NAS 1.55:3052

JAN 12 1990

NASA Conference Publication 3052

CAST-10-2/DOA 2 Airfoil Studies Workshop Results

Proceedings of a workshop held at
NASA Langley Research Center
Hampton, Virginia
September 23-27, 1988

NASA

Page 578

NASA Conference Publication 3052

CAST-10-2/DOA 2 Airfoil Studies Workshop Results

Compiled by
Edward J. Ray and Acquilla S. Hill
Langley Research Center
Hampton, Virginia

Proceedings of a workshop sponsored by
the National Aeronautics and Space Administration
and held at NASA Langley Research Center
Hampton, Virginia
September 23–27, 1988

National Aeronautics and
Space Administration
Office of Management
Scientific and Technical
Information Division
1989

II

PREFACE

During the period of September 23 through 27, 1988, the Transonic Aerodynamics Division at the Langley Research Center hosted an International Workshop on CAST-10-2/DOA 2 Airfoil Studies. These airfoil studies were the outgrowth of several cooperative study agreements among the National Aeronautics and Space Administration (NASA), the National Aeronautical Establishment (NAE) of Canada, the Deutsche Forschungsanstalt für Luft- und Raumfahrt (DLR) of West Germany, and the Office National d'Études et de Recherches Aérospatiales (ONERA) of France. Each of the visiting organizations was represented by at least two participants. The NASA and visiting researchers reviewed both theoretical and experimental CAST-10 airfoil results which had been obtained from an extensive series of tests and studies. These results provided an opportunity to make direct comparisons of adaptive wall test section (AWTS) results, taken in the NASA 0.3-Meter Transonic Cryogenic Tunnel and ONERA T-2 AWTS facilities, with "conventional" ventilated wall wind-tunnel results taken in the Canadian High-Reynolds Number Two-Dimensional Test Facility.

On the first day of the workshop there were eleven informal papers presented. The second working day of the workshop was devoted to sessions with three working groups dealing with: theoretical predictions of CAST-10 airfoil characteristics, possible residual corrections for AWTS's and wall corrections for "conventional" tunnels, and validity and correlation of AWTS and "conventional" results. The final working day of the workshop was used to make concluding announcements, review findings, and tour several of Langley's major testing facilities.

The overall results of the workshop were very positive. Correlations of corrected "conventional" results, AWTS data, and predictions were generally good. The present report contains the individual papers presented during the workshop. A summary of the major activities and accomplishments of the workshop is included.

CONTENTS

PREFACE iii

ATTENDEES vii

SUMMARY COMMENTS 1

NONLINEAR TRANSONIC WALL-INTERFERENCE ASSESSMENT/CORRECTION (WIAC) PROCEDURES AND APPLICATION TO CAST-10 AIRFOIL RESULTS FROM THE NASA 0.3-M TCT 8- X 24-INCH SLOTTED WALL TEST SECTION (SWTS) 9
Clyde R. Gumbert, Lawrence L. Green, and Perry A. Newman

COMPARISON OF CONVENTIONAL AND ADAPTIVE WALL WIND TUNNEL RESULTS WITH REGARD TO REYNOLDS NUMBER EFFECTS 37
E. Stanewsky and P. Freimuth

HIGH REYNOLDS NUMBER TESTS OF THE CAST-10-2/DOA 2 TRANSONIC AIRFOIL AT AMBIENT AND CRYOGENIC TEMPERATURE CONDITIONS 47
E. Stanewsky, F. Demurie, E. J. Ray, and C. B. Johnson

SOME NAVIER-STOKES CALCULATIONS FOR THE CAST-10 AIRFOIL 61
D. Schwamborn

MAIN RESULTS OF CAST-10 AIRFOIL TESTED IN T2 CRYOGENIC WIND TUNNEL 83
A. Blanchard, A. Seraudie, and J. F. Breil

TEST DATA ANALYSIS AND THEORY - EXPERIMENT COMPARISONS 99
J. J. Thibert

AN EXPERIMENTAL AWTS PROCESS AND COMPARISONS OF ONERA T2 AND 0.3-M TCT AWTS DATA FOR THE ONERA CAST-10 AEROFOIL 137
Stephen Wolf and Renaldo Jenkins

INVESTIGATION OF CAST-10-2/DOA 2 AIRFOIL IN NAE HIGH REYNOLDS NUMBER TWO-DIMENSIONAL TEST FACILITY 155
Y. Y. Chan

RESIDUAL INTERFERENCE AND WIND TUNNEL WALL ADAPTATION 175
Miroslav Mokry

COMPARISON OF NAE POROUS WALL AND NASA ADAPTIVE WALL TEST RESULTS USING THE NAE CAST-10 AIRFOIL MODEL 195
Raymond E. Mineck

EXPERIENCE WITH SOME REPEAT TESTS ON THE 9" CHORD CAST-10-2/DOA 2 AIRFOIL MODEL IN THE LANGLEY 0.3-M TCT ADAPTIVE WALL TEST SECTION 213
A. V. Murthy and E. J. Ray

COMPARISON OF TWO- AND THREE-DIMENSIONAL NAVIER-STOKES SOLUTIONS WITH NASA EXPERIMENTAL DATA FOR CAST-10 AIRFOIL 233
R. Charles Swanson, Rolf Radespiel, and V. Edward McCormick

ATTENDEES

Dr. Harold L. Atkins
NASA/Langley Research Center
MS 159
Hampton, VA 23665-5225

Dr. A. Blanchard
ONERA/CERT-DERAT
BP 4025
31055 Toulouse Cedex
FRANCE

Mr. Walter E. Bruce, Jr.
NASA/Langley Research Center
MS 267
Hampton, VA 23665-5225

Dr. Y. Y. Chan
High-Speed Aerodynamics Laboratory
NRC Canada
National Aeronautical Establishment
Ottawa K1A OR6
CANADA

Mr. Jerome T. Foughner
NASA/Langley Research Center
MS 198
Hampton, VA 23665-5225

Mr. Lawrence L. Green
NASA/Langley Research Center
MS 159
Hampton, VA 23665-5225

Mr. Clyde R. Gumbert
NASA/Langley Research Center
MS 159
Hampton, VA 23665-5225

Mr. Roy V. Harris, Jr.
NASA/Langley Research Center
MS 116
Hampton, VA 23665-5225

Dr. Hassan A. Hassan
North Carolina State University
NASA/Langley Research Center
MS 159
Hampton, VA 23665-5225

Mr. Renaldo V. Jenkins
NASA/Langley Research Center
MS 359
Hampton, VA 23665-5225

Dr. Robert A. Kilgore
NASA/Langley Research Center
MS 287
Hampton, VA 23665-5225

Mr. Charles L. Ladson
NASA/Langley Research Center
MS 287
Hampton, VA 23665-5225

Mr. Linwood W. McKinney
NASA/Langley Research Center
MS 198
Hampton, VA 23665-5225

Mr. Raymond E. Mineck
NASA/Langley Research Center
MS 294
Hampton, VA 23665-5225

Dr. Miroslav Mokry
High-Speed Aerodynamics Laboratory
NRC Canada
National Aeronautical Establishment
Ottawa K1A OR6
CANADA

Mr. Harry L. Morgan
NASA/Langley Research Center
MS 359
Hampton, VA 23665-5225

Dr. Annageri V. Murthy
Vigyan Research Associates
NASA/Langley Research Center
MS 287
Hampton, VA 23665-5225

Dr. Perry A. Newman
NASA/Langley Research Center
MS 159
Hampton, VA 23665-5225

Dr. Rolf Radespiel
DLR-Am Flughafen
NASA/Langley Research Center
MS 159
Hampton, VA 23665-5225

Mr. Edward J. Ray
NASA/Langley Research Center
MS 276
Hampton, VA 23665-5225

Mr. Manuel D. Salas
NASA/Langley Research Center
MS 159
Hampton, VA 23665-5225

Dr. D. Schwamborn
DLR-AVA
SM-ES
Bunsenstrasse 10
D-3400 Goettingen
WEST GERMANY

Dr.-Ing. Egon Stanewsky
DLR-AVA
SM-ES
Bunsenstrasse 10
D-3400 Goettingen
WEST GERMANY

Dr. Roy C. Swanson, Jr.
NASA/Langley Research Center
MS 159
Hampton, VA 23665-5225

Dr. J. J. Thibert
ONERA - BP 72
92322 Chatillon Cedex
FRANCE

Dr. Stephen Wolf
Vigyan Research Associates
NASA/Langley Research Center
MS 287
Hampton, VA 23665-5225

SUMMARY COMMENTS

During the period of September 23 through 27, 1988, the Transonic Aerodynamics Division at the Langley Research Center hosted an International Workshop on CAST-10-2/DOA 2 Airfoil Studies. Mr. Roy Harris, Jr., the Director for Aeronautics, Langley Research Center, NASA, delivered the opening welcome and remarks to the workshop attendees.

The CAST-10 studies were the outgrowth of several cooperative study agreements among the NASA, the NAE of Canada, the DLR of West Germany, and the ONERA of France. Each of the visiting organizations was represented by at least two enthusiastic participants. Since the workshop was conducted at Langley, there was a comparatively large NASA participation. This group of about twenty researchers reviewed both theoretical and experimental CAST-10 airfoil results which had been obtained from an extensive series of tests and studies.

The major objectives of the CAST-10 Airfoil Workshop were as follows:

* Develop a CAST-10 airfoil "corrected" data base over a broad range of Mach and Reynolds numbers.

* Evaluate current analytical methods for predicting airfoil characteristics.

* Evaluate current adaptive wall test section (AWTS) techniques.

* Examine the range and suitability of current techniques for correcting "conventional" wind tunnel results.

* Evaluate correlations of AWTS, "corrected" "conventional" and analytical results.

* Document advantages and disadvantages of various experimental and theoretical methods used in the determination of "interference-free" airfoil results.

The wind tunnel tests which were considered during the workshop were started back in the early 1980's in the slotted-wall two-dimensional test section of the 0.3-Meter Transonic Cryogenic Tunnel (TCT). For this original test and all following tests, extreme care was taken to use highly accurate and carefully validated airfoil models. All of the models were designed and fabricated by the Germans, French, and the Canadians. These detailed airfoil tests were conducted under highly controlled

conditions in both "conventional" and adaptive wall test sections (AWTS's) over large ranges of Mach and Reynolds numbers. The results provided an opportunity to make direct comparisons of AWTS's results, taken in the NASA 0.3-Meter Transonic Cryogenic Tunnel and ONERA T 2 facility, with ventilated wall (floor and ceiling) wind tunnel results taken in widely recognized "conventional" airfoil facilities such as the Canadian High-Reynolds Number 2-D test facility.

The theoreticians were very active during the workshop and it was refreshing to see analytical and wind tunnel personnel working together to accomplish a common goal. The theoreticians presented an interesting array of topics covering a NASA Nonlinear Transonic Wall-Interference Assessment/Correction (WIAC), Navier-Stokes Computations, AWTS Residual Interference studies, and correlations of theoretical and experimental results. In general, it appears that the CAST-10 theoretical and experimental results represent one of the most complete, systematic collections of supercritical-type airfoil/wall interference studies available.

On Friday the 23rd, the first active day of the conference, there were eleven, very informative, informal papers presented. These presentations represented an overview of the CAST-10 airfoil data base and experimental and theoretical state of the art. The weekend offered an opportunity for the visiting team members to tour Colonial Williamsburg, Virginia, visit the General MacArthur Memorial and Waterside of Norfolk, Virginia and test some of the local restaurants. On Monday the second working day of the workshop, the attendees were divided into working groups to identify key issues and provide action items in the evaluations of the CAST-10 results. There were three working groups. Group 1 considered "Theoretical Predictions of Airfoil Characteristics for the CAST-10 Airfoil." Group 2 dealt with the "Possible Residual Corrections for Adaptive Wall Test Sections and Wall Corrections for "Conventional" Ventilated Wind Tunnels as Applied to the CAST 10 Airfoil Tests." The third group concentrated on "Validity and Correlation of Experimental Adaptive Wall and "Conventional" Wind Tunnel Results for the CAST-10 Airfoil Tests."

The second working day of the workshop was devoted to working sessions with the three groups. In areas where working group members had interests in another group, workshop attendees were encouraged to participate with more than one group. During these proceedings the entire working group was periodically assembled to identify issues or action items of interest to all attendees.

The third working day was used to make final announcements, review conclusions, and tour some of Langley's major testing facilities. The overall results of the workshop were very positive. Not all of the objectives defined earlier were met, but definite progress was accomplished. Manny Salas, Head of the Theoretical Aero Branch, made a recommendation to the group to consider continued effort with the Canadian CAST-10 airfoil. His proposal was to extend Navier-Stokes computations to "model"

airfoil/sidewall juncture behavior and perform additional CAST-10 tests in the Langley 0.3-m TCT. The flow-juncture study as proposed would consider advanced diagnostic methods to map the actual flow behavior. Workshop members were very receptive to the proposal and the Canadians have agreed to loan their model to NASA for additional testing. The NASA team pointed out that they have experienced non-unique convergence situations with their original wall adaptation procedure. This weakness has been addressed and a "real-time" residual correction process has been incorporated as an independent check on the "convergence." Dr. A. Murthy's paper number 11 discussed these findings. ONERA indicated that they would perform additional tests in their T2 tunnel to resolve identified problems with test conditions, need for additional data, and refinements to their adaptation process. The correlations between corrected conventional results, AWTS data, and predictions were fairly good. However, there were some obvious differences at the high Mach Number conditions, which will require further study.

All in all, the attendees agreed that the workshop had been beneficial and enjoyable and tentative plans were made to meet again in the Fall of 1989 in Toulouse, France.

INITIAL WORKING GROUP ASSIGNMENTS

CAST-10 AIRFOIL WORKSHOP 23 - 27 SEPTEMBER 1988

Group 1 - Perry Newman/NASA *Theoretical Predictions of Airfoil Characteristics for the CAST-10 Airfoil*

Co-leader: M. Salas, NASA

Members: H. Hassan, N.C. State U.
R. Swanson, NASA
J. Thibert, ONERA
D. Schwarnborn, DLR
R. Radespiel, DLR
H. Morgan, NASA
H. Atkins, NASA

Group 2 - Miroslav Mokry/NAE, *Possible Residual Corrections for Adaptive Wall Test Sections and Wall Corrections for "Conventional" Ventilated Wind Tunnels as Applied to the CAST-10 Airfoil Tests*

Members: L. Green, NASA
C. Gumbert, NASA
C. Ladson, NASA
A. Murthy, Vigyan Research Assoc.
S. Wolf, Vigyan Research Assoc.

Group 3 - Egon Stanewsky/DLR, *Validity and Correlation of Experimental Adaptive Wall and "Conventional" Wind Tunnel Results for the CAST-10 Airfoil Tests*

Members: E. Ray, NASA
R. Kilgore, NASA
R. Jenkins, NASA
R. Mineck, NASA
A. Blanchard, ONERA
L. Chan, NAE

Note: These assignments are tentative and are subject to change during workshop proceedings. In fact, groups may "merge" or split during the working sessions.

MAJOR OBJECTIVES
CAST-10 AIRFOIL WORKSHOP 23 - 27, SEPTEMBER 1988

- Develop a CAST-10 airfoil "corrected" data base over a broad range of Mach and Reynolds numbers.
- Evaluate current analytical methods for predicting airfoil characteristics.
- Evaluate current adaptive wall test section (AWTS) techniques.
- Examine the range and suitability of current techniques for correcting "conventional" wind tunnel results.
- Evaluate correlations of AWTS, "corrected" "conventional" and analytical results.
- Document advantages and disadvantages of various experimental and theoretical methods used in the determination of "interference-free" airfoil results.

Manuel Salas, NASA, with his working Group 1, Theoretical Predictions of Airfoil Characteristics for CAST-10 Airfoil.

Miroslav Mokry, NAE, with his working Group 2, Possible Residual Corrections for the Adaptive Wall Test Sections and Wall Corrections for Conventional Ventilated Wind Tunnels as Applied to the CAST-10 Airfoil Tests.

Dr. Egon Stanewsky, DLR, with his working Group 3, Validity and Corrections of Experimental Adaptive Wall and Conventional Wind Tunnel Results for the CAST-10 Airfoil Tests.

Dr. Steve Wolf describes the Adaptive Wall Process of the Langley 0.3-Meter Transonic Cryogenic Tunnel to several of the workshop attendees.

Workshop attendees viewing the Boeing 767 model installed in the Langley National Transonic Facility, NTF.

Dr. Balakrishna describes the third generation Mach, Pressure, and Temperature Controller of the Langley 0.3-Meter Transonic Cryogenic Tunnel.

NONLINEAR TRANSONIC WALL-INTERFERENCE ASSESSMENT/CORRECTION (WIAC) PROCEDURES AND APPLICATION TO CAST-10 AIRFOIL RESULTS FROM THE NASA 0.3-M TCT 8- X 24-INCH SLOTTED WALL TEST SECTION (SWTS)

Clyde R. Gumbert,
Lawrence L. Green, and
Perry A. Newman
NASA Langley Research Center
Hampton, Virginia

Introduction

From the time that wind tunnel wall interference was recognized to be significant, researchers have been developing methods to alleviate or account for it. Despite the best efforts so far, it appears that no method is available which completely eliminates the effects due to the wind tunnel walls. This report will discuss procedures developed for slotted wall and adaptive wall test sections of the Langley 0.3-m TCT to assess and correct for the residual interference by methods consistent with the transonic nature of the tests.

WIAC Concept

The underlying concept of both procedures is depicted below. There are two basic elements: the wind tunnel which generates the flow in which measurements are made, and the computer which now solves two related flow problems. In the full nonlinear correction procedure at least two transonic flow problems are solved on the computer. The first is an equivalent inviscid tunnel flow where measured pressures near the wall and on the model are used as boundary conditions. The result of this first calculation is an equivalent inviscid model defined in terms of either its shape or its distribution of singularities. The second problem to be solved on the computer is a sequence of inviscid transonic calculations in which the equivalent model is used as the inner boundary condition and free-air conditions are used at the outer boundaries. The freestream Mach number and angle of attack are perturbed during this sequence in order to satisfy a best-fit criterion for the calculated model pressures and the measured model pressures. The two results obtained from these computer calculations are: corrections to the freestream conditions M and α, and a measure of residual interference.

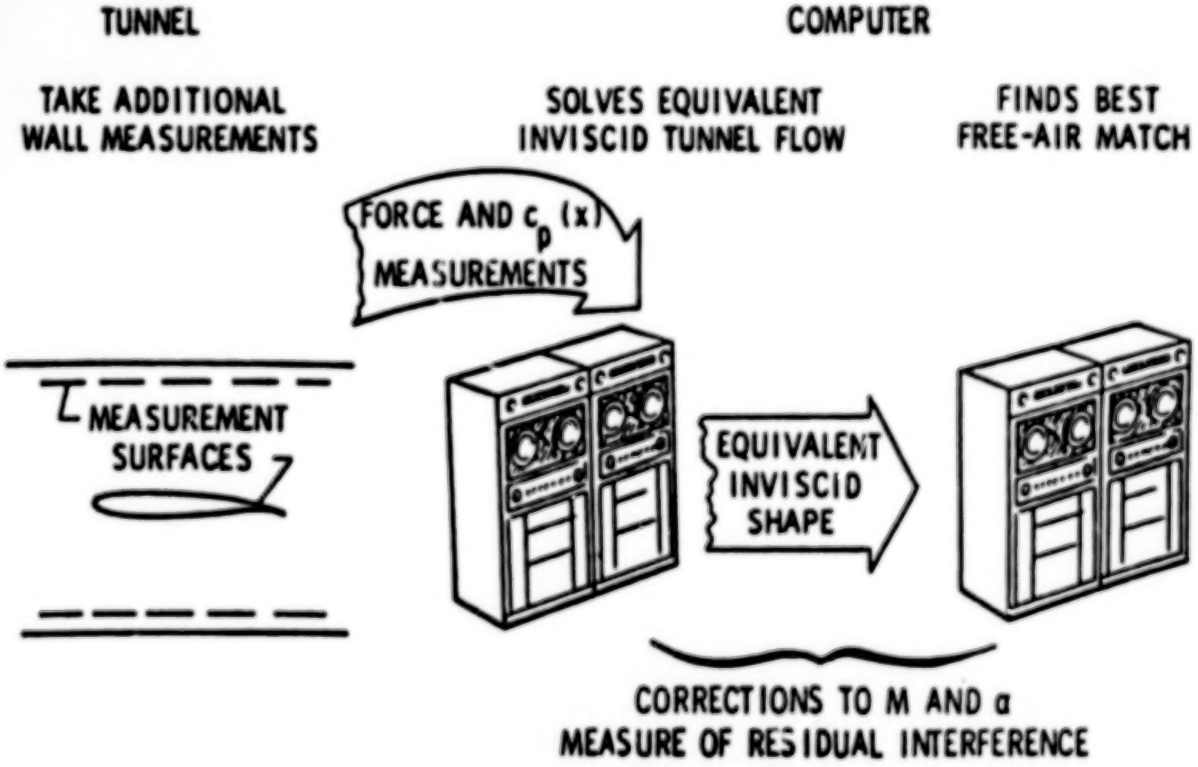

Transonic WIAC Codes

This WIAC concept was conceived by Kemp (ref. 1), developed into the TWINTAN code for slotted wall test sections (ref. 2) and extended by Kemp and Adcock (ref. 3) to include the effects of the tunnel sidewall boundary layer. The resulting code, TWINTN4, was enhanced by Green (ref. 4) to allow data on shaped walls to be used as the outer boundary condition for the equivalent tunnel flow calculation.

- Transonic flows
- Broad range of lift coefficient
- Nonlinear TSDE
- Uses measured wind tunnel data in BC's
  - Airfoil C_p, C_l and C_d
  - Top & bottom wall C_p
  - Tunnel empty SWBL δ^* and H
- Three SWBL approximations
  - 2-wall (top & bottom only)
  - Barnwell-Sewall SWBL approximation
  - Murthy SWBL approximation
- Two codes
  - Kemp's TWINTN4 for slotted wall
  - TWNTN4A for adapted wall

Nonlinear TSDE for WIAC

The TWINTN4 code (and Green's derivative) performs the flow calculations using the nonlinear Transonic Small Disturbance Equations (TSDE). The three dimensional effects of the sidewall boundary layer are incorporated into the two dimensional TSDE after Barnwell and Sewall (ref. 5) by the term, S. The effect of model aspect ratio was determined by Murthy (ref. 6) as a simple modification to the Barnwell-Sewall method.

- Solves 2-D Transonic Small Disturbance Equation (TSDE)

$$\Lambda\phi_{xx} + \phi_{yy} = 0$$

$$\Lambda = 1 - M_\infty^2 + S - (\gamma+1)M_\infty^2 \frac{U_R}{U_\infty}\phi_x \left[1 + \frac{U_R}{2U_\infty}\phi_x \right]$$

$$S = \frac{2\delta^*}{b} \left[2 + \frac{1}{H} - M_f^2 \right] \left[\frac{k_2}{\sinh(k_2)} \right]$$

$$k_2 = \frac{\pi(1-M_f^2)b}{c}$$

- Three VLOR solutions
  - In-tunnel → effective inviscid body
  - Free-air → M_{cor} and α_{cor}
  - Free-air → interference field

Cartesian Grid for WIAC

The flow field is discretized onto a Cartesian grid which is similar for both the tunnel flow calculation and the free air calculations. The top and bottom wall data is applied on grid lines included in the free air grid at the mean location of the walls. The data on the airfoil surface is applied at the slit on the tunnel centerline (or mean location of the model). The boundary condition at the inflow plane of the wind tunnel was left undetermined from wind tunnel data. This remaining boundary condition is assumed during the first pass through the correction code and approximated by iteration based on the difference between the computed inclination of the equivalent inviscid model and the geometric model according to the method devised by Gumbert et al (ref. 7). The first approximate iterate value is used in the second pass through the correction code; a third pass may be required.

WIAC Procedure

In order to more easily apply the individual codes to the data, they were incorporated into a procedure by Gumbert, et al (refs. 7 and 8) to pass data from one code to the next in a somewhat automated manner. This procedure was first used for making corrections to several data sets in order to validate the procedure and the individual codes.

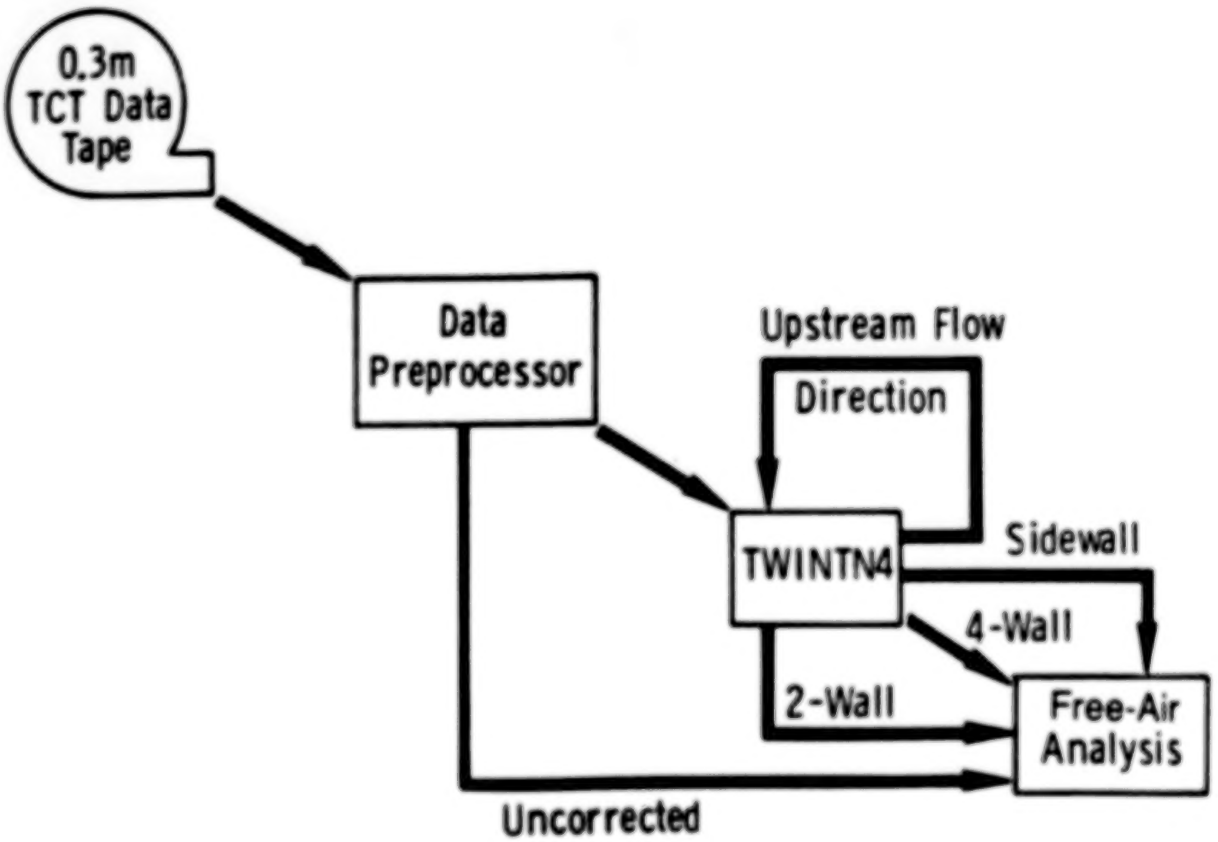

Validation of WIAC Procedure

The validation of the WIAC procedures (refs. 4 and 9) was accomplished by two types of comparisons. First, the corrected data was compared to the best available independent free-air computer code solutions. For the earlier slotted wall data comparisons (ref. 9), solutions from the conservative, transonic, full-potential equation (with viscous/inviscid interaction) GRUMFOIL code (ref. 10) were used. For the latter adaptive wall data comparisons, solutions from a Navier-Stokes code (ref. 11) were used. Second, the corrected data from several tests of the same airfoil shape were compared for consistency.

- Comparison of Corrected Data With Independent Free-Air Calculations
- Consistency of Corrected Data From Separate Tests of Common Airfoil

Test Data Matrix

The three tests of the CAST 10 airfoil under consideration here were conducted in the 8- X 24-inch slotted wall test section over a span of several years. Two of the tests were conducted using a six-inch-chord model. During the period between the two tests, several changes were made to the test section toaccommodate different instrumentation and flow visualization techniques. The other test used a three-inch-chord model. It was the only non-six-inch chord model tested in the 8- X 24-inch slotted wall test section. More specific information about the tests can be found in references 12 through 15. The figure shows the ranges of Mach number and Reynolds number over which the three tests were run. The WIAC procedure was applied to data for the three tests at those conditions which are similar for all three tests. These eleven common points are denoted as ● in the figure below.

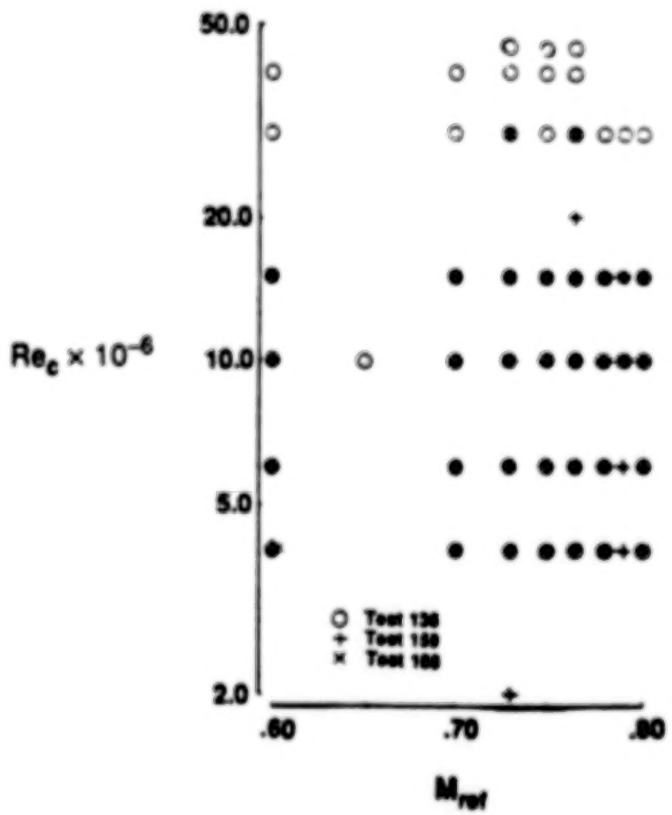

Preprocessor Plots of Airfoil C_p

The first step in the WIAC procedures is the preprocessor code where the primary function is to select only the pertinent information from the data tapes and generate an input file for TWINTN4. In the process it generates plots of the uncorrected data which are to be used as inner boundary conditions for the WIAC code solutions. Shown in the figure are the uncorrected pressure coefficient distributions on the model for each test at nearly the same conditions: $Re_c = 15$ million, $M_{ref} = 0.765$, and $C_L = .55$.

$$M_{ref} \approx 0.765,\ C_L \approx 0.55,\ Re_c \approx 15 \times 10^6$$

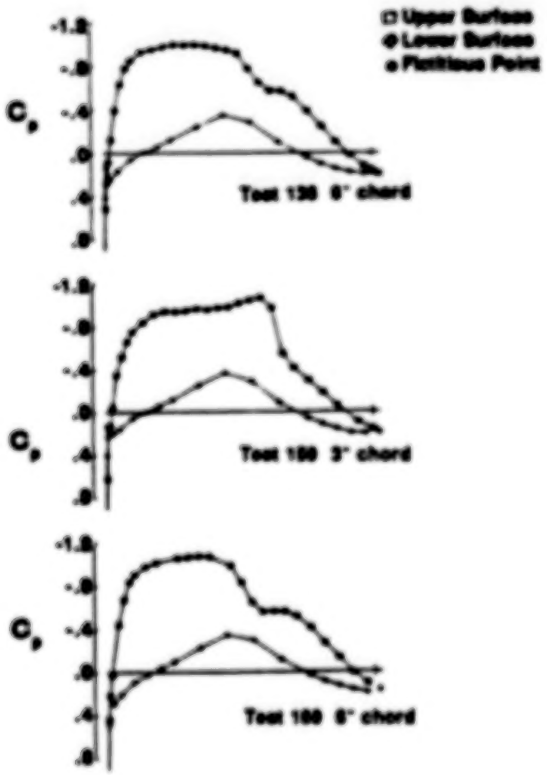

Preprocessor Plots of Wall C_p

The preprocessor also generates plots of the pressure coefficient distribution on the center slats of the top and bottom walls as shown in the figure. The circled points in the bottom figure indicate data that was conspicuously inconsistent. The data point over the leading edge was removed and the data point ahead of the model was modified as shown by the filled square symbol. These are the data to be used as outer boundary conditions for the WIAC code solutions.

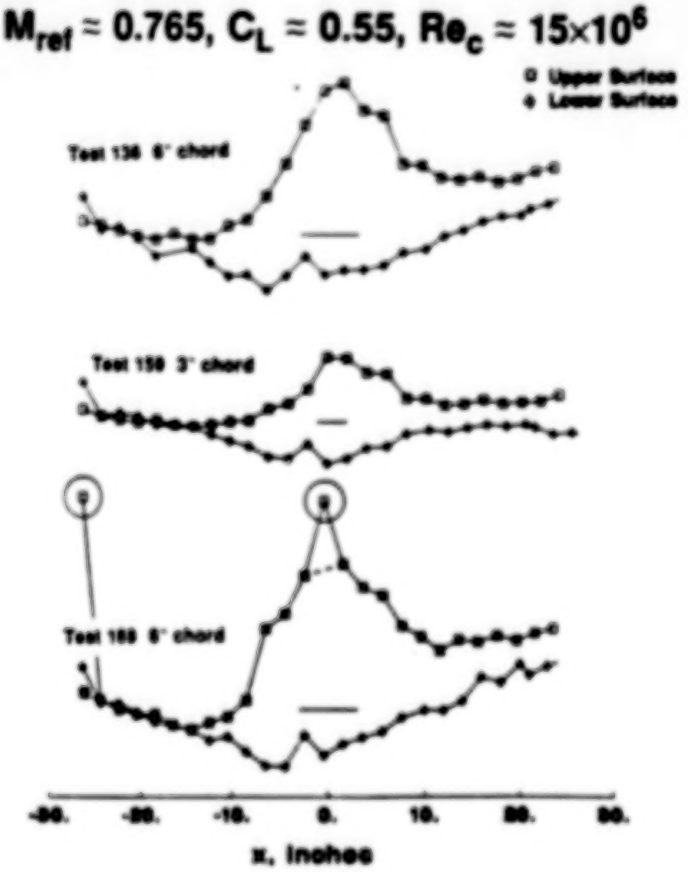

Uncorrected Lift Curves

The correction to the angle of attack can best be shown in plots of the lift coefficient versus angle of attack. Shown in the figure is the comparison of the uncorrected lift curves for the three tests at $M_{ref} = 0.73$ and $Re_c = 10$ million. For comparison, the results from GRUMFOIL are shown. The data from the three tests are quite scattered and each shows a different slope.

$M_{ref} \approx 0.730$, $Re_c \approx 10 \times 10^6$.

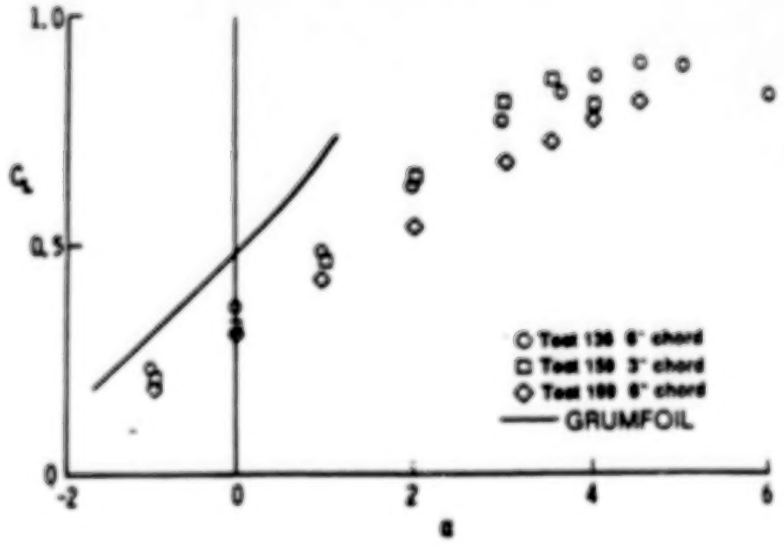

First Pass WIAC Lift Curves

The results from the first pass through the correction code, TWINTN4, are shown below. The lift curve slopes seem more consistent between the three tests, yet there is an unresolved shift between the data sets and with respect to the GRUMFOIL curve.

$M_{ref} \approx 0.730$, $Re_c \approx 10 \times 10^6$

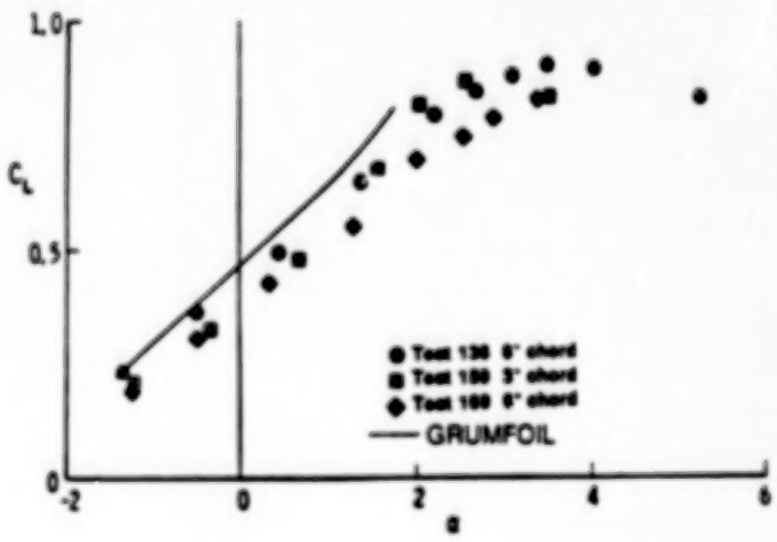

Second Pass WIAC Lift Curves

The results from the second pass through the correction code are shown below. All three tests show good agreement over the low lift range and the comparison with the independent free-air code is good. However, the data from test 169 tend to be inconsistent at moderate lift and all three data sets show different behavior near maximum lift. The early breakdown of the test 169 data and its correction may be due to the known inaccuracy of the top wall pressure data in the vicinity of the model. Subsequent correction comparisons will involve data from test 136, the early test of the six-inch-chord model and test 159, the test of the three-inch-chord model.

$M_{ref} \approx 0.730$, $Re_c \approx 10 \times 10^6$

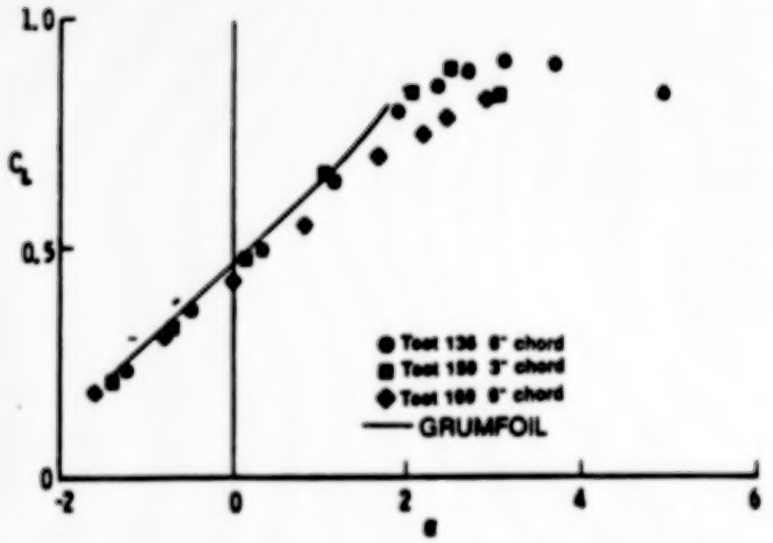

Drag Rise Curves, $C_L = 0.3$

The following three figures show the Mach number correction in the form of uncorrected and corrected drag rise curves. The corrections are shown with and without the Murthy aspect ratio factor (ref. 6) on the Barnwell-Sewall sidewall boundary layer term (refs. 3 and 5). The first figure below shows the comparison for $Re_c = 15$ million at $C_L = 0.3$.

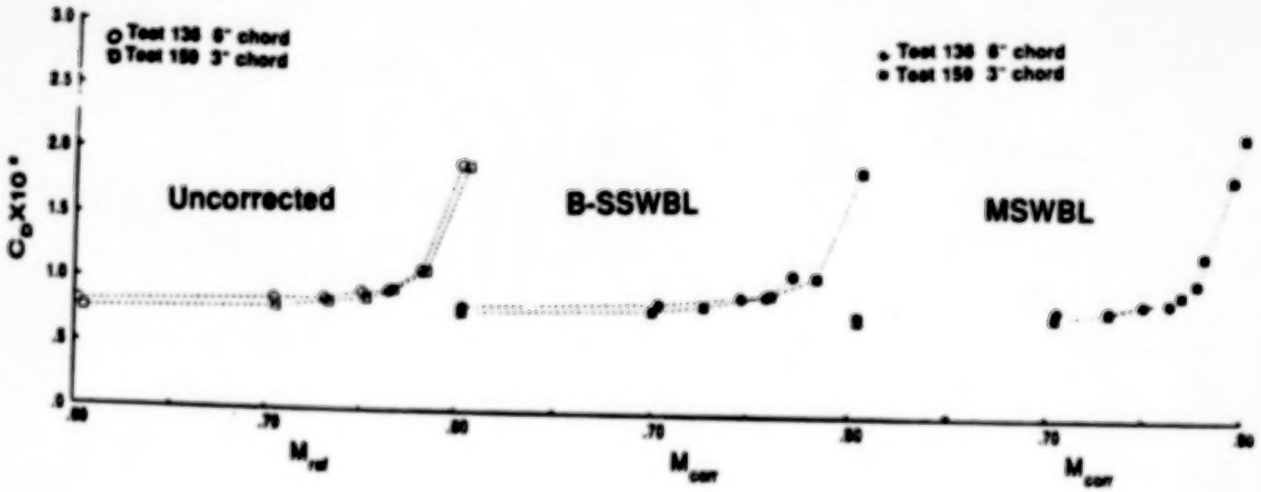

Drag Rise Curves, $C_L = 0.5$

Uncorrected and corrected drag rise curves are shown here for $C_L = 0.5$.

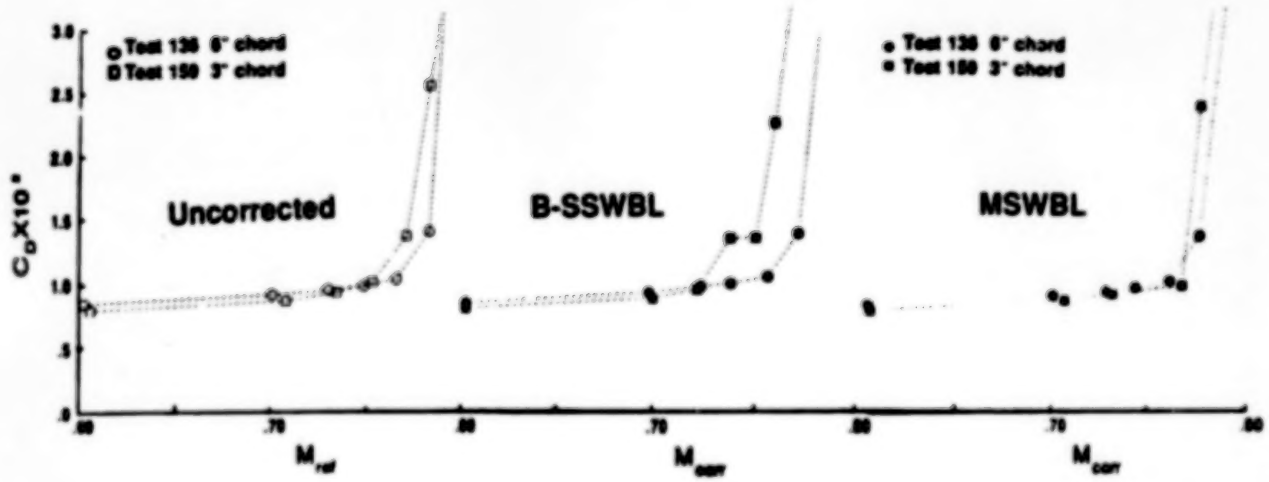

Drag Rise Curves, C_L=0.7

Uncorrected and corrected drag rise curves are shown here for C_L=0.7. In all cases, the Barnwell-Sewall Mach correction is noticeably too large for the three-inch-chord test. The agreement is pretty good for all three cases with the Murthy aspect ratio factor included; this is taken as evidence that an aspect ratio factor should appear as part of a sidewall boundary layer approximation.

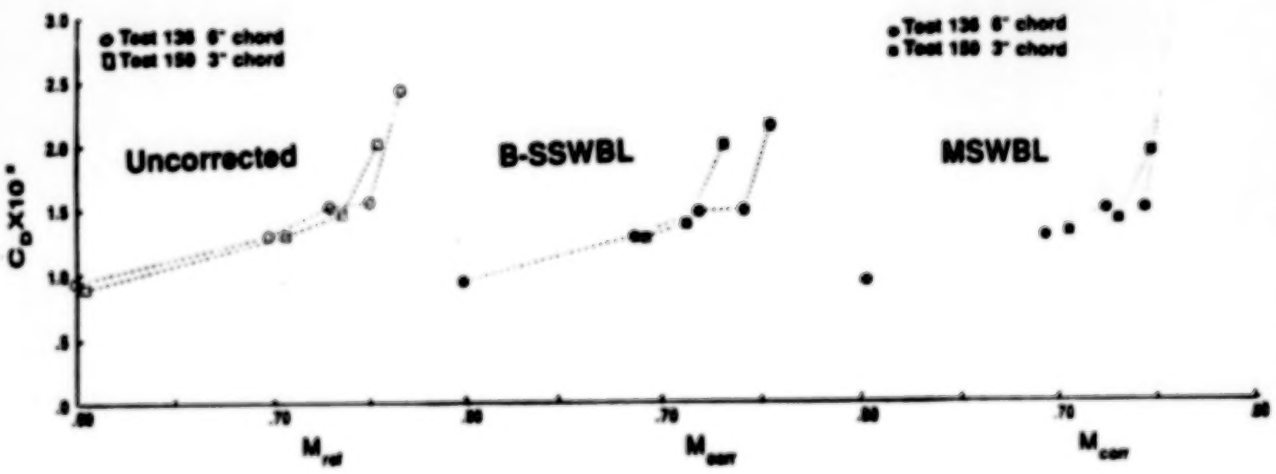

Airfoil C_p Plots

The better correction to the Mach number due to the Murthy aspect ratio factor is also evident in comparisons of the free-air calculated pressure coefficient, shown by the vertical and diagonal crosses, and the experimental pressure coefficient renormalized with the corrected Mach number, shown by the asterisks. The figure shows the comparison for the three-inch-chord model at $C_L = 0.37$, $M_{ref} = 0.765$, and $Re_c = 15$ million. The shift in the C_p's is eliminated by using the Murthy aspect ratio factor. Similar tendencies are found in the corrections for the six-inch-chord model but not to the same extent. All subsequent corrections will be made with the Murthy aspect ratio factor included in the sidewall boundary layer approximation.

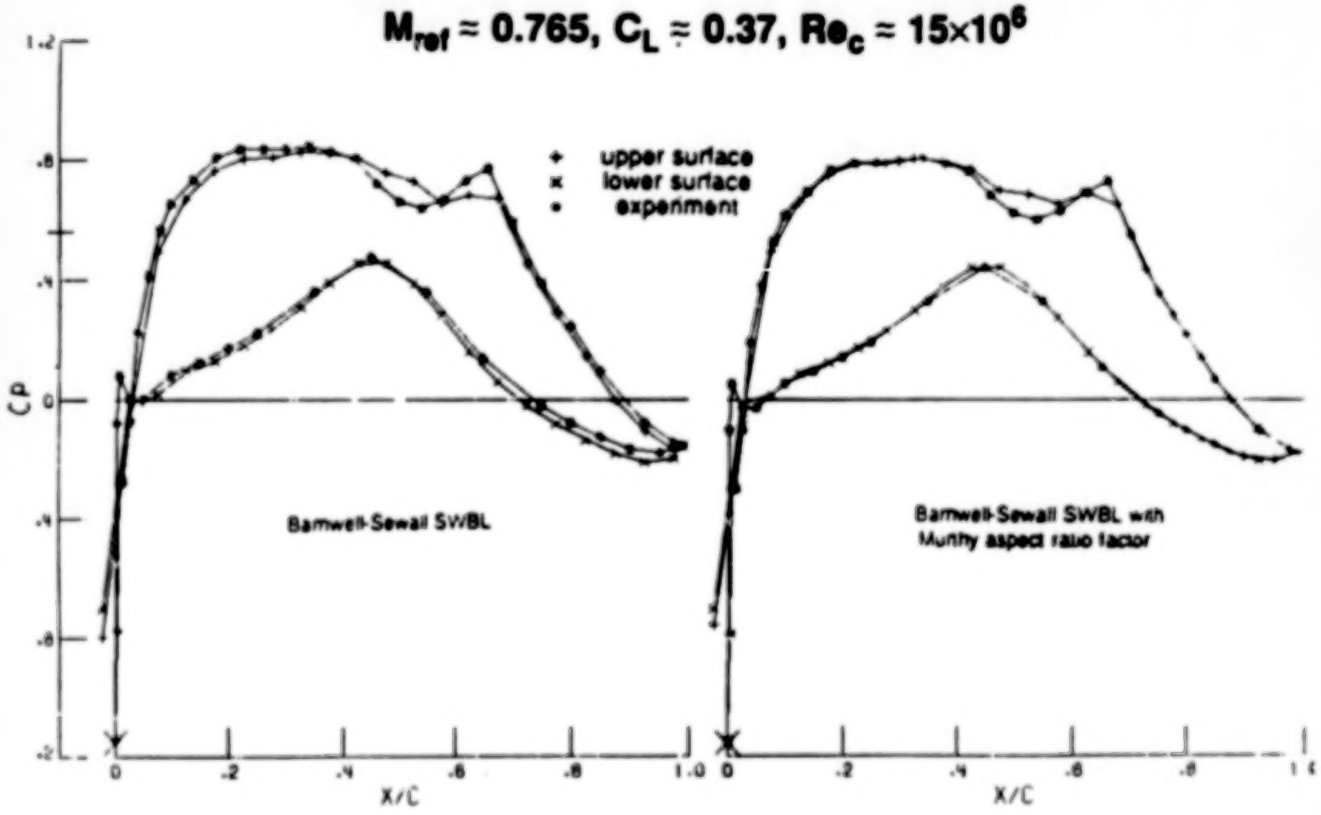

Lift Curves and Error Parameter, $M_{ref}=0.60$

The following three figures show the results of applying the WIAC procedure to data for three Mach numbers and a Reynolds number of 15 million. The corrected and uncorrected lift curves are shown for two tests. In addition, ε, the RMS matching error of the experimental and calculated airfoil surface velocity squared, is shown as an indication of the relative 'goodness' of the corrections. As the error increases the corrections are deemed to be less trustworthy. The first figure shows the lift curve and the error for $M_{ref}=0.60$.

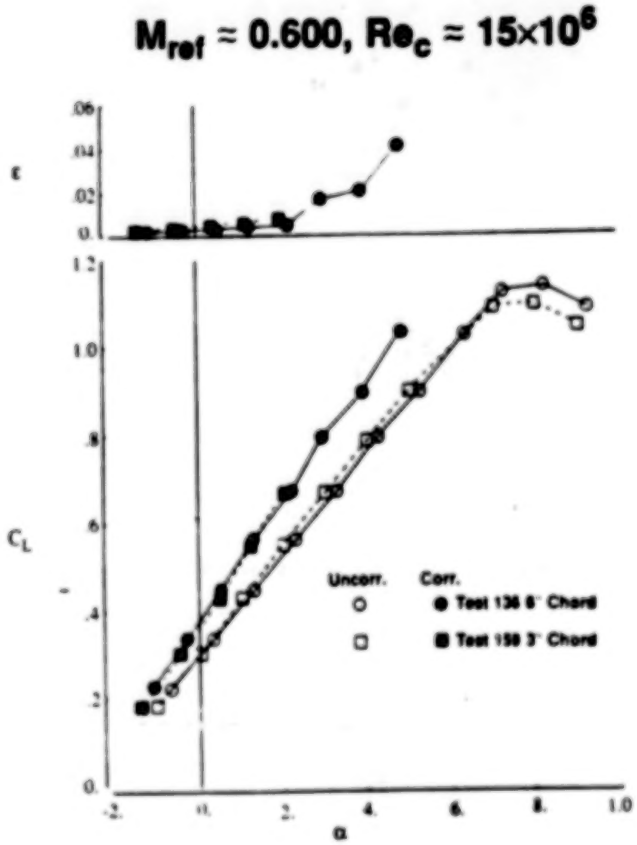

Lift Curves and Error Parameter, $M_{ref}=0.73$

This figure shows the lift curve and the error parameter for $M_{ref}=0.73$, $Re_c=15$ million. It can be seen that the error parameter, ε, becomes relatively much larger sooner with increasing α than was the case at $M_{ref}=0.60$ shown on the previous page.

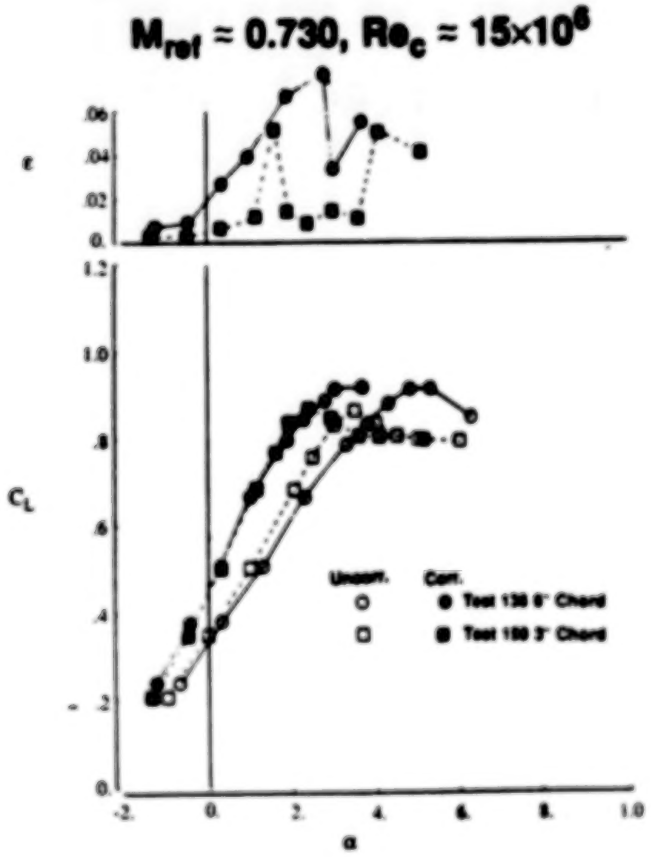

Lift Curves and Error Parameter, $M_{ref}=0.765$

This figure shows the lift curve and the error parameter for $M_{ref}=0.765$, $Re_c=15$ million. It can be seen in these three figures that as the Mach number increases and the lift increases the error parameter also increases. This is due in part to the inability of the inviscid method to adequately model a flow condition greatly influenced by viscous and viscous/shock interaction phenomena. In addition, the present sidewall boundary layer/model pressure field interaction approximations may certainly become suspect at the higher transonic flow conditions.

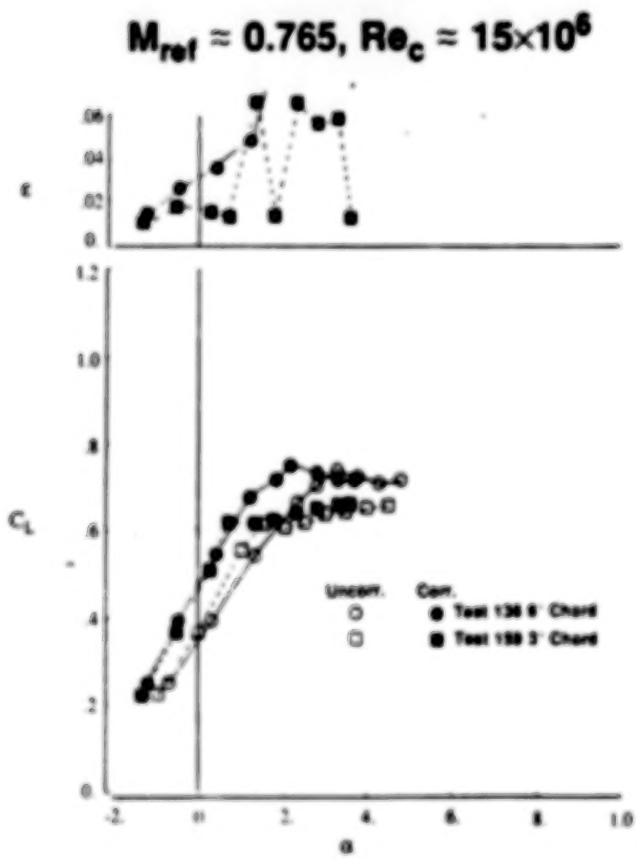

CAST 10 Airfoil Data

Comparisons of lift curve data for the French-built 18-cm (7.09 inch) chord CAST 10 model tested in both the NASA 0.3-m TCT and the ONERA/CERT T2 was recently given by Wolf and Ray (ref. 16). Both tunnels had adjusted wall test sections (AWTS) and both fixed and free transition results were given for $M_{ref} = 0.765$ and $Re_c = 4$ million. The curves shown in black by the squares and X's on the figure below denote the fixed transition data. Lift curve data shown as open and closed circles on the figure are from a 6-inch-chord model tested in the 8- by 24-inch slotted wall test section (SWTS) of the NASA 0.3-m TCT with transition fixed at 7% chord. Uncorrected data are indicated by open symbols while the (second pass, 4-wall) WIAC data are given by the solid symbols. The GRUMFOIL free-air numerical results at the corrected conditions are denoted by an alternating dash-dot line when flow is attached (until very near the trailing edge) and a dotted line for separated flow. The value of $c_{n_{max}}$ appears to be larger for the slotted wall test section results. The corrected slotted wall data and GRUMFOIL results were taken from Gumbert and Newman (ref. 9).

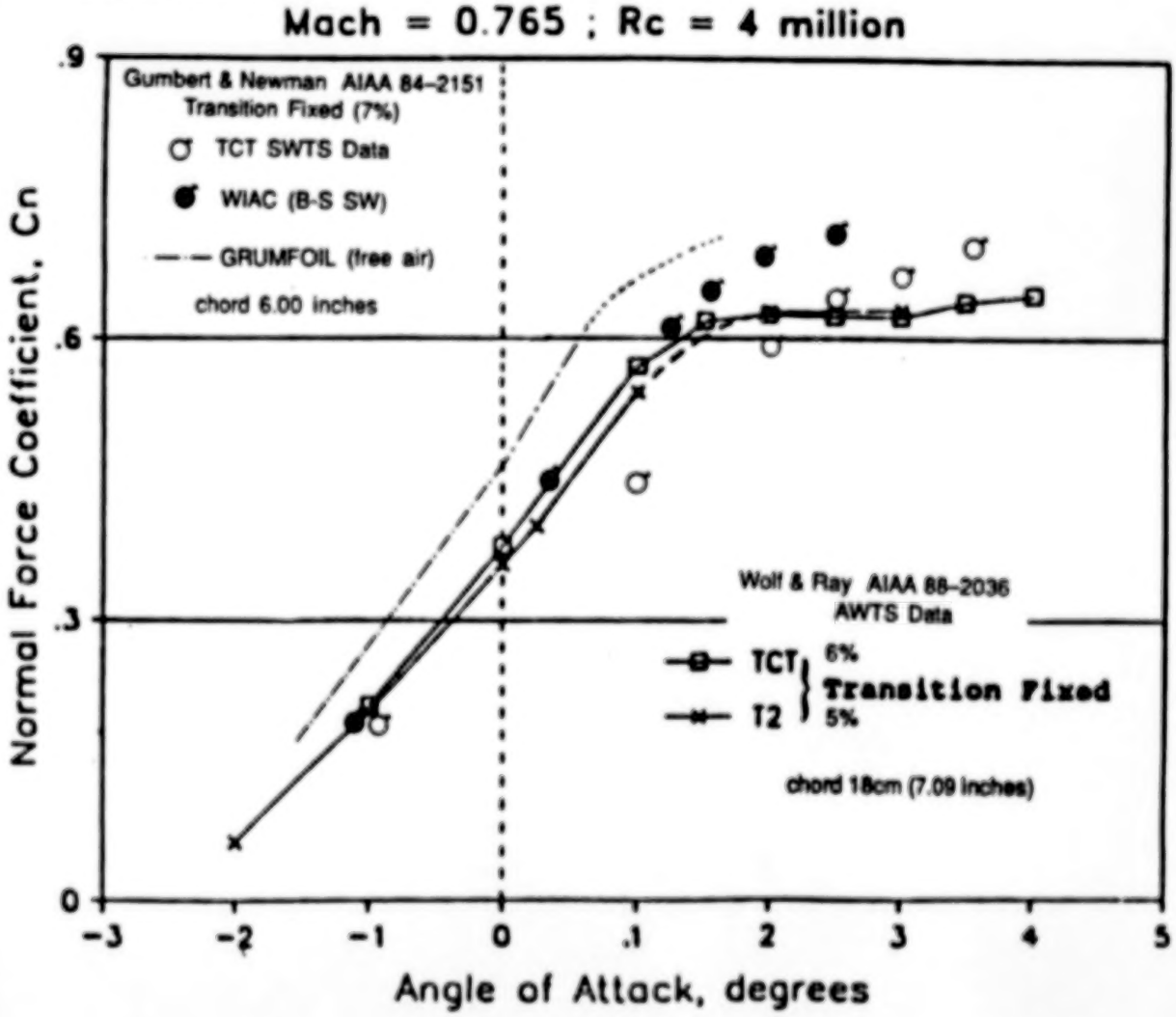

CAST 10 Airfoil Data

Lift curve data shown by the solid lines is again that from the AWTS tunnels as described on the previous page. Data shown here by the open and closed circles is for "free" transition in the slotted wall test section of the TCT. Again the open symbols are uncorrected data, the filled symbols are WIAC data and the dashed curves are for GRUMFOIL free-air results. As pointed out in reference 9, the various GRUMFOIL results are for different transition locations (denoted n% at end of line) and it appears that the transition location in the tunnel tests is changing with lift level. The relative location of the curves in the present comparison indicates that the slotted wall test section appears to cause more premature transition than the adaptive wall test section.

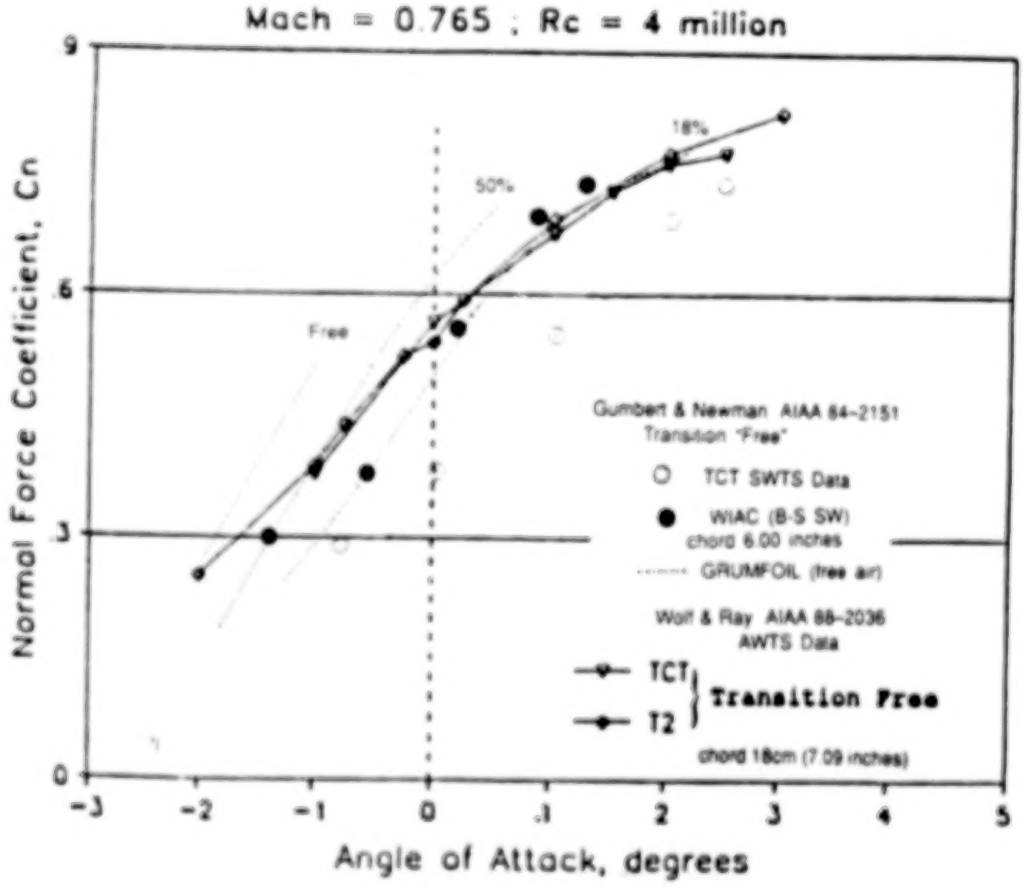

CAST 10 Airfoil Data

Comparison of lift curve data for the Canadian-built 9-inch chord CAST 10 model tested in the NASA 0.3-m TCT AWTS with that from the NAE 5-foot by 5-foot Blowdown Wind Tunnel with perforated top and bottom wall airfoil test section (15- by 60-inch) were also given by Wolf and Ray (ref. 16). These results, shown by the X's and the squares on the viewgraph below, are for transition fixed at 5% chord at M_{ref} = 0.765 and Re_c = 10 million. The Canadian data have been corrected for the top and bottom perforated wall interference. Lift curve data shown as circles are from a 6-inch-chord model tested in the 8- by 24-inch slotted wall test section of the NASA 0.3-m TCT with transition fixed (flagged symbols) and "free" (open symbols). The filled symbols represent the (second pass, 4-wall) WIAC data for free transition. Broken line curves are again GRUMFOIL free-air results with transition denoted at the end of the curve. The shift in the angle of attack scale was simply due to different definitions for the zero angle of attack.

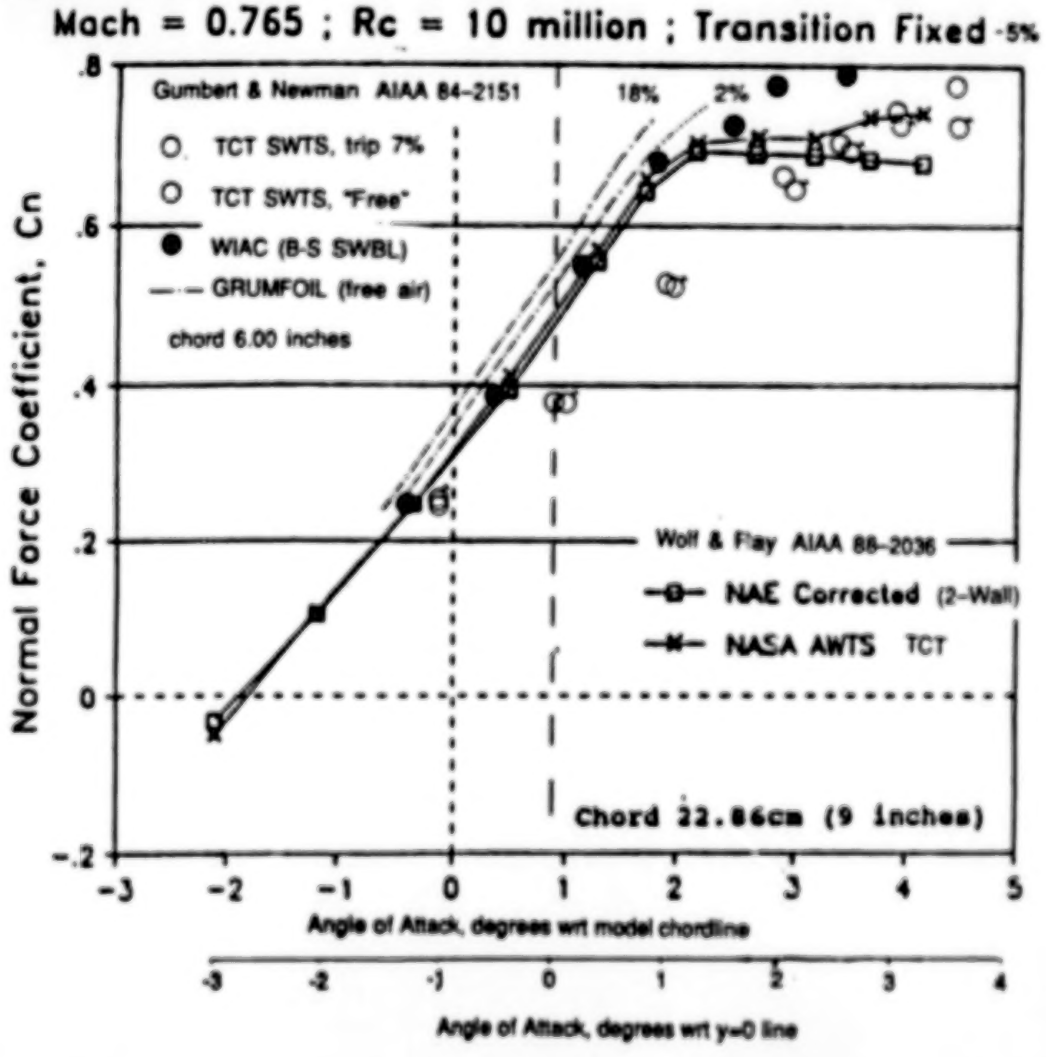

CAST 10 Airfoil Data

Lift curve data shown by the X's and squares is again that from the NAE perforated and NASA AWTS tunnels as described on the previous page. Data shown here by the "plus" symbol are for the 4-wall AWTS WIAC (ref. 4) applied to the NASA AWTS data by Mineck using the Murthy sidewall boundary layer option. The Navier-Stokes results denoted by the solid and dashed lines are due to Swanson et al and are discussed in the final talk of this workshop. At the higher lift levels for this Mach number, the Mach number corrections appear to be too large; apparently the subsonic wavy-wall solution invoked by Murthy (ref. 6) to approximately model the sidewall boundary layer effect is no longer valid for extensive supercritical flow and certainly not for large separated flow regions. This will also be discussed by Swanson.

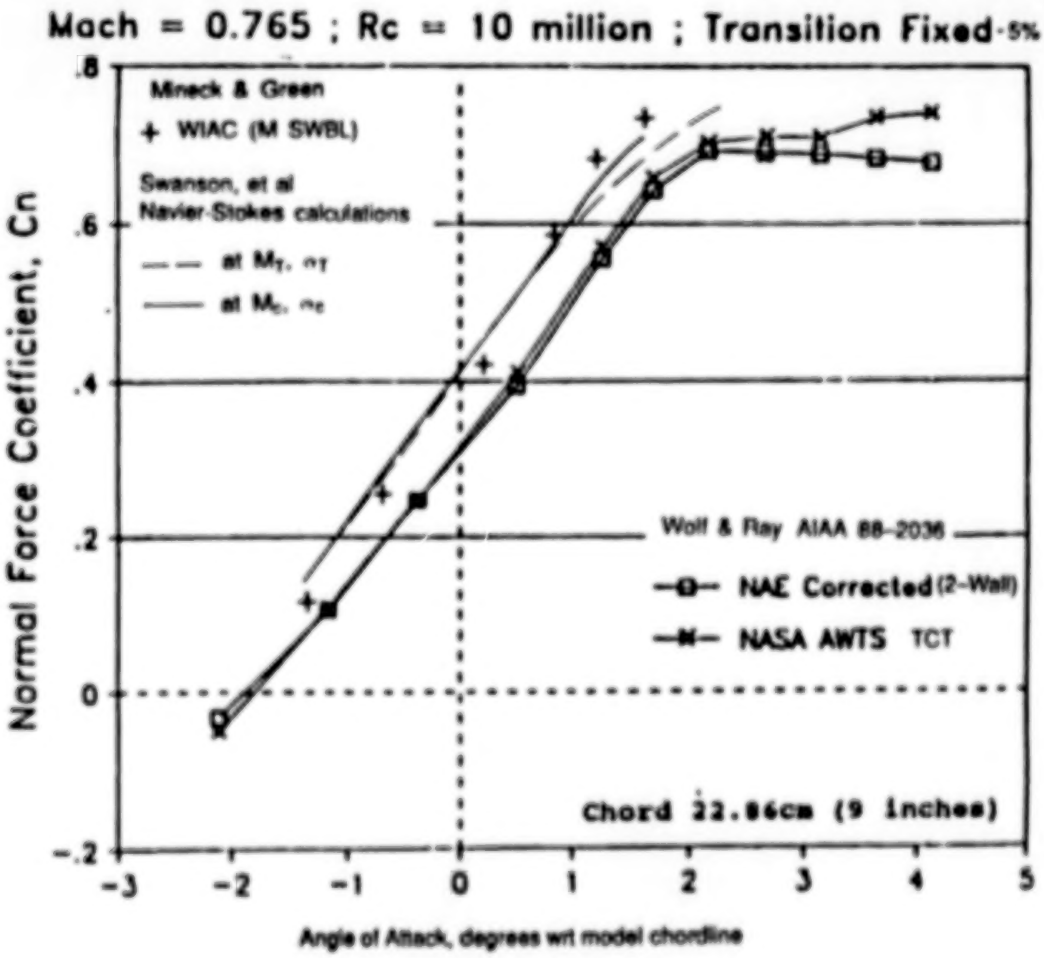

CONCLUDING REMARKS

PREMISE: All "airfoil tunnel" data contains some wall interference

- Conclusions Concerning Data
  - **Wall interference assessment must be made**
  - **Wall interference corrections have been required to date**
  - **Corrections smaller for AWTS data than for SWTS data**
  - **SWBL influence can be significant at transonic high-lift conditions**
  - **Airfoil and tunnel-wall C_p data required for TWINTN4**
  - **Transition location needs to be known**

- Conclusions Concerning WIAC
  - **Transonic 4-wall approximations are required**
  - **Multiple passes needed to assess upstream flow angle**
  - **SWBL approx. needs to contain aspect ratio effect**
  - **Reasonable corrections seem to be obtained**
  - **Fairly easy to use**
  - **SWBL approx. may be inadequate for extensive supercritical flow**
  - **Interpretation of error parameter not yet established**

References

1. Kemp, W. B., Jr.: Transonic Assessment of Two-Dimensional Wind Tunnel Wall Interference Using Measured Wall Pressures. Advanced Airfoil Technology Research - Volume I, NASA CP-2045, Part 2, 1979
2. Kemp, W. B., Jr.: TWINTAN: A Program for Transonic Wall Interference Assessment in Two-Dimensional Wind Tunnels, NASA TM-81819, 1980
3. Kemp, W. B., Jr. and Adcock, J. B.: Combined Four-Wall Interference Assessment in Two-Dimensional Wind Tunnel Tests, AIAA Paper 82-0586, March 1982
4. Green, Lawrence L. and Newman, Perry A.: Transonic Wall Interference Assessment and Corrections for Airfoil Data from the 0.3-m TCT Adaptive Wall Test Section, AIAA 87-1431, June 1987
5. Barnwell, R. W. and Sewall, W. G.: Similarity Rules For Effects of Sidewall Boundary Layer in Two Dimensional Wind Tunnels, Paper 3, AGARD CP-335, 1982
6. Murthy, A. V.: Effect of Aspect Ratio on Sidewall Boundary Layer Influence in Two-Dimensional Airfoil Testing, NASA CR-4008, 1986
7. Gumbert, C. R.; Newman, P. A.; Kemp, W. B.; Adcock, J. B.: Adaptation of a Four-Wall Interference Assessment/Correction Procedure for Airfoil Tests in the 0.3-m Transonic Cryogenic Tunnel, Paper 25, NASA CP-2319, 1984
8. Gumbert, C. R.: User Manual for 0.3-m TCT Wall Interference Assessment/Correction Procedure: 8- by 24-Inch Test Section, NASA TM-87582, 1985
9. Gumbert, C. R. and Newman, P. A.: Validation of a Wall Interference Assessment/Correction Procedure for Airfoil Tests in the 0.3-m Transonic Cryogenic Tunnel, AIAA Paper 84-2151, August 1984.
10. Melnik, R. E.; Mead, N. R.; and Jameson, A.: A Multi-Grid Method for the Computation of Viscid/Inviscid Interaction on Airfoils, AIAA Paper 83-0234, January 1983
11. Swanson, R. C. and Turkel, Eli, "A Multistage Time-Stepping Scheme for the Navier Stokes Equations," AIAA Paper 85-0035, January 1985
12. Dress, D. A.; Johnson, C. B.; McGuire, P. D.; Stanewsky, E.; and Ray, E. J.: High Reynolds Number Tests of the CAST 10-2/DOA 2 Airfoil in the Langley 0.3-m Transonic Cryogenic Tunnel - Phase I, NASA TM-84620, 1983
13. Stanewsky, E.; Demurie, F.; Ray, E. J. and Johnson,C. B.: High Reynolds Number Tests of the CAST 10-2/DOA 2 Transonic Airfoil at Ambient and Cryogenic Temperature Conditions, Paper 10, AGARD CP-348, 1984

14. Murthy, A. V.; Johnson, C. B.; Ray, E. J.; Stanewsky, E.: Investigation of Sidewall Boundary Layer Removal Effects on Two Different Chord Models in the Langley 0.3-m Transonic Cryogenic Tunnel, AIAA Paper 84-0598, March 1984

15. Dress, D. A.; McGuire, P. D.; Stanewsky, E.; Ray, E. J.: High Reynolds Number Tests of the CAST 10-2/DOA 2 Airfoil in the Langley 0.3-m Transonic Cryogenic Tunnel - Phase II, NASA TM-86273, 1984

16. Wolf, Stephen W. D. and Ray, Edward J.: Highlights of Experience with a Flexible Walled Test Section in the NASA Langley 0.3-Meter Transonic Cryogenic Tunnel, AIAA 88-2036, May 1988

Comparison of Conventional and Adaptive Wall Wind Tunnel Results with Regard to Reynolds Number Effects

E. Stanewsky and P. Freimuth
Deutsche Forschungs- und Versuchsanstalt für
Luft- und Raumfahrt e.V.
Institut für Experimentelle Strömungsmechanik
D-3400 Göttingen, F.R. Germany

Introduction

Studies of the CAST 10-2/DOA2 airfoil commenced in the early seventies with the verification of the design in tests in the 1 x 1 Meter Transonic Wind Tunnel Göttingen (TWG) [1]. Part of these studies were devoted to the investigation of viscous effects, i.e., the influence of the state and condition of the boundary layer, on the flow development. Viscous conditions were varied by changing the Reynolds number itself, although in a very limited range, and transition location; it was found that the flow development on this airfoil was very sensitive to changes in the viscous conditions [1]. This led to an investigation of the airfoil under contract in the Lockheed Compressible Flow Wind Tunnel (CFWT) at Reynolds numbers up to $Re = 30 \times 10^6$ and fixed and free transition [2] and, finally, to tests in the slotted 0.3-m Transonic Cryogenic Wind Tunnel of NASA Langley (0.3-mTCT) within a NASA/DFVLR cooperation. The objective of the latter series of experiments was twofold: to determine the effect of Reynolds number on the flow about a certain class of transonic airfoils characterized by extreme rear adverse pressure gradients, thus susceptible to rear separation, and to study the influence of the Reynolds number on the model-wind-tunnel system, i.e., on wall interference, be it sidewall or top and bottom wall induced, in conventional partly open wind tunnels. Here, two different size models having chords of $c = 76$ mm and $c = 152$ mm, respectively, were investigated. The results of these studies were summarized at the AGARD Symposium on Wind Tunnels and Testing Techniques in Cesme, Turkey, 1983 [3].

The continuation of the CAST 10-2/DOA2 airfoil studies in the adaptive wall TCT and the adaptive wall ONERA/CERT T2 - ONERA joined the NASA/DFVLR airfoil study program in 1983 - provided the opportunity to confirm or reject the postulations of the previous analysis [3] of viscous effects on airfoil flow and wall interference. In the following, we will revisit the results obtained in the conventional wind tunnels and compare them to the adaptive wall data. In the discussion, we will frequently refer to the Cesme paper [3] which is, therefore, attached for easy access (see page 47).

Sidewall Interference Effects

It was shown in [3] that the sidewall or sidewall boundary layer development may have a pronounced effect on the non-linearity of the lift curves, Fig. 5 of [3]: only a small deviation from a linear lift variation with angle of attack occurred for the large chord, small aspect ratio TCT model, while the small chord TCT and the CFWT airfoil models with their substantially higher aspect ratios showed a very pronounced non-linear increase in lift. It was concluded that sidewall interference effects suppress the non-linear lift increase as a result of the influence on the upper surface shock which assumes a more foreward position due to the interaction of the airfoil flow field with the sidewall boundary layer, Fig. 6 of [3].

Let us now turn to the investigation in the adaptive wall wind tunnel (TCT only) where lift interference effects are substantially reduced: Figure 1 shows the lift curves measured in the slotted TCT with the two different size CAST 10-2 models mentioned above and the lift curve obtained in the adaptive wall TCT with a 180 mm

chord model. Remarkable is firstly the large difference in angle of attack for a given lift coefficient but close agreement in maximum lift for the Mach number of $M_\infty = 0.73$ considered here. In order to compare the linearity of the lift development with incidence, the lift curves were shifted to match in the lower incidence range, Figure 2. One observes a close agreement between the non-linear behavior of lift measured in the adaptive TCT and the slotted TCT with the smaller model, despite the smaller aspect ratio in case of the former. Considering the maximum non-linear lift, ΔC_{L_1}, as function of the aspect ratio in Figure 3, one tends to conclude that even at an aspect ratio of 1.8 - as existed in the adaptive wall test - sidewall interference effects are minor. This is somewhat surprising since it was previously inferred from a number of experimental results that aspect ratios of AR $>$ 2 were required for sidewall effects to be negligible [4]. It is quite possible that (horizontal) wall adaptation is here of influence; however, this is a matter for further research. Concerning the influence of the Reynolds number on sidewall interference, the reader is again referred to [3] where it was concluded that the interference becomes slightly more severe at higher Reynolds numbers.

Lift Interference

It was shown in [3], see, e.g., Figs. 14 and 15, that the influence of the Reynolds number on lift interference is negligible at lift coefficients prior to maximum lift so that for these conditions true Reynolds number effects on the flow about the airfoil could be exposed. Here, we want to confirm this observation utilizing the adaptive wall interference free wind tunnel results. To proceed, let us first consider the lift curves for the various model-wind-tunnel configurations at the (nominal) Mach number of $M_\infty = 0.765$, Figure 4: The data for the large chord model in the slotted TCT exhibit the lowest lift curve slope while the adaptive wall TCT shows the highest slope reflecting the range of lift interference encountered for the model-wind-tunnel configurations considered in this test series. Note, that even for the small model in the slotted TCT with a test section height to chord ratio of H/c = 8, wall interference is still substantial. The deviations in lift indicate that in order to determine the influence of the Reynolds number on lift for the various configurations, it is necessary to suitably correct the data either by theory or empirically. Here, a simple procedure was employed, Figure 5: for given freestream conditions, here $M_\infty = 0.765$, $Re = 10\times10^6$, transition fixed, a lift coefficient was selected in the range of interest, here $C_L = 0.55$, and the angles of attack necessary to generate this lift coefficient in the various model-tunnel systems was noted. For these angles of attack the Reynolds number dependence of lift for free and fixed transition was then plotted, Figure 6. One observes that for fixed transition and at high Reynolds numbers, where the movement of the transition point with increasing Reynolds number has ceased, the data of the adapted TCT fall within the band of results previously established (Fig. 15a of [3]). The ONERA T2 data follow this band only up to a Reynolds number of about 20×10^6, then drop abruptly below the data band but still follow the trend given by the data band as the Reynolds number is further increased; this behavior seems unrealistic and must be checked.

The adaptive wall data of TCT and T2 confirm the conclusion that Reynolds number effects on lift interference are negligible, i.e., the wall characteristics are not changed by viscous effects to a degree noticeable in the Reynolds number dependence of lift prior to maximum lift. Note, that the considerable difference in the lift dependence between the various model-wind-tunnel configurations at low Reynolds numbers and free transition reflects the different model/wind tunnel environments; from the very

late onset of the rapid transition point movement as Reynolds number is increased, indicated by the late drop in lift coefficient, one may conclude that the ONERA/CERT T2 adaptive wall tunnel is a very low turbulence facility.

The dependence of the pressure distribution on Reynolds number corresponding to the data points of the adaptive wall TCT measurements is, for completeness sake, depicted in Figure 7.

Maximum Lift and Drag Rise (Blockage Interference)

It was shown in [3], Fig. 11 and 12, that very pronounced differences existed in the Reynolds number dependence of maximum lift and the drag-rise Mach number between the various model-wind-tunnel configurations. From an analysis of the results it was concluded that this was essentually due to the influence of the Reynolds number on the characteristics of partially open test section walls responsible for blockage interference. It was, furthermore, judged that perforated walls were more sensitive to Reynolds number changes than slotted ones.

Again, the results from the adaptive wall wind tunnels, which are essentially interference free, are well suited to confirm or reject the above conclusions. For this reason we have depicted in Figure 8 for a (nominal) Mach number of $M_\infty = 0.765$ maximum lift for the various model-wind-tunnel configurations, including the adaptive wall tunnels TCT and T2, as function of the Reynolds number. Considering only the gradient of the maximum lift curves which is a measure of the viscous effects on wall interference (here essentially blockage interference), one observes that there is a large deviation from the "interference free" gradient in case of the perforated wind tunnels TWG and CFWT, but only minor discrepancies for the slotted TCT, independent of model size. (The large deviation in the level of max. lift between the facilities considered is, of course, also an influence mainly of blockage interference.)

For a better comparison of the gradients of the maximum-lift curves, these curves were shifted parallel to intersect the interference free results at a Reynolds number of $Re = 4 \times 10^6$, Figure 9. Clearly indicated is the considerably stronger Reynolds number dependence of the perforated tunnels TWG and CFWT and the slotted tunnel TWB compared to the interference free results. The larger gradients in the Reynolds number dependence confirm the conclusion of [3], namely that the diminishing viscous effects with increasing Reynolds number raise the effective open area ratio of the walls thus reducing the effective freestream Mach number which results, in turn, in higher maximum lift. The slotted-TCT results are fairly close to the interference free data, exhibit, however somewhat lower gradients in the Reynolds number dependence. This means that the open area ratio reduces slightly with Reynolds number which might be due to the special design of the TCT slots. Still, the lower sensitivity of the characteristics of slotted walls to viscous changes is indicated by both the TWB and TCT results thus confirming the earlier conclusion.

It was shown in [3] that there also existed differences in the dependence of the drag-rise Mach number on Reynolds number between the various model-wind-tunnel systems considered, Fig. 12 of [3]; these differences have the same cause, namely the influence of the Reynolds number on wall characteristics. Determining the maximum lift at the drag-rise Mach number and plotting this parameter as function of the Reynolds number should, it was postulated, therefore lead to the correct maximum

lift dependence on viscous effects. Comparing the latter results with the interference free data in Figure 10 indicates that this approach comes close to reality with only minor disagreement in gradient and level of the Reynolds number dependence. Nevertheless, the conclusions of [3] are essentially confirmed.

Conclusions

A comparison of results from conventional and adaptive wall wind tunnels with regard to Reynolds number effects has been carried out. The special objective of this comparison was to confirm or reject earlier conclusions, solely based on conventional wind tunnel results, concerning the influence of viscous effects on the characteristics of partially open wind tunnel walls, hence wall interference. The following postulations could be confirmed:

- Certain classes of supercritical airfoils exhibit a non-linear increase in lift which is, at least in part, related to viscous-inviscid interactions on the airfoil. This non-linear lift characteristic can erroneously be suppressed by sidewall interference effects in addition to being affected by changes in Reynolds number. Adaptive walls seem to relieve the influence of sidewall interference.
- The degree of (horizontal) wall interference effects can be significantly affected by changes in Reynolds number, thus appearing as "true" Reynolds number effects.
- Perforated wall characteristics seem much more susceptible to viscous changes than the characteristics of slotted walls; here, blockage interference may be most severely influenced by viscous changes.
- "Real" Reynolds number effects are present on the CAST 10-2/DOA2 airfoil; they have been shown to be appreciable also by the adaptive wall wind tunnel tests.

References

[1] Stanewsky, E. and Zimmer, H., "Development and wind tunnel test of three supercritical airfoils for transport aircraft", Z. Flugwiss. 23 (1975), Heft 7/8, pp. 246-256.

[2] Stanewsky, E., "Interaction between the outer inviscid flow and the boundary layer on transonic airfoils", Z. Flugwiss. Weltraumforsch. 7 (1983), Heft 4, pp. 242-252 (also see Ph. D. Thesis, Technical University Berlin (D83), 1981).

[3] Stanewsky, E., Demurie, F., Ray, E.J. and Johnson, C.B., "High Reynolds number tests of the CAST-10-2/DOA 2 transonic airfoil at ambient and cryogenic temperature conditions", AGARD-CP-348, 1983, pp. 10-1 to 10-13 (see page 47 in this CP).

[4] Ganzer, U., Stanewsky, E. and Ziemann, J., "Sidewall effects on airfoil tests", AIAA Journal, Vol. 22, No. 2, Feb. 1984, pp. 297-299.

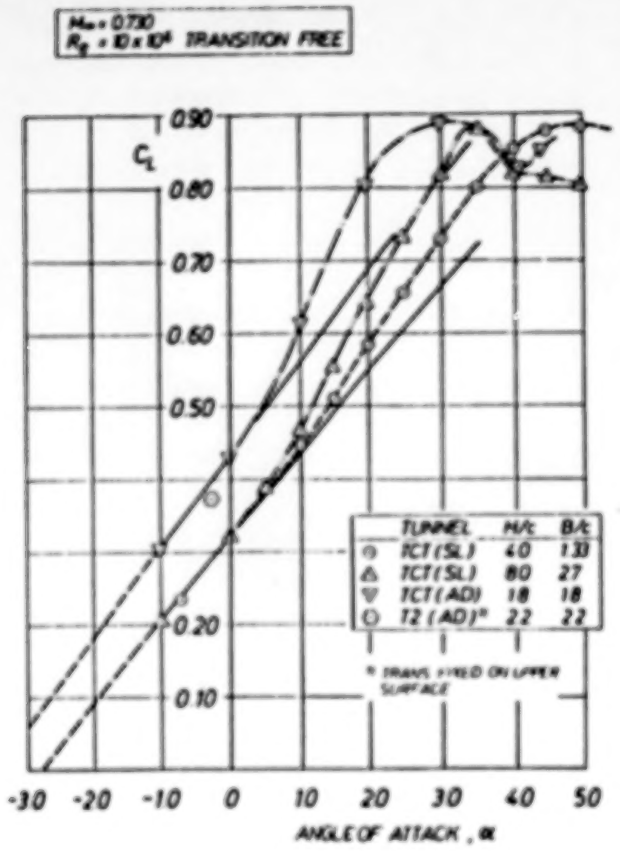

Figure 1: Lift curves obtained in conventional and adaptive wall wind tunnels

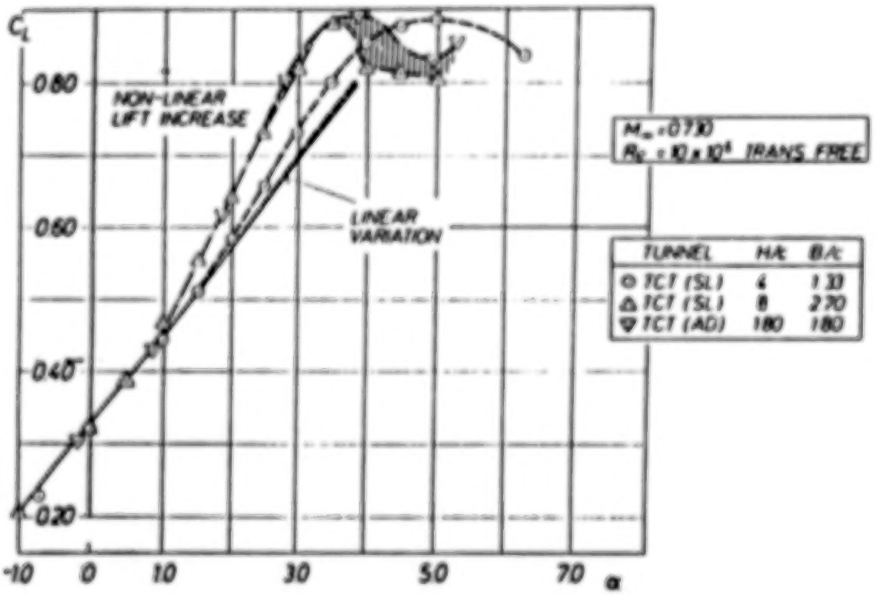

Figure 2: Lift curves of Fig. 1 shifted to match in the lower incidence range

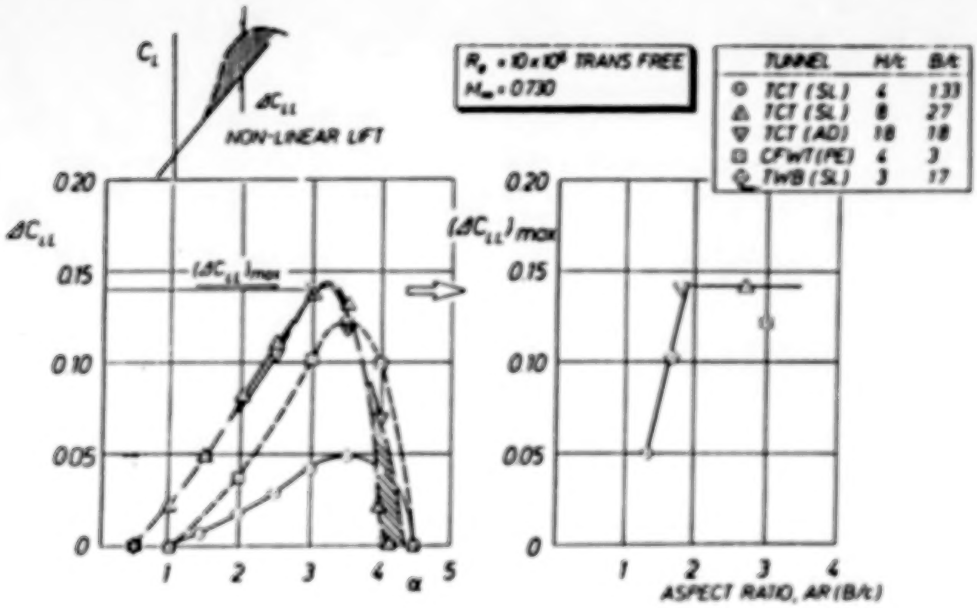

Figure 3: Effect of aspect ratio on the deviation from lift linearity

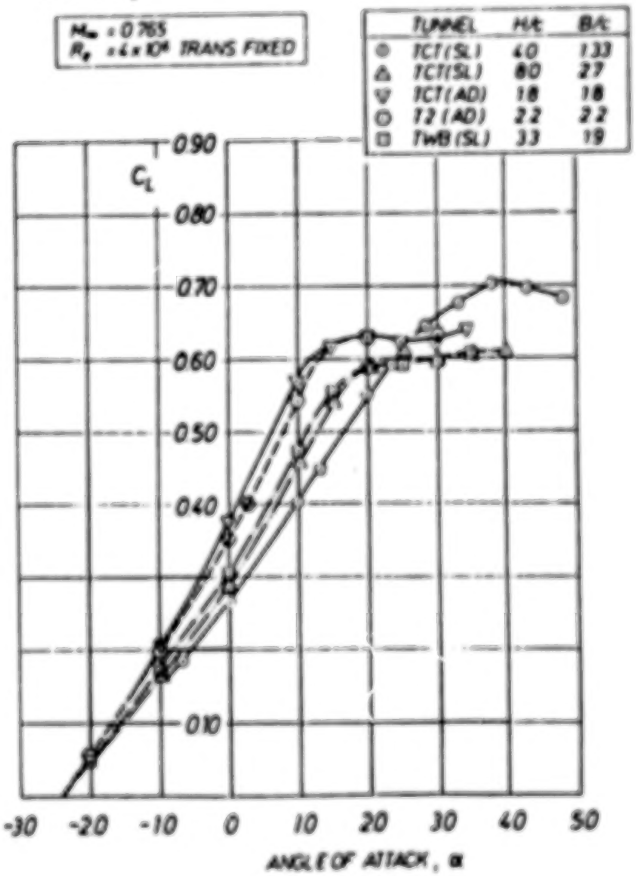

Figure 4: Lift curves for various model-wind-tunnel configurations

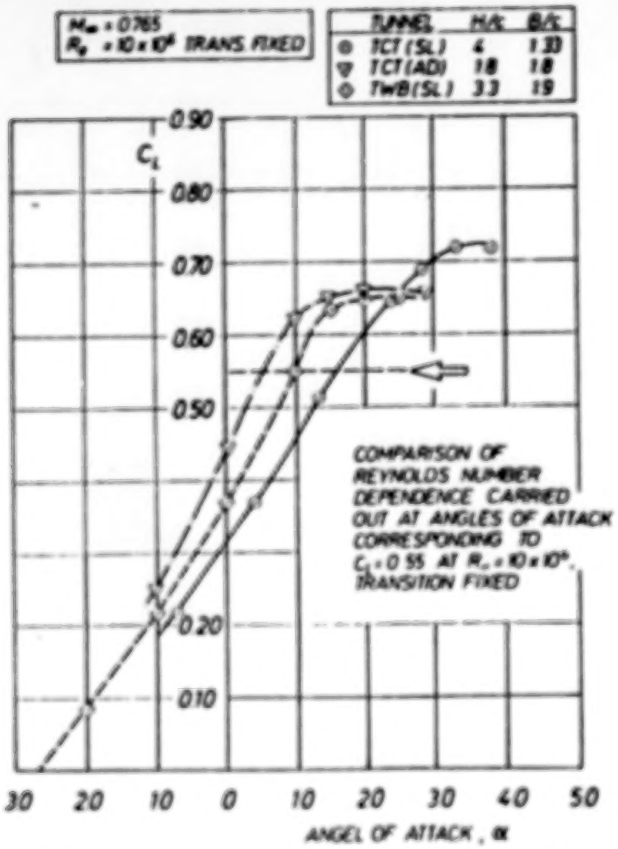
M∞ = 0.765
R_e = 10 x 10^6 TRANS FIXED
TUNNEL H/c B/c
TCT (SL) 4 1.33
TCT (AD) 1.8 1.8
TWB (SL) 3.3 1.9
C_L
0.90
0.80
0.70
0.60
0.50
0.20
0.10
COMPARISON OF REYNOLDS NUMBER DEPENDENCE CARRIED OUT AT ANGLES OF ATTACK CORRESPONDING TO C_L = 0.55 AT R_e = 10 x 10^6, TRANSITION FIXED
30 20 10 0 10 20 30 40 50
ANGEL OF ATTACK, α

Figure 5: Selection of angles of attack to determine the Reynolds number dependence of lift for the various model-wind-tunnel systems

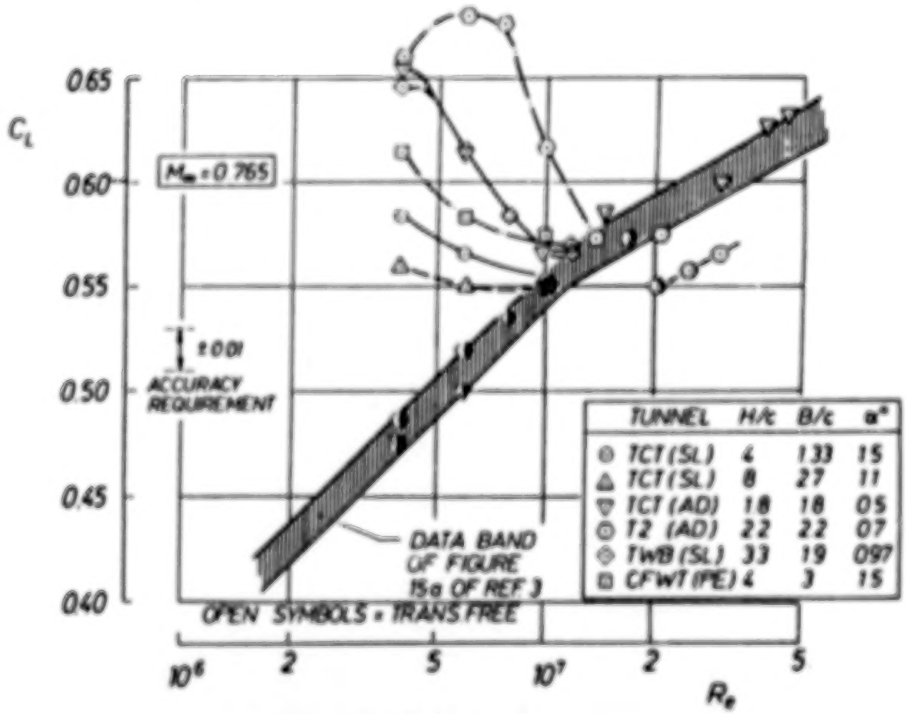

Figure 6: Effect of Reynolds number on lift

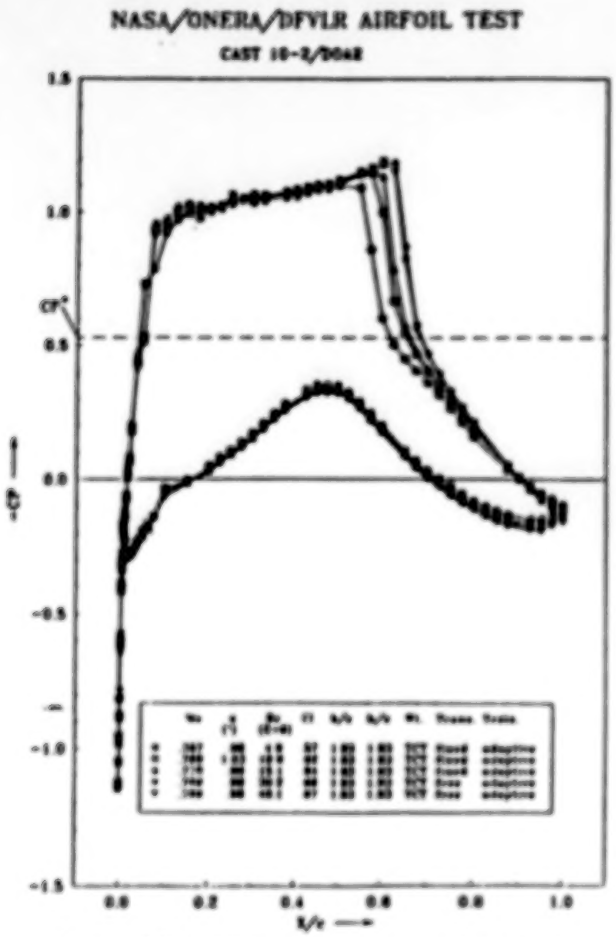

Figure 7: Reynolds number effect on the pressure distribution, adaptive TCT tests

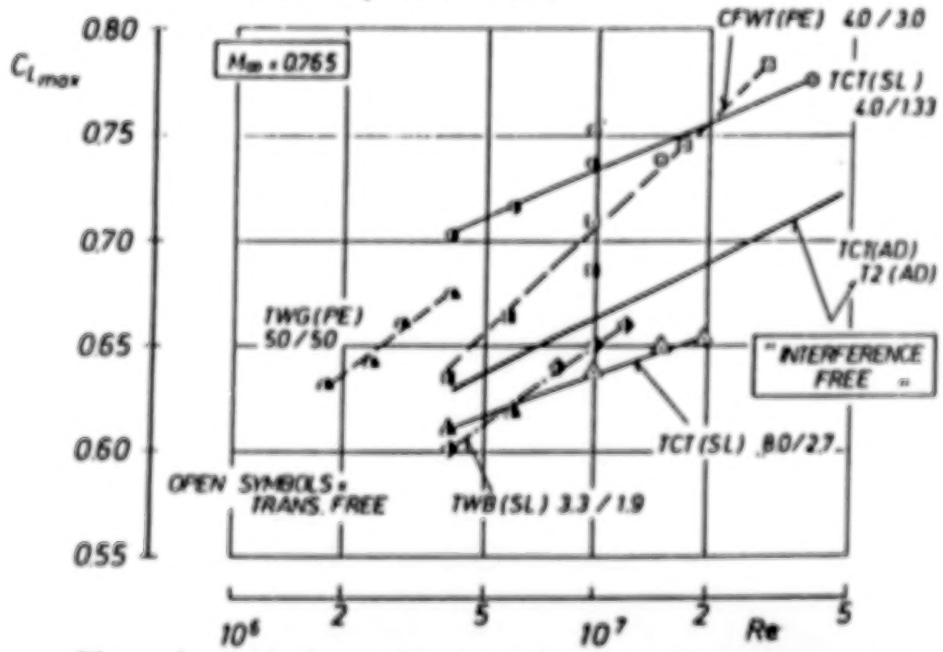

Figure 8: Maximum-lift dependence on Reynolds number for conventional and adaptive wall wind tunnels

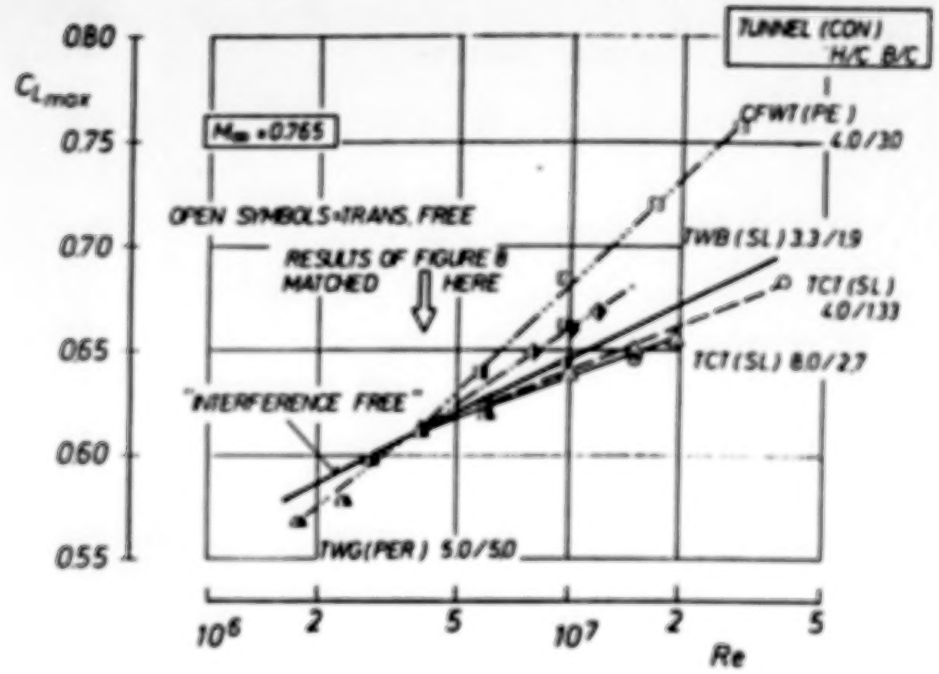

Figure 9: Maximum lift versus Reynolds number: Data of Fig. 8 shifted parallel to intersect interference free results at $Re = 4 \times 10^6$

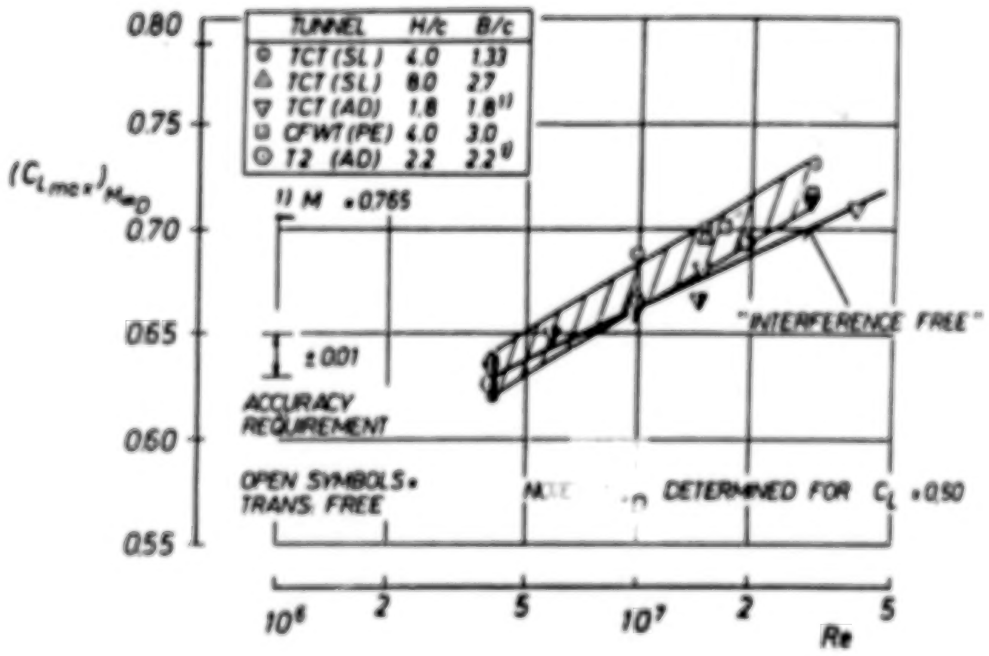

Figure 10: Effect of Reynolds number on the maximum lift at drag rise

HIGH REYNOLDS NUMBER TESTS OF THE CAST-10-2/DOA 2 TRANSONIC AIRFOIL AT AMBIENT AND CRYOGENIC TEMPERATURE CONDITIONS *

B. Stanewsky and F. Deneurie
Deutsche Forschungs- und Versuchsanstalt für Luft- und Raumfahrt e.V.
Institut für Experimentelle Strömungsmechanik
Göttingen, FRG

and

E.J. Ray and C.B. Johnson
National Aeronautics and Space Administration
Langley Research Center, Hampton, Va 23665

*Paper reprinted from AGARD Conference Proceedings No. 348.

SUMMARY

The transonic airfoil CAST 10-2/DOA2 was investigated in several major transonic wind tunnels at Reynolds numbers ranging from Re=1.3 x 10^6 to 45 x 10^6 at ambient and cryogenic temperature conditions. The main objective was to study the degree and extent of the effects of Reynolds number on both the airfoil aerodynamic characteristics and the interference effects of various model-wind-tunnel systems. The initial analysis of the CAST 10-2 airfoil results has revealed appreciable "real" Reynolds number effects on this airfoil and, moreover, shown that wall interference can be significantly affected by changes in Reynolds number thus appearing as "true" Reynolds number effects.

LIST OF SYMBOLS

AR	aspect ratio, B/c
B	tunnel width (model span)
c	airfoil chord
C_D	drag coefficient
C_L	lift coefficient
δC_{LL}	deviation from linear lift curve slope
δC_{DL}	spanwise drag variation, $C_{DB/2}-C_{DB/4}$
c_p	pressure coefficient, $(p-p_\infty)/q_\infty$
H	tunnel height
M_∞	freestream Mach number
$M_{\infty C}$	corrected freestream Mach number
$M_{\infty D}$	drag-rise Mach number
p	static pressure
q	dynamic pressure
Re	Reynolds number based on freestream conditions and chord
T_g	transonic sensitivity parameter (FIG.1)
x, y, z	Cartesian coordinates (x in chordwise direction)
α	angle of attack

Subscripts

∞	freestream conditions

Abbreviations

SL	slotted
PE	perforated
BLC	boundary layer control
Cts	Counts

I INTRODUCTION

The CAST 10-2/DOA2 airfoil, designed by Dornier, has been shown in previous tests to be extremely sensitive to changes in the initial boundary layer conditions. The high sensitivity of this airfoil compared to other contemporary supercritical type airfoils is demonstrated in FIG.1 where the change in lift with changing transition point location is plotted against the transonic similarity parameter T_g derived in REF.1. Due to this unusual sensitivity, the CAST 10-2 airfoil was selected by the DFVLR and NASA for a cooperative study to consider the following objectives:

- Assessment of the degree and extent of the effects of Reynolds number on both the aerodynamic characteristics of the airfoil and the interference effects of various model-wind-tunnel systems.
- Correlation of the results obtained in the Langley 0.3-m Transonic Cryogenic Tunnel (TCT) with results from other major facilities.
- Evaluation of current analytical and experimental techniques to account for wall interference effects over a wide range of Reynolds numbers.

Since the evaluation of analytical and experimental correction techniques has not yet progressed sufficiently, we will concentrate here on the first two objectives. This paper must, furthermore, be considered as an interim report since the data analysis as well as the experimental program are continuing.

II EXPERIMENTS

The CAST 10-2 airfoil and characteristic airfoil related data are presented in FIG. 2. Further information concerning the airfoil, including design procedures, is given in REF. 2. As shown in TABLE 1, CAST 10-2 airfoil models have been tested in the DFVLR Transonic Wind Tunnel Göttingen (TKG) [3], the DFVLR Transonic Wind Tunnel Braunschweig (TWB) [4], the Lockheed Georgia Compressible Flow Wind Tunnel (CFWT) [5] and the NASA Langley 0.3-m Transonic Cryogenic Tunnel (TCT) [6]. The matrices of model-wind-tunnel system parameters and test conditions considered in the program have been extensive and have included tunnel-height to model-chord ratios ranging from 4 to 8, tunnel-width to model-chord ratios between 1.3 and 5 and slotted and perforated test section walls. In the 0.3-m TCT phase of the studies, two models with chord lengths of 152.4 and 76.2 mm were tested with and without boundary layer control[1] to enable a determination of wall interference effects in the same tunnel as well as by comparisons with results obtained in other test facilities. The study included tests at subsonic and transonic velocities over a large angle-of-attack range. Note, that the overall scope of the study has recently been expanded to include a cooperative effort with the ONERA to test a CAST 10-2 airfoil model provided by that institution in the ONERA T2 and the NASA 0.3-m TCT Cryogenic Self-Streamlining Wall Facilities.

FIG. 3 illustrates the broad two-dimensional Reynolds number and Mach number envelopes provided by the test facilities utilized during the present CAST 10-2 studies. Traditionally, the transport aircraft design trend, shown by the solid curve, has established the upper requirements for airfoil testing. In recent years there has been a dramatic increase in these requirements as illustrated by the design conditions shown for current transport aircraft such as the Airbus and the Boeing 747 and the cargo aircraft envisioned for the not too distant future. As can be seen from FIG. 3, the two-dimensional 0.3-m TCT provides an adequate Reynolds number and Mach number capability to simulate the design flight conditions for current transport aircraft and will provide an even higher Reynolds number capability for the forthcoming CAST 10-2 self-streamlining wall tests.

Both the model-wind-tunnel system and test condition variables considered in the present program have been very extensive. Some of the major effects of these variables will be addressed in the following sections of this paper.

III ANALYSIS OF EXPERIMENTAL RESULTS

The wind-tunnel results obtained with the CAST 10-2 airfoil models have shown some rather surprising and unexpected characteristics. For instance, the extreme sensitivity of the airfoil to tunnel wall effects and, as mentioned in the introduction, the effects due to viscous-inviscid interactions on the airfoil is manifested in what might be considered to be an unusual variation of lift with angle-of-attack at supercritical Mach number conditions. This behavior is illustrated qualitatively in FIG. 4 which shows at the left the typical effects of model-tunnel systems on the variations of lift with incidence at a given Reynolds number. In general, the supercritical lift behavior is here characterized by a low angle-of-attack linear lift variation which is well understood and correctable by approaches suggested, for instance, in REF. 7 and 8. The linear lift region, however, is followed by non-linear lift and flow break-down regions which are highly susceptible to both Reynolds number effects and the complicated effects of the integrated model-wind-tunnel system. In addition, since the various model-wind-tunnel arrangements are affected by changes in boundary layer condition as integrated systems, changes in Reynolds number will affect the wall interference characteristics as well as the aerodynamic characteristics of the airfoil.

Non-linear and flow-break-down regions will be examined in more detail to study the combined effects of model-tunnel system and Reynolds number on the (measured) aerodynamic behavior of the airfoil. Essentially "pure" Reynolds number effects, depicted on the right hand side of this figure, will then be considered at conditions believed to be virtually unaffected by wall interference.

---

[1] BLC on the sidewalls upstream of the model

COMBINED WALL INTERFERENCE AND REYNOLDS NUMBER EFFECTS

Non-linear lift

Let us first examine in more detail the relationship between the non-linear lift region and the sidewall interference effects of several model-wind-tunnel systems. In FIG. 5 lift has been plotted against angle-of-attack for three different model-wind-tunnel configurations. Lift results are shown for the 152 mm chord airfoil and the 76 mm airfoil in the 0.3-m TCT and for a CAST 10-2 model in the Lockheed CFWT facility. For this case, the models were tested at a supercritical Mach number of 0.73 at a Reynolds number of Re = 10 x 10^6, transition free. The studies have indicated that at this Reynolds number the boundary layer is basically turbulent with a relatively stable transition point located near the leading edge of the airfoils.

It will be noted that there is only a small deviation from a linear lift variation for the large chord TCT model, denoted by circular symbols. This lift behavior might be considered to be normal and expected; however, the small chord TCT and the CFWT airfoils with the substantially higher aspect ratios, i.e. tunnel-breadth to model-chord ratios, show a very pronounced non-linear increase in lift. This comparison suggests that in the case of the large chord, small aspect ratio TCT model, the tunnel sidewall interference effects suppress the non-linear lift increase. This is supported by the spanwise drag distributions which clearly demonstrate the degree of three-dimensional effects due to the interaction with the sidewall boundary layer. The small insert figures indicate the drag levels measured with a "spanwise" wake rake located downstream of the model. The values were measured at stations extending from slightly beyond the centerline of the tunnel to the tunnel sidewall. In the low incidence case, when the lift variation is fairly linear for all of the airfoils, there are only small drag variations across the span of the tunnel. At the higher angles-of-attack, in the area of appreciable divergence in the linear lift behavior large spanwise variations in drag were shown for the large chord TCT model, while the spanwise variation in drag for the small chord TCT airfoil is still quite small. The large drag decreases noted for the large chord model midway between the tunnel wall and centerline are believed to be caused by compression waves originating from the separated sidewall boundary layer which locally reduce the shock losses on the airfoil. The increase in drag shown near the wall of the tunnel suggests that at this condition the separated boundary layer region extends to a point beyond the pitot probe nearest to the wall. Although not as extensive, a similar boundary layer growth process must take place for the smaller model. However, the boundary layer "thickening" process here takes place closer to the wall of the tunnel. Comparing corresponding pressure distributions taken for the two TCT airfoils at low and high lift conditions, respectively, FIG. 6, one notes that the large differences in lift at a given angle-of-attack are mainly caused by differences in the upper surface shock locations and rear pressure distributions. It seems that, while the pressure distribution on the lower surface is not at all affected, the shock on the upper surface is pulled towards the leading edge due to the interaction of the airfoil flow field with the sidewall boundary layer.

FIG. 7 presents on the left a summary of the deviation from linearity determined from the lift results shown in the previous figure. The deviation parameter, ΔC_{LL}, as shown in the small insert sketch, represents the lift increment at a given angle-of-attack between the actual lift and a linear lift slope variation established by the low lift values. It will be noted again that the small chord TCT model and the CFWT model having about the same aspect ratio, but different tunnel-height to model-chord ratios display about the same maximum deviation from linearity. The onset of the divergence from linearity, i.e., the incidence for incipient divergence, however, is different for these two model-wind-tunnel system, while there is close agreement in the incidence for the onset of non-linear lift between the CFWT and the large chord TCT airfoils which have about the same tunnel-height to model-chord ratios. These results suggest that, while the magnitude of the non-linear lift variation is primarily influenced by aspect ratio, the onset of the divergence is dependent on tunnel-height to model-chord ratio and the associated degree of lift-interference effects. The filled triangular symbols reflect data obtained with the small chord TCT model while applying sidewall boundary layer suction amounting to 2% of the tunnel mass flow. The increase in the non-linear lift value, although small, supports the premise that the three-dimensional effects caused by the interaction of the model flow field with the sidewall boundary layer influence the overall flow development of the model-tunnel system in this range of lift coefficients. Results concerning sidewall BLC in the 0.3-m TCT have been reported in REF.9 for the NASA SC(3)0712 supercritical airfoil. Documentation of the CAST 10-2 sidewall BLC study is in progress.

At the right of this figure the maximum non-linear lift parameters, $(\Delta C_{LL})_{max}$, determined at M_∞ = 0.765 and Re = 10 x 10^6 are plotted as a function of model aspect ratio, AR (B/c). One data point, the diamond symbol, has been added here to indicate results obtained with a 1.7 aspect ratio airfoil in the DFVLR Transonic Wind Tunnel Braunschweig (TWB). If it is assumed that the maximum deviation from linearity parameter provides an indication of the extent of three-dimensional wall effects, these results suggest a leveling off of wall effects for aspect ratios above about 2.0. This value in aspect ratio is in close agreement with the conclusion from other investigations [7].

In the preceding discussion we addressed some of the major effects of the model-wind-tunnel system on wall interference effects at a given Reynolds number. Let us now turn briefly to the related subject and examine the effects of Reynolds number on (a) the actual airfoil aerodynamic characteristics associated with the non-linear lift behavior, and (b) the degree of the sidewall interference effects on the model flow field. The variation of the maximum non-linear lift-parameter, $(\delta C_{L_1})_{max}$, with Reynolds number has been selected to illustrate these effects. In FIG. 8 data are shown for the two TCT airfoils and the CFWT model at a constant Mach number over a Reynolds number range varying from about 4 to 30 million. Note, that the data shown for the Re = 4 x 10^6 case were selected from fixed transition results to avoid any erroneous conclusion due to "unstable" shifts in the point of boundary layer transition.

A review of these results indicates that for all three model-tunnel systems the maximum non-linear lift parameter is reduced with increasing Reynolds number. This trend suggests that the non-linearity is, at least in part, influenced by the viscous-inviscid interaction on the airfoil. In addition to starting at a much lower value of non-linear lift, the Reynolds number dependence for the low aspect ratio (B/c = 1.33) model-tunnel system, shown by the circular symbols, is appreciably less than for the higher aspect ratio model-tunnel configuration. This example provides a good illustration as to how pure Reynolds number effects can be obscured by the complex interaction between the model flow field and the boundary layer development on the test section sidewalls.

The attention given thus far to the non-linear lift characteristic of this class of airfoil might be considered to be somewhat academic. However, a thorough understanding of this development, eventually leading to the flow break-down, and its relationship to the effects of the model-tunnel system and Reynolds number is essential in the overall assessment of actual airfoil performance at the simulated flight equivalent conditions.

Let us consider a second example: When the Reynolds number is increased, the boundary layer developing on the sidewalls will become thinner if left "undisturbed". It might be expected then that shock induced sidewall boundary layer separation would be delayed for the "thinner" boundary layers at the higher Reynolds number thereby decreasing the resulting three-dimensional effects.

In FIG. 9 we have illustrated the effects of Reynolds number on the spanwise drag variation parameter, δC_{D_1}, for the large and the small TCT models. The spanwise drag parameter is defined in the insert sketch, represents the difference between the drag levels measured at the tunnel centerline and a station midway between the centerline and the tunnel sidewall. As shown here, the drag variation across the tunnel at low angles-of-attack, prior to the onset of any significant non-linear lift effects, is small and virtually independent of model-tunnel system and Reynolds number effects. At an angle-of-attack of 3.5 degrees, however, at a condition which is well into the range of non-linear lift effects, there is not only the noticeable influence of the aspect ratio, but also a somewhat unexpected increase in spanwise drag variation with increasing Reynolds number. The latter may be related to the downstream movement of the airfoil upper surface shock and the increased shock strength at the higher Reynolds number. This illustration cites an example where the thinner sidewall boundary layer, at conditions which might be expected to be more stable and resistant to disturbance, may actually increase three-dimensional effects by promoting a more severe interaction between the tunnel sidewall and the airfoil flow field.

Maximum lift and drag rise

We have discussed in some detail the complex relationship between the aerodynamic behavior of the airfoil and the sidewalls of the model-tunnel system. In order to provide additional understanding regarding the related effects of model-tunnel systems and Reynolds number, let us now examine other characteristics, such as maximum lift and the drag divergence Mach number, which may be strongly influenced by the effects of the floor and ceiling of the test section.

At the left of FIG. 10, the maximum lift coefficient, $C_{L_{max}}$, is plotted as a function of Mach number for the large and small chord TCT models and the Lockheed CFWT model at a Reynolds number of 10 million. It will be noted that there is a pronounced difference in the maximum lift values, particularly at the higher Mach numbers. These results suggest that there is a significant difference in the effective freestream Mach numbers for the various model-tunnel configurations considered.

This is confirmed by the results at the right of the figure where the drag coefficients determined at C_L = 0.50 and a Reynolds number of 10 million are plotted as a function of Mach number for the same three model-tunnel systems. There is a pronounced difference in the drag-rise Mach numbers between the TCT H/c = 4 and H/c = 8 configurations while there is a closer agreement between the TCT and CFWT H/c = 4 results. This suggests that there is a prevailing influence of the tunnel-height to model-chord ratio on the aerodynamic characteristics considered here. That the causes for the differences in maximum lift and the drag-rise Mach number are of the same origin is substantiated by empirically correcting the Mach numbers for maximum lift at constant maximum lift by the difference in drag-rise Mach number relative to the small-chord TCT model. This correction results in a surprisingly good correlation in the maximum lift results shown in the left figure by the half-filled symbols. However, it must be noted that at higher lift coefficients this empirical procedure gives less satisfying, although qualitatively correct, results.

Having reviewed examples of the primary effects of wind-tunnel walls on the maximum lift and drag rise characteristics, let us now consider the effects of Reynolds number on the same parameters. In FIG. 11 the maximum lift determined at a Mach number of 0.765 is plotted as a function of Reynolds number for the same model-tunnel systems just discussed. In addition results are shown at relatively low Reynolds numbers which were obtained in the DFVLR-TKG facility. The open symbols indicate transition free results, the half closed symbols show transition fixed data. The comparison again vividly demonstrates the dominant influence of the model-wind-tunnel system on the maximum lift parameter with the small height-to-chord ratio airfoils displaying the highest values of maximum lift. All of the model-tunnel configurations exhibit an increase in maximum lift with increasing Reynolds number up to the highest conditions investigated. However, there is an interesting difference in the rate of increase with Reynolds number between the various model-tunnel set-ups. The two models in the slotted TCT display a similar gradient; the results obtained in the perforated CFWT and TKG tunnels are similar to each other but reflect a higher rate of change with Reynolds number. Since the free and fixed transition results show about the same dependence on Reynolds number, it is unlikely that differences in the transition fixing devices caused any significant change in the Reynolds number dependence of maximum lift. It can be assured then, that the difference noted in the family of slopes for the slotted and perforated tunnels is due to the effect of Reynolds number on the degree of wall interference effects.

Turning to the second characteristic parameter, FIG. 12 presents the variation of the drag-rise Mach number at C_L = 0.50 with Reynolds number for the two TCT models and the CFWT model. As in the case of the preceding maximum lift example, there is a pronounced difference in the Reynolds number dependence of the drag-rise Mach numbers determined for the TCT models and the CFWT model-tunnel system. For the TCT configurations, a slight decrease in the drag-rise Mach number is exhibited with increasing Reynolds number. An opposing trend is displayed for the CFWT airfoil, which shows a noticeable increase in the drag-rise Mach number with increasing Reynolds number. If it is assumed that the TCT results for these conditions represent the proper Reynolds number dependence, the increase in the drag-rise Mach number would suggest that the effective freestream Mach number in the CFWT decreases with increasing Reynolds number. If this assumption were correct, it would mean that the wind-tunnel walls behave in a more "open" fashion with increasing Reynolds number. This is supported by the previously shown results which indicated a much higher rate of increase in the maximum lift coefficient with Reynolds number for the CFWT model. It will also be noted here that the two TCT systems show about the same Reynolds number dependence even though there is a great difference in the aspect ratios, B/c, which substantiates that the differences in the drag-rise characteristics discussed here are primarily caused by the influence of the floor and ceiling and the associated effects of Reynolds number.

Both, the drag-rise Mach number and the maximum lift coefficients reflect differences due to changes in Mach number which occur as a result of undesirable model-tunnel wall interference effects. The unknown regarding Mach number can be eliminated by combining the drag rise and maximum lift parameters into a new parameter, the maximum lift at drag rise, $(C_{Lmax})_{M=D}$. In FIG. 13 the maximum lift at drag rise parameter is plotted as a function of Reynolds number for the two TCT and the CFWT model-tunnel systems. A review of the results indicates that when the maximum lift and drag rise characteristics are combined in this manner, all three model-tunnel systems exhibit essentially the same degree of dependence on Reynolds number. The slight scatter in the data is within the lift accuracy requirements quoted by an AGARD Conveners Group on "Data Accuracy and Flow Quality Requirements in Wind Tunnels"[10]. These results provide a strong indication that for some wind tunnels, the Reynolds number dependence of certain aerodynamic parameters are, indeed, due in part to the influence of Reynolds number on the wall characteristics. In comparing the results for the TCT and CFWT tests it appears that perforated wall tunnels are much more susceptible to Reynolds number effects than slotted wall tunnels. It must, furthermore, be realized that it is not possible to eliminate this "pseudo" Reynolds number effect by simply calibrating the empty tunnel over the unit Reynolds number range of the facility. The actual flow characteristics of the partially open walls over the desired Reynolds number range must be determined but this represents a very rigorous process and does not always guarantee success. The only feasible way, short of adaptive walls, then seems to be to determine the wall boundary conditions as input to a suitable wall interference correction method. It must be stressed that actual Reynolds number effects on the airfoil flow development can only be determined after the proper elimination of the wall interference effects at all conditions.

"PURE" REYNOLDS NUMBER EFFECTS

The third and final portion of this paper will deal with the interference-free Reynolds number effects on the aerodynamic characteristics of the airfoil. Although the wall interference effects of the various model-tunnel systems cannot be ignored completely, they will only be considered in this portion of the paper to enable an analysis of the interference-free trends in the aerodynamic characteristics.

The angle-of-attack necessary to establish a given lift coefficient provides a good indication of the sensitivity of an airfoil to Reynolds number changes as well as of the difference in lift interference effects between the various model-tunnel systems. In FIG. 14 (a), the angle-of-attack required to produce a lift coefficient of C_L = 0.55 at a Mach number of 0.765 is plotted as a function of Reynolds number for the two TCT and the CFWT models. The transition fixed and the high Reynolds number results show a steady decrease in the incidence for C_L = 0.55 up to the highest Reynolds number investigated. Considering fixed transition, the difference in the incidence angle at Re = 4 x 10^6 between the H/c = 4 airfoils and the H/c = 8 TCT model is 0.5 degrees. This change in

incidence is reduced to about 0.36 degrees at a Reynolds number of Re = 40 x 10^6. The very small change in the incidence angle between these Reynolds number extremes may be related to wall interference effects. However, since this slight difference in angle-of-attack corresponds to a change in lift coefficient of only about 0.025, which is close to the desired lift accuracy requirement of ±0.01 [10], characteristic trends noted here and in the following figures can be considered to represent the "interference-free" Reynolds number effects on the airfoil characteristics. Note, that in the case of low Reynolds number free transition the differences in incidence for C_L = 0.55 between the respective model-tunnel configurations can not be reproduced. This is likely to be due to different transition point locations caused by the various levels of turbulence and model roughness for the different model-tunnel systems.

In FIG. 14 (b), results obtained in the DFVLR TKG and TWB facilities have been added to the angle-of-attack for constant lift results shown in the preceding figure. The TCT and CFWT turbulent boundary layer trends have been summarized here and are indicated by two lines. Both, the TKG and TWB results exhibit essentially the same trends in Reynolds number dependence as was determined in the TCT and CFWT facilities. It is clearly indicated by the large incidences shown for the TKG facility that the 6-percent open, perforated test section [4] is much too open for interference free testing. The TWB with a tunnel-height to model-chord ratio of only 3 produces results which are close to the results shown for the H/c = 8 TCT system. The TWB facility has slotted walls with an open area ratio of about 2.4 percent which have been optimized for zero blockage [5]. The TWB results suggest that the wall interference effects can be significantly reduced by properly ventilating the tunnel walls even in situations where the tunnel-height to model-chord ratios might be considered unacceptably low.

Following the preceding discussion, FIG. 15 (a) then summarizes the "pure" effects of Reynolds number at a Mach number of 0.765 on lift at a given angle-of-attack for five different CAST 10-2 model-tunnel systems. The incidence angles, shown in the key for each model-tunnel set-up, were selected to provide about the same lift coefficient at Re = 10 x 10^6, transition fixed. When this procedure was followed, all of the transition fixed results fell within a relatively narrow band which corresponds to an accuracy in lift coefficient of about ± 0.01. With turbulent boundary layer conditions, i.e., either fixed transition or free transition at Re > 10 x 10^6, the lift coefficients increase throughout the entire Reynolds number range extending from about 1.9 to 40 million. The total change in lift between these Reynolds number extremes is significant and amounts to an increment in C_L of about 0.20 or 33 percent of the lift value at Re = 40 x 10^6. This rather dramatic increase in lift is believed to be due to changes in the initial displacement thickness (fluid shape of the airfoil) with increasing Reynolds number and the resulting condition of the flow leaving the trailing edge of the airfoil [1]. This assumed effect is further demonstrated by the lift behavior of the transition free results determined at the lower test Reynolds numbers. The transition point is initially far "downstream" resulting in a thin boundary layer and a correspondingly high lift coefficient. As the Reynolds number is increased, the transition point moves forward on the airfoil increasing the displacement thickness and, in turn, reducing the lift coefficient. This progression continues and slowly diminishes with increasing Reynolds number until the point of transition has reached a stable, nearly fixed position, close to the leading edge of the airfoil. The large differences in the low Reynolds number transition free results indicate a high susceptibility of the flow development to characteristics associated with the various model-tunnel systems such as wind tunnel noise, turbulence and model roughness.

This summary suggests that it would be difficult to extrapolate the free transition results for this airfoil to full-scale conditions even if data were available up to a Reynolds number of Re = 30 x 10^6. In the case of the fixed transition results where the progression of lift with Reynolds number is more systematic, an extrapolation from low to high Reynolds numbers seems possible; however, before reaching a general conclusion let us examine first the next figure.

FIG. 15 (b) illustrates the dependence of lift on Reynolds number for a second set of test conditions. Here, lift results are shown for the H/c = 4 TCT and CFWT model-tunnel systems at a Mach number of 0.75 and an angle-of-attack of $\alpha \approx 3$ degrees. The lift behavior at the lower Reynolds numbers is very similar to the results shown in the preceding figure; however, at Reynolds numbers between 10 and 20 million a reversal occurs in the Reynolds number dependency. It is obvious from this illustration that an extrapolation of low Reynolds number results to flight conditions would be impossible. This reversal, as revealed by the pressure distributions of FIG. 16, is caused by an "irregular" behavior of the upper surface shock which either ceases to move downstream or shifts upstream with increasing Reynolds number, FIG. 16 b and 16 c. The phenomenon is not yet completely understood, although some indication might be obtained from the CFWT results. Since the trailing edge pressure continues to increase with Reynolds number, it appears that here the local effects due to a reduction in displacement thickness override the global effects associated with changes in the flow conditions at the trailing edge of the airfoil. It is worthwhile noting that both of the H/c = 4 TCT and CFWT model-tunnel systems reflect this type of lift dependence on Reynolds number.

Airfoil performance is always a subject of major interest to the aerodynamicist. This presentation therefore will be concluded with what is considered to be the interference free variation of the well known aerodynamic range parameter $(C_L/C_D \cdot M_\infty)_{max}$ with Reynolds number, the latter extending here from ambient wind tunnel to flight equivalent conditions for large transport class aircraft, FIG. 17. Since this particular performance parameter is highly dependent upon the drag levels near the drag-rise Mach number, the empirical Mach number correction discussed earlier in this paper has been applied to the results for the three larger, i.e., H/c = 4 and 5, airfoil models. The adjusted results for the four model-tunnel systems exhibit a good agreement in the variation of the range parameter with Reynolds number. It is also interesting to note the surprisingly large variation in performance over the Reynolds number range of the tests which amounts to an increase in the range parameter of about 45 percent based on the value at $Re = 40 \times 10^6$. Here again, these results clearly indicate the difficulty in extrapolating performance data based on low Reynolds number characteristics.

It will be noted that there is a slight decrease in the range parameter at Reynolds numbers between 30 and 40 million which is due to a drag increase in this Reynolds number range. The exact reason for this drag increase has not yet been established, but it does serve to illustrate the importance of testing at, and possibly slightly beyond, the design and off-design flight equivalent conditions. The ability to test at the high Reynolds number conditions, furthermore, enables experimental studies of complex basic phenomena, such as for instance shock boundary layer interactions, which cannot be modeled accurately with current theroretical methods.

IV CONCLUSIONS

An extensive study has been made of the CAST 10-2/DOA2 transonic airfoil in both ambient temperature and advanced cryogenic temperature wind tunnels at transonic Mach numbers over a large range of Reynolds numbers including flight equivalent conditions. The initial analysis of the extensive CAST 10-2 airfoil results has led to the following conclusions:

1. Certain classes of supercritical airfoils may exhibit a non-linear increase in lift which is at least in part related to viscous-inviscid interactions on the airfoil. This non-linear lift characteristic can be erroneously suppressed by wall interference effects in addition to being affected by changes in Reynolds number.

2. Wind tunnel wall interference effects can be severe and completely overshadow a determination of the actual airfoil aerodynamic characteristics. Moreover, the degree of wall interference effects can be significantly affected by changes in Reynolds number, thus appearing as "true" Reynolds number effects.

3. Two-dimensional airfoil models and wind tunnels must be considered as a complete and totally integrated system for which all boundary conditions must be obtained. This approach can enable the separation of the complex and interrelated effects of the tunnel walls and the actual aerodynamic characteristics of the airfoil.

4. "Real" Reynolds number effects on the CAST 10-2 airfoils have been determined and have been shown to be very appreciable. For instance, near the airfoil design condition, a 45 percent increase in the aerodynamic range parameter was observed when the Reynolds number was increased from 2 to 40 million.

5. For certain classes of airfoils, an accurate extrapolation of low Reynolds number results to flight equivalent conditions seems not possible, making at least research facilities operating beyond flight equivalent Reynolds numbers necessary.

The CAST 10-2 high Reynolds number results have provided new insight into the aerodynamic behavior of this class of airfoils and have provided a valuable aid in the analysis of wall interference and Reynolds number effects. There are still many questions left unanswered; however, the analysis of the data is continuing and the forthcoming tests in cooperation between NASA, ONERA and DFVLR in advanced adaptive wall facilities will provide additional knowledge regarding the complex problems associated with wall interference and "true" Reynolds number effects.

REFERENCES

1. Stanewsky, E., "Interaction between the outer inviscid flow and the boundary layer on transonic airfoils", Z. Flugwiss. Weltraumforsch. 7 (1983), Heft 4, pp. 242 - 252

2. Stanewsky, E. and Zimmer, H., "Development and wind tunnel test of three supercritical airfoils for transport aircraft", Z. Flugwiss. 23 (1975), Heft 7/8, pp. 246 - 256

3. Hottner, Th. and Lorenz-Meyer, W., "The Transonic Wind Tunnel of the Aerodynamische Versuchsanstalt Göttingen", DGLR-Jahrbuch 1968, pp. 235 - 244

4. Stanewsky, E., Puffert-Meissner, W., Müller, R. and Hoheisel, H., "The Transonic Wind Tunnel Braunschweig of the DFVLR", Z. Flugwiss.Weltraumforsch. 6 (1982), Heft 6, pp. 398 - 408

5. Pounds, G.A. and Stanewsky, E., "The Research Compressible Flow Facility", Lockheed-Georgia Company Report ER-9219, 1967 (also see: Blackwell, J.A.,"Wind tunnel blockage correction for two-dimensional transonic flow", J. Aircraft, Vol.16, No.4, 1979)

6. Ray, E.J., Ladson, C.L., Adcock, J.B., Lawing, P.L. and Hall, R.M., "Review of design and operational characteristics of the 0.3-m Transonic Cryogenic Tunnel", NASA TM-80123, Sept. 1979

7. Elsenaar, A. (Editor), "Two-dimensional transonic testing methods", GARTEur/TP-011, 1983 (Final report of the GARTEur Action Group AD (AG 02))

8. Kemp, W.B., "TWINTAN: A program for transonic wall interference assessment in two-dimensional wind tunnels", NASA TM-81819, May 1980

9. Murthy, A.V., Johnson, C.B., Ray, E.J.,Lawing, P.L. and Thibodeaux, J.J., "Investigation of the effects of upstream sidewall boundary-layer removal on a supercritical airfoil", AIAA 21st Aerospace Sciences Meeting, Reno, Nevada, January 10-13, 1983, Paper No.83-0386

10. Steinle, F. and Stanewsky, E., "Wind tunnel flow quality and data accuracy requirements", AGARD Advisory Report No. 184, Nov. 1982

TABLE 1: CAST 10-2 airfoil studies

TUNNEL	MODEL CHORD (mm)	TUNNEL CHARACTERISTICS				TEST CONDITIONS			
		H/c	B/c	TYPE WALL	POROS. σ %	M_∞	α°	Re x 10^{-6}	TRANSITION
TKG	200	5	5.0	Perf.	6	0.50 ÷ 0.83	-2÷10	1.3÷ 4	Fixed & Free
TWB	200	3	1.7	Slotted	2.4	0.6;0.7;0.76	‖	3÷14	‖
CPWT	178	4	2.9	Perf.	4	0.60 ÷ 0.82	‖	6÷31	‖
0.3-m TCT[1]	152	4	1.33	Slotted	5	0.60 ÷ 0.80	‖	4÷85	‖
0.3-m TCT[1]	76	8	2.66	Slotted	5	‖	‖	4÷20	‖
0.3-m TCT TKG,TWB	ONERA and NASA streamlined wall tests and additional DFVLR tests (1984)								

[1] with/without BLC

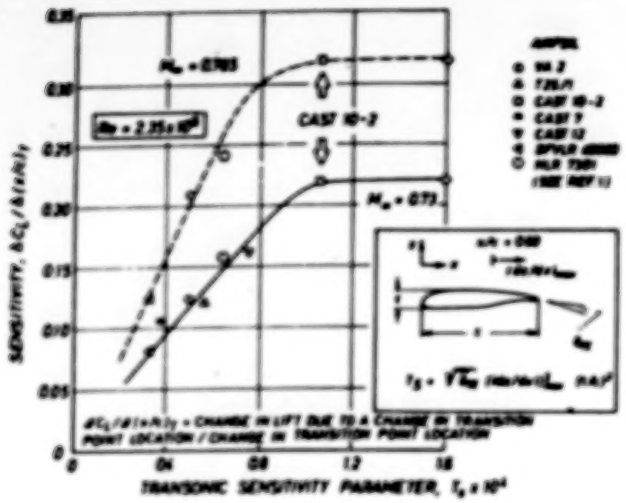

FIGURE 1: Flow sensitivity to changes in the initial boundary layer condition (from REF.1)

FIGURE 2: CAST 10-2/DOA2 characteristics

AIRFOIL CHARACTERISTICS : $t/c = 0.121$ at 45% c
$(t/c)_{TE} = 0.005$

THEORETICAL DESIGN POINT : $M_\infty = 0.76$, $C_L = 0.595$
$\alpha = 0.3°$

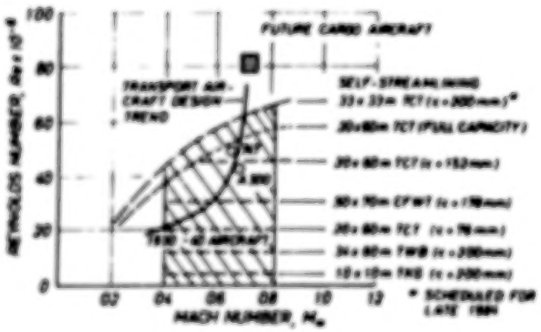

FIGURE 3: CAST 10-2/DOA2 test envelopes

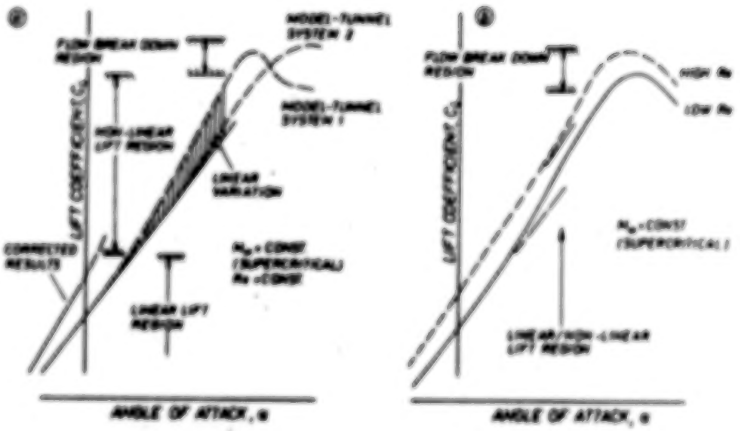

FIGURE 4: Effect of ⓐ model-wind-tunnel system and ⓑ Reynolds number on lift behavior (schematic)

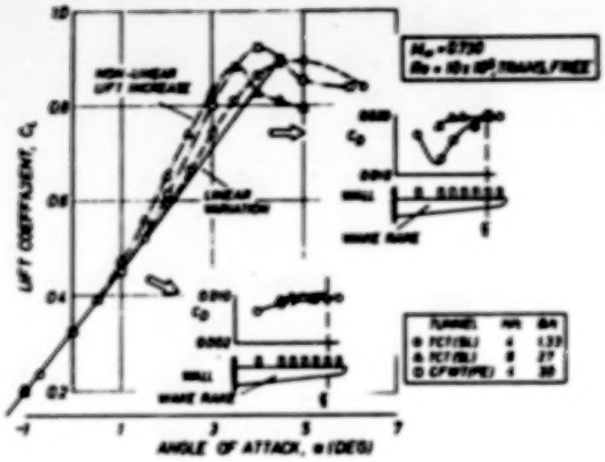

FIGURE 5: Tunnel (side) wall effects on lift increase with angle-of-attack

FIGURE 6: Tunnel (side) wall effects on the chordwise pressure distribution (test cases of FIG.5)

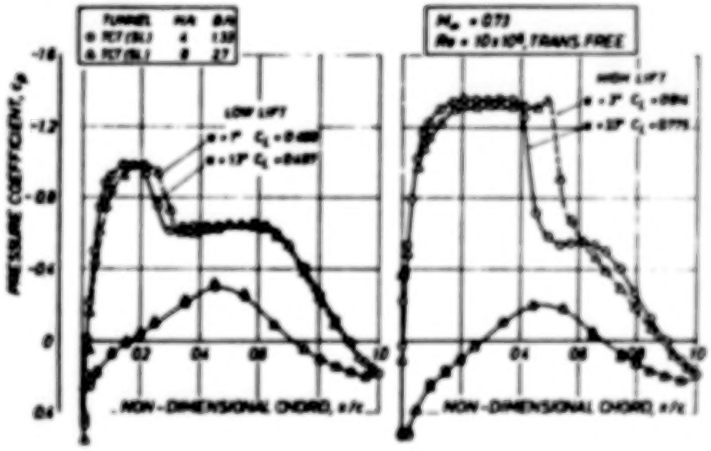

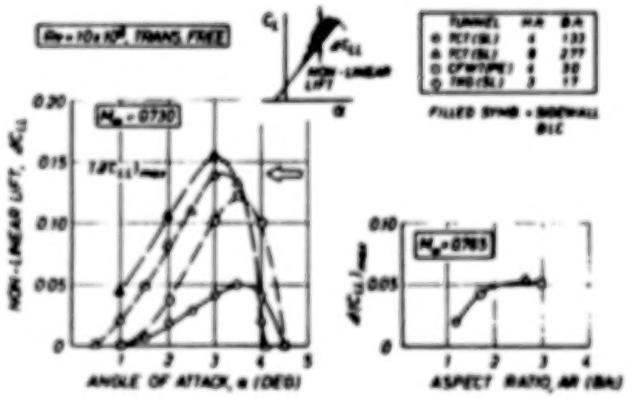

FIGURE 7: Effect of aspect ratio on the deviation from lift linearity

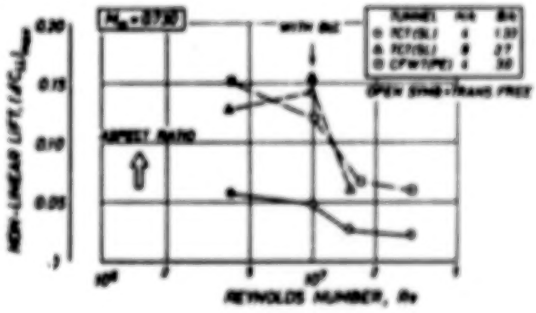

FIGURE 8: Reynolds number effects on maximum lift non-linearity

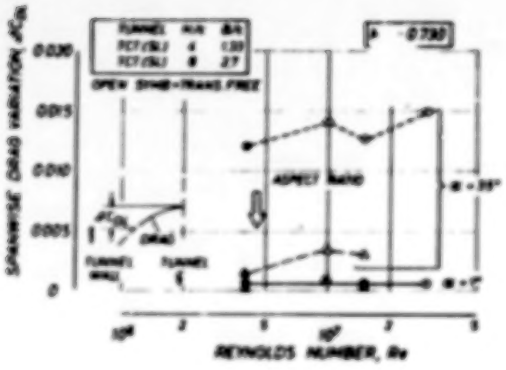

FIGURE 9: Reynolds number effects on spanwise drag variation

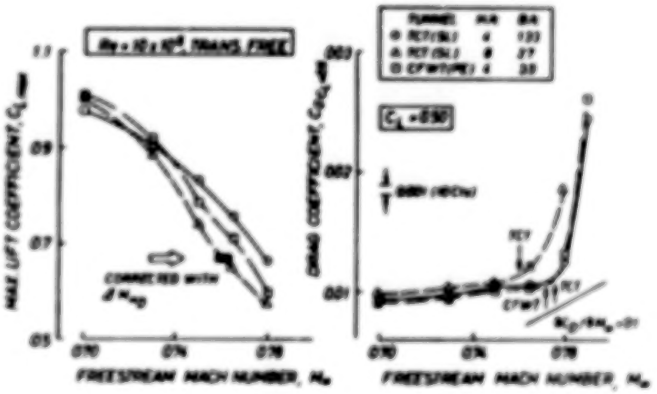

FIGURE 10: Wall interference effects on maximum lift and drag

(↓ Indicates M_{cr})

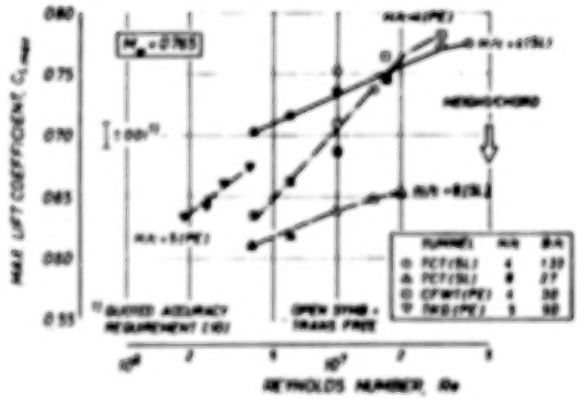

FIGURE 11: Effect of Reynolds number and model-wind-tunnel system on maximum lift

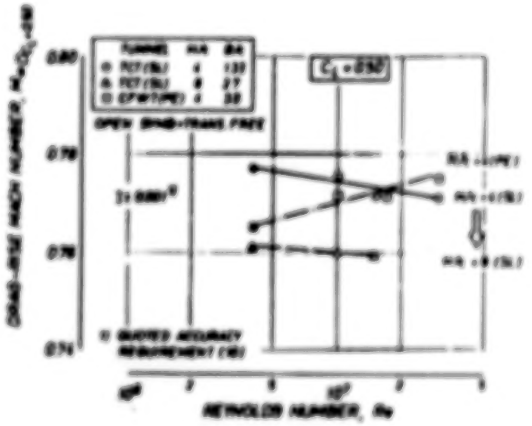

FIGURE 12: Effect of Reynolds number and model-wind-tunnel system on the drag-rise Mach number

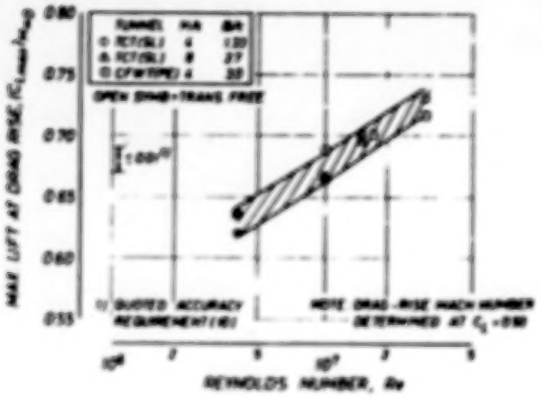
MAX LIFT AT DRAG RISE, $C_{L_{max}}$ at $M_{drag\ rise}$
REYNOLDS NUMBER, Re
OPEN SYMB = TRANS FREE
QUOTED ACCURACY REQUIREMENT (±)
NOTE DRAG-RISE MACH NUMBER DETERMINED AT C_L = 0.50

FIGURE 13: Effect of Reynolds number on the maximum lift at drag rise

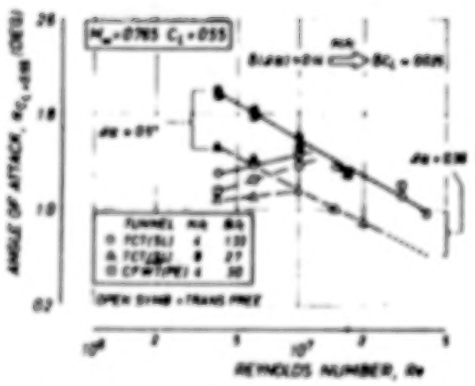

a. 0.3-m TCT and CFWT model-wind-tunnel configurations

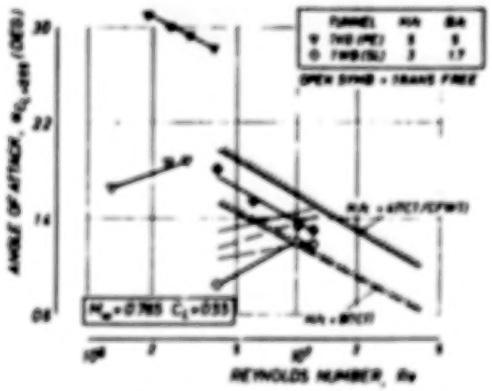

b. TWB and TEG model-wind-tunnel configurations

FIGURE 14: Reynolds number dependence of the angle-of-attack for constant lift

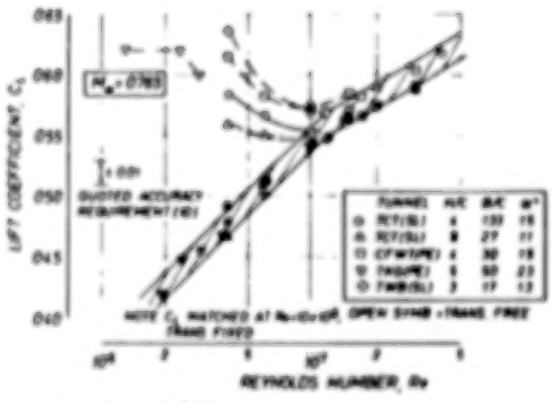

a. M_∞ = 0.765 α = const.

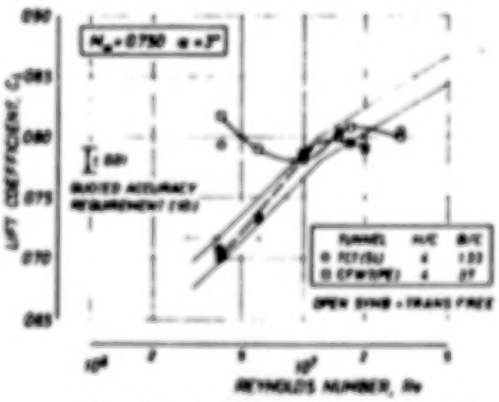

b. M_∞ = 0.750 α = const.

FIGURE 15: Effect of Reynolds number on lift

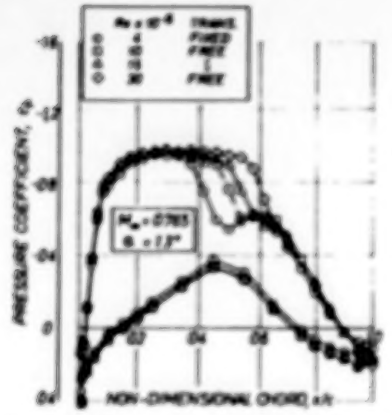

a. M_∞ = 0.765 α = 1.3° TCT-results

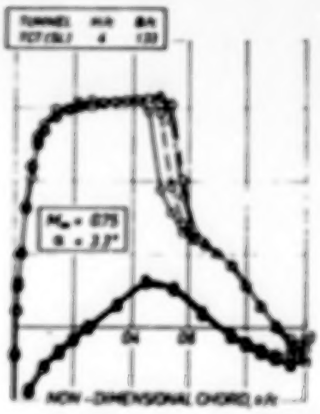

b. M_∞ = 0.750 α = 3.3° TCT-results

FIGURE 16: Effect of Reynolds number on pressure distribution (test cases of FIG.15)

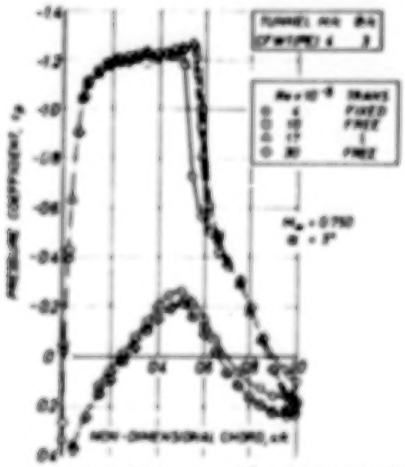

c. M_∞ = 0.750 α = 3° CFWT-results

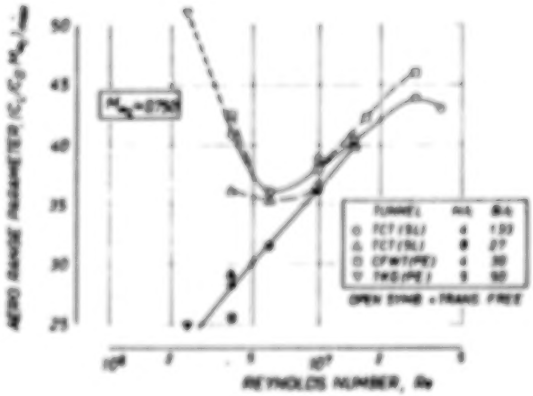

FIGURE 17: Effect of Reynolds number on the aerodynamic range parameter

Some Navier-Stokes Calculations for the CAST-10 Airfoil

D. Schwamborn
DLR, Institute for Theoretical Fluid Mechanics
Bunsenstr.10, 3400 Göttingen, FRG.

Introduction

Numerical methods for viscous transonic aerodynamics have made enormous progress in recent years, but further improvement is still needed, especially with regard to the accuracy of the prediction. This improvement will mainly result from validation of codes based on data from appropriate transonic experiments, where e.g. boundary conditions to be used in the calculation have to be measured and where also shear stress data or velocity profiles are available. Because there are not enough such experiments it is also necessary to compare numerical results with data from experiments which don't meet the requirements of code validation. Even in these cases a lot of useful information can be gained, not only for the theoretician but also for the experimentalist.

In the following a comparison is presented between the computed results of the flow about the CAST10 airfoil and the pressure distributions and force coefficents from experiments in the adaptive TCT [1].

Description of the Method

For the discretization of the complete Navier-Stokes equations a finite volume Runge-Kutta time-stepping scheme based on a cell centered formulation is used [2]. Since the fluxes across the cell faces are averaged from neighbouring cells which is equivalent to central differencing artificial diffusion terms are needed. These damping terms are the usual blend of second and fourth order differences except that a weighting function is employed. This weighting function restricts the artificial diffusion in the viscous near-wall regions or in the wake, where the unweighted formulation would otherwise result in a predominance of non-physical diffusion.

The set of ordinary differential equations resulting from the finite volume discretization is integrated in time using a linearized four-stage Runge Kutta scheme. Local time stepping is employed to accelerate the convergence to steady-state solutions, and in order to save further computation time the artificial and physical diffusion terms are updated only once per time step reducing the execution time by more than 50 per cent.

To have a well-posed problem a set of appropriate boundary conditions is needed. At the airfoil surface the no-slip and the adiabatic wall condition is used. The pressure is derived from the assumption of zero pressure gradient normal to the wall which is justified for the very small step sizes normal to the wall used in Navier-Stokes calculations for turbulent flows. At the far field boundary we use one-dimensional Riemann invariants normal to the boundary in order to obtain boundary conditions.

Since the two-dimensional flow solver used here is derived from the three-dimensional one described in [2], it allows for a block-structured approach, i.e. the computational domain can be divided in a number of subdomains called blocks. The advantage of this approach is that it is very flexible regarding the handling of complex geometries (e.g. with multiply connected domains). The flexibility is partly due to the segmentation of the block faces, which allows for the use of different types of boundary conditions and different neighbouring blocks at each

block face. This feature was used in the present calculations to model the finite thickness of the CAST10 trailing edge by using a C-type mesh past the airfoil with an extra grid in the gap behind the trailing edge. For more information on the block structure refer to [2].

To simulate the turbulence the well-known algebraic model of Baldwin and Lomax [3] is used.

Typical grid in the vicinity of the airfoil

For the flow about the airfoil the mesh consists of 260x80 cells in chordwise and wall-normal direction, respectively and the mesh extends about 10 root chords away from the airfoil. There are 200 cells on the wing surface and the first step size normal to the wing surface is chosen such that it is equivalent to $z^+ \approx 2$ in the first cell of the wall, in order to resolve the laminar sublayer of the turbulent flow.

The C-type grid is generated algebraically using a code of Sobieczky [4] resulting in a mesh with a gap of the thickness of the trailing edge. This gap is closed by a suitable interpolation which yields a smooth distribution of the stepsize in the direction normal to the wake.

The block structure in the present calculations includes three blocks; the first and second corresponding to the C-type mesh in the vicinity of the airfoil and to the interpolated mesh in the gap, respectively. In these two blocks the complete Navier-Stokes equations are solved, whereas only the Euler equations are solved in the third block for the outer part of the C-mesh. The block boundary of the later block is about 25 per cent of chord away from the airfoil and the wake, respectively.

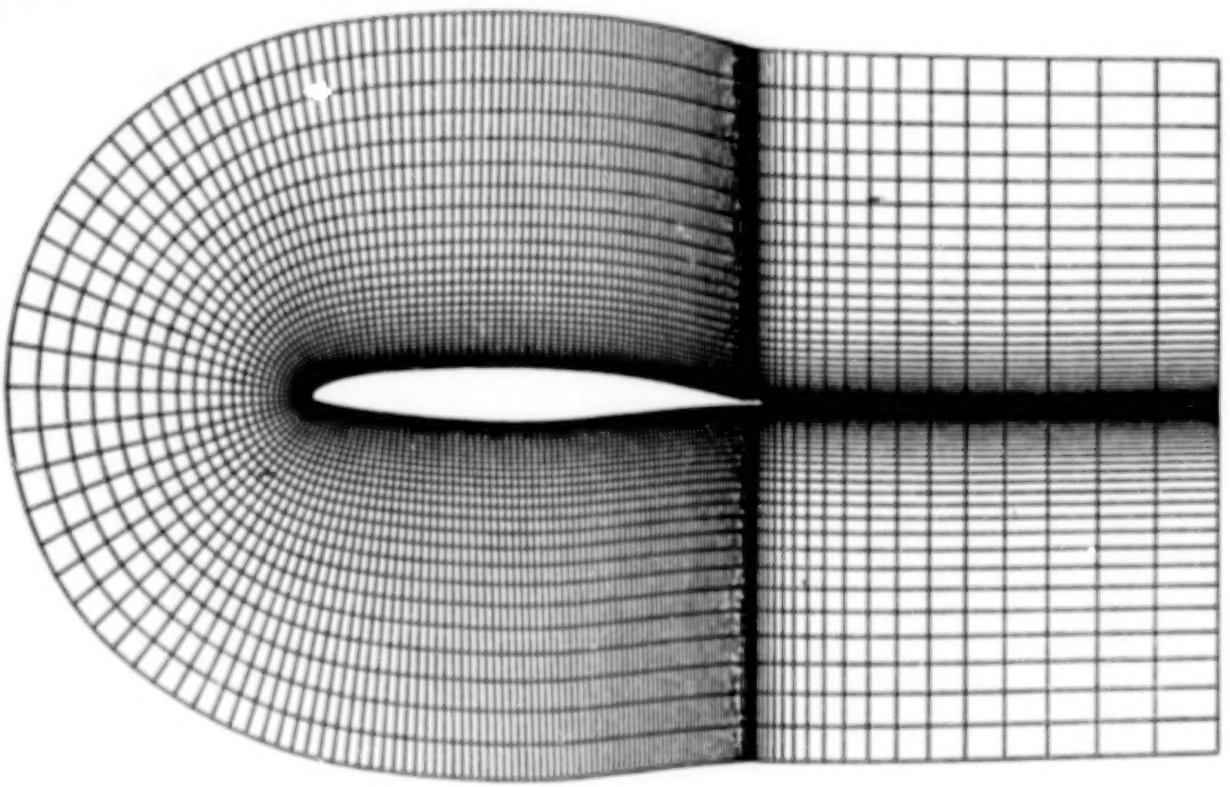

Details of the mesh near the leading and trailing edges

The figures show the strong clustering of the grid lines near the wall and give an idea of the grid in the gap behind the trailing edge. In the present calculation the mesh within the gap behind the trailing edge is fairly small, i.e. there are only ten cells over the height of the trailing edge.

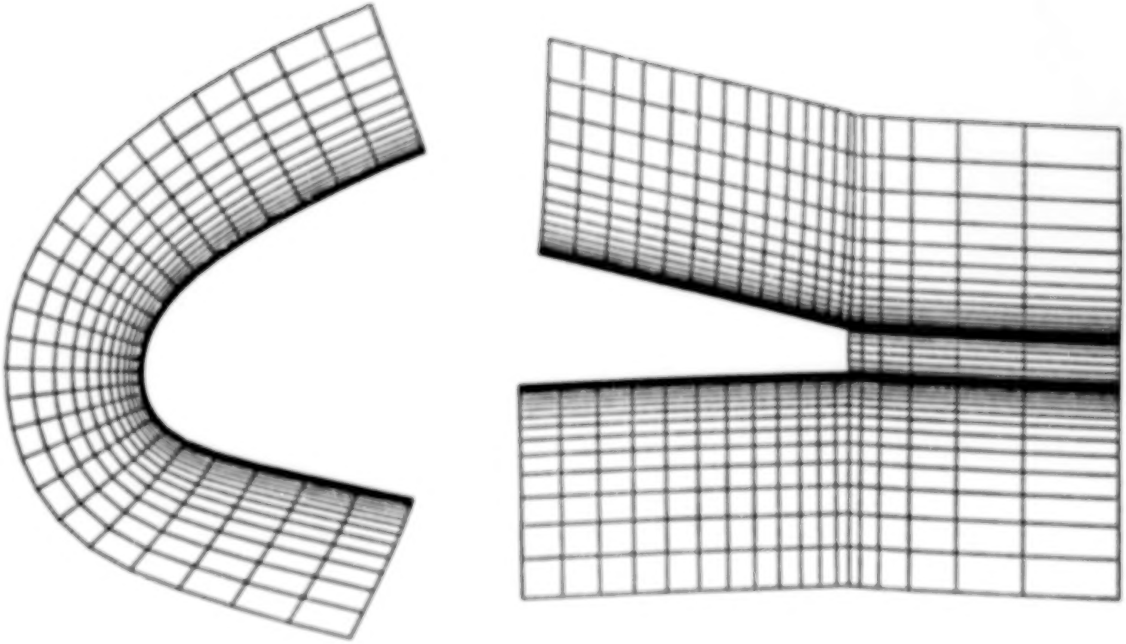

Comparison of experimental and computed lift and drag

M = .73 Re = 10 million

The table shows a comparison of the lift and drag coefficients from experiments in the TCT [1] with free transition (the transition takes place somewhere near the leading edge) and calculations where the transition point is prescribed. The transition location is given as upper/lower chord position.

As can be seen from the table the upper surface location of transition (.07 to .2 chord) has almost no influence on the coefficients, but the lift increases when the transition location is shifted downstream on the lower surface (to .15 and .2 chord).

The calculation for $\alpha = 3.0$ is slightly unsteady, i.e. the residuals stay on a certain level in the separation zone behind the shock.

For details see the following pages.

α	exp./cal.	transition	lift coeff.	drag coeff.
1.0	exp.	free	.616	.010
	cal.	.07/.07	.677	.0152
	cal.	.10/.10	.677	.0152
	cal.	.15/.15	.685	.0149
	cal.	.07/.20	.695	.0150
	cal.	.20/.07	.677	.0150
	cal.	.10/.10 (modif.turb.)	.637	.0159
.9	cal.	.10/.10	.677	.0150
3.0	exp.	free	.895	.0450
	cal.	.10/.10	.82-.90	.033-.039

Iso-Mach contours for M = .73 Re = 10 million α = 1.00

Calculation: transition at .10/.10 chord

This figure shows contour lines of the Mach number in the vicinity of the airfoil (Δ = .05) with the supersonic regime set off in gray. Also shown are the block boundaries of the computation. Since some isolines cross the boundary between the viscous inner and the inviscid outer block without any disturbance it is obvious that the block concept has no influence on the solution quality.

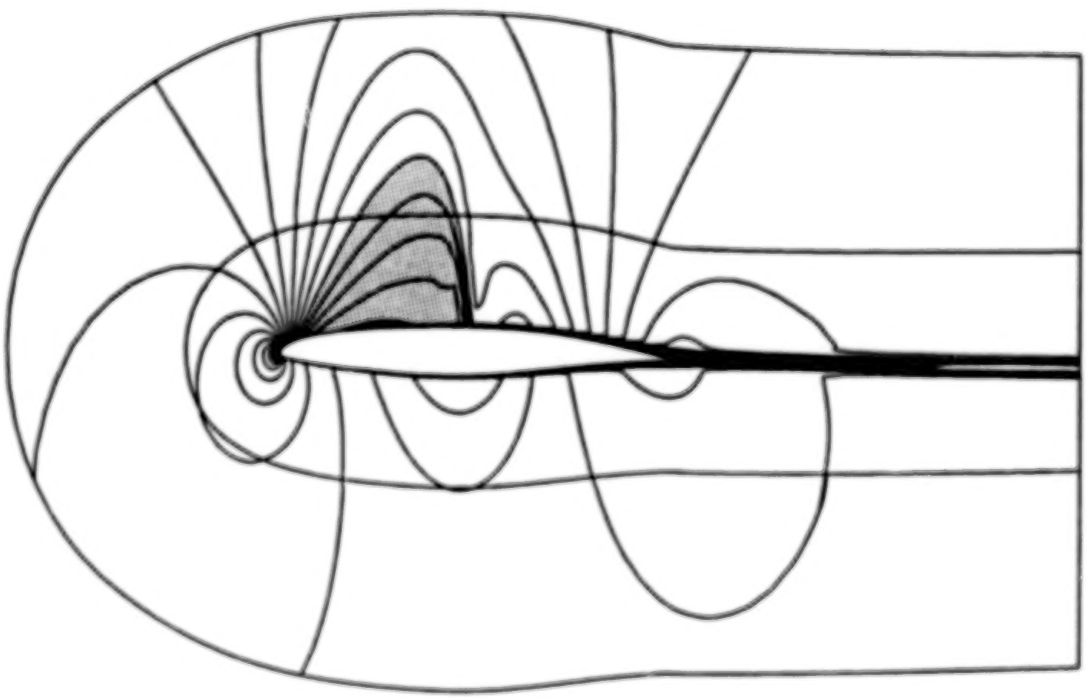

Cp-distribution at M= .73 Re= 10 million α = 1.00

1. Calculation: transition at .10/.10 (or .07/.07) chord

The symbols show the experimental data from TCT [1](point 203) and the solid line shows the computational result. The horizontal line with the crosses at its ends indicates the critical Cp value. Fixing the transition at 10 or 7 per cent chord in the calculation gives the same pressure distribution.

The results compare quite well for the major part of the surface except near the trailing edge, but there is a discrepancy in the shock location of about 10 per cent chord.

To see the influence of the chosen transition location on the results the following variations are made.

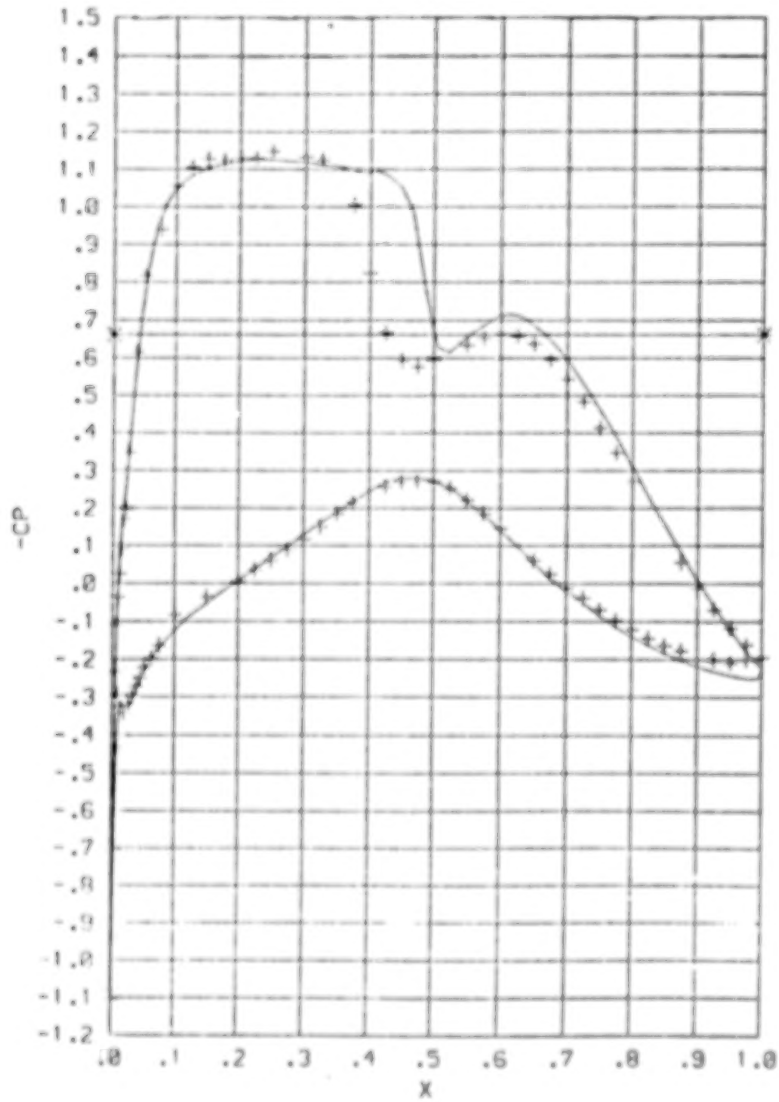

Cp-distribution M= .73 Re= 10 million α = 1.00

2. Calculation: transition at .07/.20 chord

The pressure distribution shows almost no variation compared to previous calculation.

3. Calculation: transition at .20/.07 chord

The pressure at the beginning of the pressure plateau is now even closer to the experimental one, but the shock has moved a little bit further downstream. The solution behind the shock and at the lower surface are the same as before.

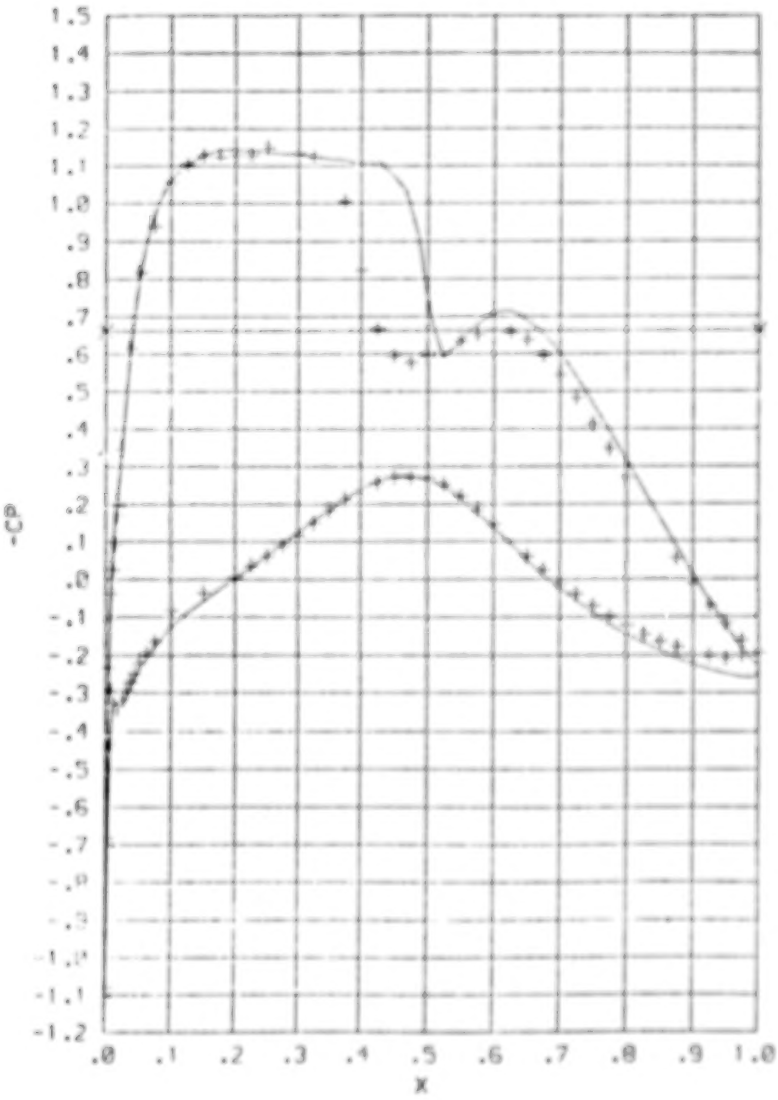

Cp-distribution M = .73 Re = 10 million α = 1.00

4. Calculation: transition at .10/.10 chord and α = .9

A decrease in the angle of attack results in less agreement regarding the plateau pressure and the pressure at the lower surface. The shock has now moved upstream, but by a far too small extent. To match the plateau pressure again a higher Mach number would be necessary, but this further variation was not tried.

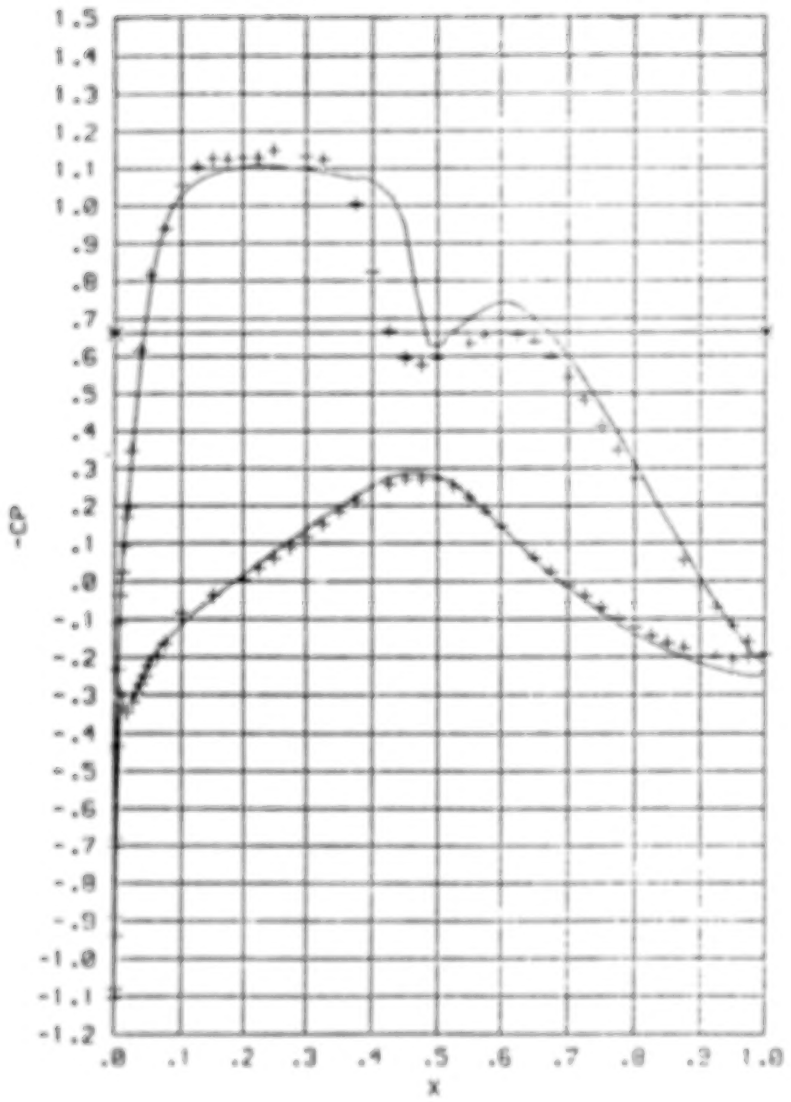

Cp-distribution M = .73 Re = 10 million α = 1.00

5. Calculation: transition at .10/.10 chord and variation of turbulence model near shocks

A modification in the Baldwin/Lomax turbulence model resulting in a local increase of the eddy viscosity is made. The shock is moved upstream almost into the right position but the plateau pressure and the pressure at the lower surface show now larger discrepancies similar to the result with the smaller angle of attack. It is obvious from the movement of the shock that there is a strong influence of the modelling on the turbulent shock boundary layer interaction.

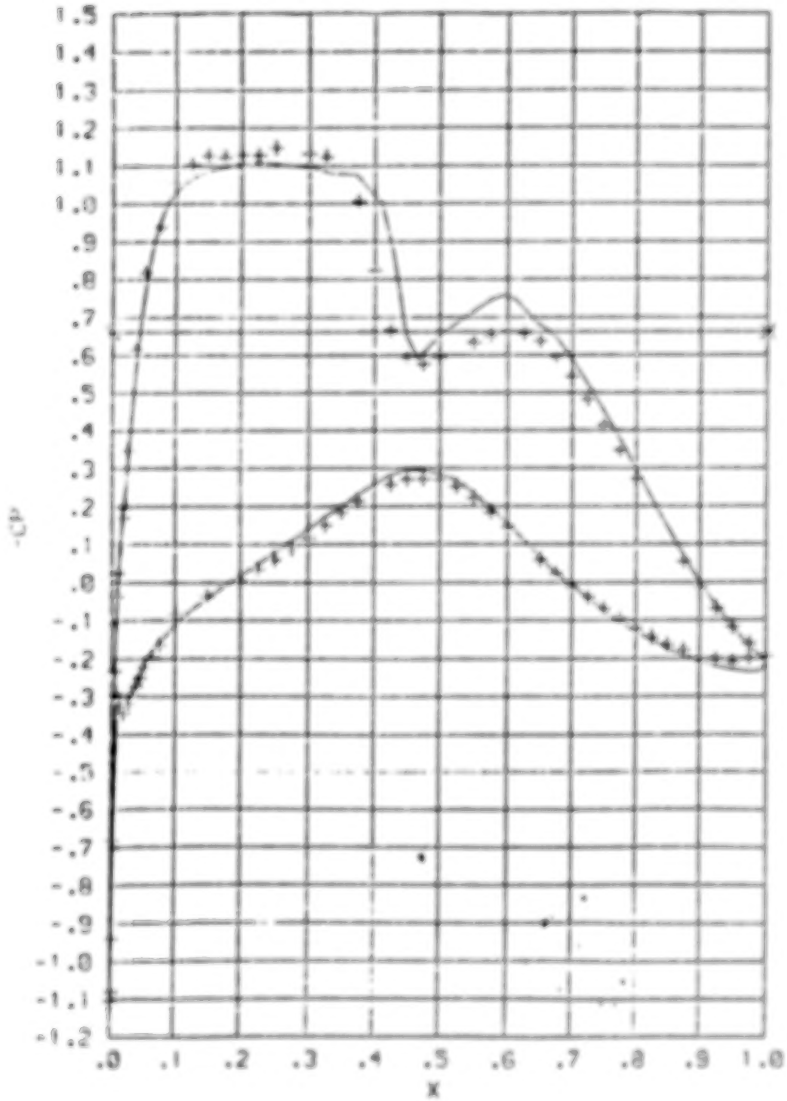

Iso-Mach contours for M = .73 Re = 10 million α = 1.00

Calculation: transition at .10/.10 chord
Modified turbulence model

This figure shows the Mach number distribution with the modified turbulence model. In comparison to the previous results one realizes the upstream movement of the shock due to this modification. Away from the supersonic region the two solutions look very similar as one could expect already from the pressure distributions.

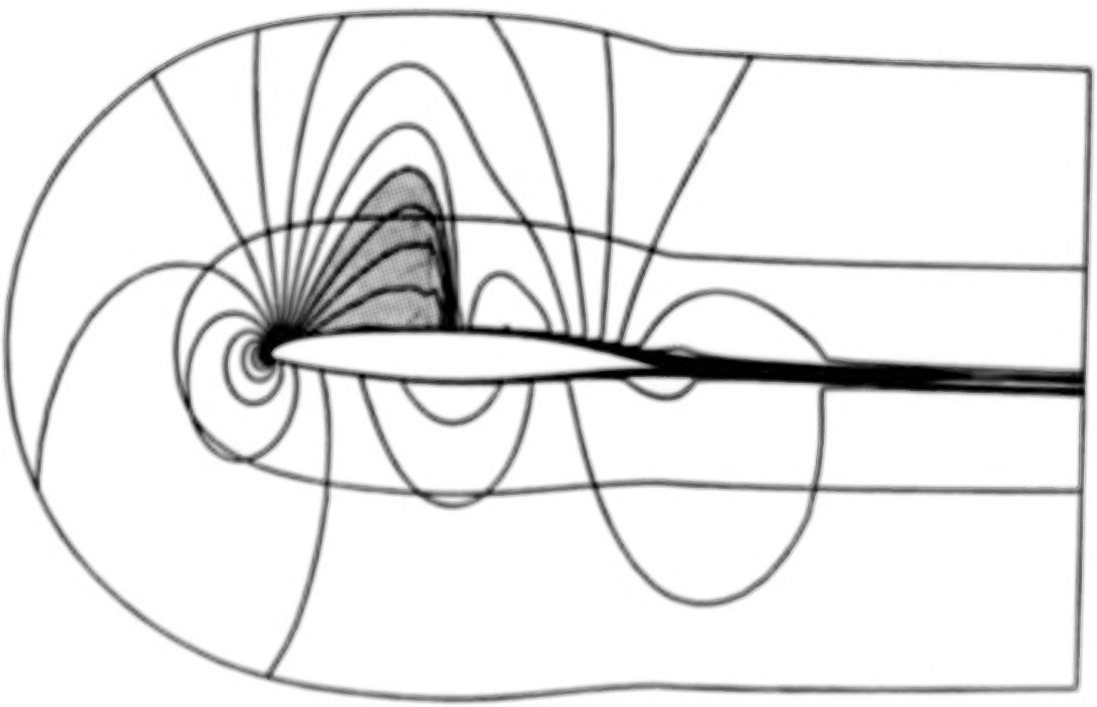

Cp-distribution M= .73 Re= 10 million α = 3.00

Calculation: transition at .10/.10 chord

For this higher angle of attack case (point 207 of TCT data[1]) the calculation indicates a slightly unsteady solution in the separated region on the upper surface near the trailing edge. Again the results compare quite well for the major part of the surface, but we find again the discrepancy in the shock location. In this case with separated flow the aforementioned modification of the turbulence model shows almost no influence on the solution, maybe because the modification is only local at the shock and does not extend over the whole separated region.

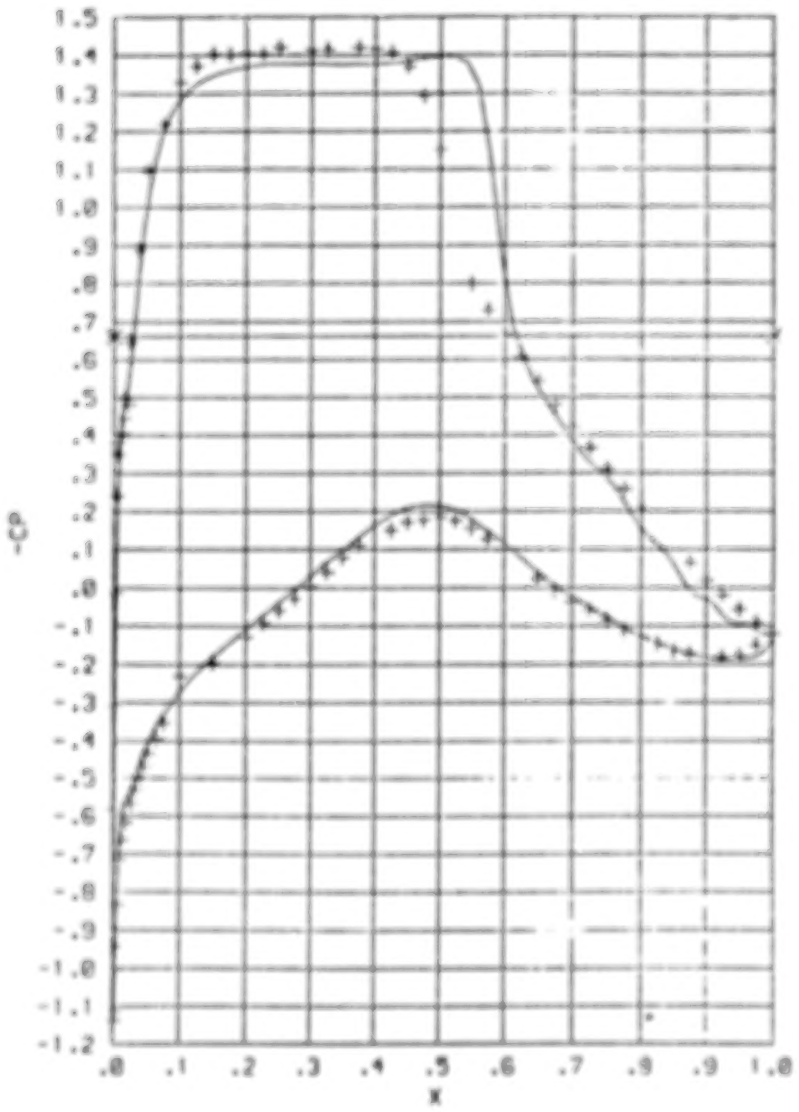

Iso-Mach contours for M = .73 Re = 10 million α = 3.00

Calculation: transition at .10/.10 chord

This figure shows the Mach number distribution for the higher angle of attack case, where the shock has moved downstream. Due to the separation behind the shock the boundary layer has thickened considerably as can be seen in comparison to the Mach number distribution for $\alpha = 1$.

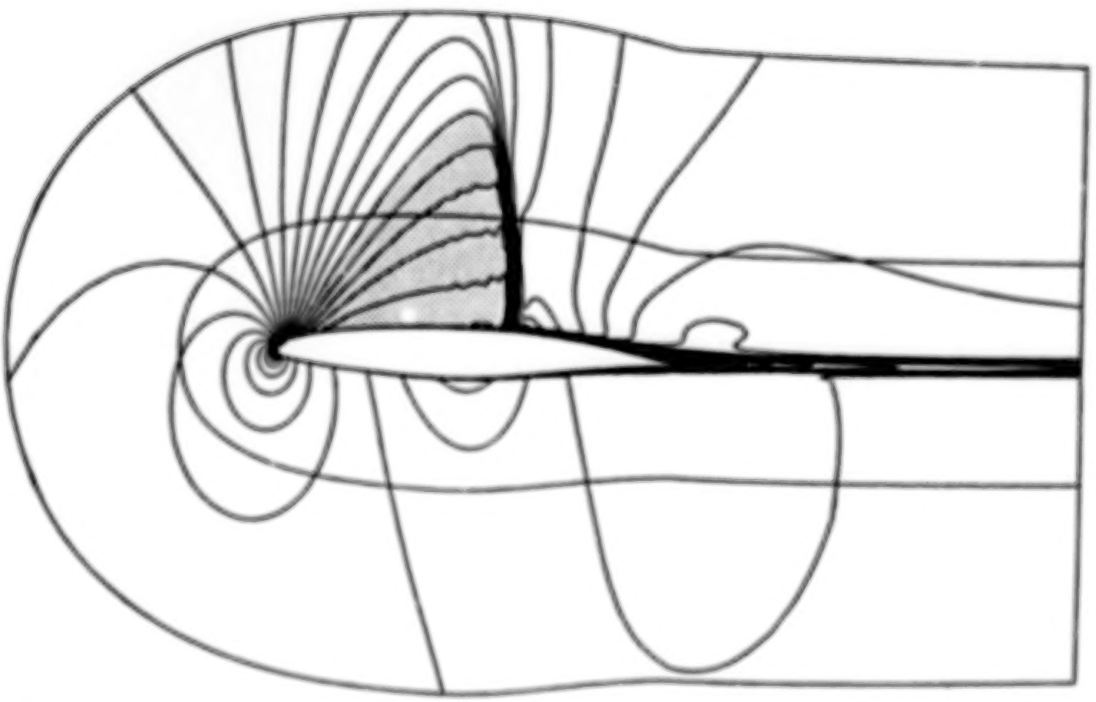

Comparison of experimental and computed lift and drag at M= .765

The table shows a comparison of the force coefficients from experiments with fixed and free (for the higher Re numbers) transition to those from calculations where the transition location is always at .07/.07. Results are presented for different angles of attack and different Re numbers.

For more details regarding the calculated results see the following pages.

α	Experiment lift / drag	Calculation lift / drag
Re = 4 million		
0	.378 / .012	.53 / .0169
.5	-	.604 / .0216
1.	.57 / .020	.53-.65 / .019-.028
Re = 10 million		
0	.45 / .011	.53 / .0155
.5	.588 / .015	.575 / .0185
1.	.623 / .024	.58-.63 / .019-0.25
Re = 40 million		
0	.538 / .012	.41-.43 / .010-.011

Cp-distribution M= .765 Re= 4 million α = 0.00

Transition at .07/.07 chord (calculation) and .06/.06 chord (experiment)

For this higher Mach number case (point 39 of TCT data [1]) the numerical result compares not so well with the experimental data, not even at the lower surface. The computation exhibits a pressure plateau with an expansion peak in front of the shock, whereas the experiment shows a double structure of weaker shocks. The calculated pressure distribution results in a higher lift (and drag) and in a higher trailing edge pressure.

According to previous experience the difference in the transition location between calculation and experiment is estimated to have practically no influence.

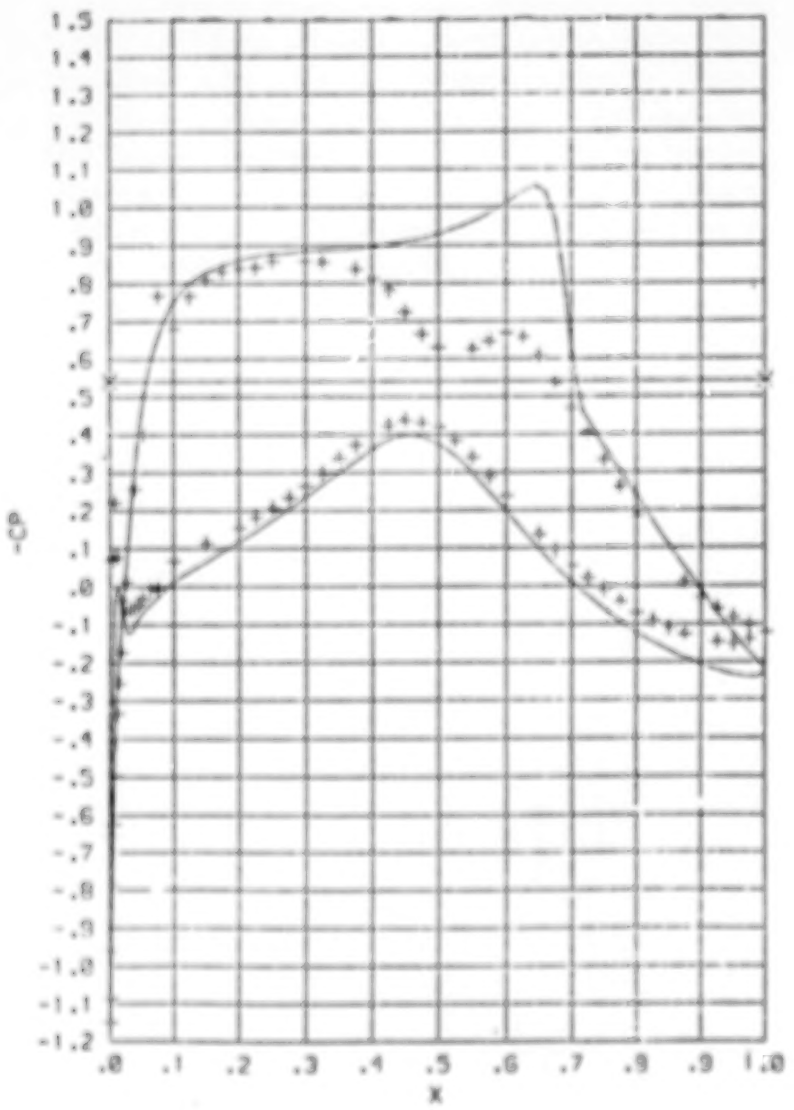

Cp-distribution M= .765 Re= 10 million α = 0.00

Transition at .07/.07 chord (calculation) and .06/.06 chord (experiment)

Increasing the Reynolds number results in almost no change in the computed pressure distribution. The experimental pressure (point 79 in TCT data [1]) is now slightly higher on the lower surface and slightly lower on the upper surface thus producing a higher lift due to the reduced decambering by the thinner boundary layers. Now the pressure distributions compare better except for the region of the shocks where we find again the double shock in the experimental data.

It is far from clear why the calculation at the lower Reynolds number doesn't show the decambering effect found in the experiment.

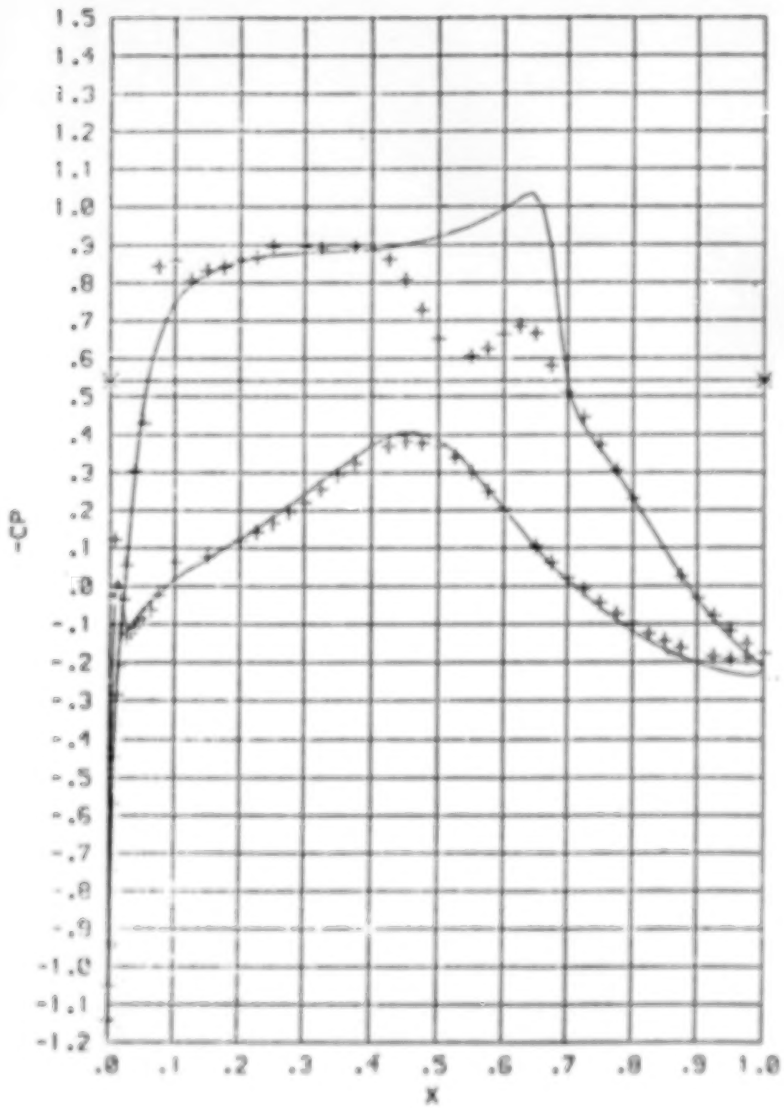

Cp-distribution M= .765 Re= 40 million α = 0.00

Transition at .07/.07 chord (calculation) and .06/.06 chord (experiment)

A further increase in Reynolds number changes the situation in the experiment (point 284), i.e. the double shocks merge and form a stronger single shock downstream. Again the pressure is increased at the lower and decreased at the upper surface. Although the qualitative result of the computation compares now better to the experimental pressure distribution, the quantitative result is much worse. This is due to the poor resolution of the very thin boundary layer. With a better resolution, however, the computed shock position is again found downstream of the experimental one whereas the plateau pressure and the pressure at the lower surface are recovered. As for the lower Mach number cases we assume that this effect is at least partly due to the turbulent shock boundary layer interaction which is not correctly modelled by the Baldwin-Lomax turbulence model.

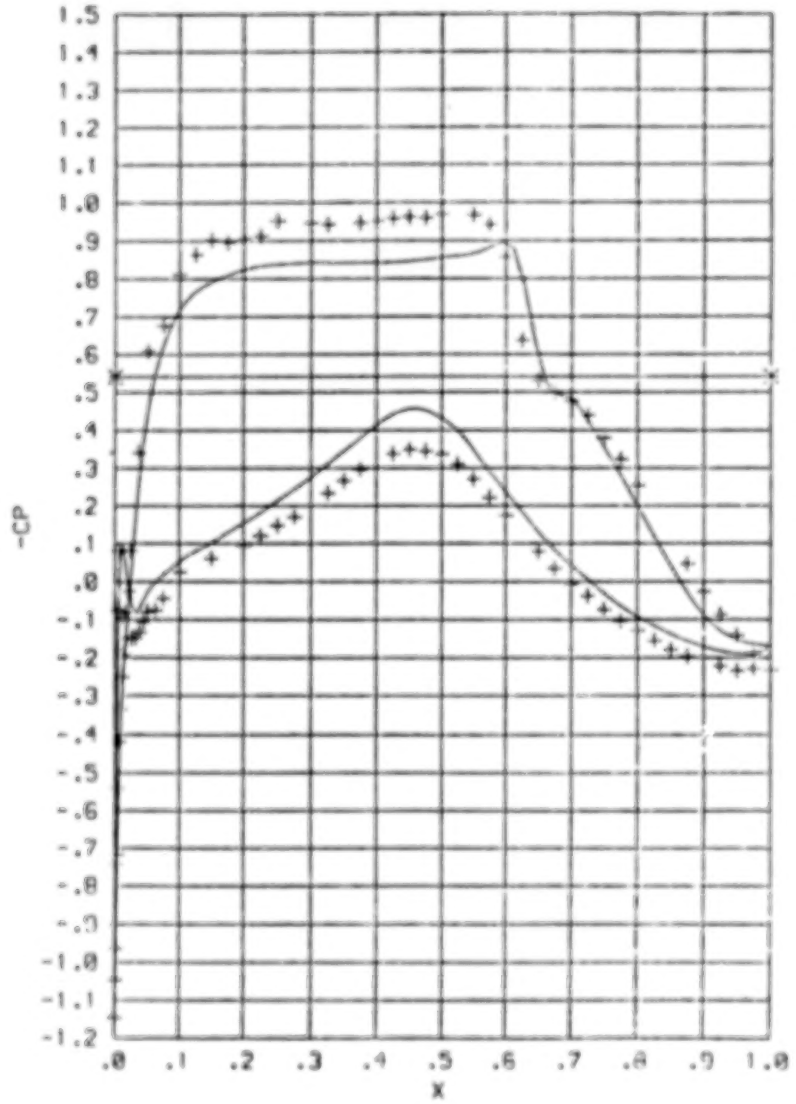

Cp-distribution M= .765 Re= 4 million α = 1.00

Transition at .07/.07 chord (calculation) and .06/.06 chord (experiment)

For a higher angle of attack and the low Reynolds number (point 40 of TCT data [1]) we find only a single shock in the experimental data and, as is seen in most of the other cases, the numerical result compares quite well except at the shock. But this depends on the picked iteration cycle where the results are plotted, as will be discussed on the next page.

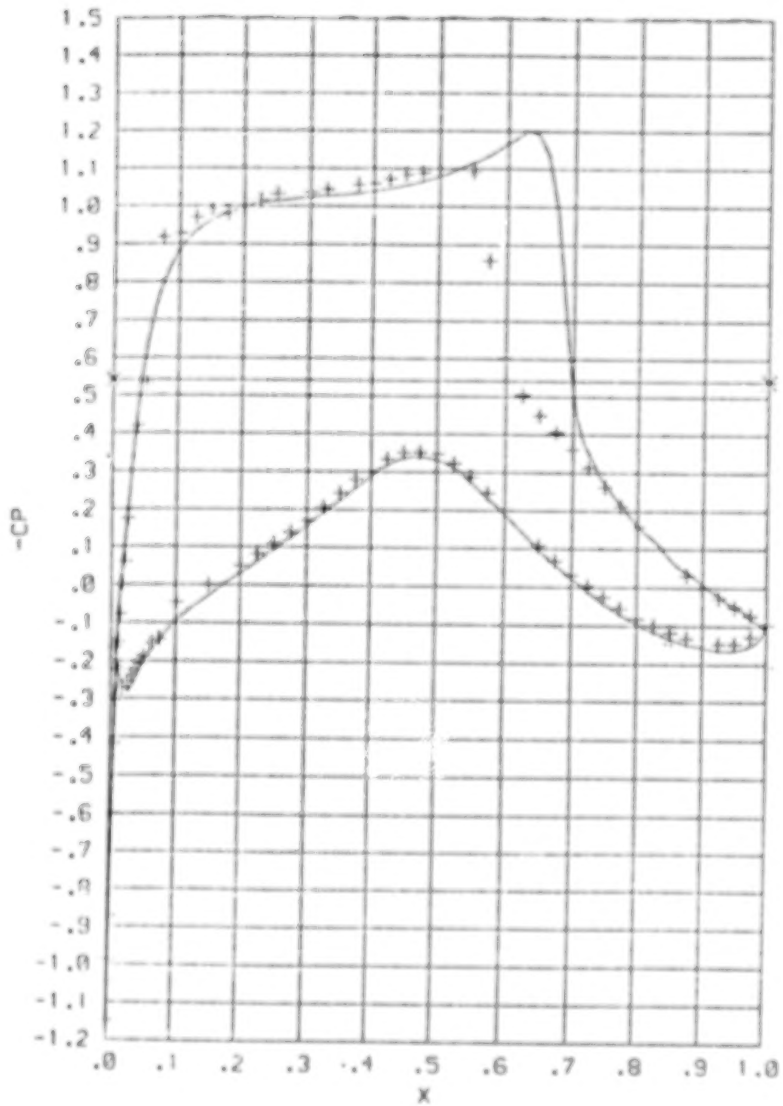

Cp-distribution M= .765 Re= 10 million α = 1.00

Transition at .07/.07 chord (calculation) and .06/.06 chord (experiment)

Increasing the Reynolds number again (point 339 of TCT data [1]) has little influence in the experimental data; only the shock is shifted downstream a little bit. One would expect the same for the computed results keeping in mind the results for zero incidence. But as is seen from the variation of lift and drag in the preceding table there is an unsteadiness in the numerical results at this angle of attack, i.e. the solutions do not converge to a steady state. The result shown here was obviously taken at a moment where the lift in the calculation was low, whereas the result on the previous page corresponds to a situation where the lift was high.

Since the numerical method uses local time stepping as an acceleration technique the unsteadiness cannot be interpreted in a physically meaningful way, although it indicates that a time accurate calculation at this angle of attack would yield an unsteady flow behavior, too.

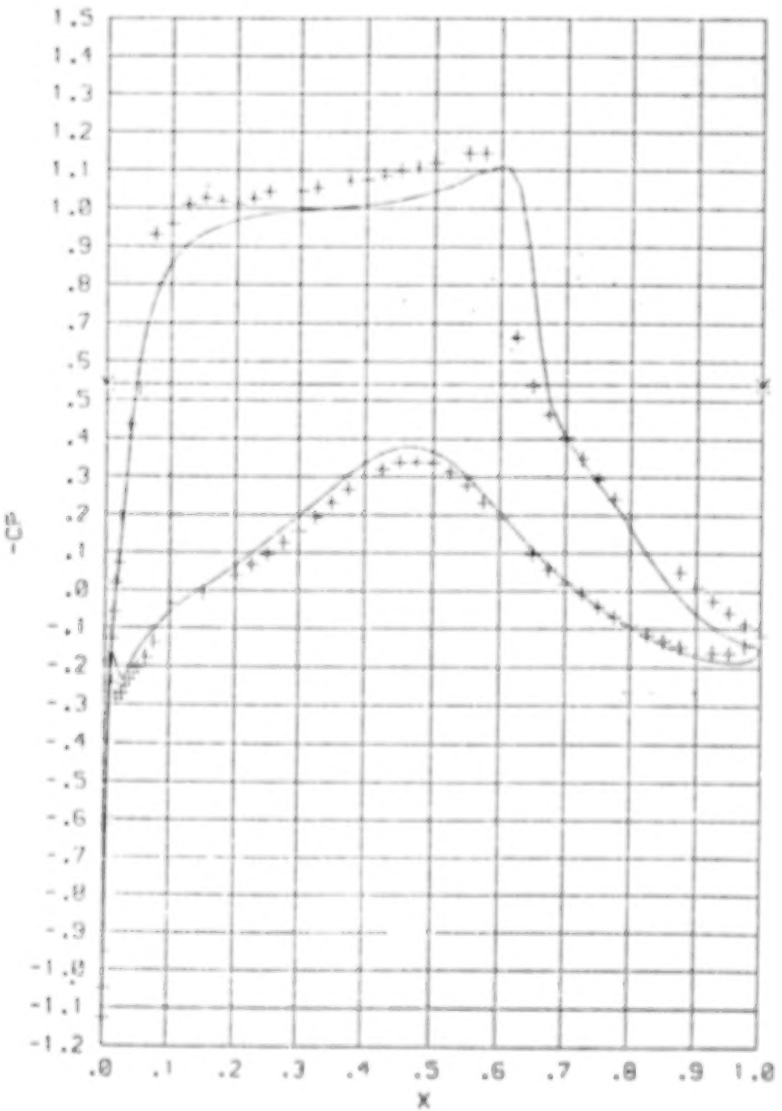

Concluding Remarks

Results of the simulation of the viscous flow past the CAST10 airfoil have been shown for different flow conditions. Since the experiments provide only surface pressures and force coefficents the comparison to the numerical results relies on these.

Good agreement of the results is found for the lower Mach number cases except for the shock position. As numerical experiments indicate, this seems to be due to the turbulent shock boundary layer interaction which is not correctly modelled by the algebraic turbulence model employed.

For the lower Mach number case the influence of the transition location has been investigated, too. Changing the transition location at the lower surface has much more influence on the pressure distribution than changing it on the upper side.

For the higher Mach number case the double shock structure found in the experiment for the lower Reynolds numbers was not reproduced by the numerical solutions. The reason for this is unknown though it may be due to the turbulence modelling. For the higher Reynolds number a better resolution of the boundary layer is needed in the computation in order to recover the experimental pressure plateau; but then the shock position is still found downstream of the experimental one.

REFERENCES

[1] TCT data provided by E. Stanewsky, DLR-Institute for Experimental Fluid Mechanics, Göttingen.
The TCT is Described in:
Ladson, C.L., Ray, E.J.: Evolution, Calibration, and Operational Characteristics of the Two-Dimensional Test Section of the Langley 0.3 Meter Transonic Cryogenic Tunnel, NASA Technical Paper 2749, Sept. 1987.

[2] SCHWAMBORN, D.: Simulation of the DFVLR-F5 Wing Experiment Using a Block-Structured Explicit Navier-Stokes Method. Notes on Numerical Fluid Mechanics Vol.22, Vieweg Publishers,1988.

[3] BALDWIN, B.S., LOMAX, H.: Thin Layer Approximation and Algebraic Model for Separated Turbulent Flows. AIAA Paper 78-257, (1978).

[4] SOBIECZKY, H.: Analytical Surfaces and Grids. AGARDOGRAPH on Current Practices in Numerical Grid Generation

Main Results of CAST-10 Airfoil Tested in T2 Cryogenic Wind Tunnel

A. Blanchard, A. Seraudie, and J. F. Breil
ONERA/CERT
DERAT
Toulouse-France

INTRODUCTION

The aims of the cooperation NASA/DFVLR/ONERA

* Examine Re, M, and Transition effects on a very sensitive airfoil, systematically tested previously.

* Evaluation of the airfoil characteristic prediction
  - comparison experimental/theoretical results
  - comparison adaptive walls/conventional wind tunnel results

* Mutual help for T2 , 0.3m TCT , TWB (Braunschweig)
  - Gives us more experience for airfoil tests under cryogenic operation (second cryogenic airfoil tests)
  - lots of experience with adaptive wall techniques

2 Series of Tests in T2

-1st in November 1984
-2nd in April 1985

Model

* Designed by Dornier
* Manufactured by ONERA
* Chord= 180mm , Width= 560mm
* 103 pressure tapes (L.E. Ø 0.1mm)
  21 thermocouples (15 in the skin region)

T2 Wind Tunnel

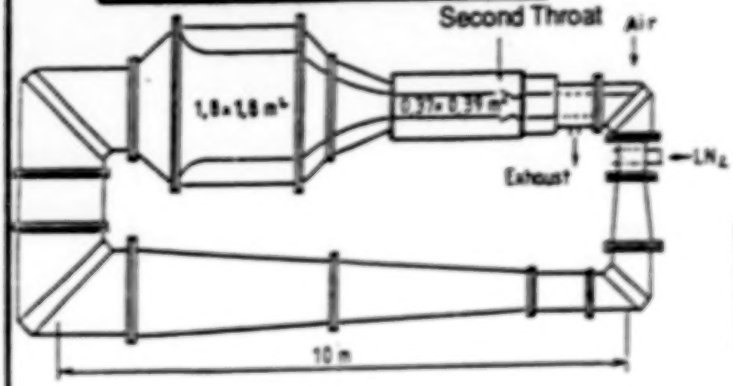

- Transonic
- Pressurized
- Cryogenic
- Adaptive walls

- Air induction
- LN2 injection
- Internal insulation

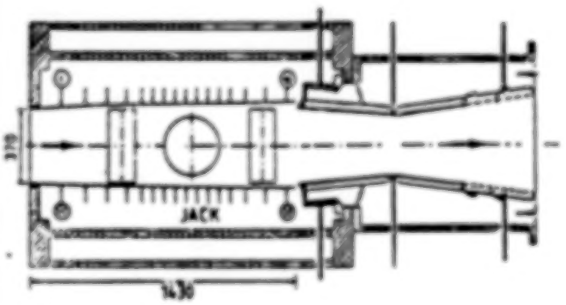

WALL DISPLACEMENT MECHANISM

Adaptive Walls

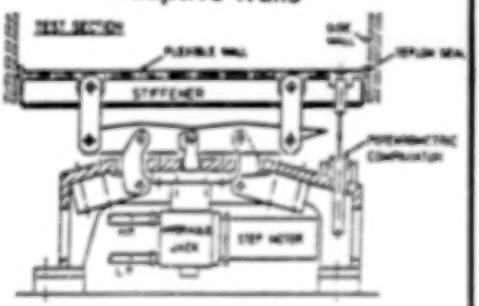

- Control by computer
- Runs ≈ 30s to 60s
- Model precooling
  - outside
  - in the test section

$\frac{\sqrt{p'^2}}{q} = 0.004$

Tu = 0.1 %

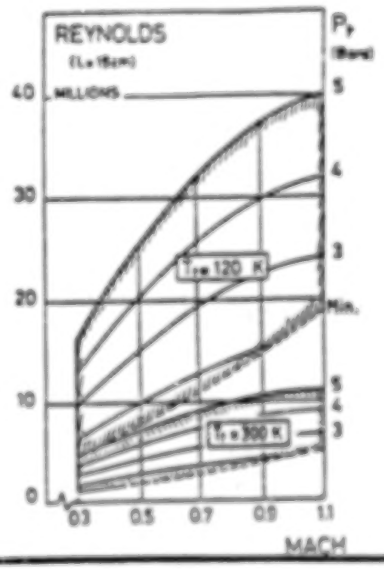

Operational envelope

0.6 < Mo < 0.9

1.6 < Pt < 3 bars

110K < Tt < T.amb

100mm< Chord <200mm

Rc < 30.10^6

T2 Run

CAST 10

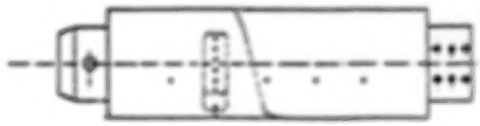

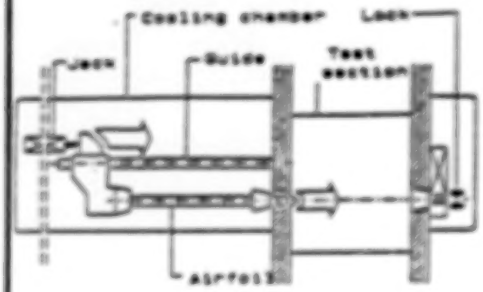

Model Precooling

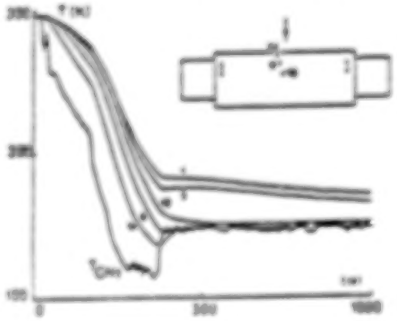

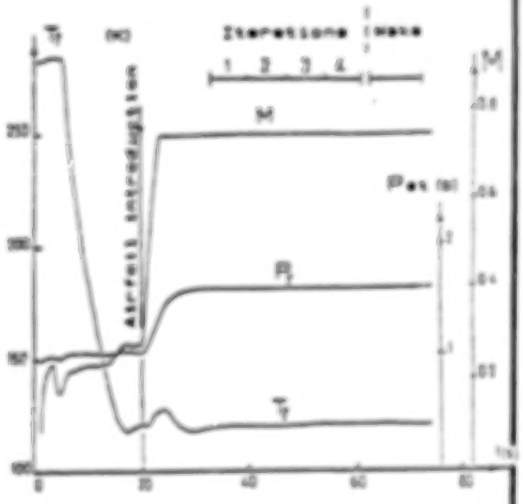

RUN

* A part of the model is hollow

- Model is cooled outside before the run
- Start of the run at low Mach number (0.3)
  low pressure (1.1 b)
  selected temperature
- Introduction of the model in the test section
  (T model ≈ T flow)
- Increase of (M,Pt) at the required level

- Wall adaptation, measurements on the walls and on the model
- Other measurements (Wake)

- End of the run (one configuration has been tested)

2-D Adaptation

2-D Adaptation Strategy

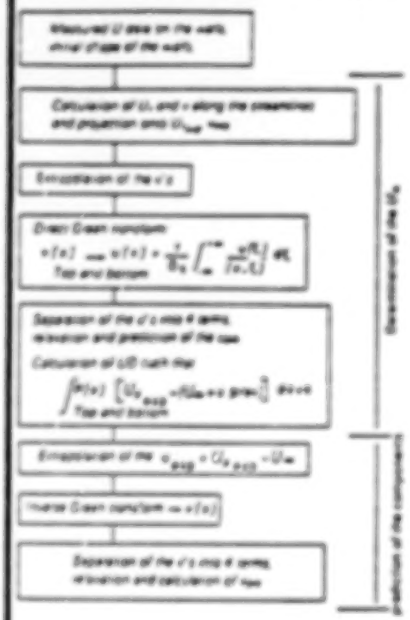

Adaptation Flowchart

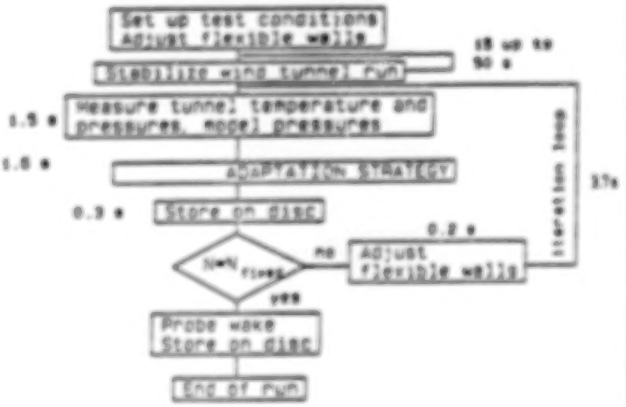

* **Regulation** by computer. (M,P,T) independent

Measurements → Pt , Tt , Pwalls , Zwalls , Pmodel, ...

Mo

theoretically $\Delta\alpha$, ΔM =0 ← **Adaptation**

* Principle rather simple

  internal field- measured (walls) } iterations until they are
  external field-calculated(Green) } equal on the control surf.

Accuracy of the method

  u,v extrapolation --> $\pm\infty$

  u,v streamline projection on a straight line

Stategy rather complicated to obtain rapidly the convergence

  - Mo calculation (field around the model)
  - separation in 4 elementary terms
  - relaxation coefficients

Convergence criterion: until no variations (Pwalls,Zwalls, Pmodel)

* Convergence in 3 or 4 iterations in a run (each one ≈ 5s)

* Residual errors $\Delta M \approx 0.002$, $\Delta\alpha \approx \pm 0.02°$

Measurement Accuracy

* **Model : good quality (shape, surface roughness,...)**
  (very important for Natural Transition,
  some problems at High Reynolds Number)

* **Steady flow accuracy**

P_t =3 bars T_t =120 K M = 0.8 C_L = 0.5	Instrumentation * Calibration	Control * Computer process * Mechanical limits	Aerodynamic Field *Adaptive walls	 * Gradients
Pressure	0.001 bar	0.004 bar		
Temperature	0.3 K	0.4 K		< 0.5 K (wall: 10 K)
Mach number	0.002	0.001	0.002	
Angle of attack	0.02°		0.02°	

Control / Adaptive walls : $\Delta M = 0.005$ Flexible wall shape : $\Delta y = \pm 0.1$ mm
Model temperature $T_w/T_{aw} = 1.015$

* **Flow quality** (important for Natural Transition)
  - **Pressure fluctuations** (low levels)
  - **Velocity fluctuations** (due to pressure fluctuations)
  - **Temperature fluctuations** (seem reasonable)
  - **Uniformity in the test section** (good enough)
  - **Purity of the fluid** (moisture is the most important problem for flow quality in a cryogenic wind tunnel)

* **Side wall boundary layers**
  seems a real problem ($\Delta\alpha = 0.1$ to $0.2°$)

CAST 10 Tests in T2

1st series of tests — * Natural Transition — T.N.

		0.69 < M < 0.77
Rc = 4 . 10^6	+3° α -2°	lot of values

$6 .10^6 < Rc < 30 .10^6$

- M=0.7 α=+1°
- M=0.73 α=-0.25°
- M=0.76 α=+0.25°
- M=0.765 α=+0.25°
- +some scatter points

Nb of runs = 160

2nd series of tests — * Tripped Transition — T.D.

h=0.045mm Xt/C = 5%

		0.7 < M < 0.765
Rc = 4 . 10^6	+4° α -2°	lot of values

$6 .10^6 < Rc < 27. 10^6$

- M=0.7 α = +1°
- M=0.73 α = -0.25°
- M=0.76 α = +0.25°
- M=0.76 α = +1°
- M=0.765 α = -2°
- M=0.765 α = +2°

Nb of runs = 90

* Half Tripped Transition — T.1/2D.

(lower surface)

		0.73 < M < 0.78
Rc = 4 . 10^6	+2° α -2°	some values

$6 .10^6 < Rc < 14. 10^6$

- M=0.73 α = -0.25°
- M=0.76 α = +0.25°

Nb of runs = 45

Measurements at each run

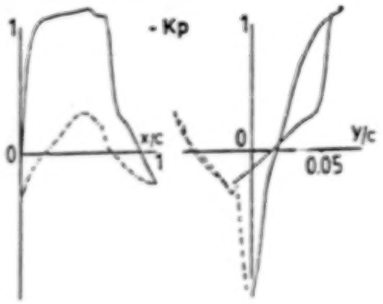

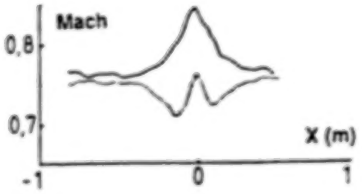

On the Model

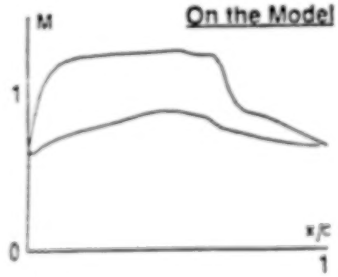

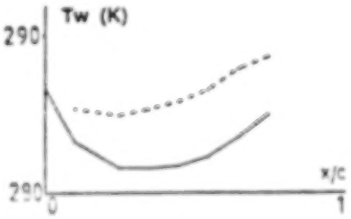

On the Walls

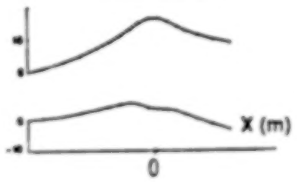

Wake

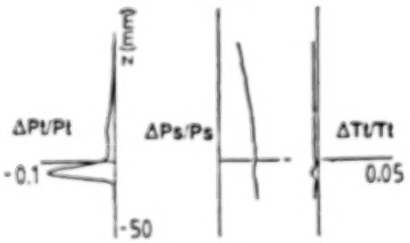

+ Oil Visualisation ---> 2-D of the flow
(Shock, Transition, Bubble, Separation,...) locations .

* **Tunnel** ---> **Pt , Tt**
* **M** walls ---> Infinite conditions **Mo**
  Z walls Streamline convergence
  (C_L not exploited here)
* **Kp** ---> **C_L** $(C_D)_{pressure}$
* **M** model ---> Shock location, B.L./Shock wave interaction
  lam. Bubble , T.E. separation , L.E. peak , ...
* **Tw** ---> Equilibrium
  (B.L. information not exploited here)
* **Wake** ---> **C_D** (Pt Ps and Tt probes, 400 pts in a wake)
  B.L./Shock wave interaction

Transition Detection in a Transonic Cryogenic Tunnel

Measure

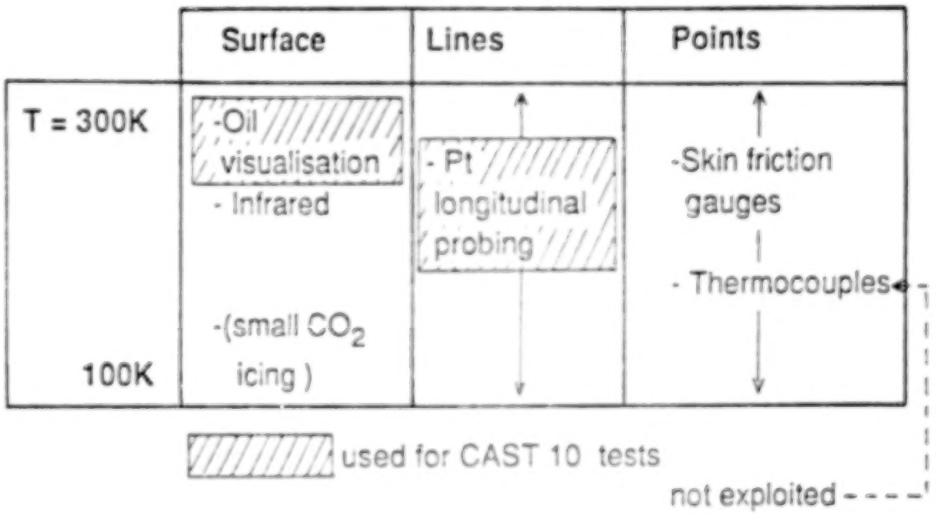

Identification

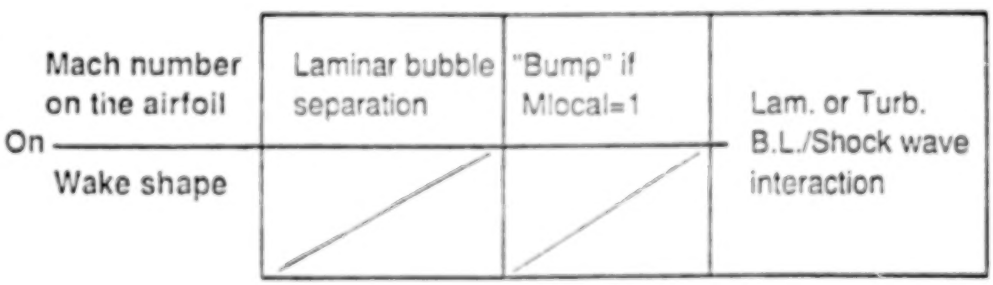

Estimation

- Aerodynamic coefficients $C_D(Re)$, $C_L(Re)$
- T.N. / T.D. comparisons
- Experiment / calculation comparisons

Reynolds Number Effects

α =-0.25°
M = 0.73

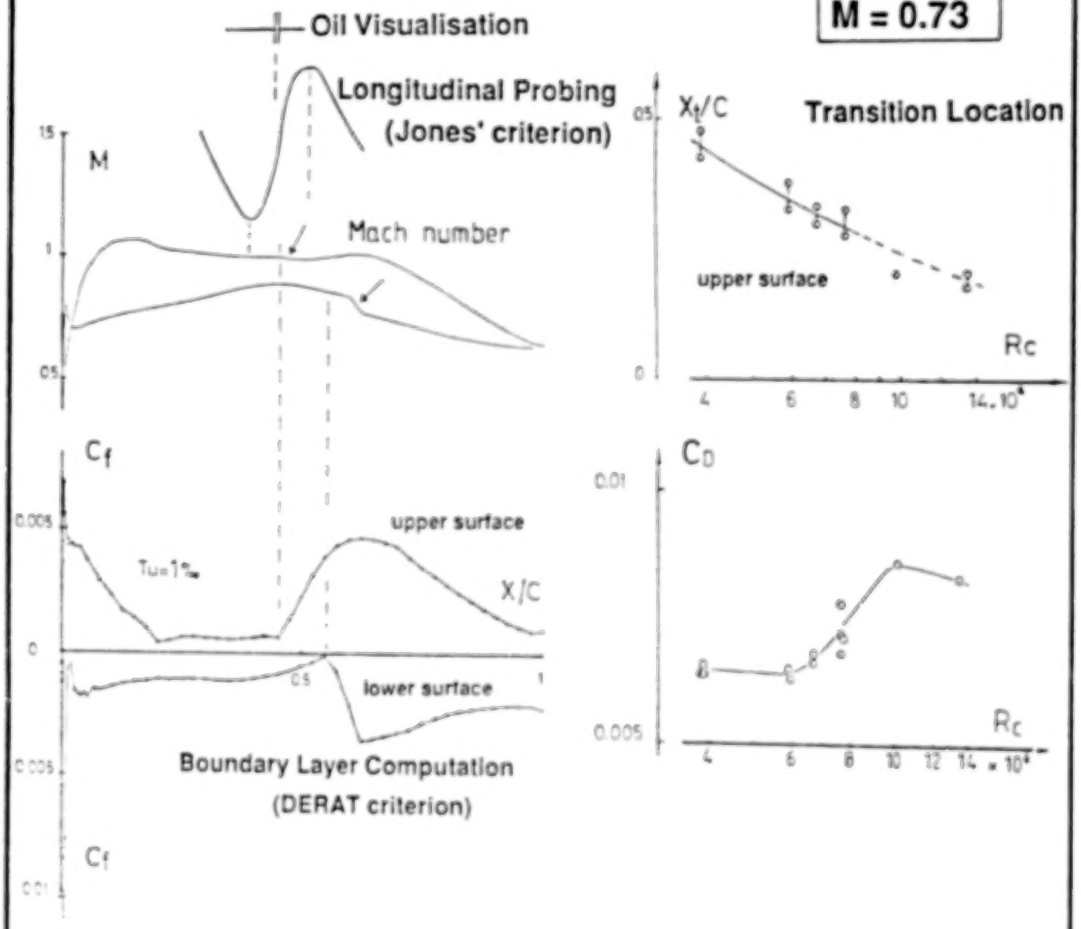

* Good correlation of the estimated transition locations
  from : - oil visualisation
  - longitudinal probing
  - local Mach number distortion
  - computation

* The transition location moves with the Reynolds number
  - regularly on the upper surface
  - suddenly on the lower surface (60%--->L.E. for $Rc=7.10^6$)

* These transition displacements explain the $C_D(Re)$ evolutions
  - direct Re effect : (Re ↗) ---> (C_D ↘)
  -indirect Re effect : (Re ↗) ---> (Xt/C ↘) ---> (C_D ↗)

Natural Transition

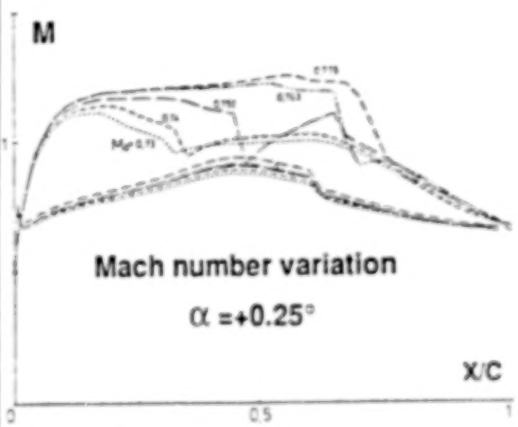

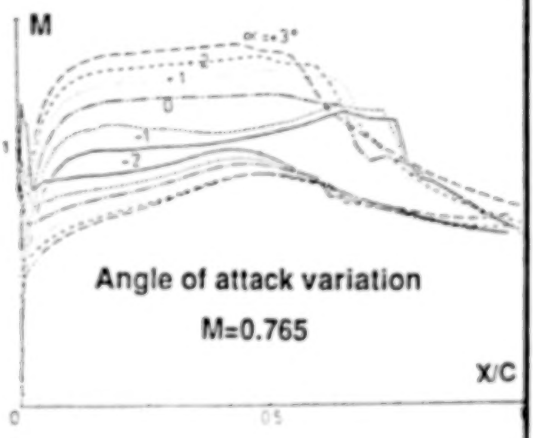

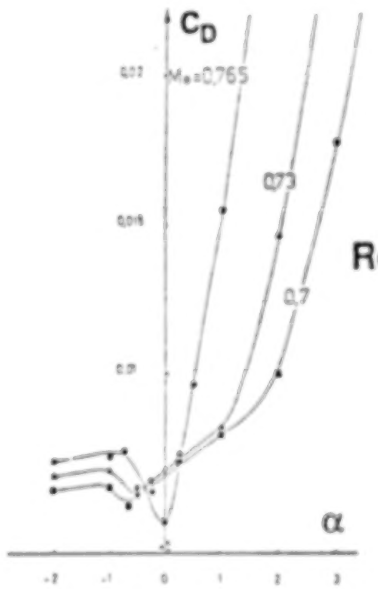

Rc = 4 .10^6

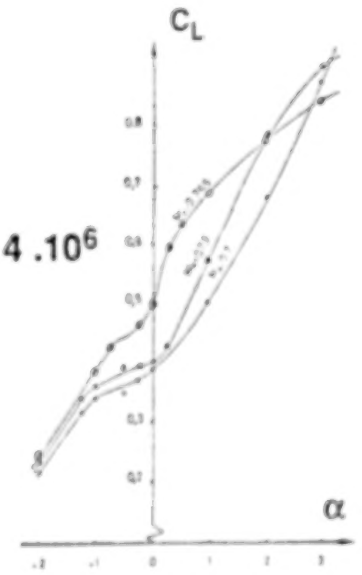

*Unusual $C_L(\alpha)$ and $C_D(\alpha)$ evolutions at Rc=4 .10^6 due to transition displacements

	upper surface	lower surface
α<-1°	lam.	Peak at the L.E.
α=0°	(turb.)	
α> 0°	lam.	60%

(must be examined for each Mo)

* + Classical effects of shock wave, and T.E. separation

T.N / T.1/2D. / T.D. Comparison

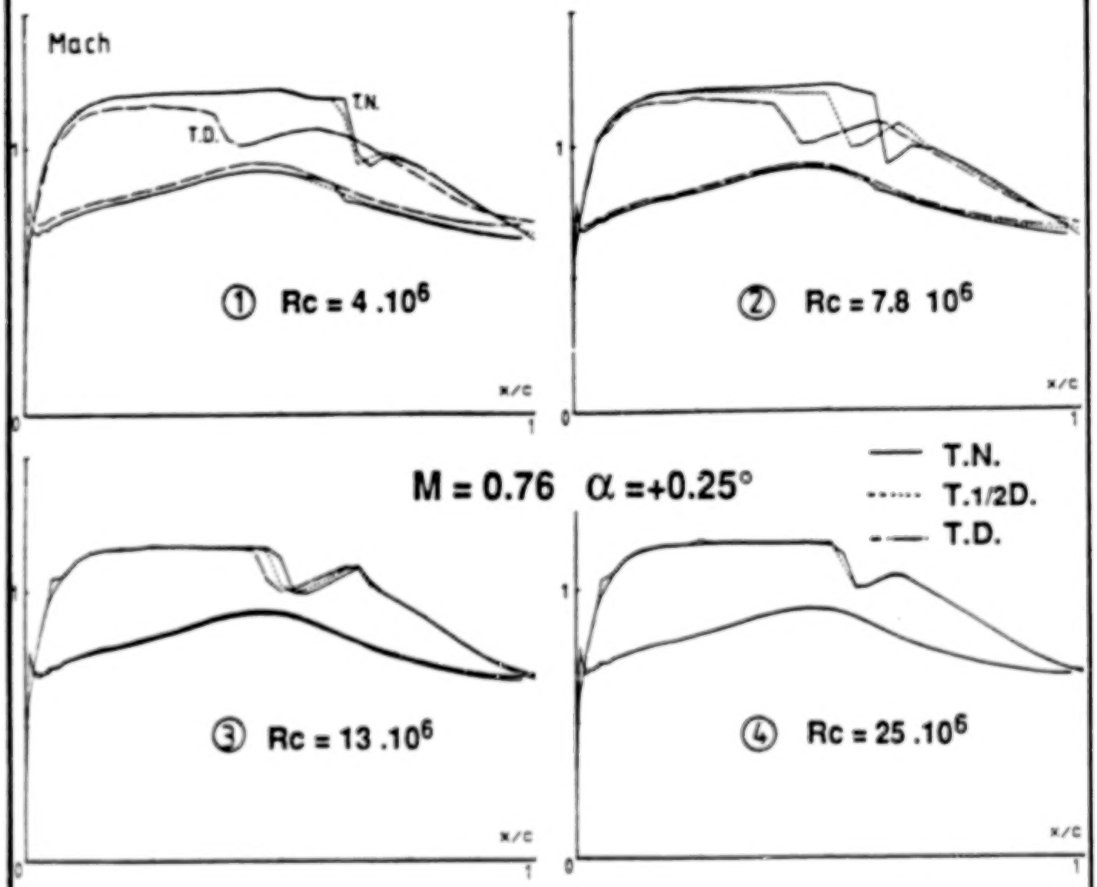

* At low Re : very different

* T.1/2D. upper surface = T.N.
lower surface = T.D.
? —— NO
upper/lower S. coupling

* Shock wave location

with Re

* Transition T.N.
L.E. | <—— Xt/C with Re

* At high Re : T.N. = T.D.

CAST 10 Airfoil Characteristics

$Rc = 4 .10^6$

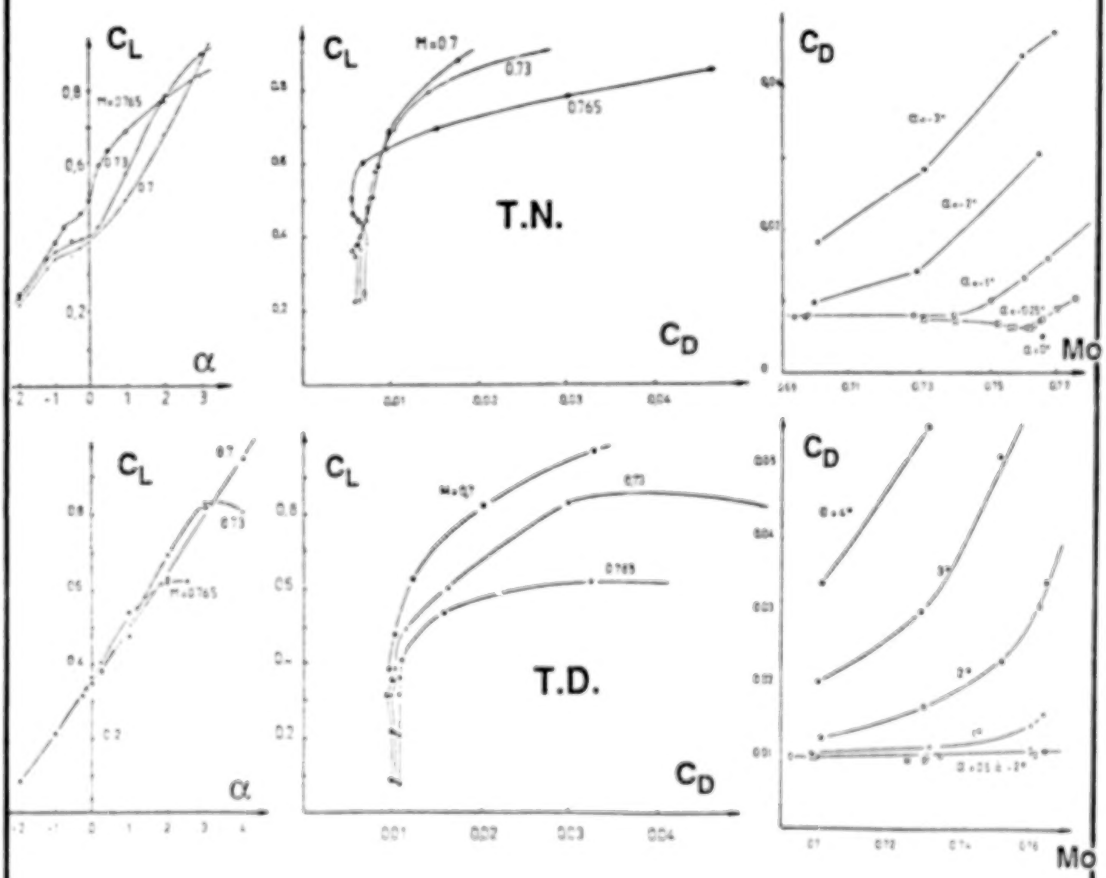

* Very different results with boundary layer conditions
* Smoother curves in T.D.
* The divergence Mach number is not very affected but, C_D levels are different
* $(C_L)_{max}$ is higher in T.N.
* Typical $C_L(C_D)$ laminar airfoil shape (M=0.765)
* (C_L / C_D) ratio higher in T.N.

Aerodynamic Coefficient Evolutions with the Reynolds Number

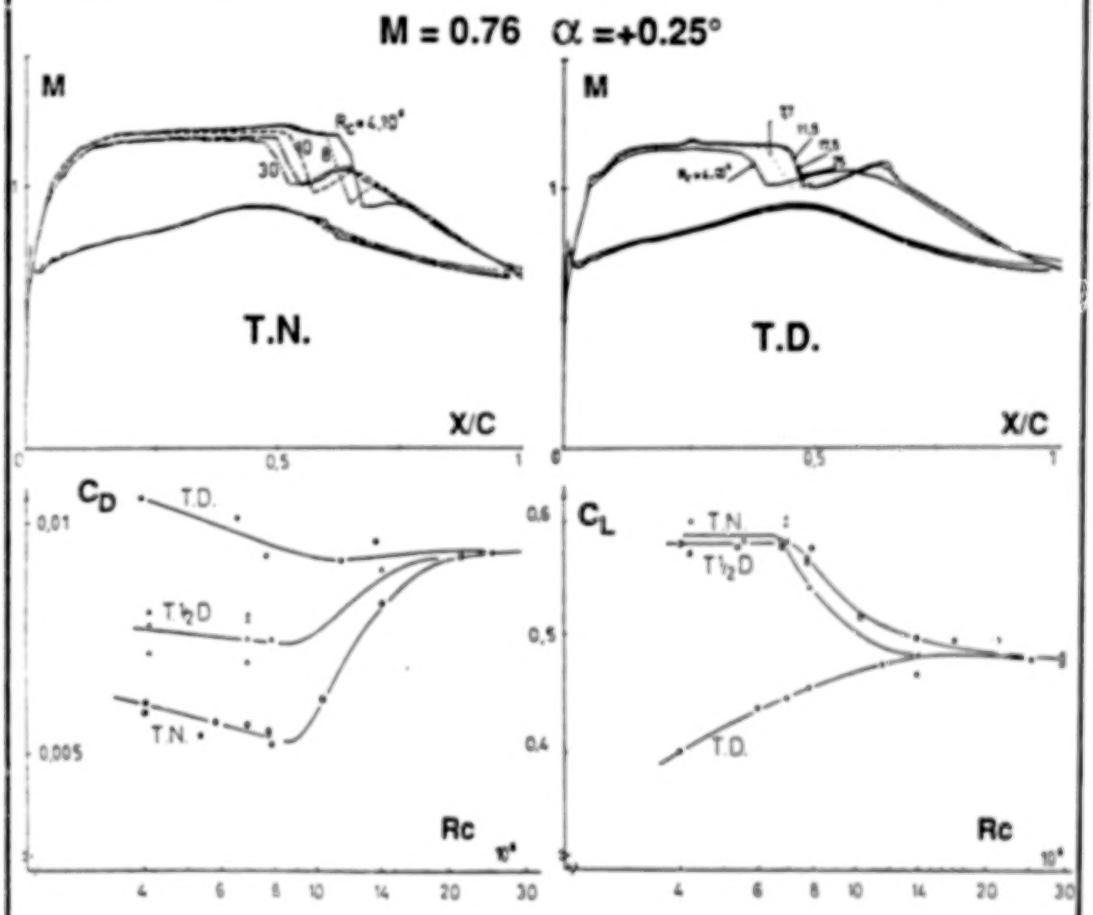

* Comparison of (T.N. / T.1/2D. / T.D.)
  - precises the transition motion in T.N. ,
  - precises the C_D and C_L evolutions ,
  - partly dissociates what is due to upper and lower surfaces
  - gives confidence in the results

* **The CAST 10 airfoil is still laminar at $Rc = 8 .10^6$ this must be considered as a success for T2 performances**

* **At $Rc \geq 20 .10^6$, transition is near the L.E.**

Airfoil Performances

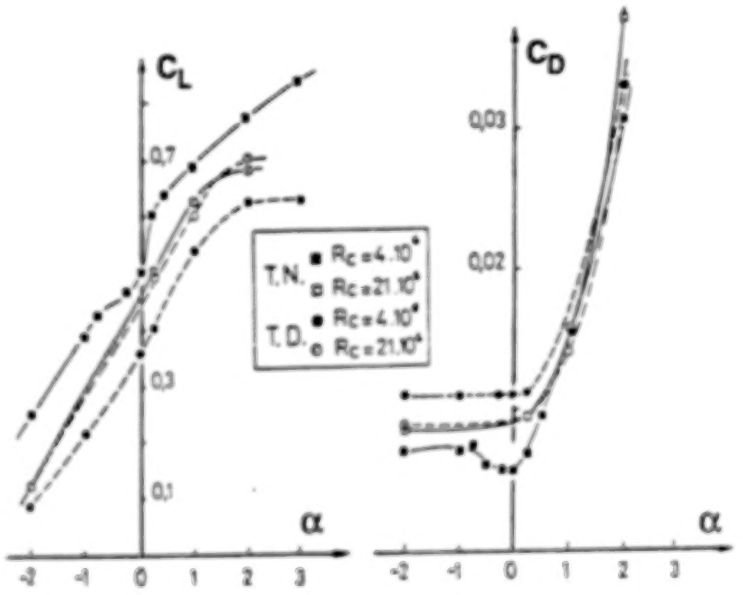

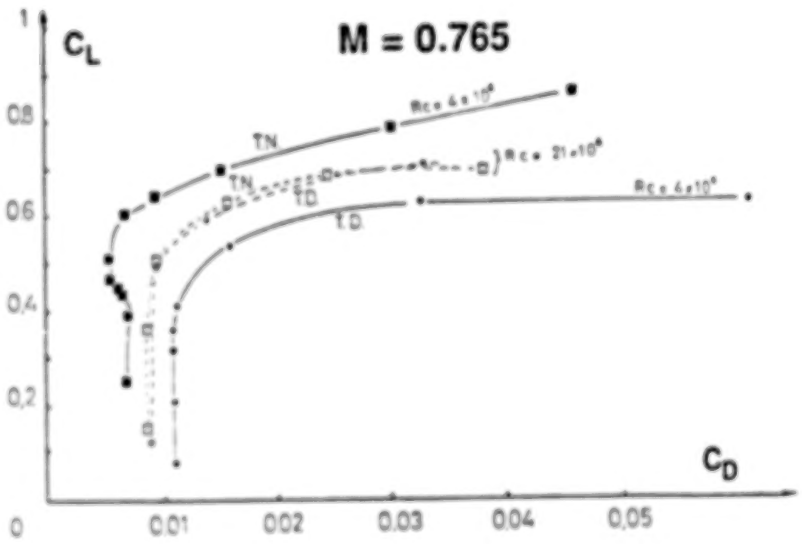

* High airfoil performances in laminar flow

* Inverse evolutions with the Reynolds number in T.N. and T.D

* Same results at Rc= 20 .10^6

Conclusions

- **Good model quality** (necessary for T.N. measurements)

* T2 tests

- **General characteristics of the CAST 10 airfoil**
  (M , α , Rc , Free/Fixed transition)

- **Fundamental studies on Reynolds number effects**
  - The T.N. and T.D. evolutions are very different
  - Comprehension of phenomenon in T.N.
  - Interest of the laminar airfoil

- **Analysis of some special points**
  - Tw / Taw effects
  - Thermal equilibrium
  - Estimation of the transition location under cryogenic operation
  - Cross control for Rc (P,T)

- **Good T2 cryogenic operation**
  - Adaptive wall functioning = T.amb.
  - Laminar studies : O.K. for Rc $\leq 8.10^6$
    pbs at higher Reynolds Number
  - Improvements must be done
    for moisture elimination
    for side wall boundary layer effects

* Comparison with prediction methods

----> **ONERA results** (J. Thibert)

* Comparison with others tunnel results

----> (J. Thibert) **and** (workshop)

TEST DATA ANALYSIS
AND
THEORY - EXPERIMENT COMPARISONS

J. J. THIBERT
TRANSPORT AIRCRAFT DIVISION
AERODYNAMICS DEPARTMENT
ONERA (FRANCE)

ONERA / DFVLR / NASA COOPERATION

ON CRYOGENIC AND ADAPTIVE WALLS

TECHNOLOGIES FOR AIRFOIL TESTING

- OBJECTIVES

EXPERIMENTAL TEST ON THE CAST 10 AIRFOIL IN THE ONERA T2 TUNNEL IN ORDER TO PROVIDE DATA AT FLIGHT EQUIVALENT REYNOLDS NUMBER ON A SUPERCRITICAL AIRFOIL

COMPARISON OF DATA ON THE SAME MODEL IN SEVERAL WIND TUNNELS

CAST 10 AIRFOIL WORKSHOP
SUMMARY OF THE PRESENTATION

T2 TEST ANALYSIS

T2 - TCT DATA COMPARISONS

COMPUTER CODES DESCRIPTION

THEORY - EXPERIMENT COMPARISONS

CONCLUSION

T2 TEST ANALYSIS

-- TRANSITION EFFECT

$M = 0.765 \quad Re = 4 \times 10^6$

-- REYNOLDS NUMBER EFFECT

$M = 0.765 \quad \alpha = 0.25$

-- TRANSITION EFFECT

$M = 0.765 \quad Re = 20 \times 10^6$

-- MACH NUMBER EFFECT

fixed transition

$Re = 25 \times 10^6 \quad \alpha = 0.25$

-- REYNOLDS NUMBER EFFECT

$M = 0.73 \quad \alpha = 0.25$

CAST 10 AIRFOIL MODEL

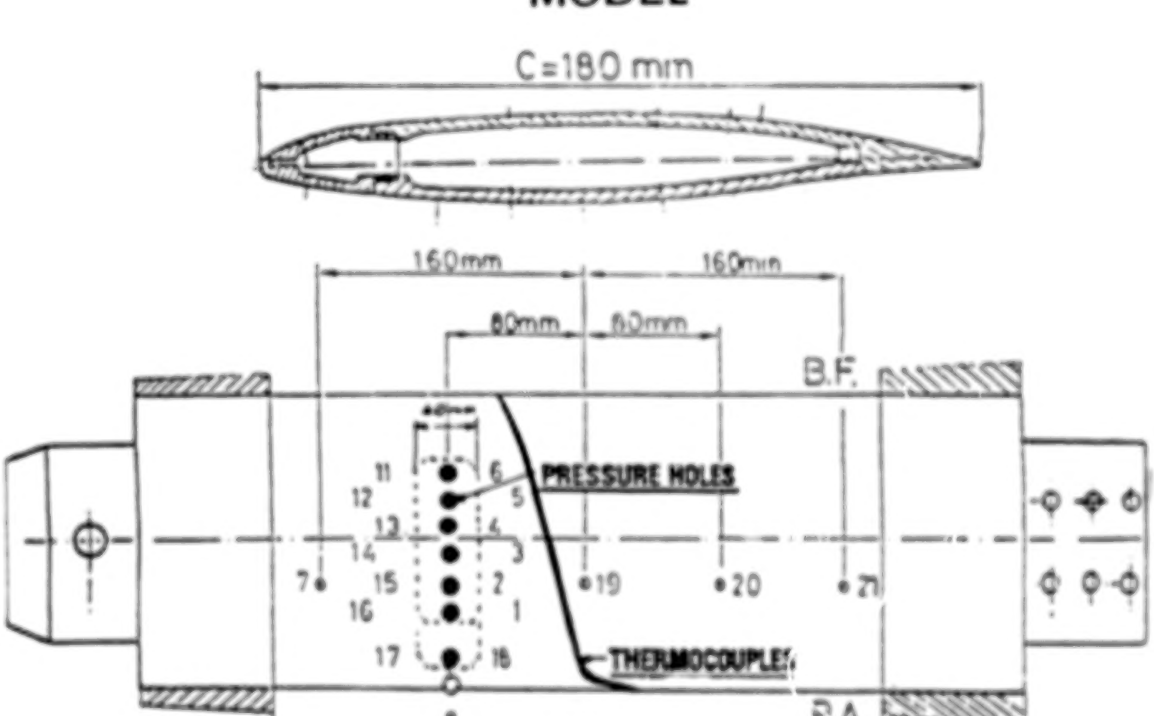

TRANSITION EFFECT

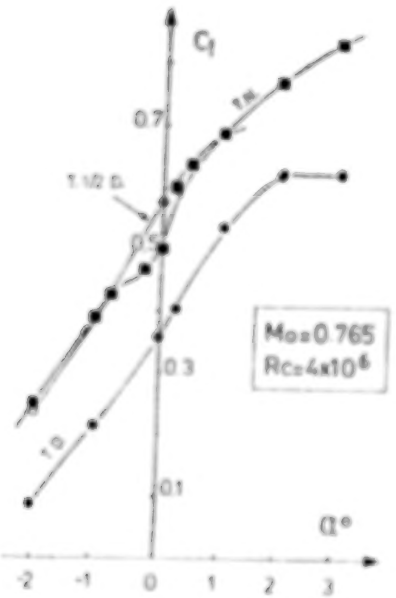

TRANSITION EFFECT

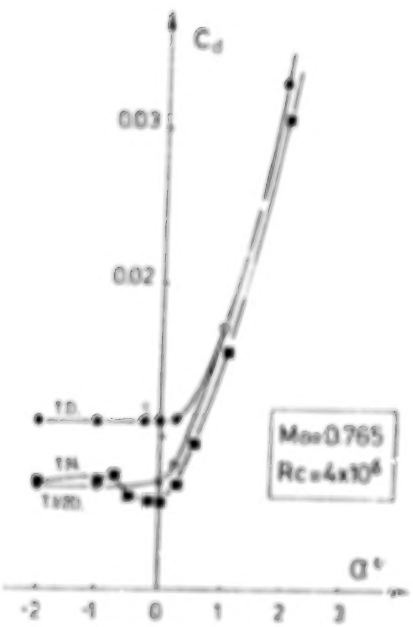

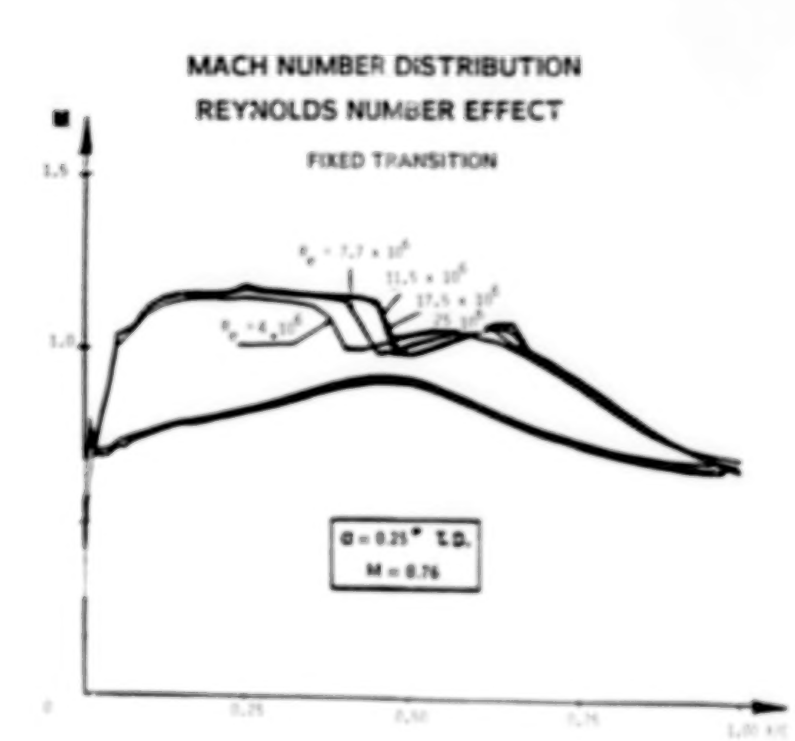
MACH NUMBER DISTRIBUTION
REYNOLDS NUMBER EFFECT
FIXED TRANSITION
M
1.5
1.0
α = 0.25° T.D.
M = 0.76

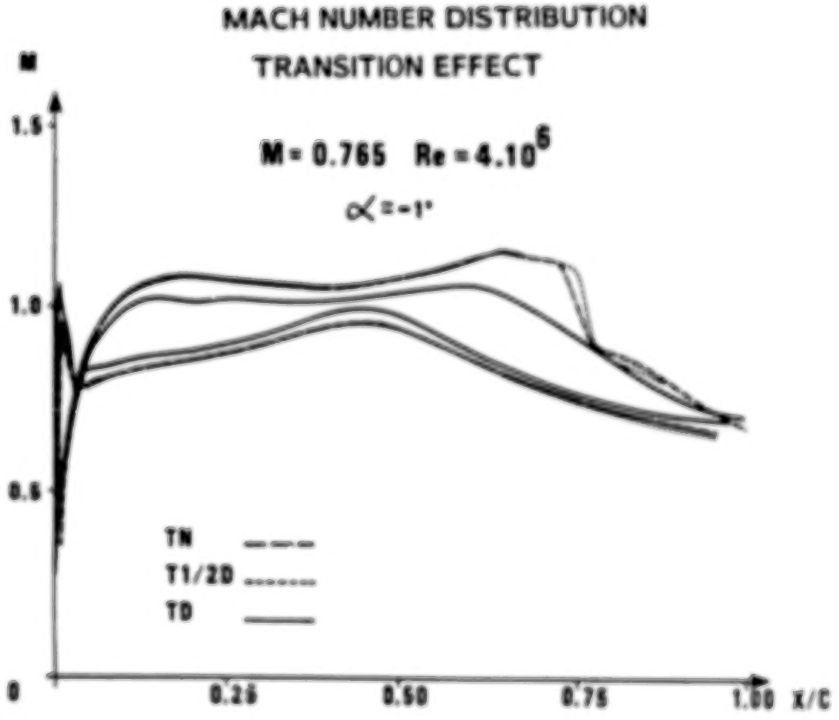
MACH NUMBER DISTRIBUTION
TRANSITION EFFECT
M
M = 0.765 Re = 4.10^6
α = -1°
1.5
1.0
0.5
0
TN
T1/2D
TD
0.25
0.50
0.75
1.00 X/C

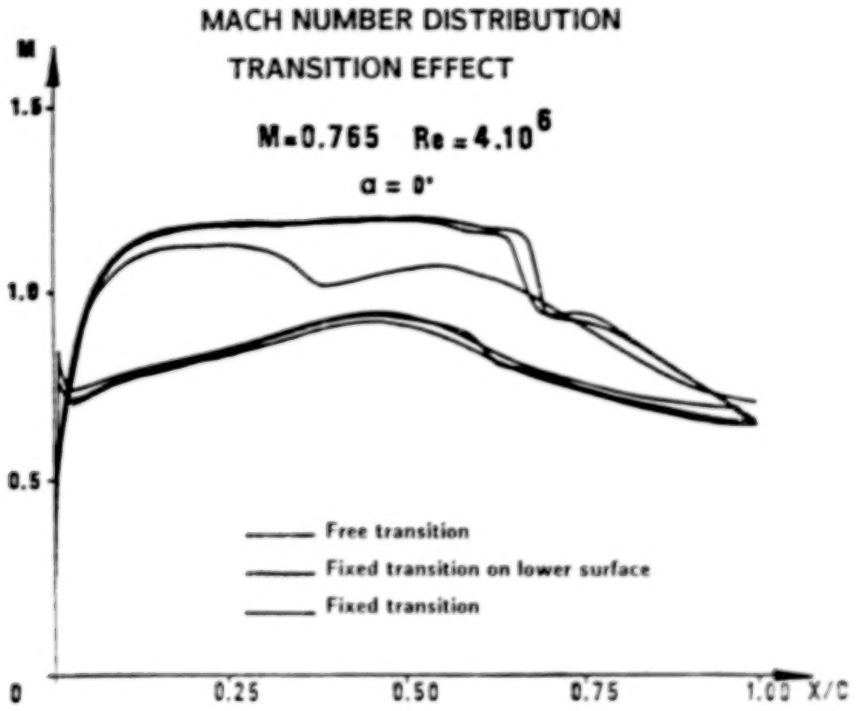
MACH NUMBER DISTRIBUTION
TRANSITION EFFECT
M=0.765 Re = 4.10^6
α = 0°
M
1.5
1.0
0.5
0
0.25
0.50
0.75
1.00 X/C
Free transition
Fixed transition on lower surface
Fixed transition

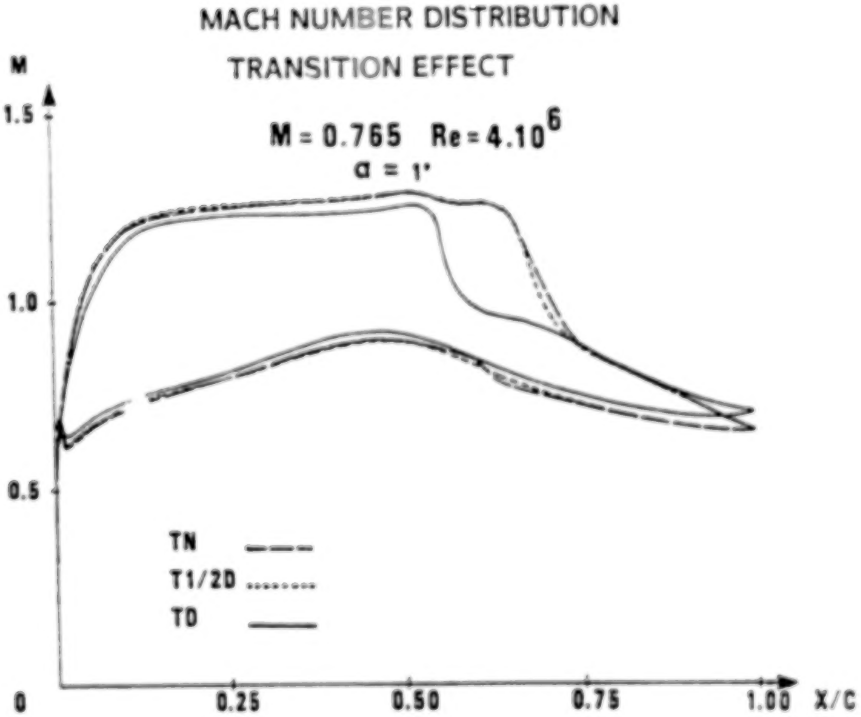
MACH NUMBER DISTRIBUTION
TRANSITION EFFECT
M = 0.765 Re = 4.10^6
α = 1°
M
1.5
1.0
0.5
0
0.25
0.50
0.75
1.00 X/C
TN
T1/2D
TD

T2 TESTS

EVOLUTION OF THE LIFT COEFFICIENT WITH THE REYNOLDS NUMBER

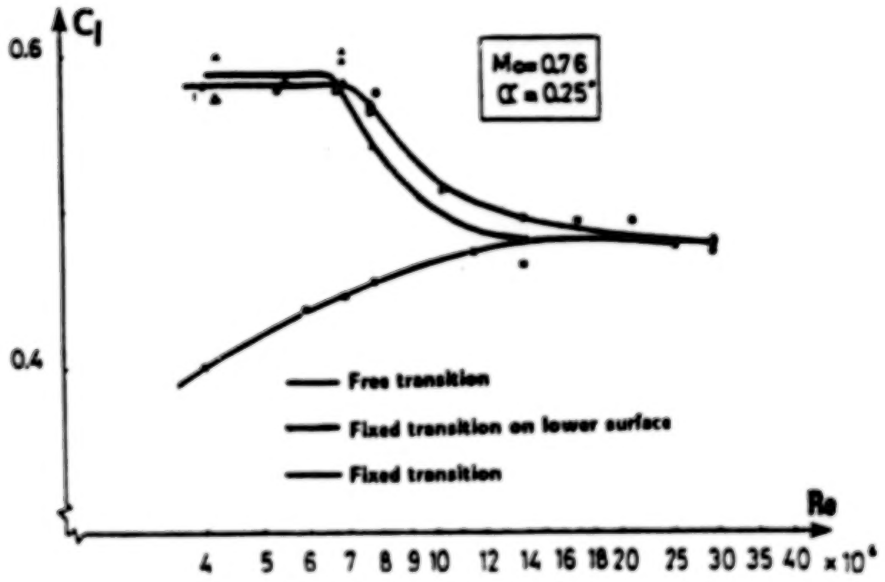

T2 TESTS

EVOLUTION OF THE DRAG WITH THE REYNOLDS NUMBER

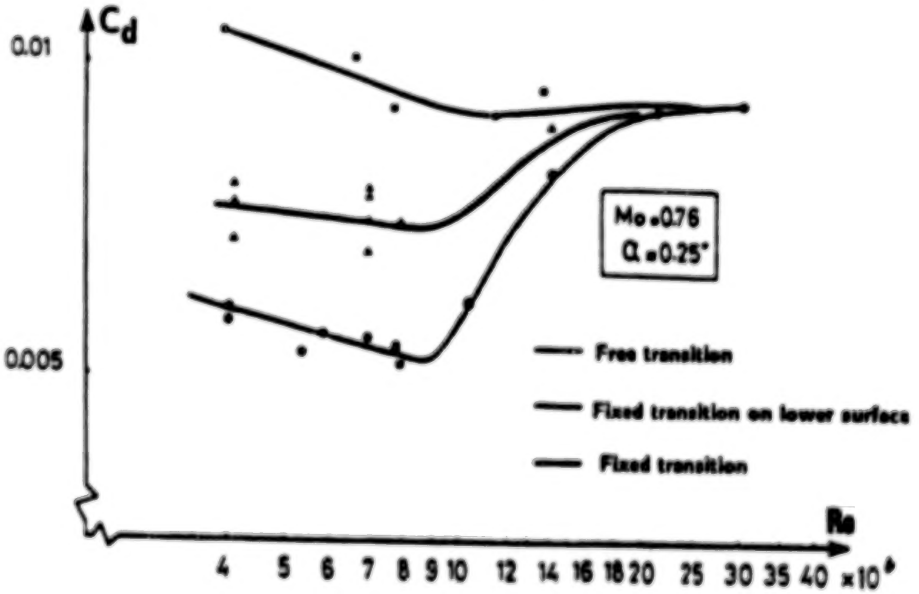

MACH NUMBER DISTRIBUTION

FREE TRANSITION - Re EFFECT

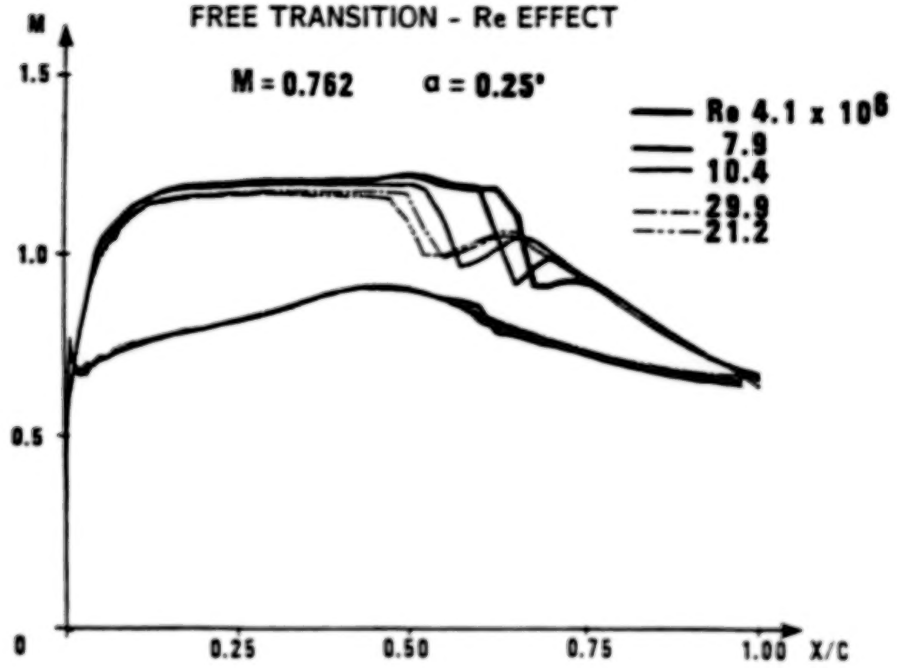

SHOCK LOCATION

TRANSITION EFFECT

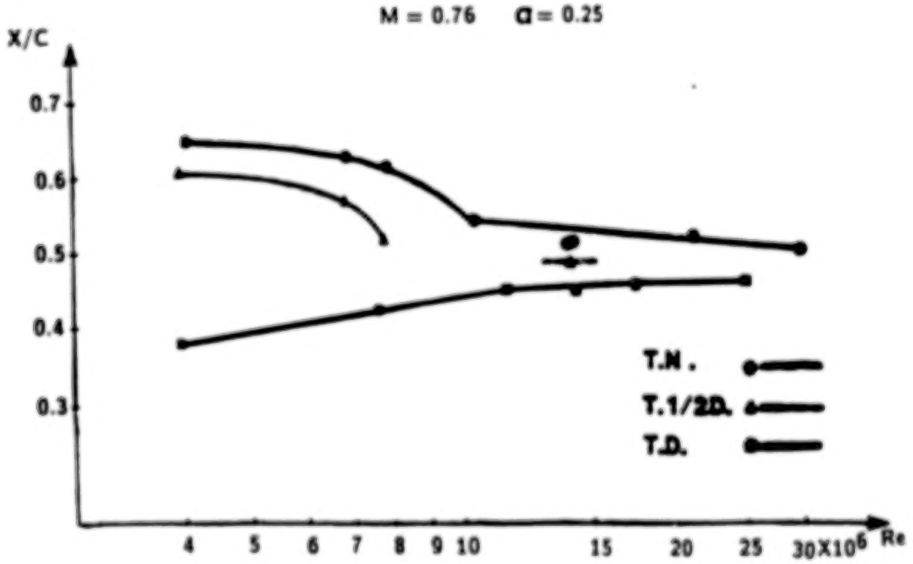

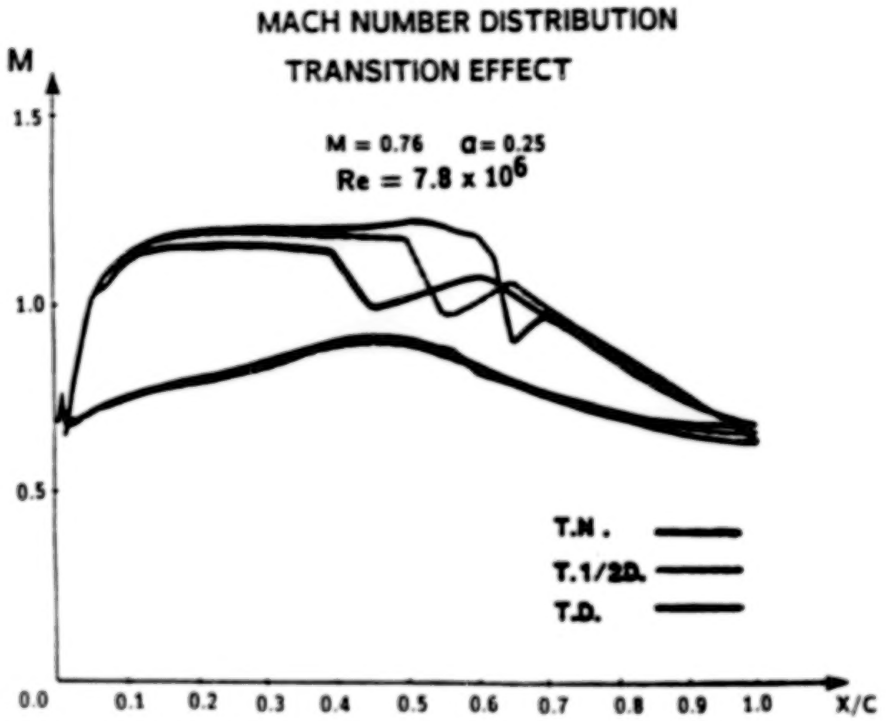
MACH NUMBER DISTRIBUTION
TRANSITION EFFECT
M
M = 0.76 α= 0.25
Re = 7.8 x 10^6
1.5
1.0
0.5
0.0
0.1
0.2
0.3
0.4
0.5
0.6
0.7
0.8
0.9
1.0
X/C
T.N.
T.1/2D.
T.D.

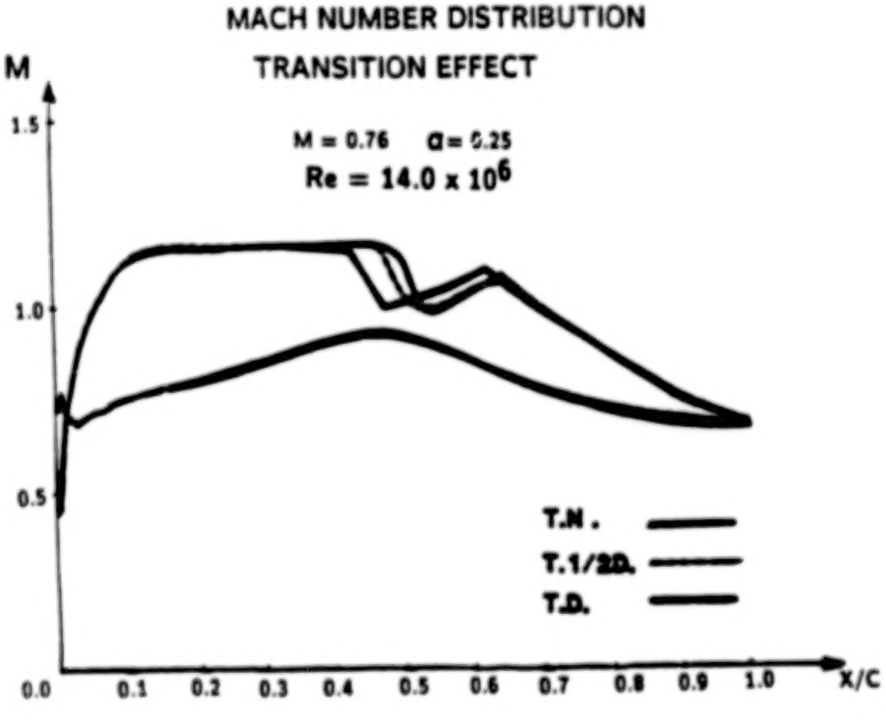
MACH NUMBER DISTRIBUTION
TRANSITION EFFECT
M
M = 0.76 α= 0.25
Re = 14.0 x 10^6
1.5
1.0
0.5
0.0
0.1
0.2
0.3
0.4
0.5
0.6
0.7
0.8
0.9
1.0
X/C
T.N.
T.1/2D.
T.D.

REYNOLDS NUMBER EFFECT
M = 0.765
FREE TRANSITION

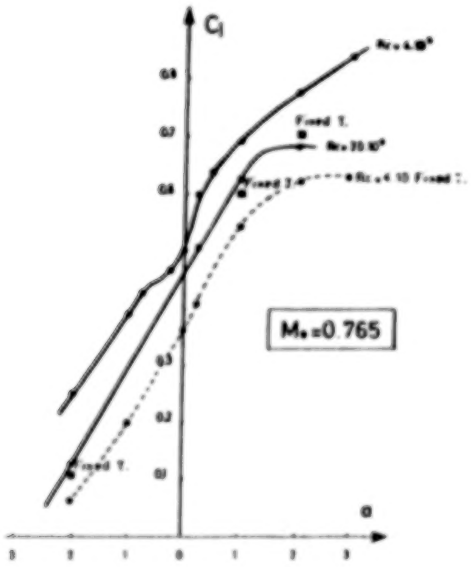

REYNOLDS NUMBER EFFECT
M = 0.765
FREE TRANSITION

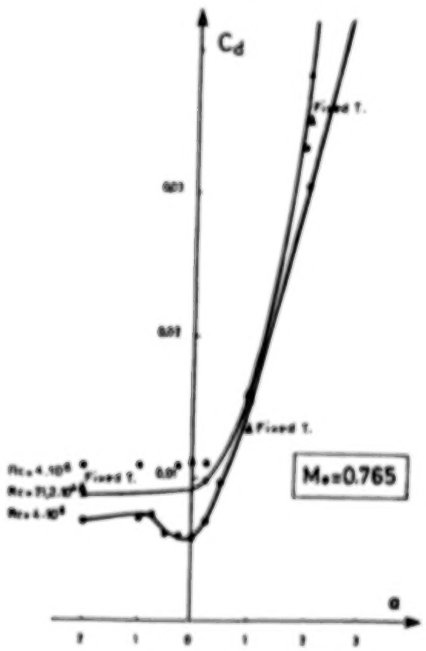

T2 T.N. M=0.765 RE=21.106

NUM	MACH	ALPHA	RE	CZ	CX	CM
121	.764	-2.00	21.3	.110	.00870	-.07500
77	.762	.25	21.2	.497	.00930	-.07500
101	.762	1.00	21.2	.620	.01480	-.08100
116	.769	2.00	21.3	.675	.04050	-.07600

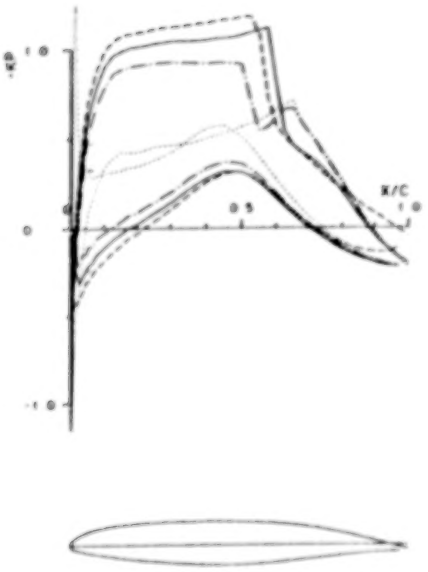

T2 T.D. M=0.765 RE=21.106

NUM	MACH	ALPHA	RE	CZ	CX	CM
315	.765	-2.00	20.9	.108	.00910	-.07500
311	.764	1.00	21.2	.597	.01360	-.07800
320	.767	2.00	21.0	.692	.03500	-.07600

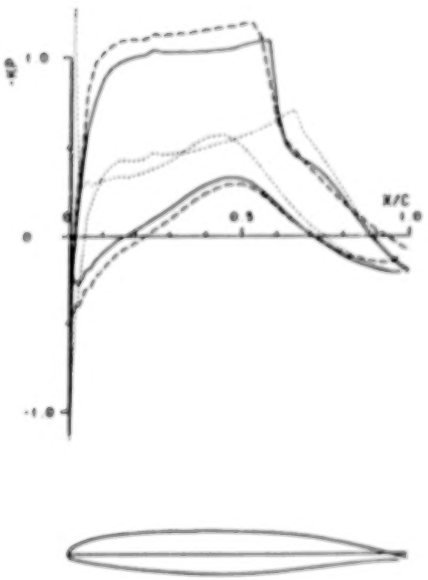

T2 T.N.-T.D. M=.765 RE=21.106 AL=-2

	NUM	MACH	ALPHA	RE	CZ	CX	CM
TD	315	.765	-2.00	20.9	.108	.00910	-.07500
TN	121	.764	-2.00	21.5	.110	.00870	-.07500

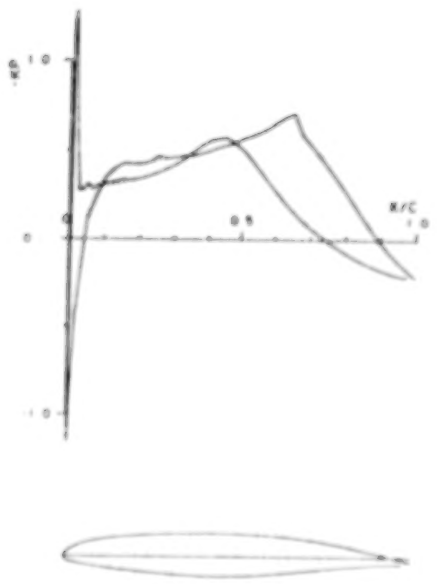

T2 T.N.-T.D. M=.765 RE=21.106 AL=+1

	NUM	MACH	ALPHA	RE	CZ	CX	CM
TD	311	.764	1.00	21.2	.597	.01360	-.07800
TN	101	.762	1.00	21.2	.620	.01480	-.08100

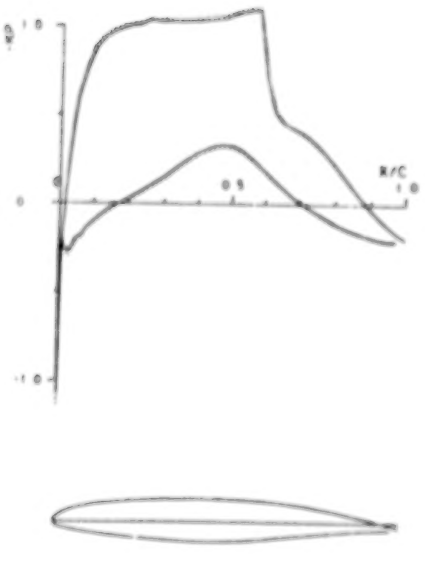

T2 T.N.-T.D. M=.765 RE=21.106 AL=+2

	NUM	MACH	ALPHA	RE	CZ	CX	CM
TD	320	.767	2.00	21.0	692	03500	-.07600
TN	116	.769	2.00	21.3	675	04050	-.07600

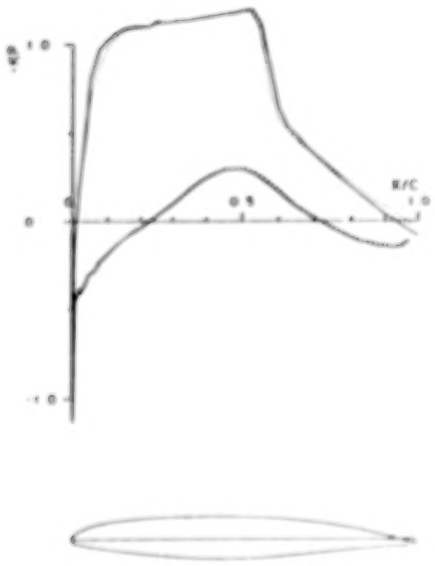

T2 EFFECT MACH EN T.D. RE=25.106 AL=0.25

	NUM	MACH	ALPHA	RE	CZ	CX	CM
———	336	.729	25	24.5	450	00870	-.06700
- - - - -	296	.760	25	25.2	478	00940	-.07000
———	332	.766	25	25.0	485	00970	-.07200
— · — · —	333	.777	25	25.3	508	01150	-.08100
— - — - —	335	.780	25	25.7	478	01660	-.08200

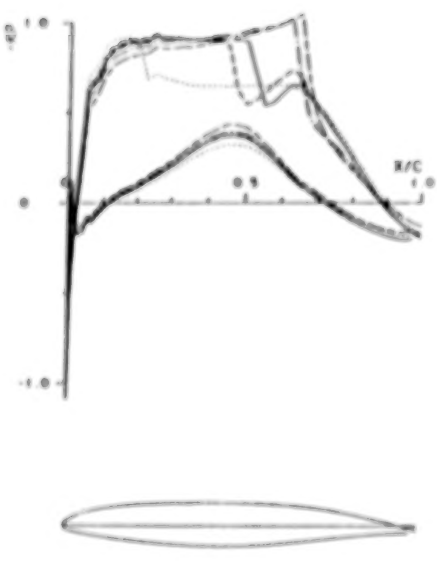

LIFT EVOLUTION WITH REYNOLDS NUMBER

$M_o = 0.73 \quad \alpha = -0.25$

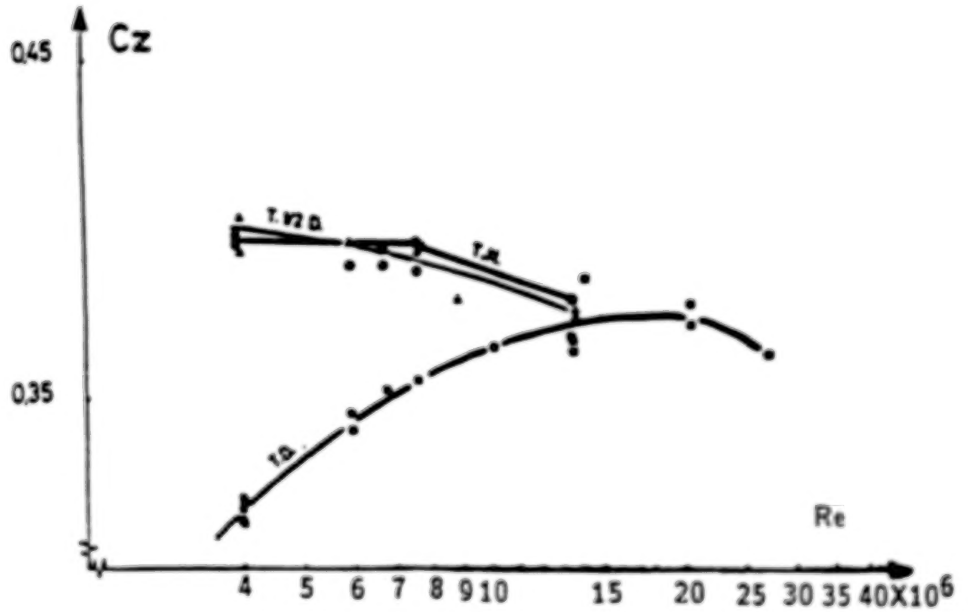

DRAG EVOLUTION WITH REYNOLDS NUMBER

$M_o = 0.73 \quad \alpha = -0.25$

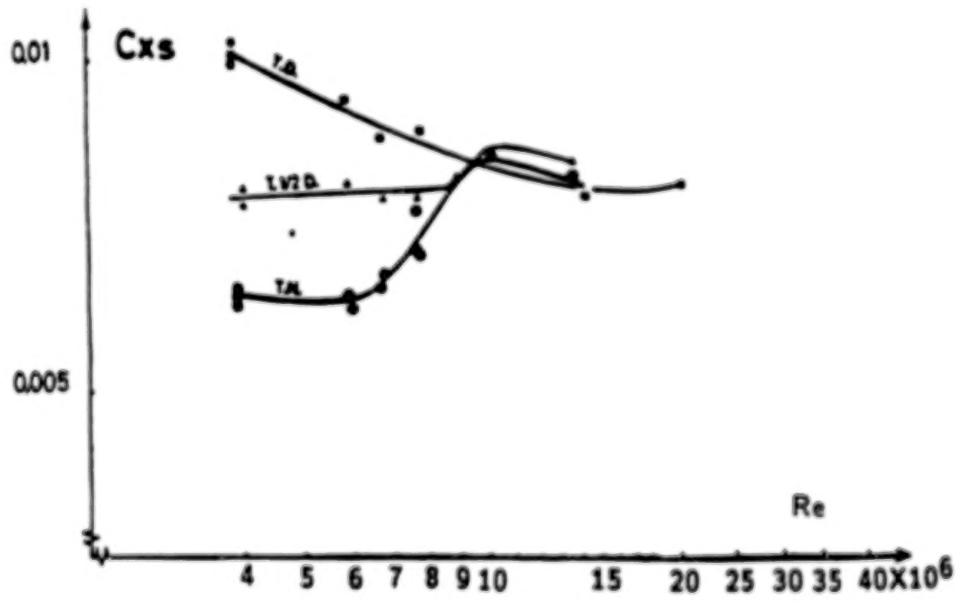

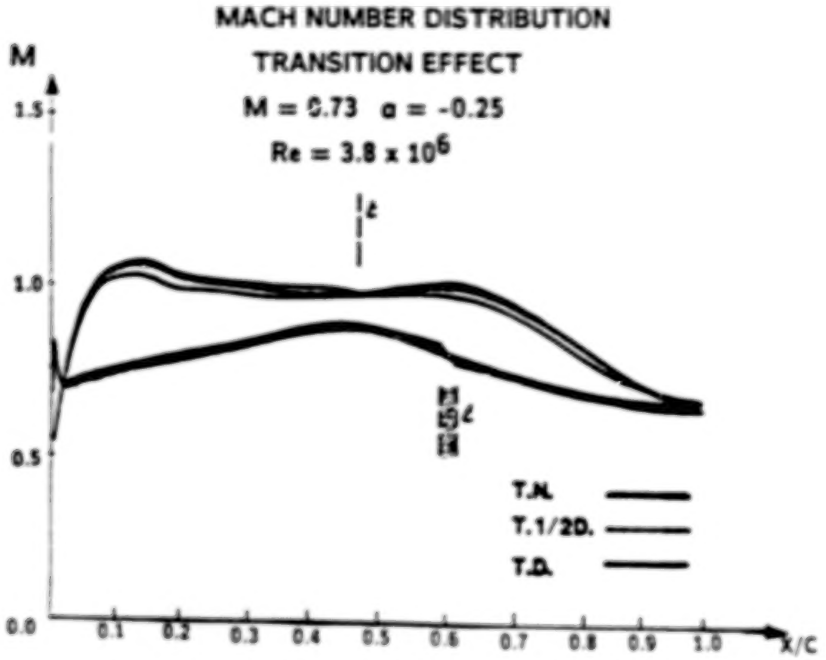
MACH NUMBER DISTRIBUTION
TRANSITION EFFECT
M = 0.73 α = -0.25
Re = 3.8 x 10^6
M
1.5
1.0
0.5
0.0
T.N.
T.1/2D.
T.D.
0.1
0.2
0.3
0.4
0.5
0.6
0.7
0.8
0.9
1.0
X/C

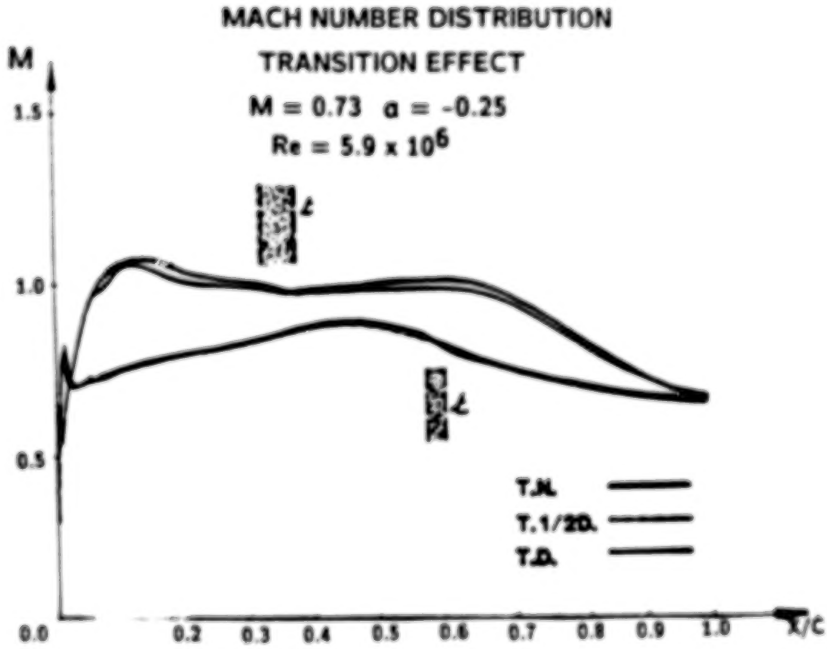
MACH NUMBER DISTRIBUTION
TRANSITION EFFECT
M = 0.73 α = -0.25
Re = 5.9 x 10^6
M
1.5
1.0
0.5
0.0
T.N.
T.1/2D.
T.D.
0.2
0.3
0.4
0.5
0.6
0.7
0.8
0.9
1.0
X/C

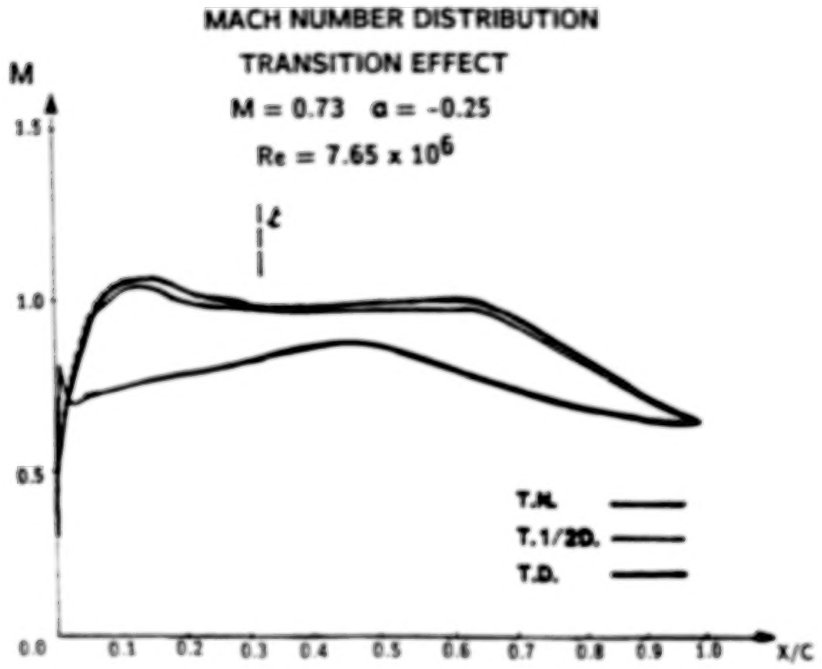
MACH NUMBER DISTRIBUTION
TRANSITION EFFECT
M = 0.73 α = -0.25
Re = 7.65 x 10^6
M
1.5
1.0
0.5
0.0
0.1
0.2
0.3
0.4
0.5
0.6
0.7
0.8
0.9
1.0
X/C
T.N.
T.1/2D.
T.D.

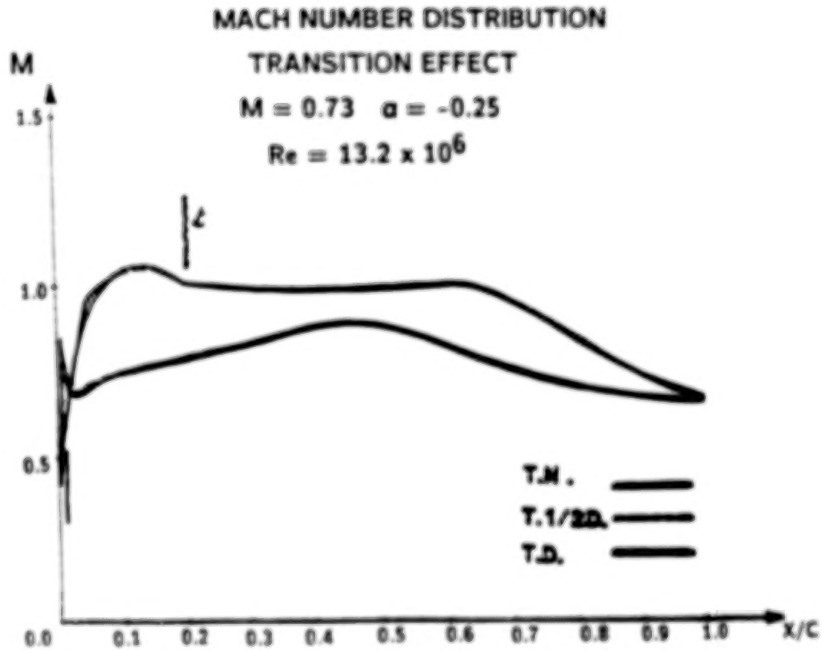
MACH NUMBER DISTRIBUTION
TRANSITION EFFECT
M = 0.73 α = -0.25
Re = 13.2 x 10^6
M
1.5
1.0
0.5
0.0
0.1
0.2
0.3
0.4
0.5
0.6
0.7
0.8
0.9
1.0
X/C
T.N.
T.1/2D.
T.D.

T2 - TCT DATA COMPARISON

- M = 0.765 Re = 4×10^6
  fixed and free transition
  Total forces
  Pressure
- REYNOLDS NUMBER EFFECT
  M = 0.76 $\alpha = -0.25°$

CAST 10 MODEL
AND WIND TUNNEL CHARACTERISTICS

- MODEL

  CRYOGENIC TECHNOLOGY

  CHORD : 180 mm

  POSSIBILITY OF MOUNTING IN THE T2, TWB, TCT TUNNELS

  EQUIPMENT : 103 PRESSURE HOLES (Ø 0.1 mm AND 0.3 mm)
  19 THERMOCOUPLES

- WIND TUNNEL CHARACTERISTICS

TUNNEL	WALLS	TEST SECTION	Re x 10^{-6}
T2	ADAPTIVE	0.4 x 0.4 m^2	4 - 30
TWB	SLOTTED	0.34 x 0.6 m^2	4 - 12
TCT	ADAPTIVE	0.2 x 0.6 m^2	4 - 45

LIFT COEFFICIENT
TRANSITION EFFECT
M = 0.765
$R_N = 4 \times 10^6$

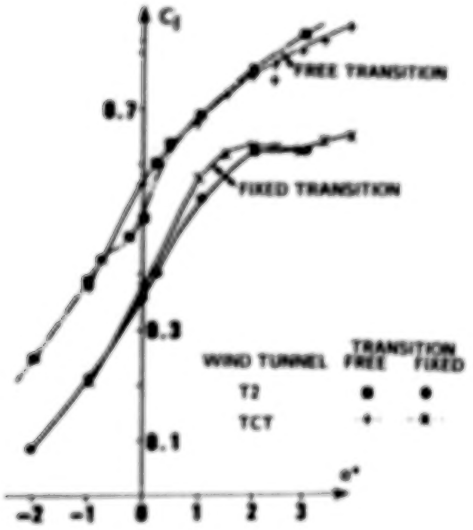

DRAG COEFFICIENT
TRANSITION EFFECT
$M_\infty = 0.765$
$R_N = 4 \times 10^6$

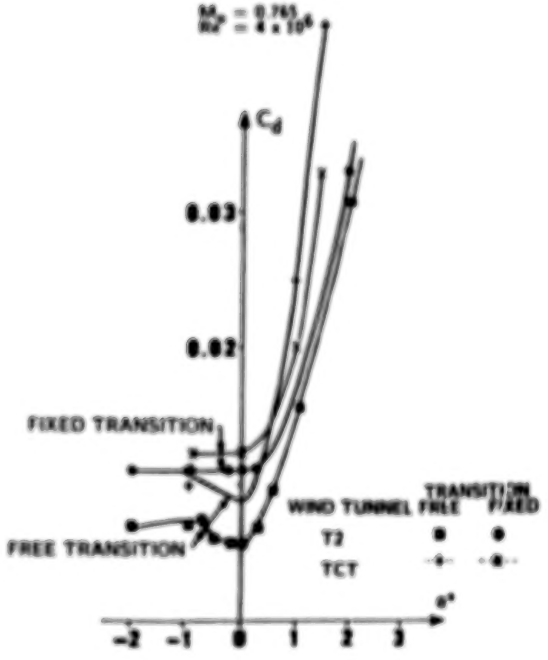

TCT T.D. M=0.765 RE=4.10⁶

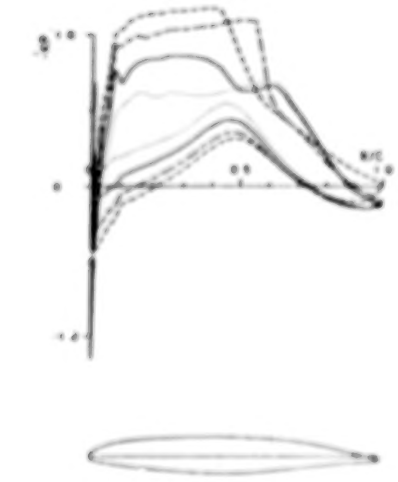

TCT T.N. M=0.765 RE=4.10⁶

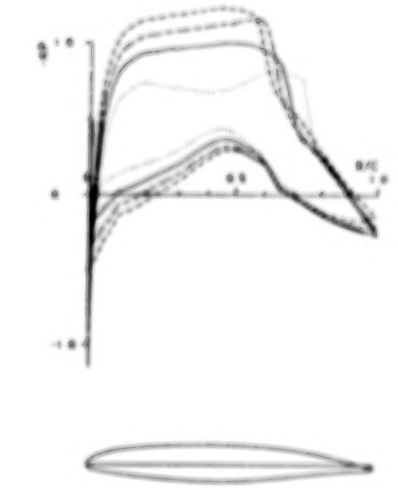

TCT T.N.-T.D. M=.765 RE=4.106 AL=-1.

	MACH	ALPHA	RE	CZ	CX	CM
Tc	.438	.771	-.99	4.0	.206	.01193	-.05952
Tv	.31269	.764	-1.02	4.0	.577	.01042	-.09748

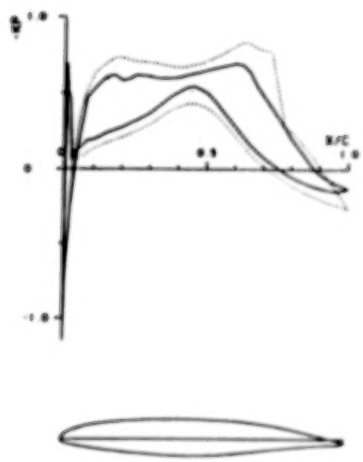

TCT T.N.-T.D. M=.765 RE=4.106 AL=0

	MACH	ALPHA	RE	CZ	CX	CM
Tc	.439	.766	.01	4.0	.378	.01197	-.05732
Tv	.31270	.765	-.02	4.0	.565	.00920	-.09794

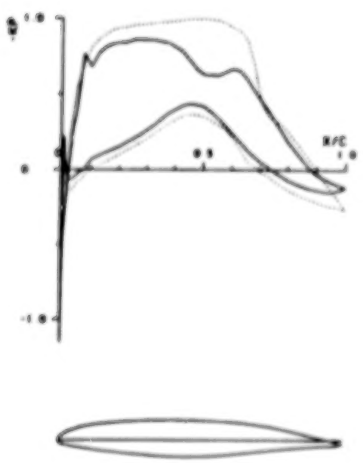

TCT T.N.-T.D. M=.765 RE=4.106 AL=-1

	NUM	MACH	ALPHA	RE	CZ	CX	CM
T6	440	.767	.98	4.0	.570	.02048	-.06661
T7N	31272	.766	.95	4.0	.675	.02453	-.09748

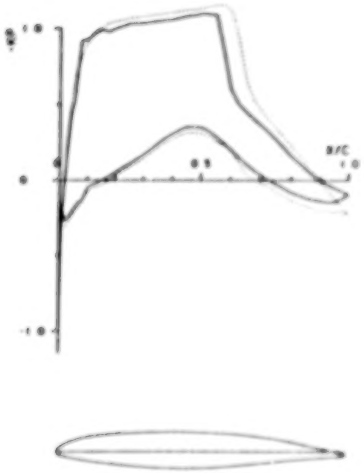

T2-TCT T.N. M=.765 RE=4.106 AL=-1

	NUM	MACH	ALPHA	RE	CZ	CX	CM
T8	24	.765	-1.00	4.1	.580	.00750	-.09900
T8T	31269	.764	-1.02	4.0	.577	.01042	-.09748

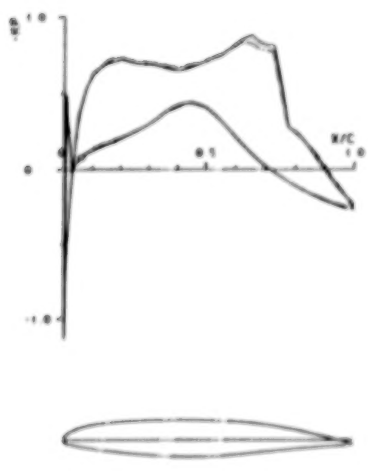

T2-TCT T.N. . M=.765 RE=4.106 AL= 0.

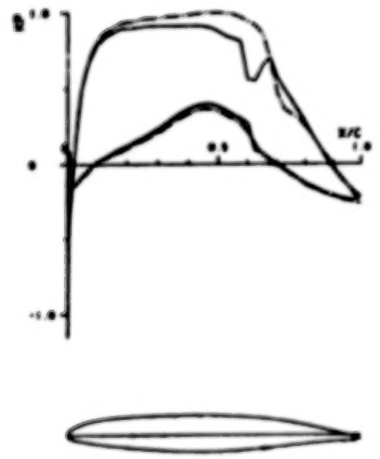

T2-TCT T.N. . M=.765 RE=4.106 AL=-1.

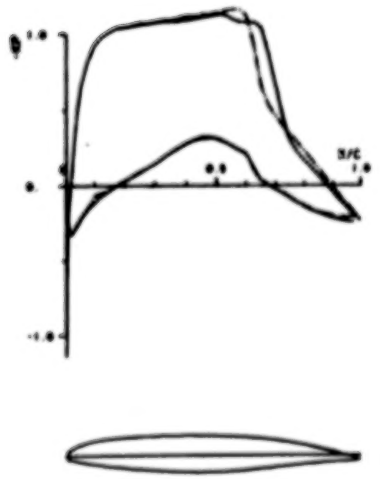

T2-TCT T.D. M=.765 RE=4.106 AL=-1.0

	NUM	MACH	ALPHA	RE	CZ	CX	CM
ZX	270	765	-1.00	40.0	.199	.01080	-.05800
ZCP	436	771	-.99	4.0	.206	.01193	-.05952

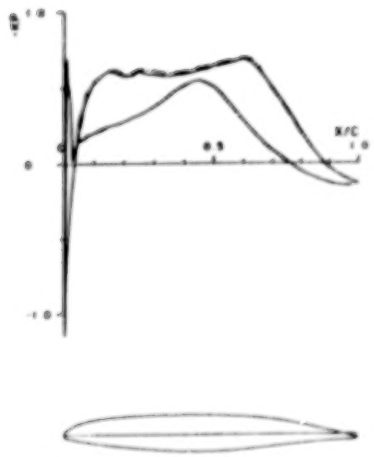

T2-TCT T.D. M=.765 RE=4.106 AL=0.0

	NUM	MACH	ALPHA	RE	CZ	CX	CM
ZX	251	762	.00	4.0	.359	.01090	-.05600
ZCP	439	766	-.01	4.0	.378	.01197	-.05732

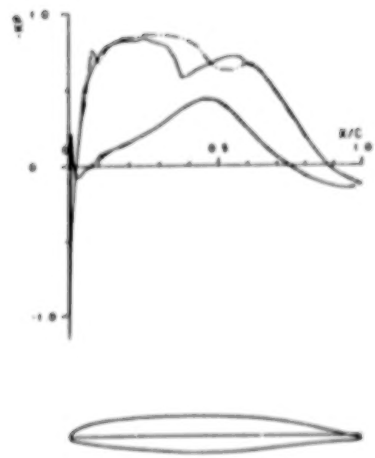

T2-TCT T.D. M=.765 RE=4.106 AL=-1.0

	NUM	MACH	ALPHA	RE	CZ	CX	cl
TZ	246	.765	1.00	4.1	.542	.01580	-.063000
TCT	440	.767	.98	4.0	.570	.02048	-.066661

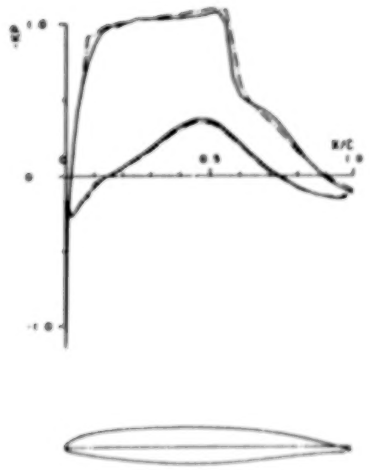

EVOLUTION OF THE LIFT COEFFICIENT
WITH THE REYNOLDS NUMBER
TRANSITION EFFECT

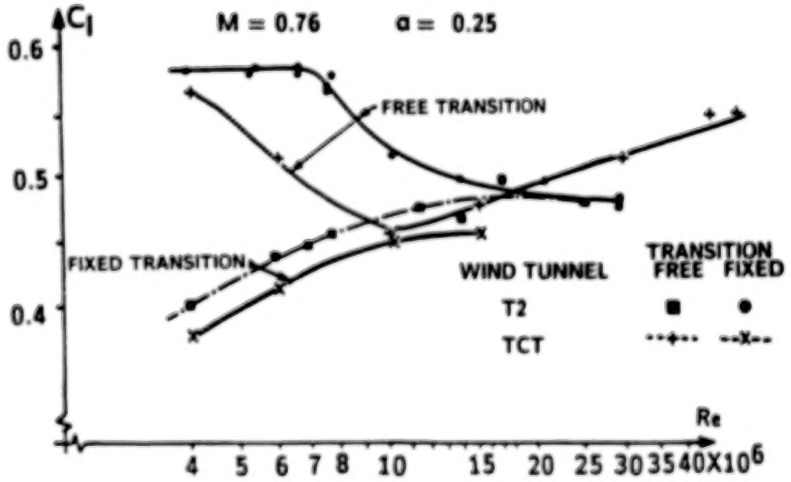

EVOLUTION OF THE DRAG WITH THE REYNOLDS NUMBER

M = 0.76 α = 0.25

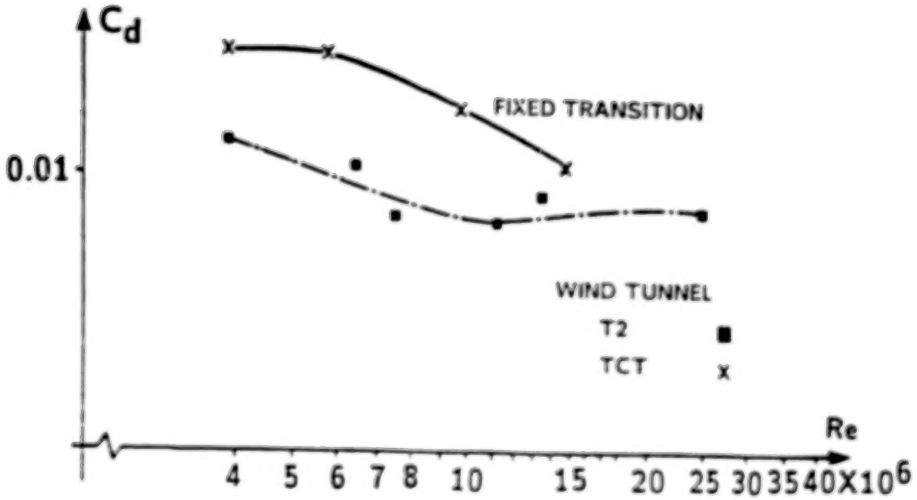

COMPUTER CODES DESCRIPTION

. POTENTIAL CODES
(finite difference)

- AP 27

Inviscid flow : Garabedian and Korn method (nonconservative)
Boundary layer : Michel method
Weak coupling
No wake computation

- VISC 05

Inviscid flow : Chattot method
Boundary layer
Strong coupling } Le Balleur method
Wake computation
Nonconservative or conservative options
C type mesh

. NAVIER STOKES CODE
(Veuillot-Cambier)

Compressible N.S equation with constant total enthalpy 3 possible turbulence models (Michel, Baldwin-Lomax, K-ℓ)
Explicit finite difference scheme
Local time step
Multigrid acceleration technique
Far field boundary conditions treatment using characteristics relations
C type mesh

THEORY - EXPERIMENT COMPARISONS

- M = 0.765 Re = 21x10^6
  Total forces
  Pressure: free transition Cl ~ 0.5
  Side wall B.L. effect simulation
- M = 0.765 Re = 25x10^6
  Pressure: fixed transition Cl ~ 0.5
- Mach number effect Re = 25x10^6
  fixed transition
  Pressure
  Total forces
- M = 0.73 Cl ~ 0.35
  fixed transition
- Reynolds number effect
  M = 0.73 α = -0.25°
  Total forces

THEORY EXPERIMENT COMPARISON

M = 0.765 Re = 21 x 10^6

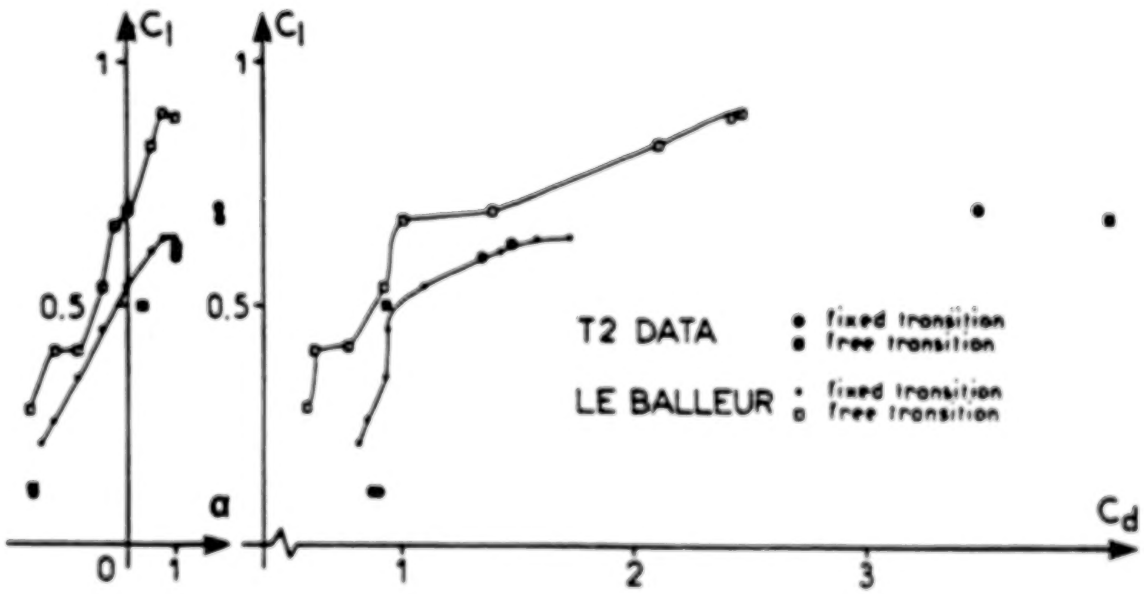

THEORY-EXPERIMENT COMPARISON

FREE TRANSITION

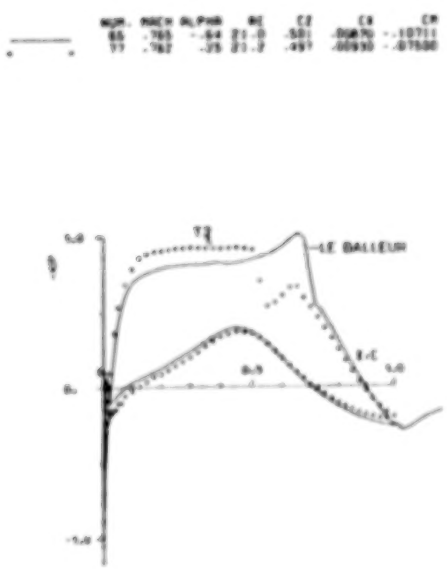

TEST - THEORY COMPARISON
FREE TRANSITION

M = 0.762 a = 0.25

Re = 21 x 10^6

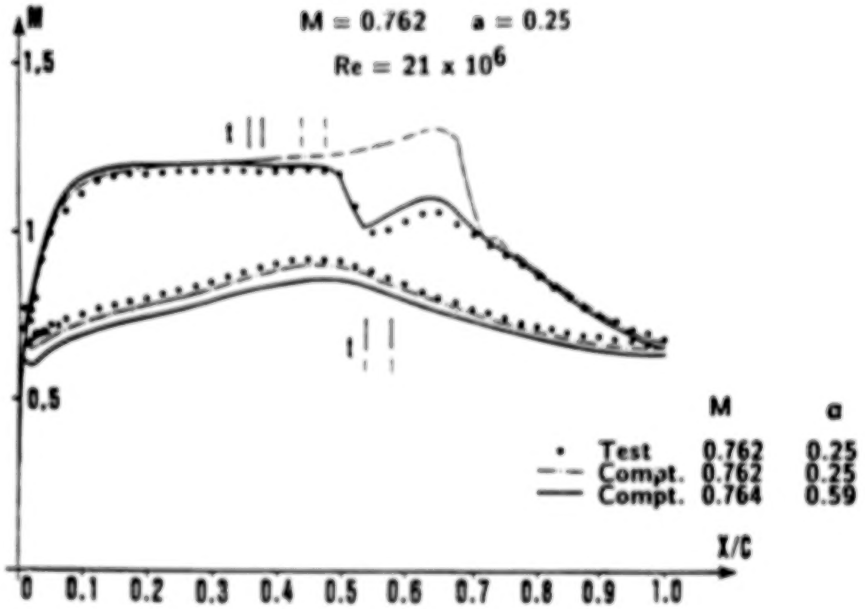

COMPUTER CODE COMPARISONS
$Re = 15 \times 10^6$

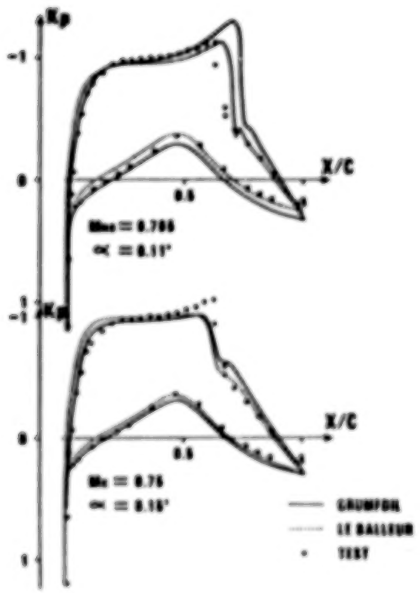

LATERAL WALL B.L.EFFECT
FIXED TRANSITION

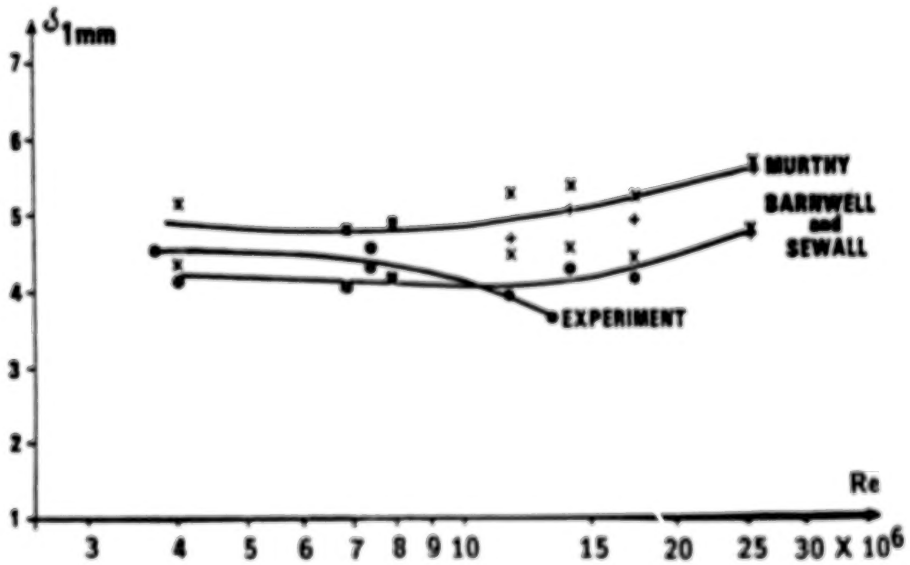

THEORY - EXPERIMENT COMPARISON

FIXED TRANSITION

	NUM.	MACH	ALPHA	RE	CZ	CX	CM
———	1	.765	.25	25.0	.481	.01279	-.09774
○ ○	332	.766	.25	25.0	.485	.00570	-.07230

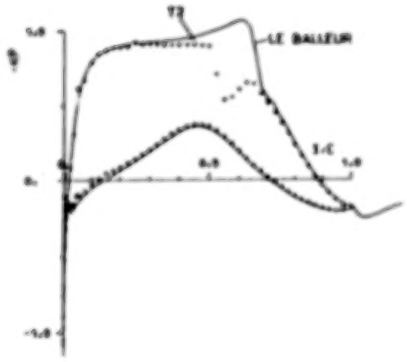

THEORY-EXPERIMENT COMPARISON

FIXED TRANSITION

	NUM.	MACH	ALPHA	RE	CZ	CX	CM
———	1	.766	.25	25.0	.484	.00590	-.09392
○ ○	332	.766	.25	25.0	.485	.00570	-.07230

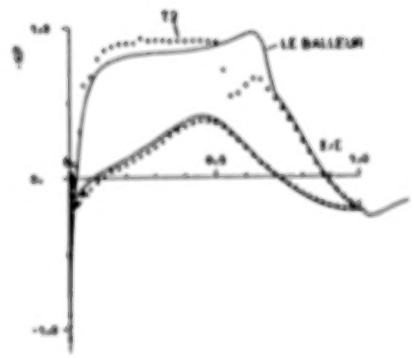

THEORY - EXPERIMENT COMPARISON

FIXED TRANSITION

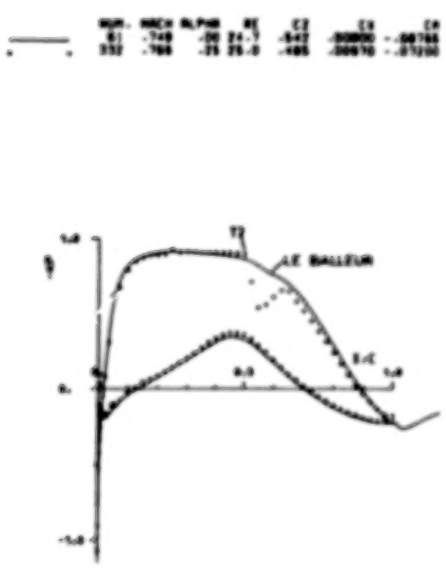

N.S. CALCULATIONS

FIXED TRANSITION

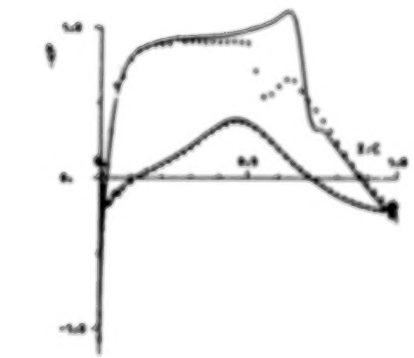

N.S. CALCULATIONS

FIXED TRANSITION

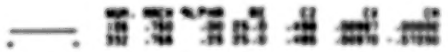

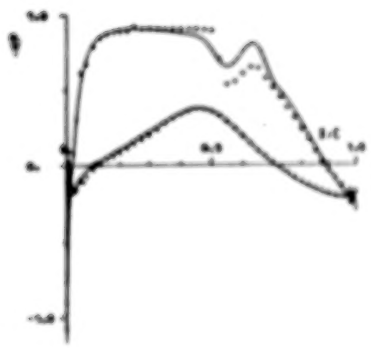

N.S. CALCULATIONS

MACH NUMBER EFFECT

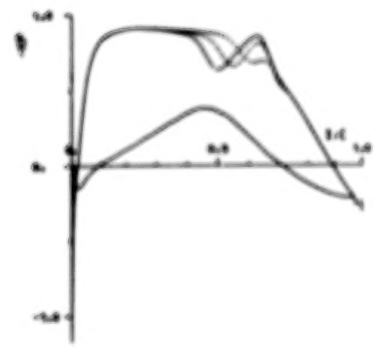

THEORY - EXPERIMENT COMPARISON

FIXED TRANSITION

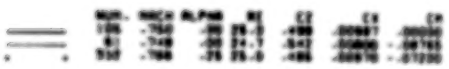

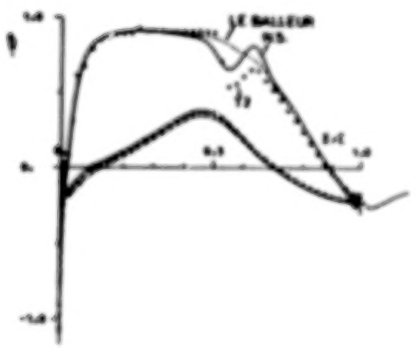

"LE BALLEUR" CALCULATIONS

FIXED TRANSITION

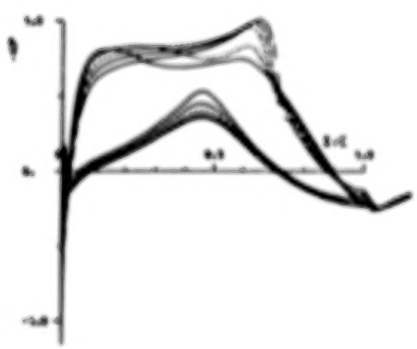

"LE BALLEUR" CALCULATIONS

FIXED TRANSITION

(corrected Mach numbers)

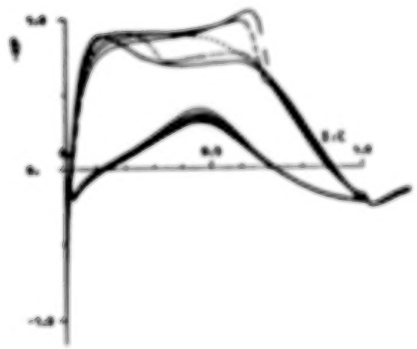

N.S. CALCULATIONS

(corrected Mach numbers)

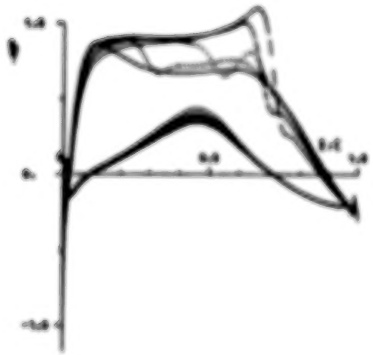

THEORY EXPERIMENT COMPARISON
FIXED TRANSITION

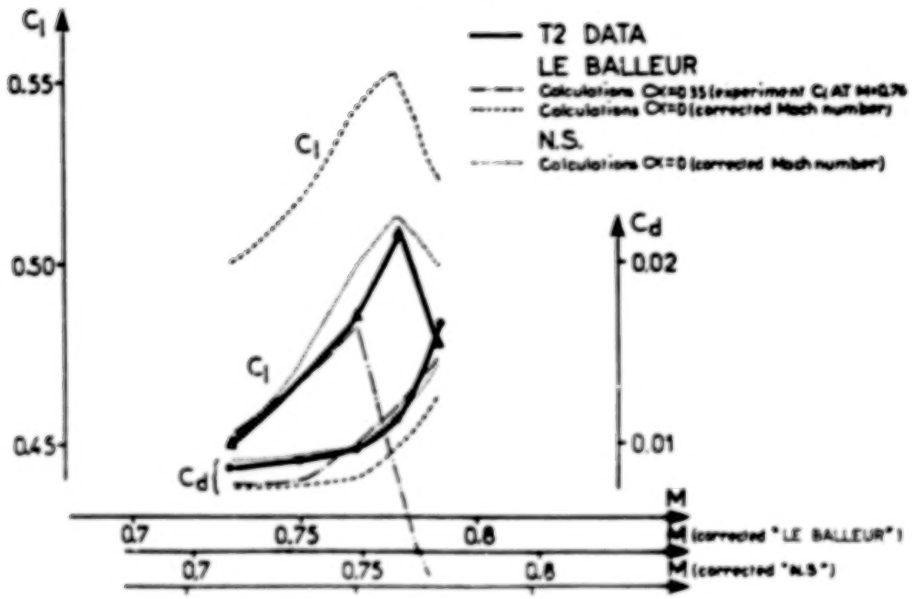

THEORY-EXPERIMENT COMPARISON

FIXED TRANSITION

	NUM.	MACH	ALPHA	RE	CZ	CX	CM
———	107	.76'	.00	25.0	.513	.01115	.00000
———	69	.759	.00	24.9	.552	.00970	-.09453
. .	333	.777	.25	25.3	.508	.01130	-.08100

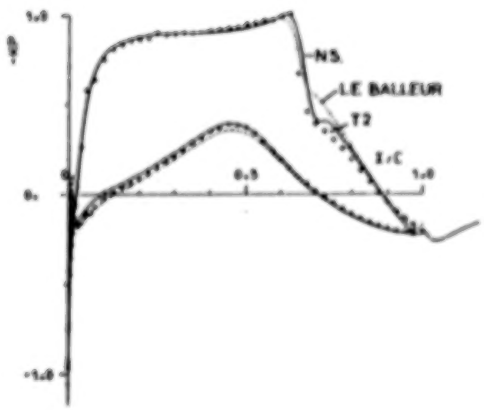

THEORY-EXPERIMENT COMPARISON

FIXED TRANSITION

	NUM.	MACH	ALPHA	RE	CZ	CX	CM
———	106	.774	.00	25.0	.499	.01461	.00000
———	70	.772	.00	25.1	.530	.01270	-.09727
° °	335	.780	.25	25.7	.478	.01660	-.08200

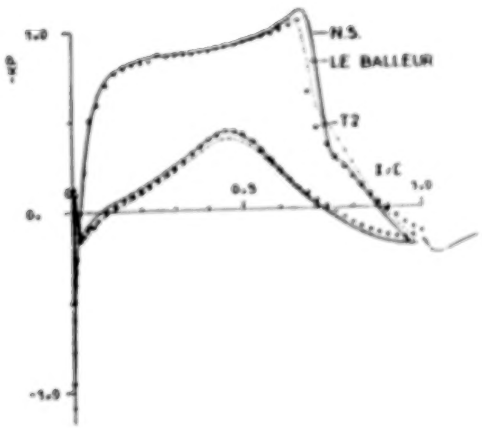

THEORY - EXPERIMENT COMPARISON

LE BALLEUR'S METHOD

FIXED TRANSITION

** REC.C.FORT ESSAI M=0.73 I=-0.25 **

	NUM.	MACH	ALPHA	RE	CZ	CX	CM
• ——— •	273	.727	-.25	7.6	.350	.00890	-.06400
———	1	.727	-.25	7.6	.409	.01167	-.07148
———	2	.715	-.25	7.5	.411	.01180	-.07233

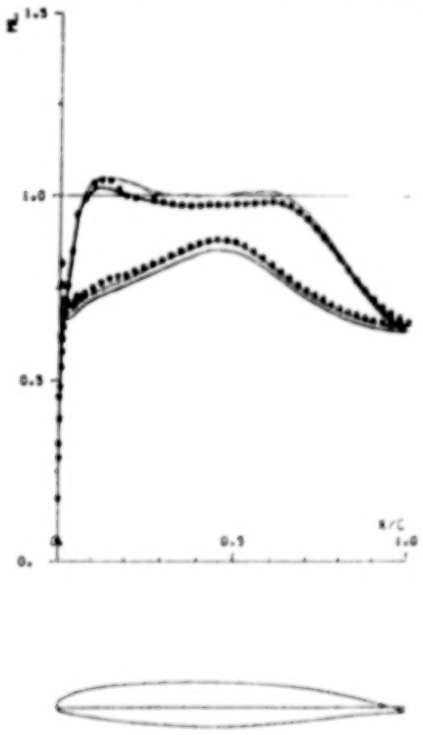

THEORY - EXPERIMENT COMPARISON

WEAK COUPLING METHOD

REC.C.FAIBLE ESSAI M=.73 I=-.25

	NUM.	MACH	ALPHA	RE	CZ	CX	CM
•	273	.727	-.25	7.6	.550	.00890	-.06400
———	1	.727	-.25	7.6	.529	.00987	-.09253
———	2	.705	-.25	7.6	.498	.00953	-.08754

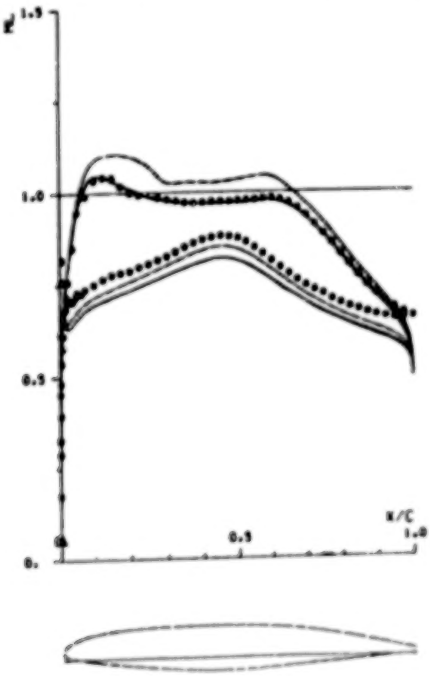

CONCLUSIONS

1) T2 DATA

. CAST 10 AIRFOIL VERY SENSITIVE TO :
- TRANSITION LOCATION
- MACH NUMBER
- REYNOLDS NUMBER

. T2 DATA VERY WELL DOCUMENTED AT LOW AND MEDIUM REYNOLDS NUMBERS

. T2 DATA SHOWS LARGE EXTENT OF LAMINAR FLOW UP TO Re 10

. TRANSITION LOCATION DISPLACEMENTS CONTROL
- Cl, CD EVOLUTIONS VERSUS ANGLE OF ATTACK
- Cl, CD EVOLUTIONS VERSUS Re NUMBER

2) T2 - TCT DATA COMPARISONS

. TCT DATA SHOW LESS LAMINAR FLOW THAN T2 AT THE SAME Re NUMBER

. FIXED TRANSITION DATA SEEMS TO CORRELATE CORRECTLY

. MORE COMPARISONS ARE NEEDED AT HIGH Re NUMBER

3) TEST - THEORY COMPARISONS

. CORRELATIONS ARE POOR USING THE SAME MACH NUMBER

. SIDEWALL B-L CORRECTIONS IMPROVE COMPARISONS

. NS COMPUTATIONS (WITH CORRECTED MACH NUMBERS) GIVE GOOD CORRELATIONS FOR :
- Cl, CD
- PRESSURE

VERSUS MACH NUMBER

BLANK PAGE

AN EXPERIMENTAL AWTS PROCESS AND COMPARISONS OF ONERA T2 AND 0.3-M TCT AWTS DATA FOR THE ONERA CAST-10 AEROFOIL

Stephen Wolf
Vigyan Research Associates

and

Renaldo Jenkins
NASA Langley Research Center

NASA Langley 0.3-m TCT

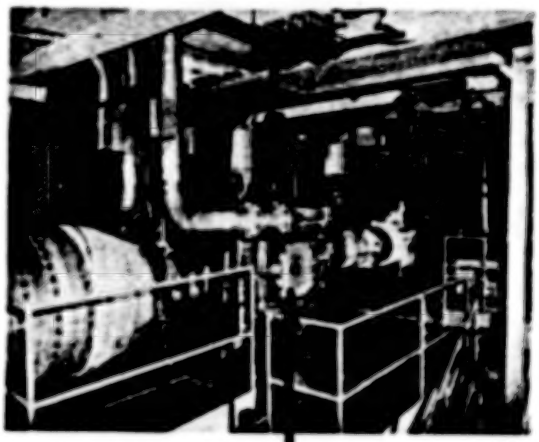

Flexible walled AWTS
installed in the 0.3-m TCT

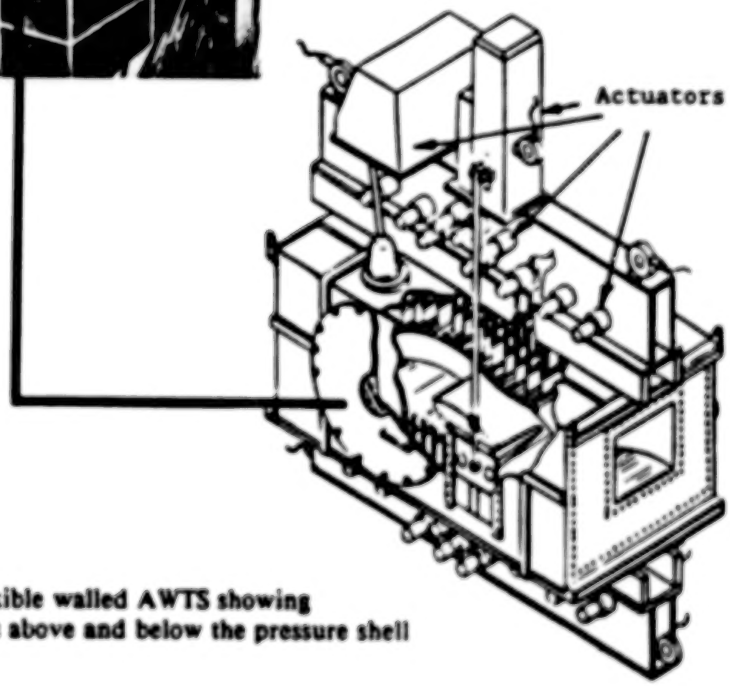

Sketch of flexible walled AWTS showing
jack actuators above and below the pressure shell

EXPERIMENTAL AWTS PROCESS IN THE 0.3-m TCT

Test Section Design - Four solid walls, floor and ceiling adjustable.
Total of 21 wall jacks per wall (note only 18 wall jacks used in wall adjustment process).

Wall Adjustment Process - Fast and iterative, based on wall data only.
Judd method with linearized compressible flow theory (2-D testing only).

Wall Data - Ceiling and floor jack positions.
Ceiling and floor pressures on the tunnel centerline.

We began operating the NASA Langley 0.3-m TCT (Transonic Cryogenic Tunnel) with an Adaptive Wall Test Section (AWTS) in March 1986.[1] The AWTS has a 33 cm (13 inch) square cross-section with four solid walls. The floor and ceiling are adjustable. We control the wall shapes with a system of 21 computer controlled jacks. We use only 18 jacks per wall in the wall adjustment process. The 3 downstream jacks simply control a variable diffuser to provide a smooth interface between the AWTS and the rigid tunnel circuit.

The wall adjustment process is both fast and iterative and requires only information on the flexible walls. The theory of the process utilizes the well-proven Judd method using linearized theory.[2]

We obtain the wall data for the wall adjustment process and residual interference assessment simply by measuring the jack positions and the wall pressures on the tunnel centerline.

QUALITY OF WALL ADJUSTMENTS / STREAMLINING

Assessment of Residual Wall Interferences

Input data - Measured and calculated wall pressures.
Aerodynamic position of floor and ceiling.
Position of model chordline in the AWTS.

Empirical Maxima -

1) Average Cp error (between streamline and measured values) along each wall - 0.01
2) Induced angle of attack at the model leading edge - 0.015°
3) Induced camber along the model chordline - 0.07°
4) Average induced streamwise Cp error along the model chordline - 0.007

We assess the quality of the wall adjustments/streamlining by calculating the residual wall interferences due to the floor and ceiling. The calculations are quick (allowing real-time use) using linearized compressible flow theory with the input data listed above.

The wall adjustment process automatically stops when all the residual wall interferences reduce below the maxima listed above. These maxima are defined empirically as a compromise between perfection (zero residual wall interferences) and unnecessary iterations of the wall adjustment process. These maxima are related to the quality of the AWTS hardware and instrumentation and stability of test conditions in the AWTS.

We do not apply any of these residual wall interference corrections to the final aerofoil data. We consider the real-time aerofoil data to be "corrected." In this adaptive wall context, "corrected" refers to the elimination of wall interferences at the source of these interferences.

COMPARISONS OF T2 AND 0.3-m TCT AEROFOIL DATA

Comparison Qualifications

Most of 0.3-m TCT data is new and preliminary.

Concentration on data at the design Mach number.

No sidewall boundary layer control involved.

Similar testing techniques in T2 and 0.3-m TCT.

No conclusions given to bias the workshop discussions.

Before we present any data comparisons, it should be known that the above qualifications apply to the comparisons. Most of the 0.3-m TCT data presented here is new and unpublished and must therefore be considered as preliminary. This new data comes from a re-test (T-224) of the ONERA CAST 10 carried out in August 1988. (Original 0.3-m TCT data came from tests T-212 and T-216.) We found it necessary to carry out this re-test due to discrepancies in the 0.3-m TCT data from the two CAST 10 models. We will not discuss these discrepancies here.

We concentrate the data comparisons on the design Mach number 0.765 because of the known sensitivity of the CAST 10 section at this Mach number. This sensitive situation acts as an excellent challenge for free air simulations.

We did not use sidewall boundary layer control during the 0.3-m TCT tests nor did the French in their tests.

The ONERA/CERT T2 tunnel and the 0.3-m TCT use similar testing techniques. Both tunnels have flexible walled AWTS's. We do not discuss the French wall adjustment process here. Suffice to say, the process is well established at ONERA and is similar to the NASA process. However the T2 wall adjustment process does not involve any residual wall interference assessment due to the intermittent tunnel operation. Interestingly, we did attempt to use the T2 wall adjustment process with the 0.3-m TCT but failed to achieve a converged solution due mainly to software problems.

We do not give any conclusions in this presentation to bias any discussion of these data comparisons. We present these data comparisons with comments as input for the forthcoming workshop discussions.

TESTING FACTS

- Aerofoil Chord - 18 cm (7.09 inches)
- Test Section Height/Chord Ratio - 1.83 (0.3-m TCT) & 2.05 (T2)
- Aspect Ratio - 1.833 (0.3-m TCT) & 2.166 (T2)
- Transition Location on both surfaces - 6% (0.3-m TCT) & 5% (T2)
- Transition Strip - 1.7% of 0.053/0.043mm dia. micro-spheres (0.3-m TCT)
  0.045mm high carborundum grit (T2)
- Mach Number Stability - 0.002 (0.3-m TCT) & 0.004 (T2)
- Data Shortfall - Sparsity of high Reynolds number data from T2

The testing facts listed above define the model condition for the data compared here. The transition strip location in the NASA tests is a compromise between the ONERA and DFVLR locations.

Mach number stability during a polar is a problem in the T2 tunnel because each data point is a separate run of this intermittent tunnel. The 0.3-m TCT is a continuously operating tunnel.

The T2 data we used here is not complete. There is a sparsity of high Reynolds number data for example. This incompleteness makes it very difficult to make more meaningful direct comparisons than shown here.

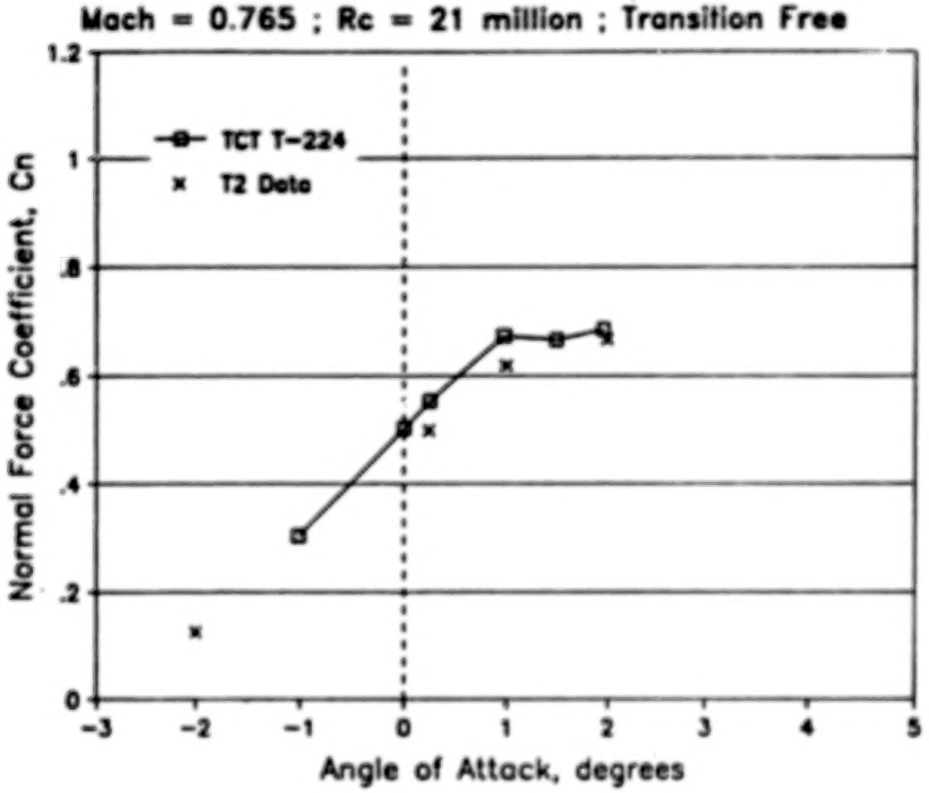

This data comparison is for the test conditions Mach 0.765, 21 million chord Reynolds number, and transition free. The Cn-v-α data shown above indicates an α difference between the two tunnels. It seems as though Cn_{max} is matched but the sparsity of T2 data does add some uncertainty. The range of Mach number in the four T2 data points is 0.007, compared with 0.0003 in the 0.3-m TCT data.

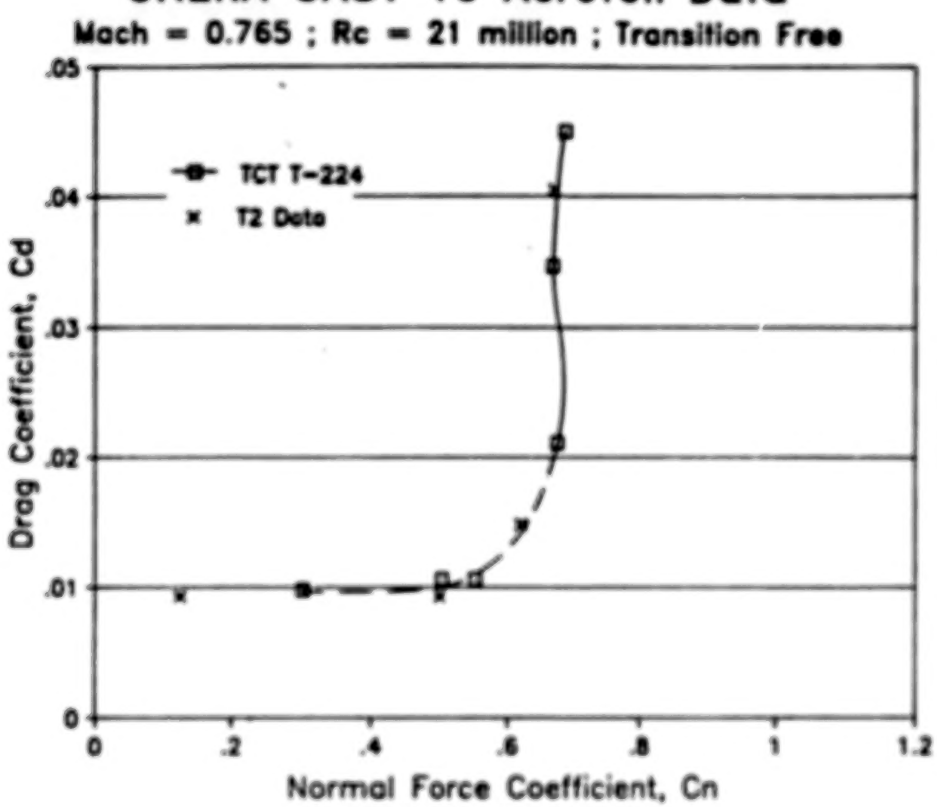

Continuing the data comparison at 21 million chord Reynolds number. The graph of Cd-v-Cn shows a remarkably good data comparison. This confirms that there is an α difference between the two tunnels. The repeatability of data on a known sensitive aerofoil is always a challenge. Add to this challenge, tests in different tunnels with natural transition and you have the very demanding situation discussed here.

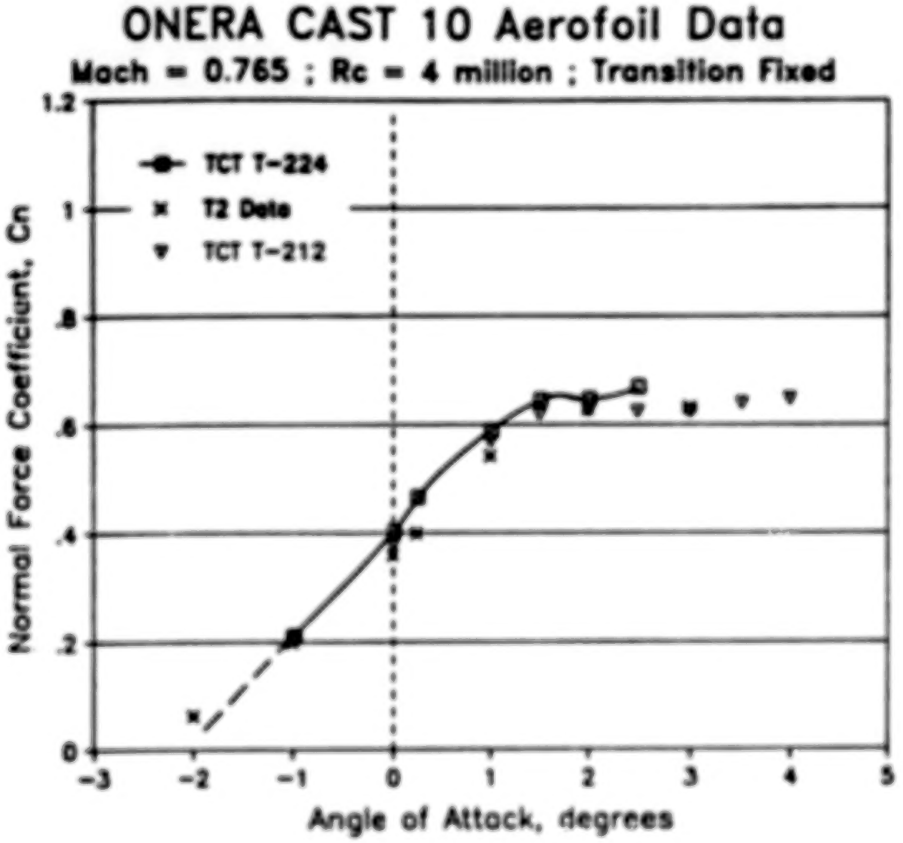

If we now reduce the chord Reynolds number in the data comparison to 4 million, we find much more T2 data. The Cn-v-α data again indicates that there is an α difference persisting between the two tunnels. We have more confidence in the matching of Cn_{max} at this lower Reynolds number. We include the original 0.3-m TCT data set (T-212) in this comparison to show data repeatability. Notice the latest set (T-224) has slightly higher Cn values. Nevertheless, both sets of 0.3-m TCT data show a higher lift curve slope than found in T2.

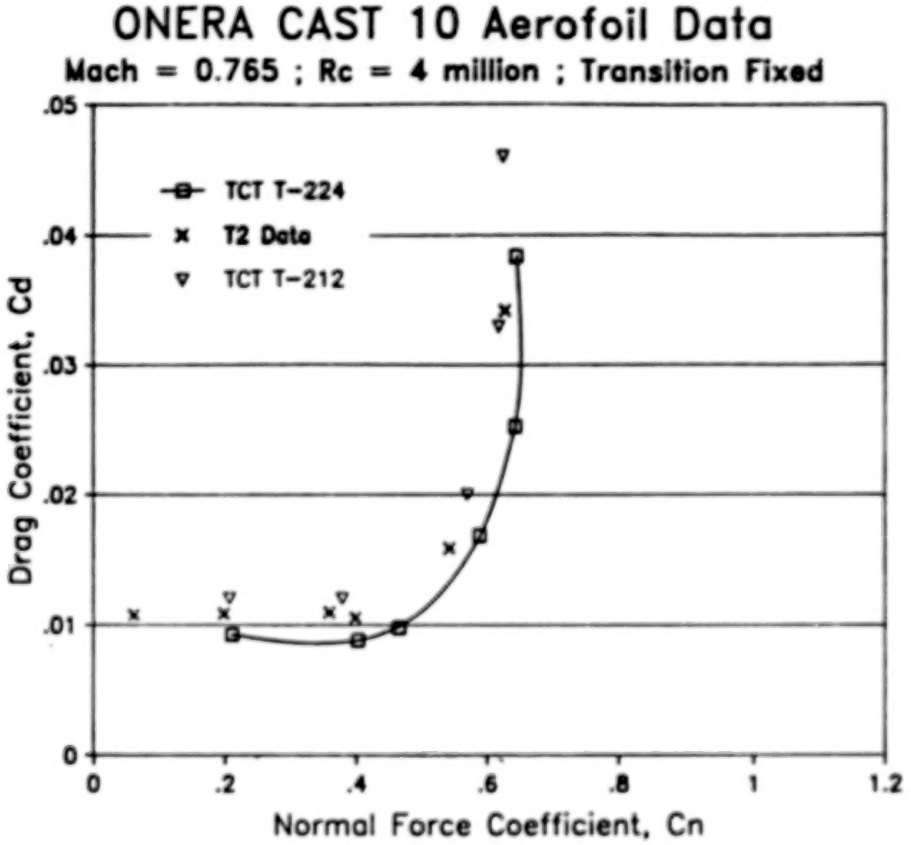

When we remove a from the 4 million Reynolds number data, we see another source of data differences. In the Cd-v-Cn graph shown above, we see that the two 0.3-m TCT data sets bracket the T2 data in terms of Cd_{min} and Cn_{max}. It is clear that the transition fixing is significantly affecting lift and drag. This highlights one of the major problems of simulating scale effects. The what, where and how much of transition fixing remains a big question. Another factor we must consider is the improved tunnel control system for the latest 0.3-m TCT test (T-224). We have more confidence in the drag from the latest tests.

ONERA CAST 10 Aerofoil Data

Mach = 0.765 ; Rc = 4 million ; Alpha = 1 degree

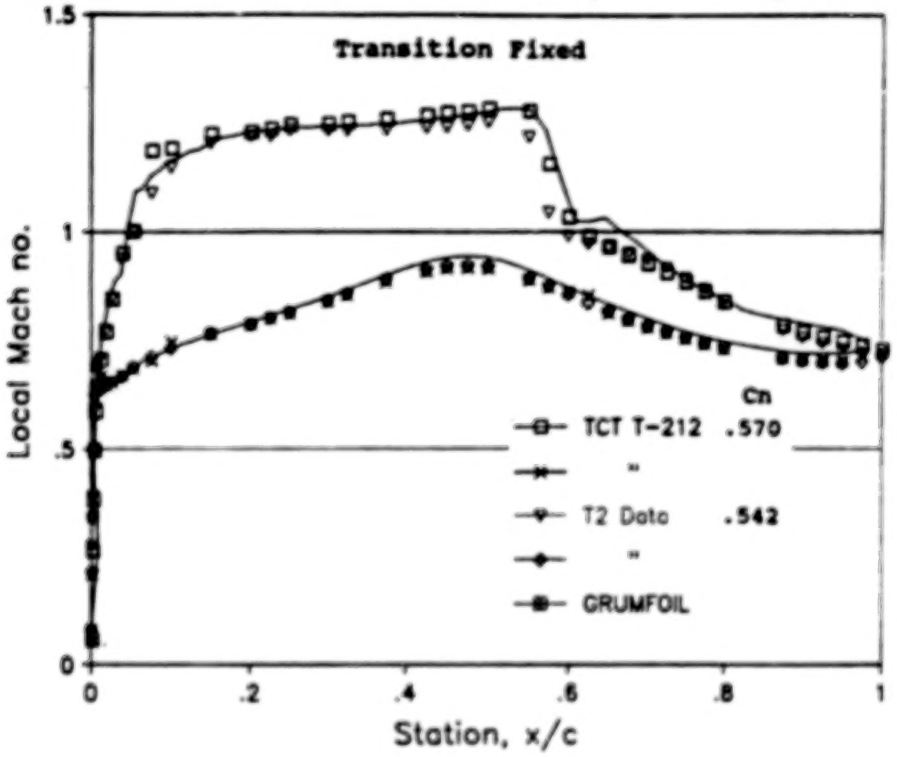

The comparison of detailed pressure distributions on the aerofoil are difficult. This is because the normal force was not matched between the two tunnels at lifting conditions. However, it is interesting to make a data comparison at $\alpha = 1^{\circ}$ and Mach 0.765, with transition fixed, as shown above. This is a challenging test condition with near maximum lift. The comparison is good with notable differences near the leading edge (due to the transition strip) and at the shock location. The movement of the shock is small, of the order of the pressure tap spacing (2.5% of chord).

We also include a GRUMFOIL free air solution in this comparison. The normal force of the GRUMFOIL result is matched to that of the 0.3-m TCT data. The comparison is very good. Incidentally, other comparisons with GRUMFOIL have been made which are also good provided Cn is less than Cn_{max} and the transition location on the aerofoil is known.

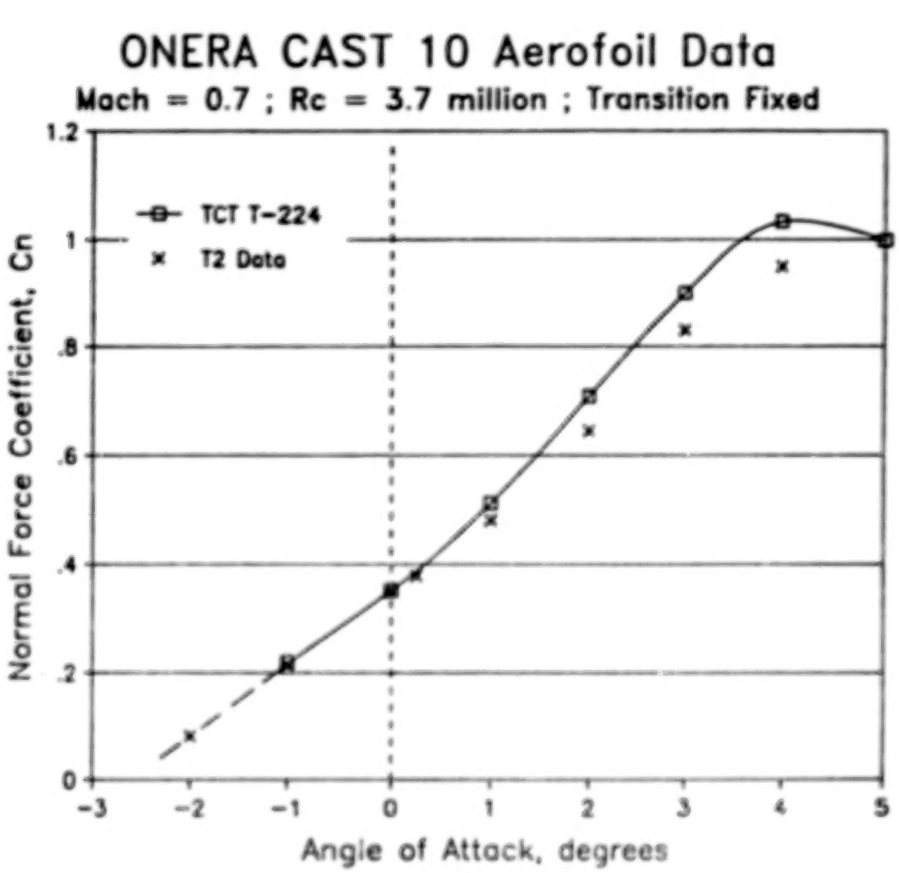

So far we have compared data at only the design Mach number. If we examine data at Mach 0.7 we see a similar trend in the Cn-v-α graph shown above. Again there is the same α difference between the two tunnels as seen at higher Mach number and Reynolds number. Unfortunately, we believe that Cn_{max} could not be obtained in the T2 tunnel at Mach 0.7, due to limitations to the flexible wall movement in the T2 AWTS. The 3.7 million chord Reynolds number of this data coincides with the majority of T2 tests at Mach 0.7.

Unfortunately, very little T2 data exists above Mach 0.765, so no data comparisons are possible for Mach numbers higher than the design value.

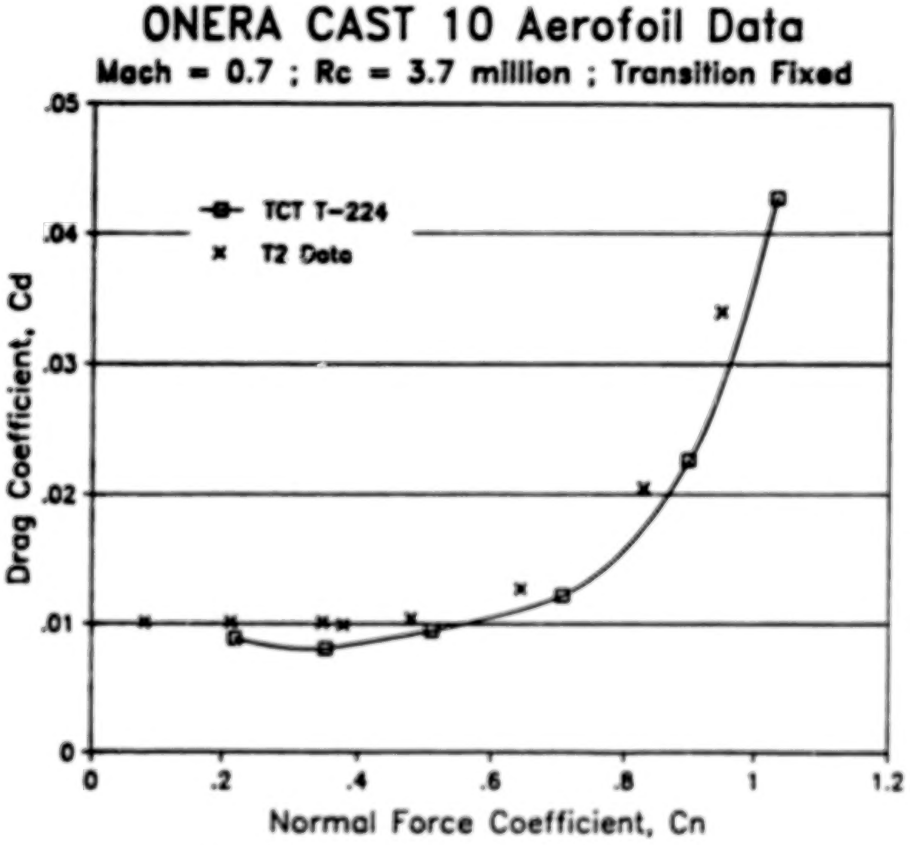

The Cd-v-Cn data at Mach 0.7 and 3.7 million chord Reynolds number shows a similar comparison as found at Mach 0.765. Once again the 0.3-m TCT data has lower drag than the T2 data by about 20 drag counts. This drag difference is due to the state of the transition fixing. The French grit is thicker than the NASA Micro-Spheres in this case.

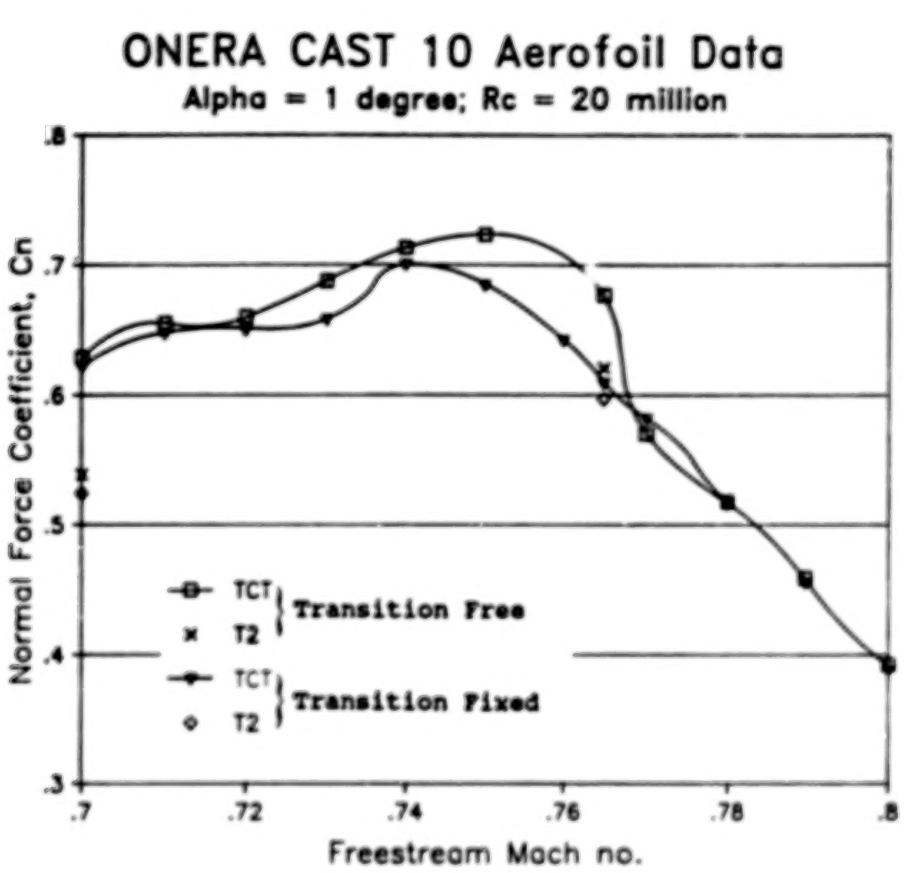

Let us now examine the effect of Mach number at a fixed α. We choose to look at data at 20 million chord Reynolds number where we expect the effects of transition fixing to be minimal. A plot of Cn-v-Mach number is shown above over the Mach number range 0.7 to 0.8. Notice the shock stall in the 0.3-m TCT data (from T-216) occurs at about Mach 0.74 transition fixed and about Mach 0.75 transition free. There is insufficient T2 data to see shock stall, but what we can see is a minimal effect of transition fixing. This indicates that the T2 transition fixing was well scaled for 20 million chord Reynolds number.

At the design Mach number, the 0.3-m TCT data indicates that Cn is very sensitive to transition fixing and Mach number at this high lift condition.

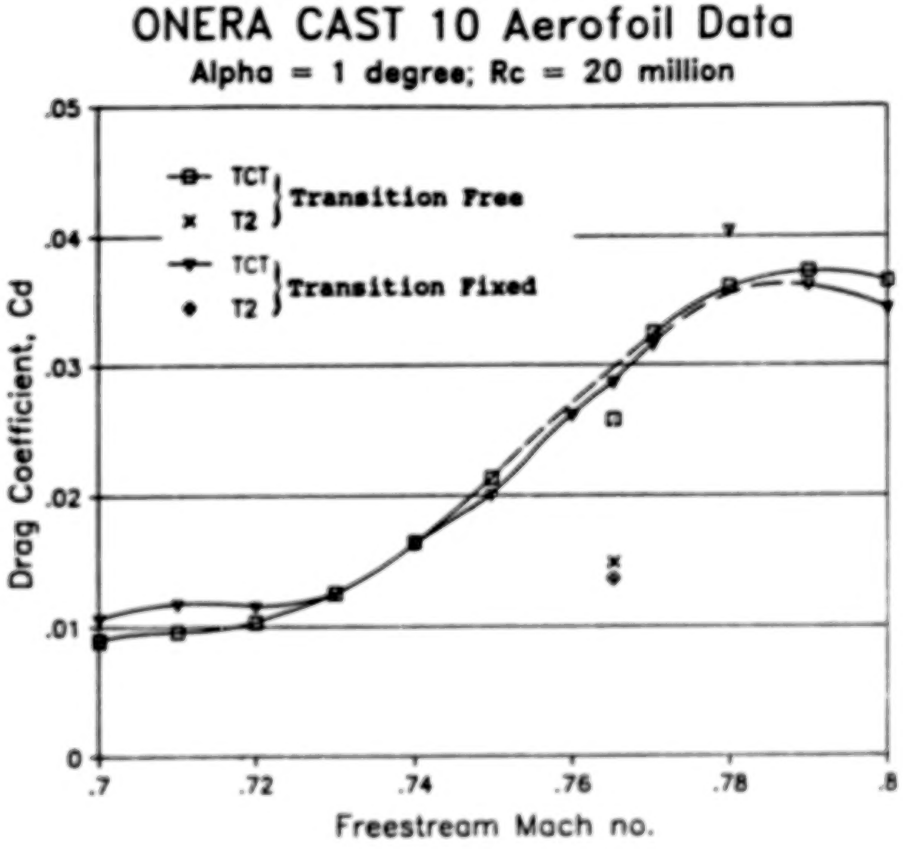

We now look at how the drag coefficient, Cd, varies with Mach number for the same conditions as shown in the previous figure. We see that the effect of transition on the 0.3-m TCT data is as small as found in the limited T2 data. The 0.3-m TCT data are faired to remove some clearly wayward data points. We attribute this scatter to the less than perfect tunnel control system used in the initial 0.3-m TCT tests (T-216).

We see that the T2 drag at Mach 0.765 is significantly lower than the 0.3-m TCT value. This seems to indicate that the effective α of the T2 data is lower than the geometrical α.

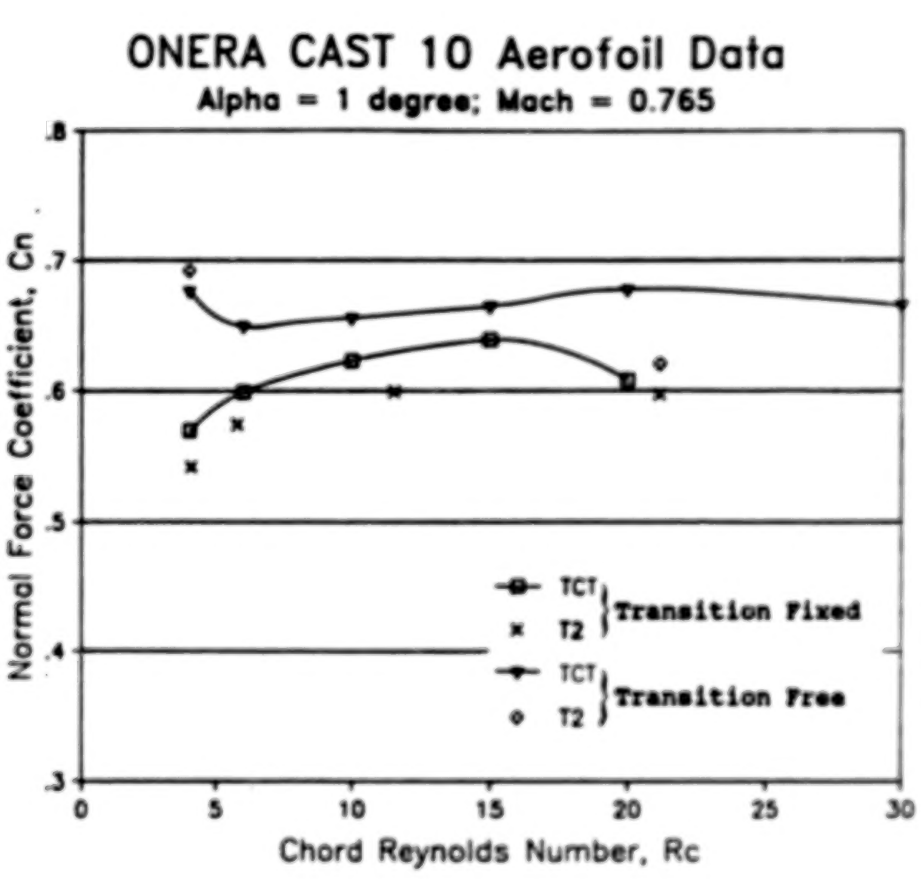

We consider Reynolds number effects at the same α of 1° using 0.3-m TCT data from the initial test (T-212). The plot of Cn-v-Rc shown above is for the chord Reynolds number range from 4 million to 21.2 million with transition fixed. We can observe that the effect of transition fixing as Reynolds number increases is not straightforward. Meanwhile, data comparisons at a lower α of 0.25° show that the effect of transition fixing reduces as Reynolds number increases, as expected.

However, we can see that the transition free data from the 0.3-m TCT shows a small Reynolds number effect concentrated between 4 and 6 million. With transition fixed, the Reynolds number effects are larger and occur over the entire Reynolds number range investigated.

The limited T2 data shows that there is minimal transition effect at 21 million chord Reynolds number, again pointing to good sizing of the transition grit for high Reynolds number testing.

The Reynolds number effects are small compared with Mach number effects. However, we can see that incorrect transition fixing can have serious consequences.

SUMMARY OF FINDINGS

Remarkable data agreement with the limited high Reynolds data from T2.

Angle of attack difference between the two tunnels.

Drag differences at low Reynolds number.

Good agreement with free air GRUMFOIL code, below Cn_{max}.

More T2 data required to confirm some observations.

References

1. Wolf, S. W. D.; and Ray, E. J.: **Highlights of Experience with a Flexible Walled Test Section in the NASA Langley 0.3-Meter Transonic Cryogenic Tunnel.** AIAA Paper 88-2036. Presented at the AIAA 15th Aerodynamic Testing Conference, San Diego, CA, May 18-20, 1988.

2. Wolf, S. W. D.; and Goodyer, M. J.: **Predictive Wall Adjustment Strategy for Two-Dimensional Flexible Walled Adaptive Wind Tunnel. A Detailed Description of the First One-Step Method.** NASA CR-181635, January 1988, N88-19409#.

INVESTIGATION OF CAST-10-2/DOA 2 AIRFOIL IN NAE HIGH REYNOLDS NUMBER TWO-DIMENSIONAL TEST FACILITY

Y. Y. Chan
National Aeronautical Establishment
National Research Council Canada

Introduction

The NAE/NRC-NASA Langley Cooperative Program on Two-Dimensional Wind Tunnel Wall Interference Research was initiated in 1984. The objective of the program is to develop the technology for elimination of correction of wall interference in transonic two-dimensional tests using the Langley 0.3-m Transonic Cryogenic Tunnel with an adaptive wall test section and the NAE 1.5-m High Reynolds Number Two-Dimensional Test Facility. A common model with the CAST 10-2/DOA-2 profile and 228 mm (9 inches) chord length has been tested in both tunnels. The tests performed in NAE covered the Mach numbers from 0.3 to 0.8 and Reynolds numbers from 10 to 30 million. The model was tested with transition free and with transition fixed at 5 percent chord for both the upper and the lower surfaces.

The NAE facility consists of a two-dimensional test section inserted into the 1.5 m transonic test section of the Trisonic Wind Tunnel. The 2-D test section is 0.38 m (15 inches) wide, 1.5 m (60 inches) high and 3.6 m (141 inches) long. The side walls are solid and the top and the bottom walls are perforated with 21% porosity, the surfaces of which are covered by fine mesh screens for elimination of edge tone generated by the perforation. A static pressure tube is installed along the center-line of each wall for monitoring the pressure distribution at the wall. The model is situated at mid-height of the test section. A balance is housed at each side wall and the model is mounted on both balances. The side wall boundary layer in the vicinity of the model is controlled by normal suction. The suction area, 0.61 m × 0.46 m (24 in. × 18 in.), is covered by a porous plate and moderate suction is applied to control the adverse growth of the boundary layer. A pitot rake with four probes is mounted 0.41 m (16 in.) downstream from the model trailing edge for measuring the wake profiles. The tunnel is precisely controlled to give the required free stream Mach number and Reynolds number. The test results are available in tabulated and graphical forms immediately after the test run. The airfoil data are corrected for the top and bottom wall interference. The effect of sidewall boundary layer is being investigated.

Conclusions

The data obtained have been analysed for the effects of Reynolds number, transition fixing and Mach number. The role of the boundary layer on the displacement effect, the interaction with the shock wave and the trailing edge separation are examined. The results are summarized as follows.

1. The airfoil performance depends strongly on Reynolds number and transition fixing.

2. With transition fixed, the aerodynamic quantities such as lift, pitching moment and drag show a monotonic variation with Reynolds number.

3. With transition free, the aerodynamic quantities vary less regularly with Reynolds number and a slight parametric dependency is shown. The weak dependency is due to the compensatory effect of the forward shift of the transition position and the thinning of the turbulent boundary layer as Reynolds number increases.

4. The shock Mach number and the shock position are weakly dependent on Reynolds number.

5. The long extent of the laminar boundary layer at transonic speeds reduces the drag appreciably at low Reynolds numbers. The drag bucket around the design Mach number can be observed below Reynolds number 15 million.

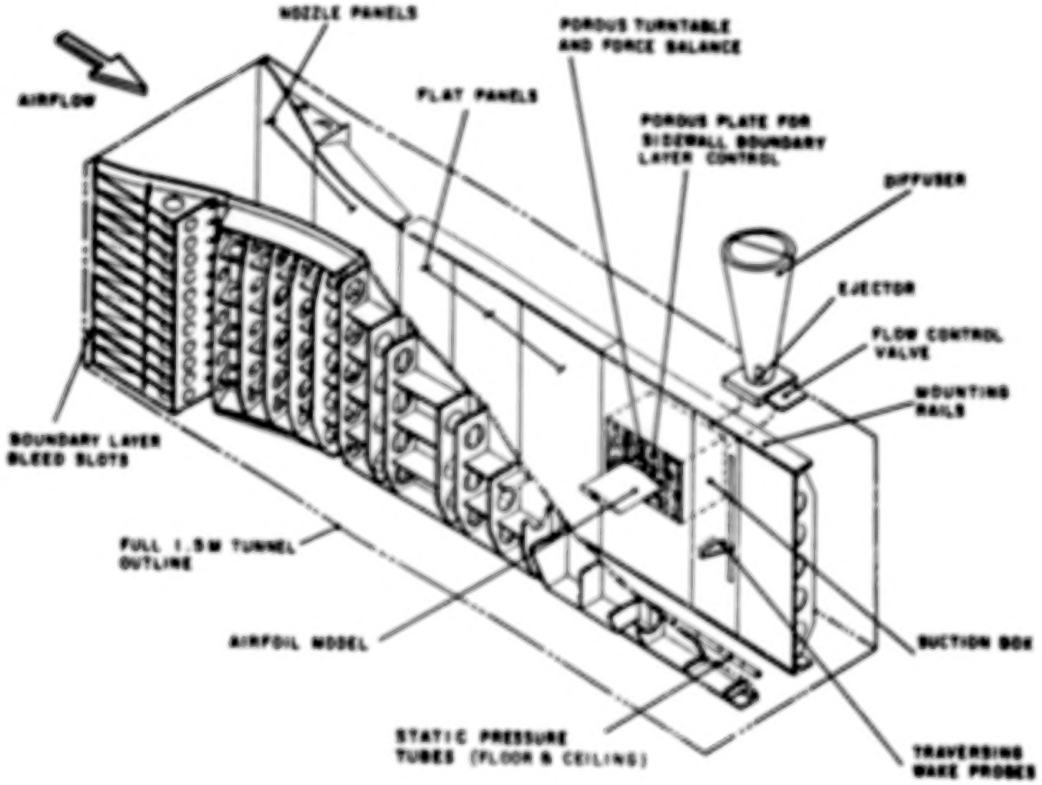

NAE 2-DIMENSIONAL TEST SECTION

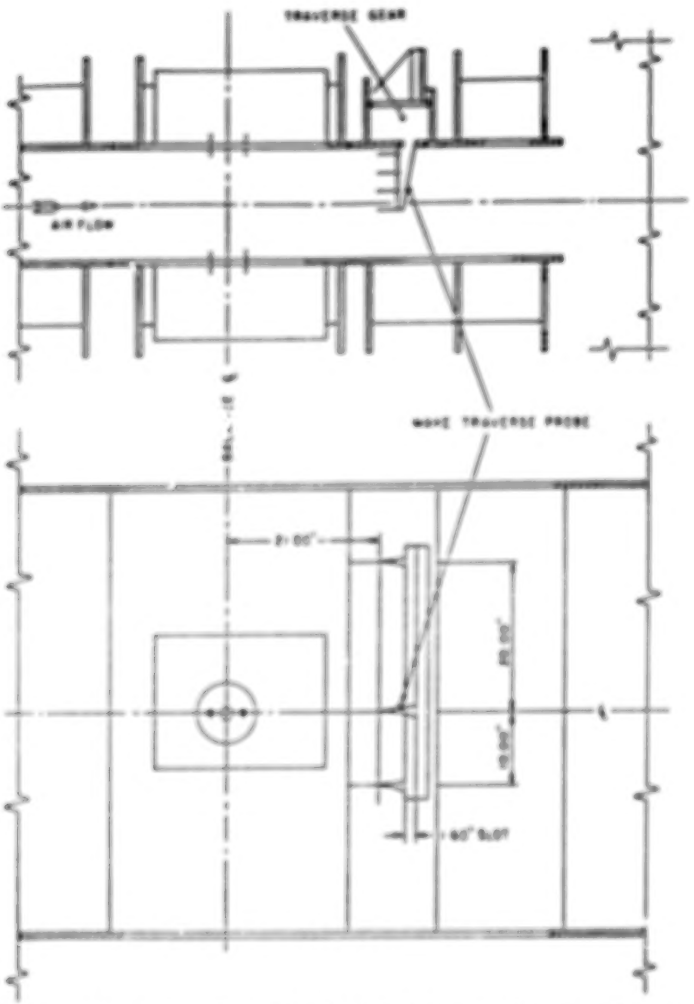

SIDEWALL MOUNTED WAKE TRAVERSE PROBE SYSTEM

HOLE NO.	X"	HOLE NO.	X"
1	-80.969	21	-0.969
2	-74.969	22	-1.422
3	-68.969	23	0.109
4	-62.969	24	1.609
5	-56.969	25	3.109
6	-50.969	26	4.609
7	-44.969	27	6.109
8	-38.969	28	7.609
9	-32.969	29	9.109
10	-26.969	30	10.609
11	-23.969	31	12.109
12	-20.969	32	15.109
13	-17.969	33	18.109
14	-14.969	34	21.109
15	-11.969	35	24.109
16	-10.469	36	27.109
17	-8.969	37	33.109
18	-7.459	38	37.109
19	-5.969	39	42.109
20	-4.469	40	47.109

PRESSURE TUBING
0.020" ID
0.032" OD

Ø .1" AL TUBING

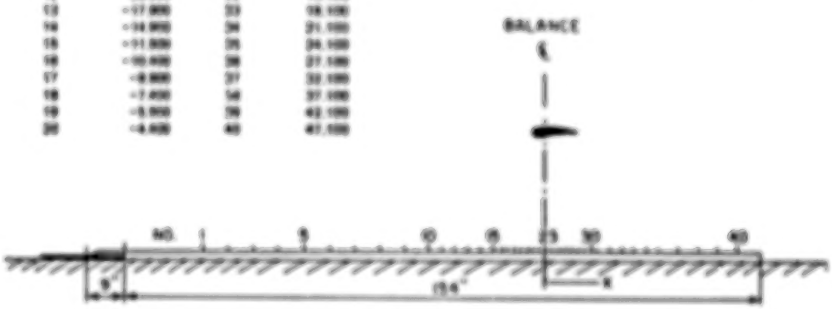

WALL STATIC TUBES

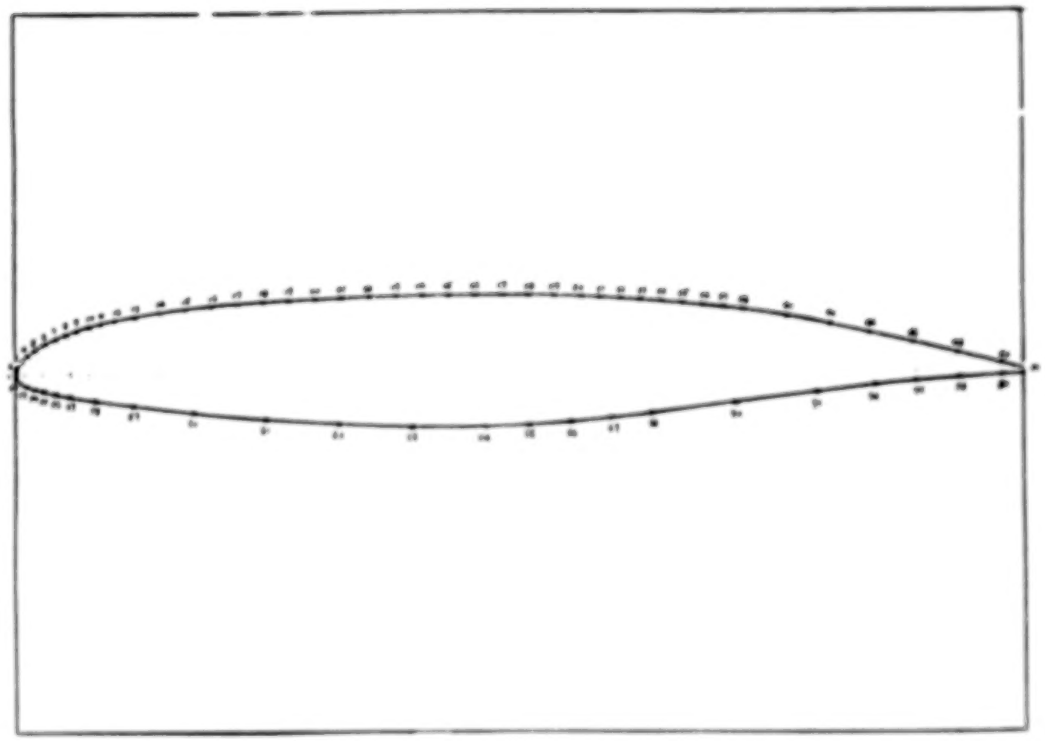

SECTION PROFILE OF CAST-10-2/DOA AIRFOIL
& PRESSURE ORIFICE LOCATION

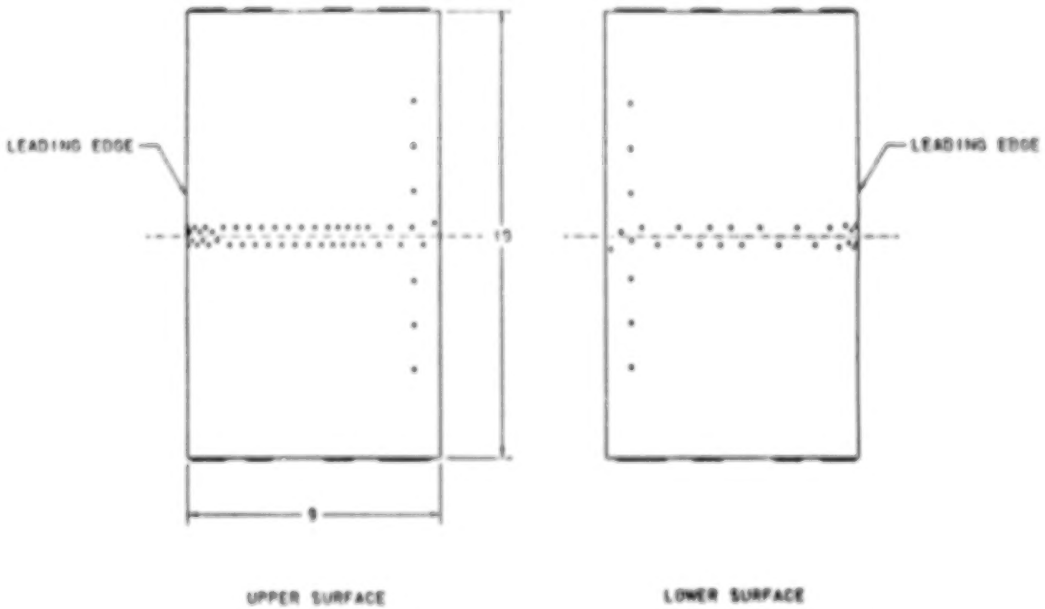

LOCATIONS OF PRESSURE ORIFICES AT UPPER AND LOWER
SURFACES PLANE VIEW

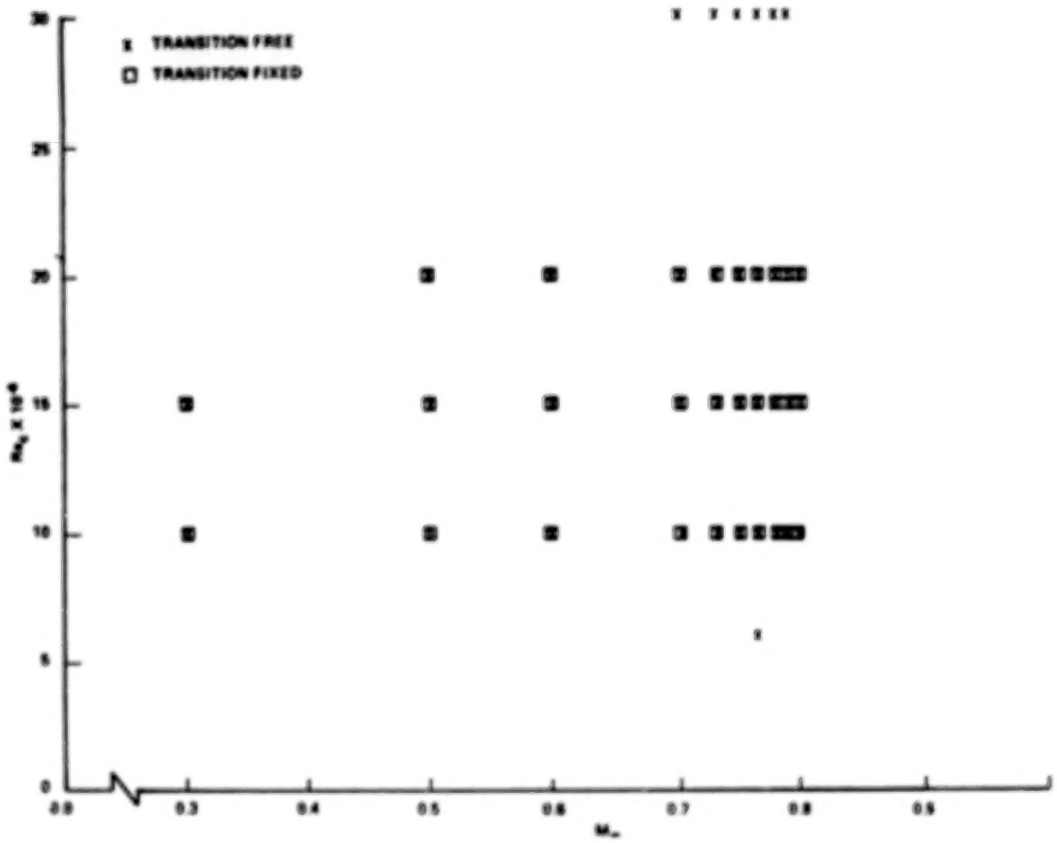

ENVELOPE OF TEST CONDITIONS

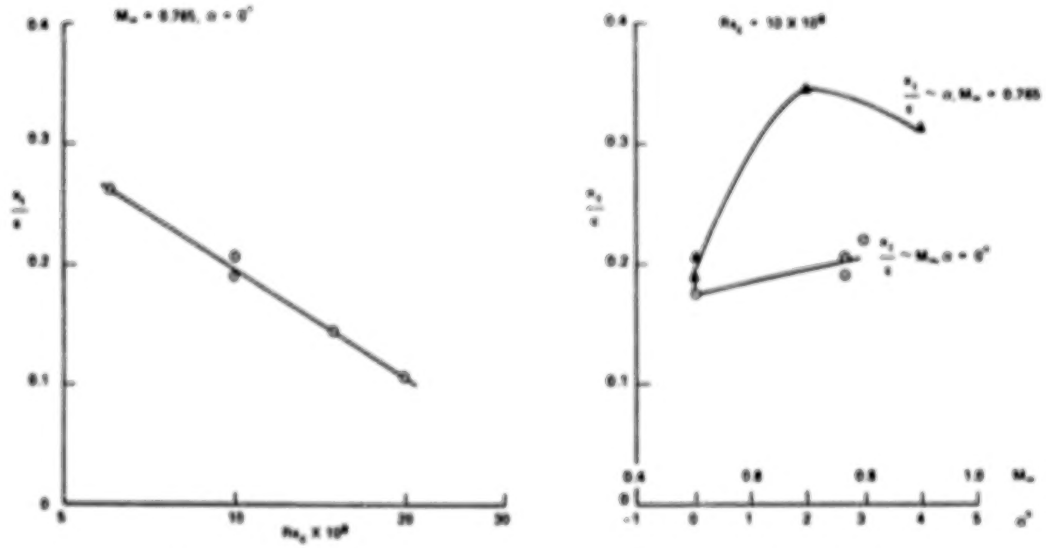

EFFECTS OF REYNOLDS NUMBER, MACH NUMBER AND INCIDENCE TO LOCATIONS OF BOUNDARY LAYER TRANSITION ON THE UPPER SURFACE OF THE MODEL

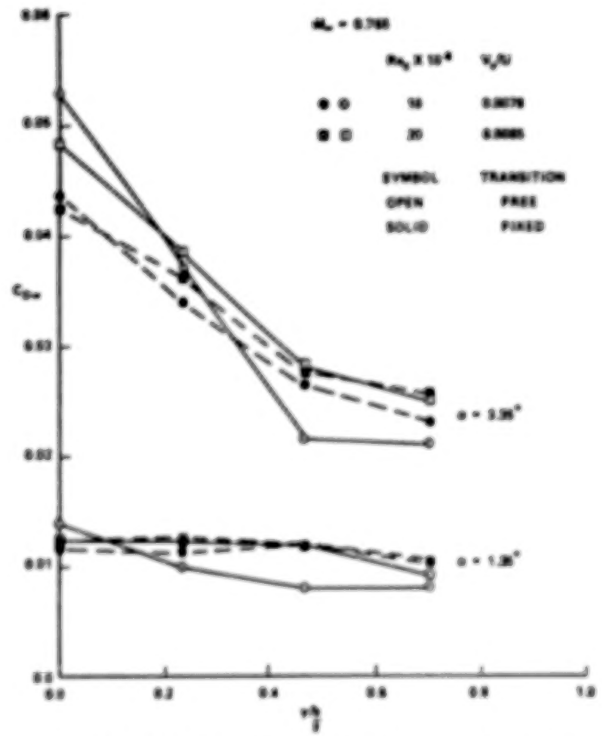

SPANWISE WAKE DRAG VARIATION AT VARIOUS REYNOLDS NUMBERS FOR TWO ANGLES OF ATTACK WITH FIXED OR FREE TRANSITION, M_∞ = 0.765

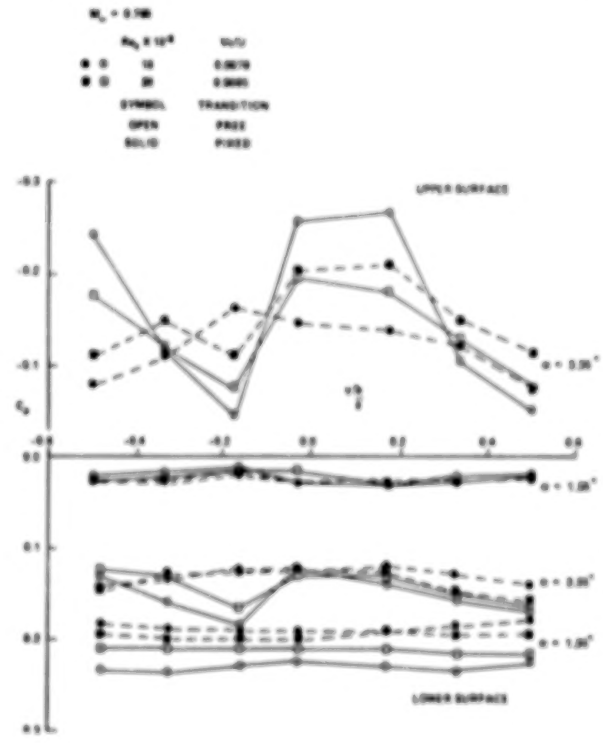

SPANWISE PRESSURE DISTRIBUTIONS AT X/C = 0.9 FOR TWO ANGLES OF ATTACK AT VARIOUS REYNOLDS NUMBERS WITH FIXED OR FREE TRANSITION, M_∞ = 0.765

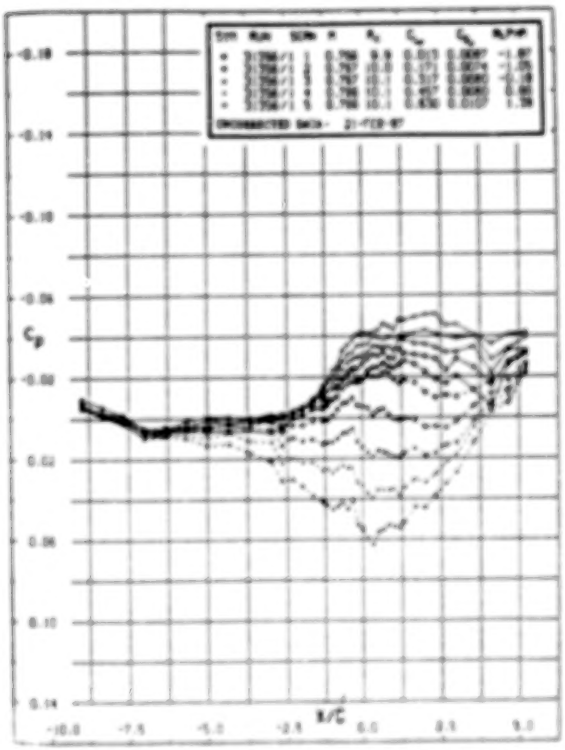

TYPICAL STATIC PRESSURE DISTRIBUTIONS ALONG TOP AND BOTTOM WALLS OF TEST SECTION.

RUN 299.2/6

R_c = 10.23×10^6
M = 0.7724
α = 2.991°
C_{N_h} = 0.6276
C_A = -0.0026
C_m = -0.0820
R = 0.0850
c/h = 0.1500

δ^* = -0.0073
δ_b = -0.663°
$\alpha + \delta\alpha^*/\delta_b$ = 0.0010
$\alpha + \delta\delta_b/\delta_b$ = -0.008°

M_{∞} = 0.7851
α_{∞} = 1.778°

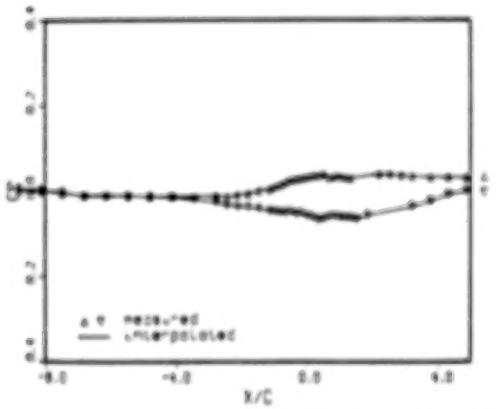

TYPICAL INTERFERENCE CALCULATION FOR SPECIFIC MODEL CONDITION.

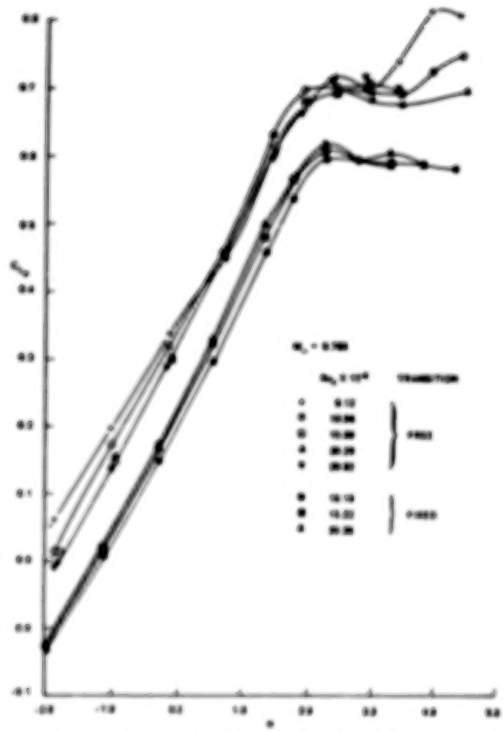

LIFT VERSUS ANGLE OF ATTACK AT VARIOUS REYNOLDS NUMBERS WITH FIXED OR FREE TRANSITION AT NOMINAL M_∞ = 0.765

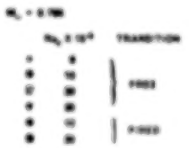

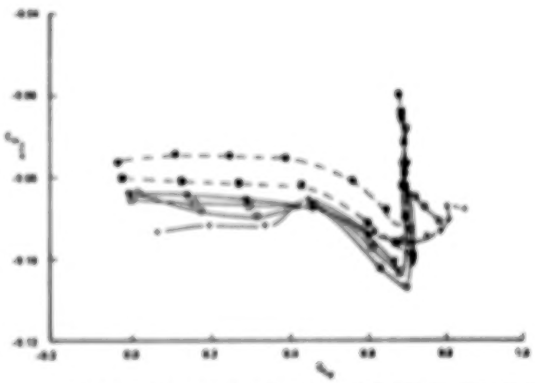

PITCHING MOMENT VERSUS LIFT AT VARIOUS REYNOLDS NUMBERS WITH FIXED OR FREE TRANSITION AT NOMINAL M_∞ = 0.765

DRAG VERSUS LIFT AT VARIOUS REYNOLDS NUMBERS WITH FIXED OR FREE TRANSITION AT NOMINAL M_∞ = 0.765

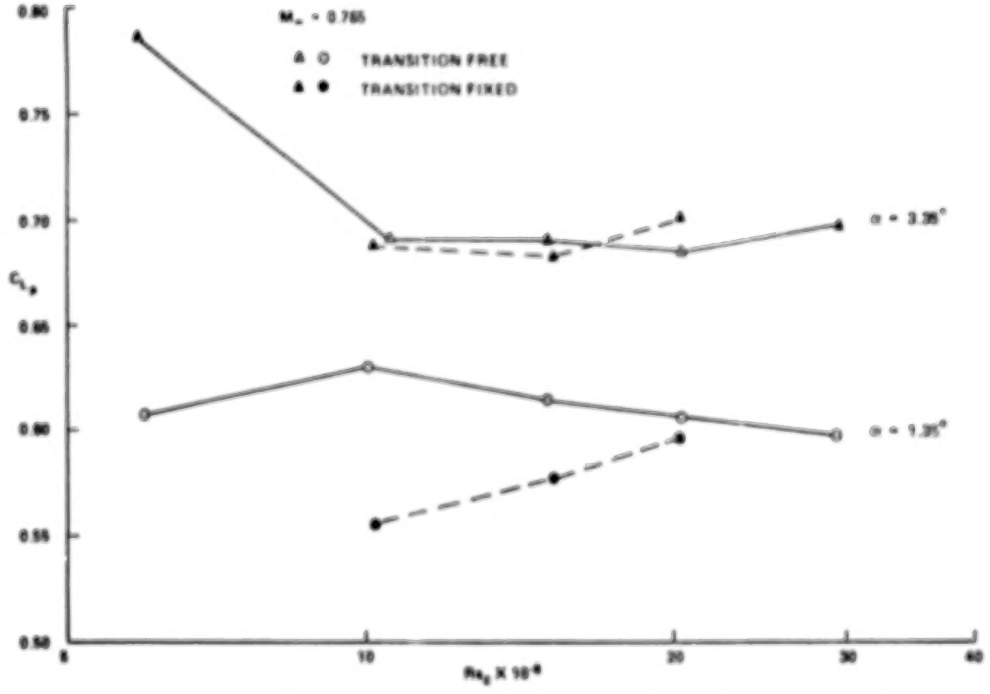

REYNOLDS NUMBER DEPENDENCE OF LIFT FOR TWO ANGLES OF ATTACK WITH FIXED OR FREE TRANSITION

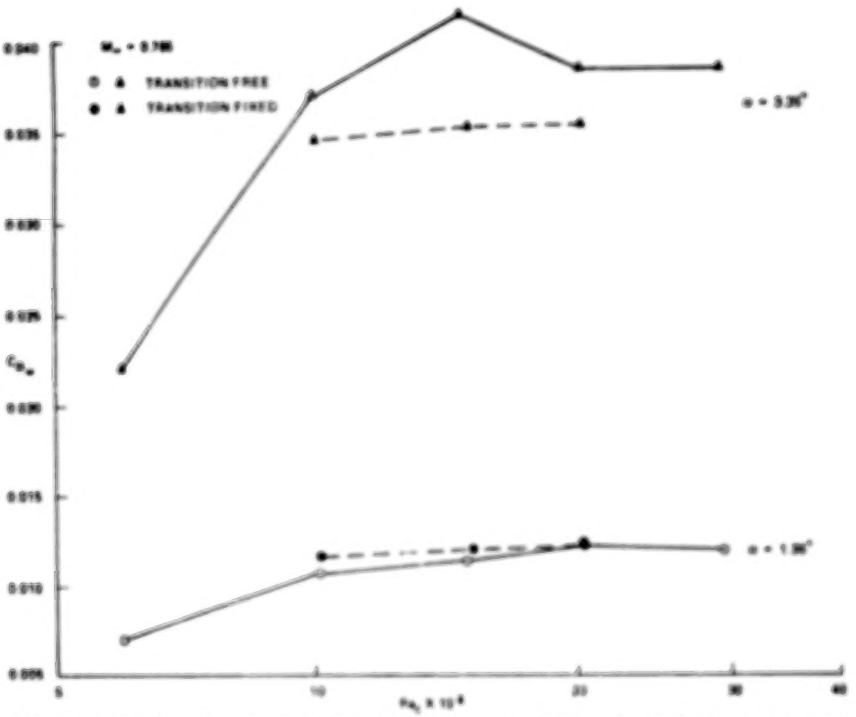

REYNOLDS NUMBER DEPENDENCE OF DRAG FOR TWO ANGLES OF ATTACK WITH FIXED OR FREE TRANSITION

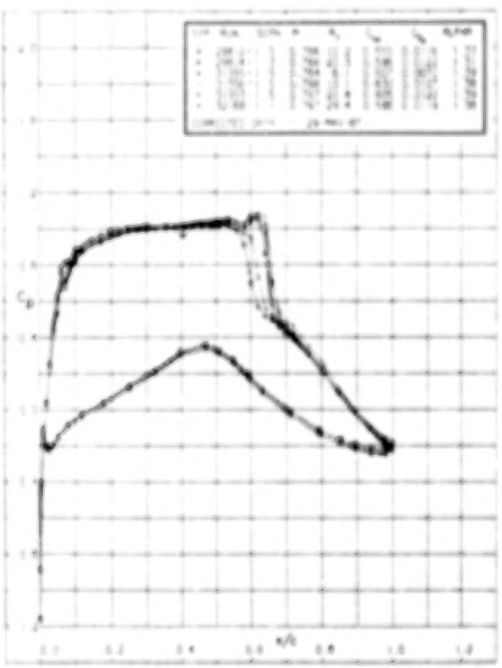

REYNOLDS NUMBER EFFECTS ON SURFACE PRESSURE DISTRIBUTIONS AT NOMINAL α = 3.35°, M_∞ = 0.765. THE FIRST TWO CASES ARE WITH TRANSITION FIXED, THE REST ARE TRANSITION FREE

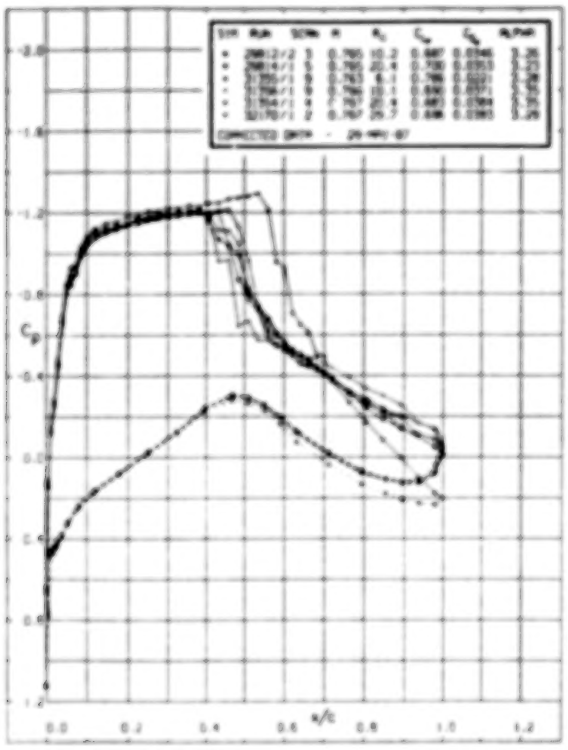

REYNOLDS NUMBER EFFECTS ON SURFACE PRESSURE DISTRIBUTIONS AT NOMINAL α = 1.35°, M_∞ = 0.765. THE FIRST TWO CASES ARE WITH TRANSITION FIXED, THE REST ARE TRANSITION FREE

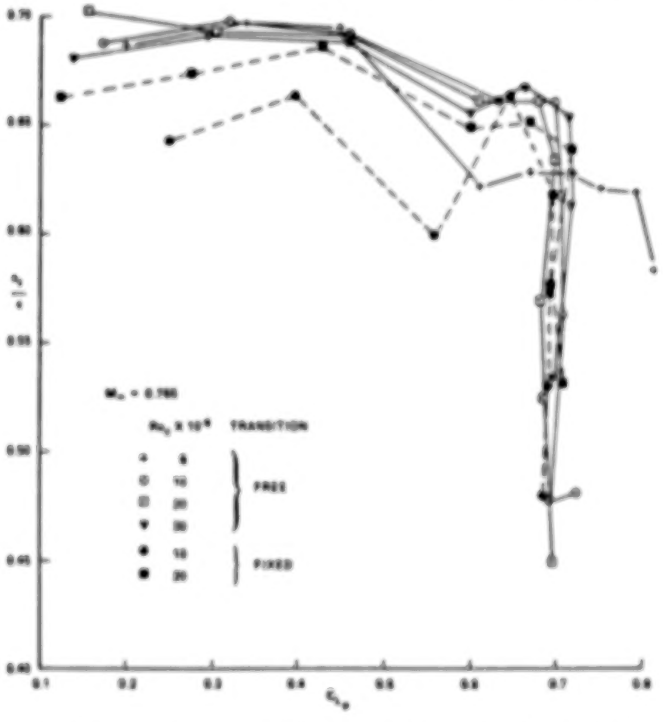

SHOCK LOCATION VERSUS LIFT AT VARIOUS REYNOLDS NUMBERS WITH FIXED OR FREE TRANSITION AT NOMINAL M_∞ = 0.765

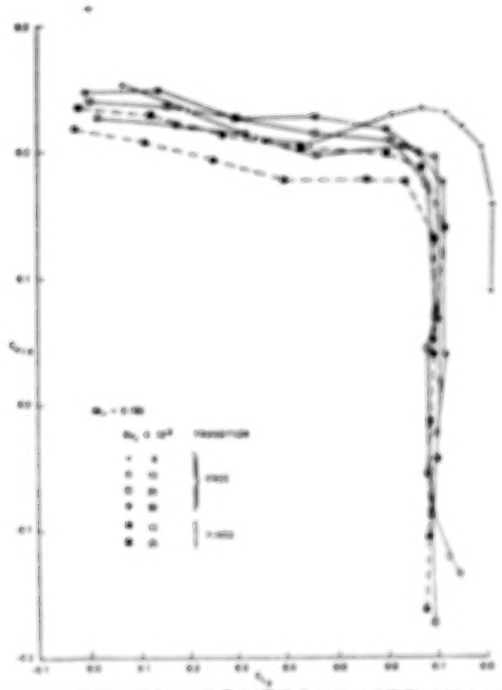

TRAILING EDGE PRESSURE VERSUS LIFT AT VARIOUS REYNOLDS NUMBERS WITH FIXED OR FREE TRANSITION AT NOMINAL M_∞ = 0.765

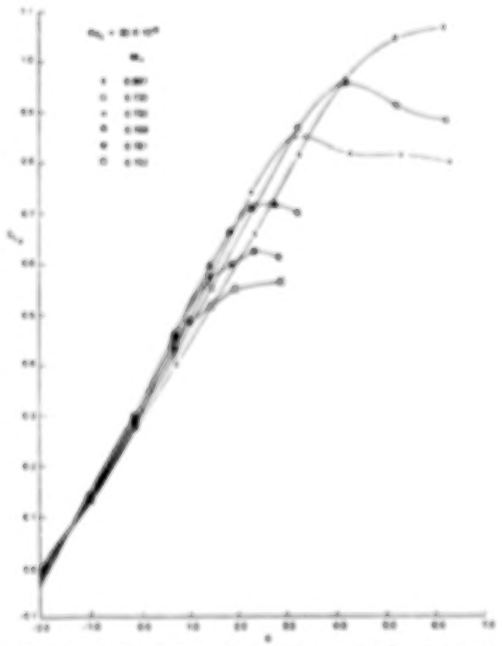

LIFT VERSUS ANGLE OF ATTACK AT VARIOUS MACH NUMBERS AT NOMINAL Re_c = 30 X 10^6 WITH FREE TRANSITION

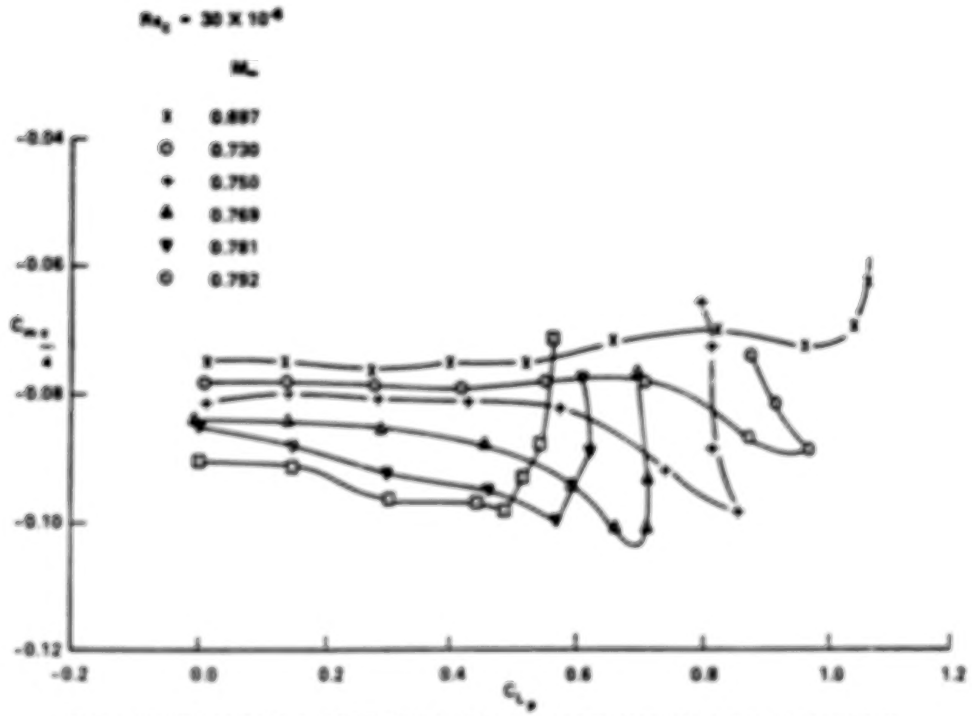

PITCHING MOMENT VERSUS LIFT AT VARIOUS MACH NUMBERS AT NOMINAL Re_c = 30 X 10^6 WITH FREE TRANSITION

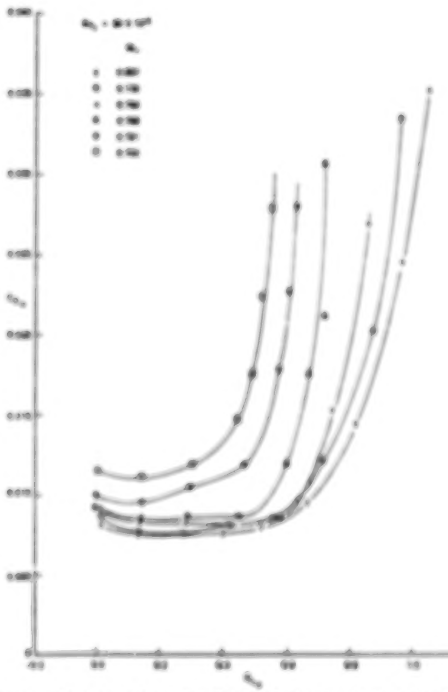

DRAG VERSUS LIFT AT VARIOUS MACH NUMBERS AT NOMINAL Re_c = 30 X 10^6 WITH FREE TRANSITION

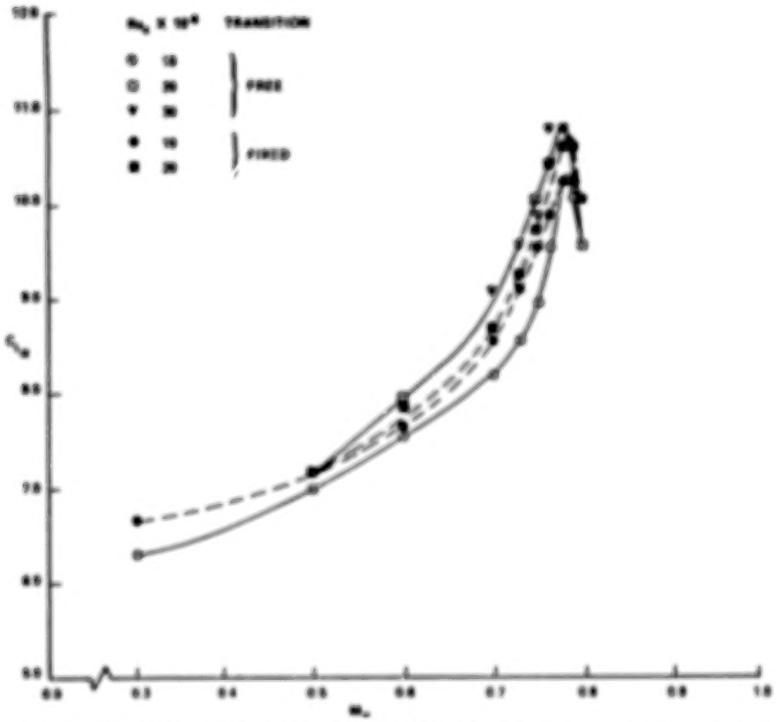

LIFT CURVE SLOPE AT ZERO LIFT VERSUS MACH NUMBER AT VARIOUS REYNOLDS NUMBERS WITH FIXED OR FREE TRANSITION

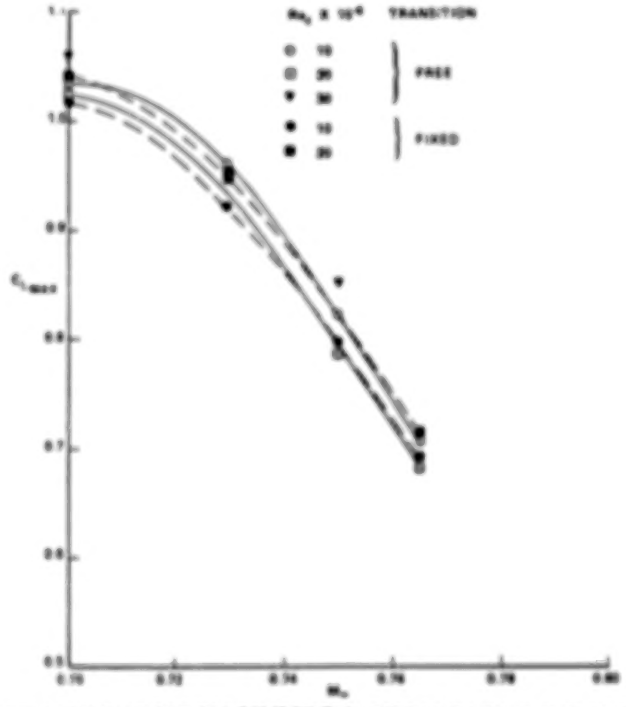

MAXIMUM LIFT VERSUS MACH NUMBER AT VARIOUS REYNOLDS NUMBERS WITH FIXED OR FREE TRANSITION

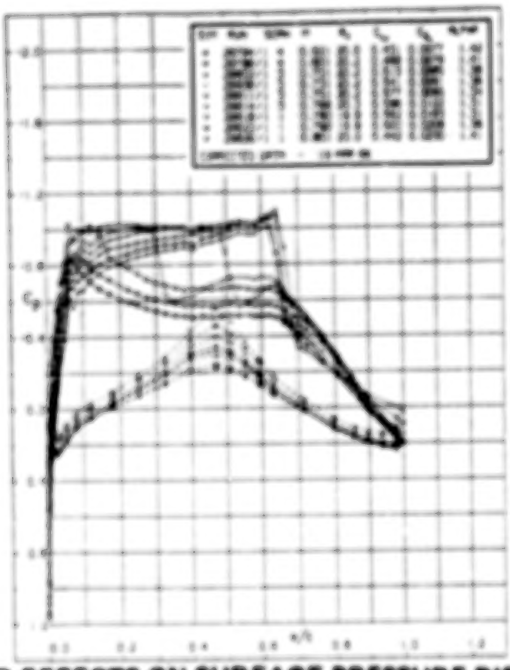

MACH NUMBER EFFECTS ON SURFACE PRESSURE DISTRIBUTIONS AT NOMINAL α = 1.35°, Re_c = 20 X 10^6 WITH FIXED TRANSITION

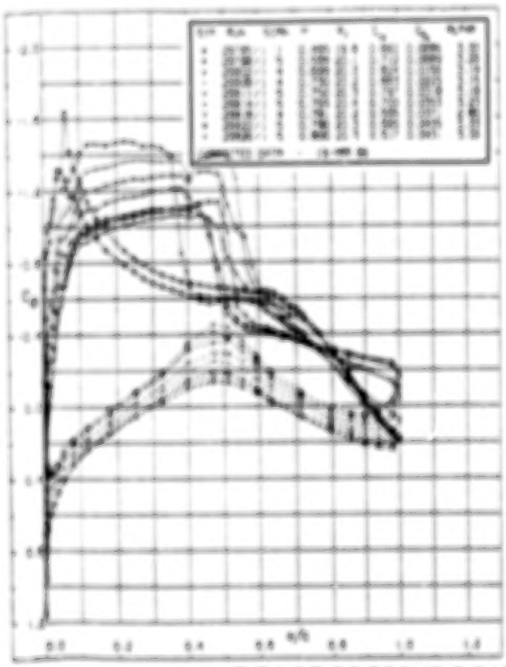

MACH NUMBER EFFECTS ON SURFACE PRESSURE DISTRIBUTIONS AT NOMINAL α = 3.35°, Re_c = 20 X 10^6 WITH FIXED TRANSITION

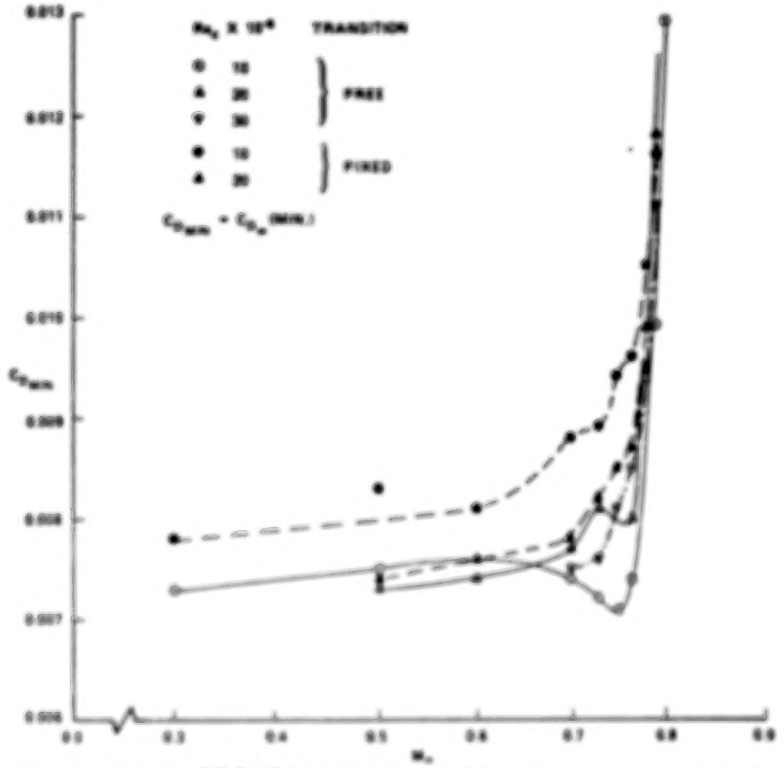

MINIMUM DRAG VERSUS MACH NUMBER AT VARIOUS REYNOLDS NUMBERS WITH FIXED OR FREE TRANSITION

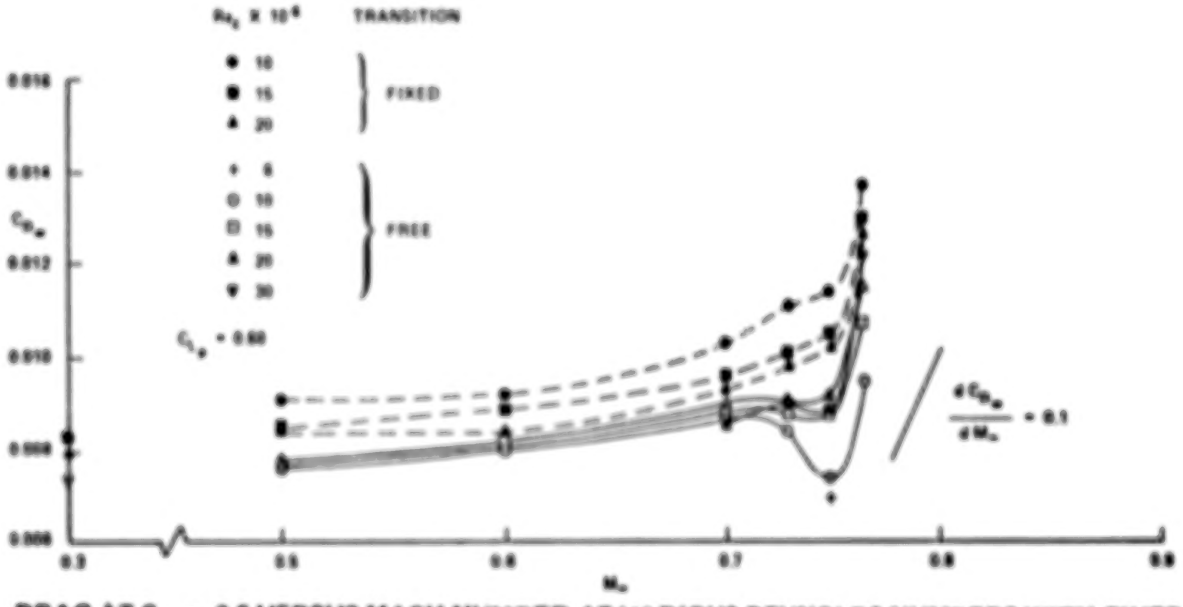

DRAG AT C_{l_p} = 0.6 VERSUS MACH NUMBER AT VARIOUS REYNOLDS NUMBERS WITH FIXED OR FREE TRANSITION

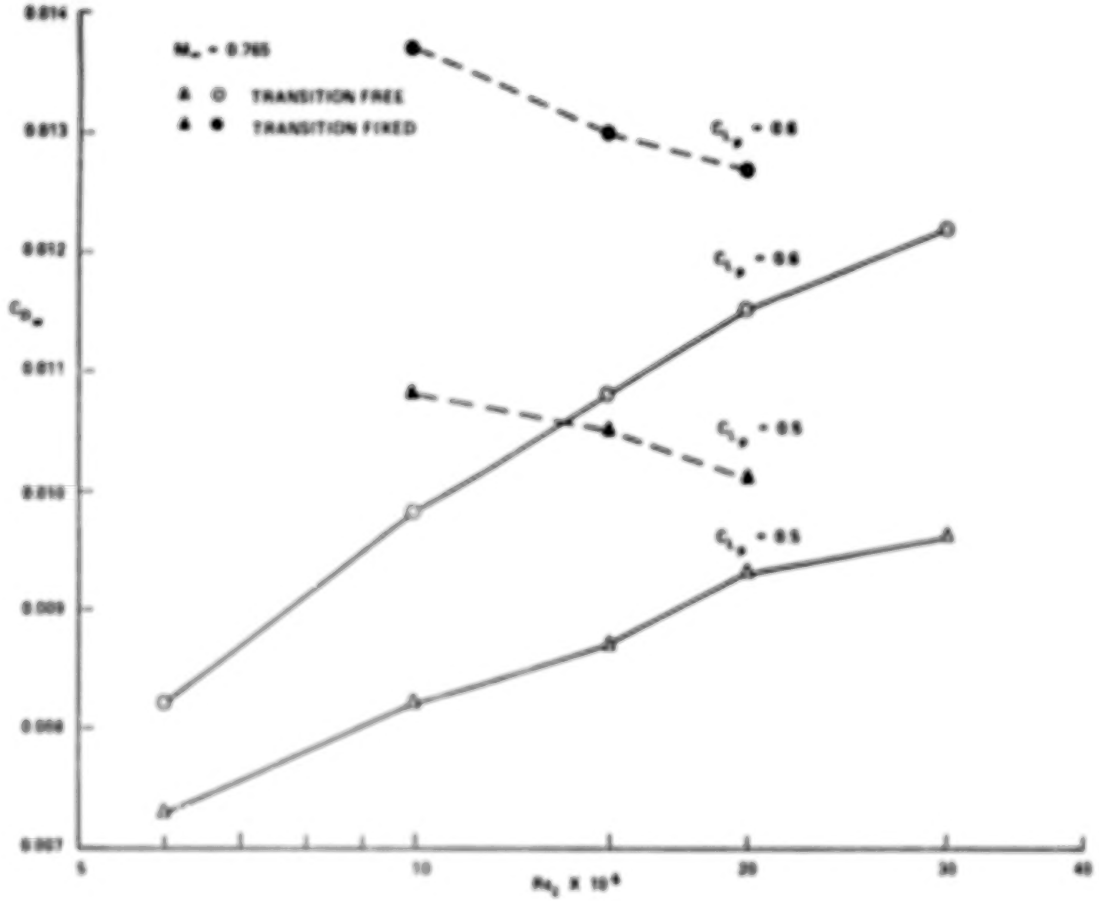

REYNOLDS NUMBER DEPENDENCE OF DRAG AT M_∞ = 0.765, C_{L_p} = 0.5, 0.6 WITH FIXED OR FREE TRANSITION

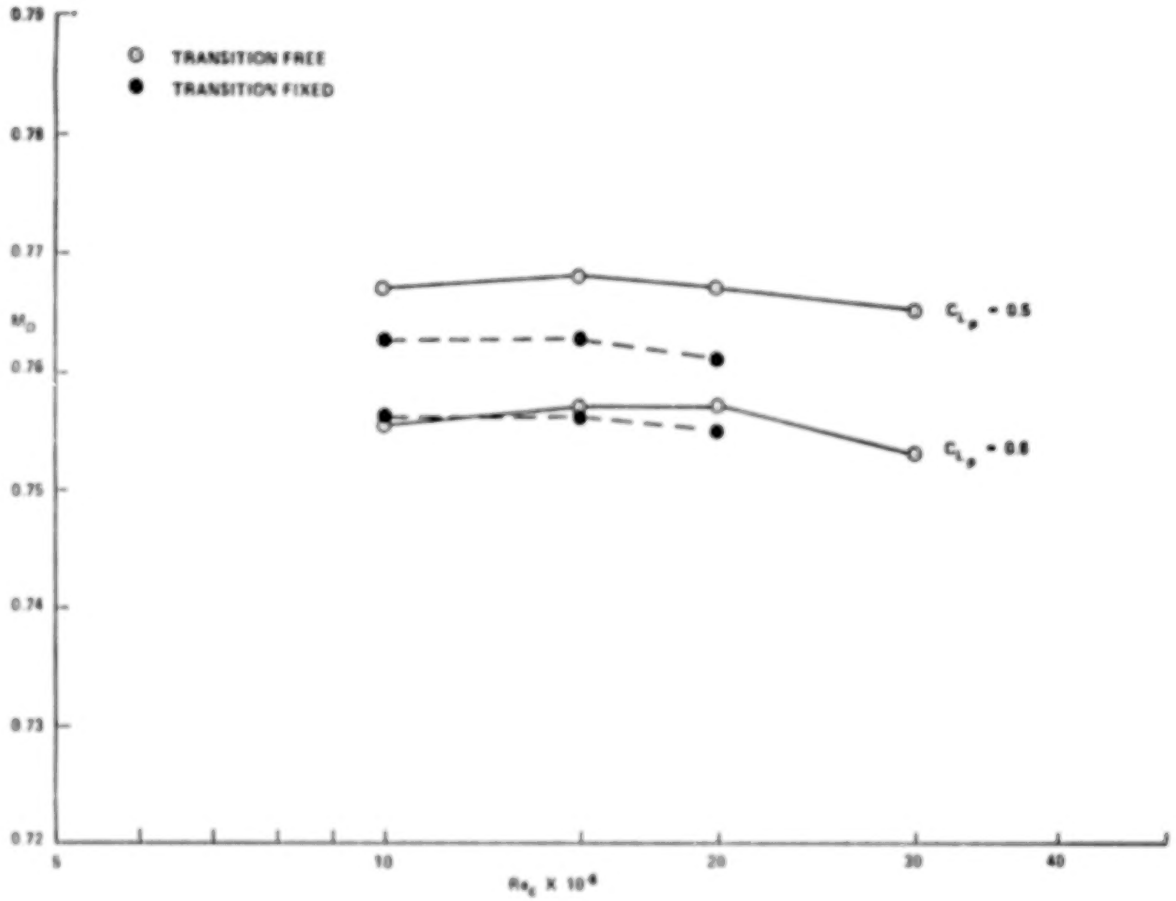

REYNOLDS NUMBER DEPENDENCE OF DRAG WITH MACH NUMBER FOR TWO LIFT CONDITIONS WITH FIXED AND FREE TRANSITION

RESIDUAL INTERFERENCE AND WIND TUNNEL WALL ADAPTATION

Miroslav Mokry

National Aeronautical Establishment
National Research Council of Canada, Ottawa

I. Introduction

Measured flow variables near the test section boundaries, used to guide adjustments of the walls in adaptive wind tunnels, can also be used to quantify the residual interference. Because of a finite number of wall control devices (jacks, plenum compartments), the finite test section length, and the approximation character of adaptation algorithms, the unconfined flow conditions are not expected to be precisely attained even in the 'fully' adapted stage [1],[2].

The procedures for the evaluation of residual wall interference are essentially the same as those used for assessing the corrections in conventional, non-adaptive wind tunnels. Depending upon the number of flow variables utilized, we speak of *one-* or *two-variable* methods [3]; in two dimensions also of *Schwarz-* or *Cauchy-type* methods [4].

The one-variable methods use the measured static pressure distribution at the test section boundary and supplement it with the far field representation of the model, estimated from its geometry and measured forces.

The two-variable methods use measurements of static pressure and normal velocity at the test section boundary, but do not require any model representation. This is clearly of an advantage for adaptive wall test sections, which are often relatively small with respect to the test model, and for the variety of complex flows commonly encountered in wind tunnel testing. For test sections with flexible walls the normal component of velocity is given by the shape of the wall, adjusted for the displacement effect of its boundary layer. For ventilated test section walls it has to be measured by the Calspan Pipes, Laser Doppler Velocimetry, or other appropriate techniques.

The *interface discontinuity method*, also described, is a 'genuine' residual interference assessment technique. It is specific to adaptive wall wind tunnels, where the computation results for the fictitious flow in the exterior of the test section are provided.

II. Linear Flow Analysis

Since the adaptive walls introduce only minor disturbances to the unconfined far field of the test model, the linearization of the potential equation near the walls is applicable as long as the flow remains subcritical there.

The governing equation for the disturbance velocity potential is

$$\beta^2 \frac{\partial^2 \phi}{\partial x^2} + \frac{\partial^2 \phi}{\partial y^2} + \frac{\partial^2 \phi}{\partial z^2} = 0, \tag{1}$$

where $\beta = \sqrt{1 - M_\infty^2}$, and $M_\infty < 1$ is the stream Mach number.

The scaling of the streamwise coordinate,

$$x' = \frac{x}{\beta}, \tag{2}$$

reduces Eq.(1) to Laplace's equation, $\nabla^2 \phi = 0$.

The linear flow region where ϕ satisfies Eq.(1) is shown schematically in Fig.1a. It excludes the volume occupied by the test model, its viscous and transonic flow regions, and the wind tunnel exterior, where no real flow exists. The outer bounding surface, enclosing the test model, is expected to lie entirely within the linear flow region, off the viscous or nonisentropic flow at the walls.

Using the principle of linear superposition, the disturbance velocity potential is split as [5]

$$\phi = \phi_m + \phi_w, \tag{3}$$

where ϕ_m is that due to the model in free air and ϕ_w is that due to wall interference.

The model potential, ϕ_m, satisfies Eq.(1) in the infinite space outside the model and the adjacent nonlinear flow regions, Fig.1b.

The wall interference potential, ϕ_w, is assumed to satisfy Eq.(1) in the entire test section interior, including the model and its nonlinear flow regions, as indicated in Fig.1c.

This assignment of the singular and nonsingular parts as the effects of the model and the walls respectively is consistent with the concept of Green's function for the Laplace operator. Accordingly, it is rigorous for an infinitesimal model, but only approximate for a finite-size model.

The derivatives of ϕ_w are interpreted as disturbances to stream velocity components. They are usually evaluated at the model reference station or as averages over the model and interpreted as *global corrections* to stream Mach number [6]

$$\Delta M_\infty = (1 + \frac{\gamma - 1}{2} M_\infty^2) M_\infty \frac{\partial \phi_w}{\partial x}, \tag{4}$$

and to flow angles (in radians)

$$\Delta \alpha_y = \frac{\partial \phi_w}{\partial y} \qquad \text{and} \qquad \Delta \alpha_z = \frac{\partial \phi_w}{\partial z}. \tag{5}$$

From the spatial variations of these corrections over the model additional streamline curvature and buoyancy effects on model force data can be determined.

In connection with adaptive wall wind tunnels, another type of the disturbance velocity potential is helpful: that corresponding to the 'fictitious' flow outside the wind tunnel.

The potential, denoted here by the symbol $\tilde{\phi}$, satisfies Eq.(1) in the exterior of the outer bounding surface, Fig.1d. The surface, separating the real wind tunnel flow and the computed exterior flow is also termed the *interface*. The aim of adaptation is to adjust the walls so that ϕ and $\tilde{\phi}$ constitute a single potential ϕ_m, continuous at the interface. There is a direct relationship between ϕ_w and the difference $\phi - \tilde{\phi}$ at the interface.

A. One-Variable Method

The method, due to *Capelier, Chevallier and Bouniol* [7], is the most popular technique for the assessment of subsonic wall interference in wind tunnels with perforated walls. It retains the essential features of the classical wall interference approach [5], but replaces the idealized wind tunnel boundary conditions by

$$\frac{\partial \phi}{\partial x} = -\frac{1}{2} C_p, \tag{6}$$

where C_p is the measured boundary pressure coefficient. The control surface along which the pressure is measured should be some distance away from the wall, where the disturbances of individual holes (perforations) are smeared out. The application of the method to test sections with slotted walls is more problematic as the flow becomes homogeneous at rather large distances from the walls, and the pressures measured directly on slat surfaces do not necessarily represent the averaged values.

The axial component of wall interference velocity,

$$u_w = \frac{\partial \phi_w}{\partial x}, \tag{7}$$

satisfying inside the test section

$$\beta^2 \frac{\partial^2 u_w}{\partial x^2} + \frac{\partial^2 u_w}{\partial y^2} + \frac{\partial^2 u_w}{\partial z^2} = 0, \tag{8}$$

is obtained from its boundary values

$$u_w = -\frac{1}{2} C_p - \frac{\partial \phi_m}{\partial x} \tag{9}$$

as a solution of the interior Dirichlet problem. The transverse velocity components,

$$v_w = \frac{\partial \phi_w}{\partial y} \qquad \text{and} \qquad w_w = \frac{\partial \phi_w}{\partial z}, \tag{10}$$

can be obtained from u_w by integrating the irrotational-flow conditions

$$\frac{\partial v_w}{\partial x} = \frac{\partial u_w}{\partial y} \qquad \text{and} \qquad \frac{\partial w_w}{\partial x} = \frac{\partial u_w}{\partial z} \tag{11}$$

along a path from the upstream end of the test section.

The Dirichlet problem for Laplace's equation is one of the best explored problems in mathematical physics and there are a large number of methods available to solve it numerically. A natural approach is to solve the problem in terms of the double layer potential [8], leading to a doublet panel method [9]. For simpler geometries, closed form solutions are obtainable using integral transforms [7] or the Fourier method [10]-[12].

The complex-variable treatment [7] of the two-dimensional problem leads, as pointed out in Ref.[4], to the Schwarz problem, consisting of determining an analytic function inside a domain from its defined real part on the boundary. Theory [13] shows that the integration of Cauchy-Riemann equations (irrotational-flow conditions) introduces an unknown imaginary constant, which needs to be specified in order to make the solution unique (specification of the upstream flow angle).

The accuracy of the one-variable method depends greatly on the accuracy with which the free air potential ϕ_m can be predicted on the control surfaces [14],[15]. Since the far field of ϕ_m is normally evaluated using the measured model loading, subject to wall interference, the prediction tends to be more exact near a fully adapted stage. However, when compared to the relative size of the model, the adaptive test sections are usually much narrower than the conventional ones, so that the representation of flow near the walls in terms of the model far field may not be satisfactory.

Another source of inaccuracy is the finite length of the test section and sparseness of the experimental pressure data. The boundary values of u_w have to be interpolated or extrapolated over a complete boundary (closed or infinite), in order to make the Dirichlet problem soluble. The adaptive test sections, which are typically longer than the conventional ones, will have a slight advantage in this regard.

The method can be used to monitor the reduction of wall interference corrections in the course of adaptation, but can also be incorporated into the adaptation algorithm [16]. Interference-free (unconfined) flow will be characterized by the vanishing boundary values of u_w:

$$u_w \equiv 0 \quad \text{on} \quad S. \tag{12}$$

Compensation for errors of reference velocity or pressure [7], also called the *autocorrective property* [15] or *autoconvergence* [17], is an important feature of the method. It applies within the limits of linearization and may be stated as follows: if the error of the (upstream) reference velocity U_∞ is δU_∞, then the perturbation velocities $U - U_\infty$ on the boundary will be offset by $-\delta U_\infty$. The ensuing incremental correction, being of equal magnitude but opposite sign to the reference velocity error, will restore U_∞ as the reference velocity.

For the one-variable method, working with measured boundary pressures p, the autocorrective property can easily be verified by introducing the pressure coefficient

$$C_p = \frac{p - p_\infty}{\frac{1}{2}\rho_\infty U_\infty^2},$$

and its error [6]

$$\delta C_p = \frac{p - (p_\infty + \delta p_\infty)}{\frac{1}{2}\rho_\infty U_\infty^2 + \delta\left(\frac{1}{2}\rho_\infty U_\infty^2\right)} \qquad C_p$$

$$\simeq \left[2 - (2 - M_\infty^2)C_p\right]\frac{\delta U_\infty}{U_\infty}$$

$$\simeq 2\frac{\delta U_\infty}{U_\infty} \qquad \text{if} \quad C_p \simeq 0.$$

From Eq.(9), considering $\partial\phi_m/\partial x$ invariant, the boundary value of u_w is found to have a constant increment

$$\delta u_w = -\frac{1}{2}\delta C_p \simeq -\frac{\delta U_\infty}{U_\infty}, \tag{13}$$

which is equal and opposite to the relative error of reference velocity. This incremental correction also applies also interior points since

$$\delta u_w(x, y, z) = -\frac{\delta U_\infty}{U_\infty} = \text{constant}$$

is a solution of Eq.(8) satisfying the boundary condition (13). There are no other possibilities, as the solution to a Dirichlet problem is unique.

Besides compensating for genuine reference velocity errors, the autocorrective principle also establishes the correspondence between U_∞ based on plenum pressure and actual stream velocity in ventilated test sections.

B. Two-Variable Method

Measurement of the static pressure and normal velocity distributions along the control surface opens the possibility of evaluating subsonic wall interference bypassing the model representation. The two-variable method is most easily applied to solid wall test sections where the walls can serve as control surfaces.

Independent formulations of this concept using Green's theorem are due to *Ashill* and *Weeks* [18] and Cauchy's integral formula (in 2D) due to *J. Smith* [4].

To describe the method, we introduce the position vectors of an interior point and a boundary point,

$$\mathbf{r}_0 = (x_0', y_0, z_0) \qquad \text{and} \qquad \mathbf{r} = (x', y, z), \tag{14}$$

and denote by

$$G(\mathbf{r}_0, \mathbf{r}) = -\frac{1}{4\pi|\mathbf{r}_0 - \mathbf{r}|} \tag{15}$$

the fundamental solution (unit-strength source) for the three-dimensional Laplace operator.

Green's second identity gives for a function ϕ_w harmonic in the test section interior

$$\phi_w(\mathbf{r}_0) = \iint_S \left[\phi_w(\mathbf{r})\frac{\partial G(\mathbf{r}_0, \mathbf{r})}{\partial n} - G(\mathbf{r}_0, \mathbf{r})\frac{\partial \phi_w(\mathbf{r})}{\partial n}\right] dS$$

and for a function ϕ_m harmonic in the test section exterior

$$0 = \iint_S [\phi_m(\mathbf{r}) \frac{\partial G(\mathbf{r}_0,\mathbf{r})}{\partial n} - G(\mathbf{r}_0,\mathbf{r}) \frac{\partial \phi_m(\mathbf{r})}{\partial n}] dS.$$

The differential and integral operations are taken with respect to the unsubscripted coordinates; S is the control surface (interface) enclosing the test section interior, and $\partial/\partial n$ is the derivative along the outward normal to the control surface in the transformed space (x', y, z).

Adding the above formulae and eliminating ϕ_m from Eq.(3), we obtain the correction formula of *Ashill* and *Weeks* [18]:

$$\phi_w(\mathbf{r}_0) = \iint_S [\phi(\mathbf{r}) \frac{\partial G(\mathbf{r}_0,\mathbf{r})}{\partial n} - G(\mathbf{r}_0,\mathbf{r}) \frac{\partial \phi(\mathbf{r})}{\partial n}] dS. \qquad (16)$$

It expresses the interior value of the wall interference potential in terms of boundary values of the (total) disturbance velocity potential.

Considering the entire space, Eq.(16) describes a sectionally harmonic function ϕ_w having a jump discontinuity ϕ across the surface S. This differs from the more conventional representation of the wall interference potential by external singularities, where ϕ_w is continuous across S and harmonic everywhere except at the singular points. Of course, inside the test section both representations are equivalent.

Physically, integral (16) can be interpreted as a surface distribution of doublets

$$\frac{\partial G(\mathbf{r}_0,\mathbf{r})}{\partial n} \qquad \text{with density} \qquad \phi(\mathbf{r})$$

and a surface distribution of sources

$$G(\mathbf{r}_0,\mathbf{r}) \qquad \text{with density} \qquad -\frac{\partial \phi(\mathbf{r})}{\partial n}.$$

The normal component of disturbance velocity $\partial\phi/\partial n$ can be measured directly, whereas the potential ϕ has to be evaluated by a streamwise integration of the measured pressure coefficient, Eq.(6).

Another possibility offers the integration by parts [19], converting the surface distribution of doublets into a surface distribution of (horseshoe) vortices

$$\Omega(\mathbf{r}_0,\mathbf{r}) = \int_{x'}^{\infty} \frac{\partial G(\mathbf{r}_0,\mathbf{r})}{\partial n} dx' \qquad \text{with density} \qquad \frac{\partial \phi(\mathbf{r})}{\partial x'} = -\frac{\beta}{2} C_p(\mathbf{r}). \qquad (17)$$

The far upstream and downstream terms are eliminated by the virtue of

$$\phi(\mathbf{r}_0,\mathbf{r}) \to 0 \quad \text{as} \quad x' \to -\infty \qquad \text{and} \qquad \Omega(\mathbf{r}_0,\mathbf{r}) \to 0 \quad \text{as} \quad x' \to \infty.$$

Taking in Eq.(16) the limit as $\mathbf{r}_0$ becomes a point of a smooth surface element, we obtain

$$\phi_w(\mathbf{r}_0) = \frac{1}{2}\phi(\mathbf{r}_0) + \iint_S [\phi(\mathbf{r}) \frac{\partial G(\mathbf{r}_0,\mathbf{r})}{\partial n} - G(\mathbf{r}_0,\mathbf{r}) \frac{\partial \phi(\mathbf{r})}{\partial n}] dS, \quad \mathbf{r}_0 \in S. \qquad (18)$$

A small circular neighbourhood of the singular point $\mathbf{r}_0$ is to be taken out from the surface S for the doublet integral; its contribution has already been accounted for by the isolated term $\frac{1}{2}\phi(\mathbf{r}_0)$. There is no ambiguity concerning the source integral, as the contribution of a small circular element around the point $\mathbf{r}_0$ is zero.

Another interesting relationship is obtained by substituting Eq.(18) in Eq.(3):

$$\phi_m(\mathbf{r}_0) = \frac{1}{2}\phi(\mathbf{r}_0) - \iint_S \left[\phi(\mathbf{r})\frac{\partial G(\mathbf{r}_0,\mathbf{r})}{\partial n} - G(\mathbf{r}_0,\mathbf{r})\frac{\partial \phi(\mathbf{r})}{\partial n}\right] dS, \quad \mathbf{r}_0 \in S. \tag{19}$$

This formula, similar to that developed in Ref.[19], determines the boundary value of the free air potential, ϕ_m, from the measured boundary values of ϕ and $\partial\phi/\partial n$. Provided that the difference between the boundary values of ϕ and ϕ_m is small, it may be possible to achieve $\phi = \phi_m$ in a single adjustment of the walls. Equation (19) will then play the role of a *single-step convergence formula*, a concept introduced in Ref.[20].

Alternative formulations of the correction method based on Green's theorem are given in Refs.[21] and [22], comparisons and accuracy aspects are discussed in Ref.[23]. Model representation, as shown above, is no longer required, but the sparseness of boundary data and incomplete test section boundary remain as a major source of inaccuracy.

The specification of *interference-free conditions* in the two-variable method is straightforward. Setting $\phi_w = 0$ in Eq.(18) or $\phi_m = \phi$ in Eq.(19), we obtain

$$\frac{1}{2}\phi(\mathbf{r}_0) = -\iint_S \left[\phi(\mathbf{r})\frac{\partial G(\mathbf{r}_0,\mathbf{r})}{\partial n} - G(\mathbf{r}_0,\mathbf{r})\frac{\partial \phi(\mathbf{r})}{\partial n}\right] dS, \quad \mathbf{r}_0 \in S, \tag{20}$$

which interrelates the values of ϕ and $\partial\phi/\partial n$ on the bounding surface of an adapted test section.

The descent to two dimensions is accomplished by putting

$$\mathbf{r}_0 = (x'_0, y_0), \quad \mathbf{r} = (x', y), \quad G(\mathbf{r}_0,\mathbf{r}) = \frac{1}{2\pi}\ln|\mathbf{r}_0 - \mathbf{r}|,$$

and replacing the surface integrals by contour integrals.

However, more readily applicable results are obtained using Cauchy's integral formula. To illustrate this approach, we introduce the complex coordinate

$$z = x' + iy = \frac{x}{\beta} + iy \tag{21}$$

and the complex disturbance velocity

$$w(z) = \beta u(x,y) - iv(x,y) = \beta\frac{\partial\phi}{\partial x}(x,y) - i\frac{\partial\phi}{\partial y}(x,y). \tag{22}$$

In accordance with Eq.(3), the complex disturbance velocity is decomposed as

$$w(z) = w_m(z) + w_w(z), \tag{23}$$

where w_w is analytic in the test section interior and w_m is analytic in the test section exterior. Applying the Cauchy integral formula to a counterclockwise oriented contour C, we obtain for an interior point z_0

$$w_w(z_0) = \frac{1}{2\pi i}\int_C \frac{w_w(z)}{z - z_0}dz$$

and

$$0 = \frac{1}{2\pi i}\int_C \frac{w_m(z)}{z - z_0}dz.$$

Adding the integrals and eliminating w_m from Eq.(23), we obtain *Smith's* correction formula [4]:

$$w_w(z_0) = \frac{1}{2\pi i}\int_C \frac{w(z)}{z - z_0}dz, \tag{24}$$

expressing the wall interference velocity in terms of boundary value of the (total) disturbance velocity.

The Cauchy type integral along a curved path can be evaluated as indicated in Appendix. Using Eq.(22), the components of the wall interference velocity are obtained as:

$$u_w(x_0, y_0) = \frac{1}{\beta}\mathrm{Re}\{w_w(z_0)\} \qquad \text{and} \qquad v_w(x_0, y_0) = -\mathrm{Im}\{w_w(z_0)\}. \tag{25}$$

An example of wall deflections and wall pressures from the tests [24] of the 9-in chord CAST 10-2/DOA 2 airfoil in the 13-in by 13-in flexible-wall test section of the Langley Transonic Cryogenic Wind Tunnel (TCT) is shown in Fig.2. The wall pressure distribution at the stream Mach number of 0.7 is subcritical as required. The downstream end of the integration contour was placed so as to cut off the last three pressure points, drifting away from the undisturbed flow conditions. The distribution of residual corrections along the wind tunnel axis, evaluated by the two-variable method, is shown in Fig.3. The flow in the test section is not interference free, but considering the size of the model with respect to the test section, the corrections are certainly small.

More detailed formulae, together with residual interference evaluated for the ONERA/CERT T2 flexible wall wind tunnel, can be found in Ref.[25].

Considering the entire complex plane, Eq.(24) describes a sectionally analytic function w_w having a jump discontinuity w across the contour C. This is obviously in contrast with the conventional representation of the complex interference velocity by external poles, allowing w_w to be analytically continued across C, but only up to the location of the poles.

The Cauchy-type integral (24) can be recast into the contour integral

$$w_w(z_0) = \int_C \left[\frac{i\gamma(z)}{2\pi(z_0 - z)} + \frac{\sigma(z)}{2\pi(z_0 - z)}\right]ds, \tag{26}$$

where $ds = |dz|$ is the counterclockwise oriented contour length element.

The integral can be interpreted as a line distribution of vortices

$$\frac{i}{2\pi(z_0 - z)} \qquad \text{with density} \qquad \gamma(z) = \mathrm{Re}\left\{ w(z) \frac{dz}{|dz|} \right\} = q_t(z) \tag{27}$$

and a line distribution of sources

$$\frac{1}{2\pi(z_0 - z)} \qquad \text{with density} \qquad \sigma(z) = -\mathrm{Im}\left\{ w(z) \frac{dz}{|dz|} \right\} = -q_n(z), \tag{28}$$

where q_t is the tangent component of disturbance velocity (positive in the counterclockwise direction) and q_n is the normal component of disturbance velocity (positive in the direction of the outward normal). The correspondence with Green's theorem approach is evident.

The *autocorrective property* of Eq.(24) again applies [15] and is easy to verify. Starting with the reference velocity increment δU_∞, the boundary value of the x-component of disturbance velocity

$$u = \frac{U - U_\infty}{U_\infty}$$

is found to have an increment

$$\delta u = \frac{U - (U_\infty + \delta U_\infty)}{U_\infty + \delta U_\infty} - u \simeq -\frac{\delta U_\infty}{U_\infty}.$$

From Eqs.(22) and (24) it follows for the increment of the complex disturbance velocity at an interior point z_0

$$\delta w_w(z_0) = \frac{\beta\, \delta u}{2\pi i} \int_C \frac{dz}{z - z_0} = \beta\, \delta u.$$

Finally, from Eqs.(25)

$$\delta u_w(x_0, y_0) = \delta u \simeq -\frac{\delta U_\infty}{U_\infty},$$

$$\delta v_w(x_0, y_0) = 0.$$

A practical verification of the autocorrective property is shown in Fig.4. The reference Mach number of our example in Fig.2 was tentatively changed from 0.700 to 0.695 and the wall pressure coefficients, used as input for the residual interference calculation, were recalculated accordingly. Comparing Fig.4 with Fig.3, we note that the resultant Mach number correction curve is displaced by 0.005 in the positive direction, so that the corrected Mach number is again the same. The angle of attack correction, as expected, is not greatly affected by the change of the reference Mach number.

Correction formula (24) is closely related to wall adaptation criteria for two-dimensional testing. In the limiting process, as z_0 becomes a point on a smooth segment of the contour C we obtain

$$w_w(z_0) = \frac{1}{2} w(z_0) + \frac{1}{2\pi i} \int_C \frac{w(z)}{z - z_0}\, dz, \quad z_0 \in C, \tag{29}$$

where the (singular) integral is to be interpreted as Cauchy's principal value.

Substituting Eq.(29) in (23), we find

$$w_m(z_0) = \frac{1}{2}w(z_0) - \frac{1}{2\pi i}\int_C \frac{w(z)}{z - z_0}dz, \quad z_0 \in C, \tag{30}$$

which is the limiting case of the formula given in Ref.[26]. It determines the boundary value w_m of the complex disturbance velocity due to the model in free air, in terms of the measured values w. This result proves again that the model representation in the two-variable method is, in theory, superfluous. However, for incomplete boundary data an independently estimated far field of w_m may conveniently be used to aid the interpolations and extrapolations.

Equation (30) may also be used as the two-dimensional *single-step convergence formula*; the case of straight line boundaries can be found in Refs.[20] and [27].

Setting $w_w = 0$ in Eq.(29) or $w_m = w$ in Eq.(30), we obtain the *interference-free condition*

$$\frac{1}{2}w(z_0) = -\frac{1}{2\pi i}\int_C \frac{w(z)}{z - z_0}dz, \quad z_0 \in C \tag{31}$$

in terms of the complex disturbance velocity on the boundary. The factor $\frac{1}{2}$ was left uncancelled, to emphasize the connection with the three-dimensional condition, Eq.(20).

Considering straight line boundaries at $y = \pm\frac{h}{2}$, we obtain in terms of disturbance velocity components

$$u(x_0, \pm\frac{h}{2}) = \mp\frac{1}{\beta\pi}\int_{-\infty}^{\infty} \frac{v(x, \pm\frac{h}{2})}{x - x_0}dx, \tag{32a}$$

$$v(x_0, \pm\frac{h}{2}) = \pm\frac{\beta}{\pi}\int_{-\infty}^{\infty} \frac{u(x, \pm\frac{h}{2})}{x - x_0}dx. \tag{32b}$$

These 'compressible-flow' versions of Hilbert's transforms, introduced by *Sears* [1] as *functional relationships* between two velocity components, define unconfined flow in a two-dimensional test section.

C. Interface Discontinuity Method

This residual interference method, closely related to the two-variable method, utilizes exterior flow calculations. The general idea, as proposed by *Sears* and *Erickson* [28] is essentially this: the flow field is considered to consist of an experimental inner region joined at an interface to a computed outer region. If the computed outer flow satisfies the unconfined flow conditions and matches along the interface the inner flow, then the combined flow field is continuous, representing unconfined flow around the model. The matching error, or discontinuity, provides a measure of the residual interference. It can be quantified by removing the discontinuity by a surface distribution of singularities. These singularities do not disturb the unconfined flow condition in the outer region, but do introduce velocity perturbations at the position of the test model, which then can be interpreted as the usual wall interference corrections.

As for the two-component method, Green's theorem will give us a quick answer as to what the suitable singularities and their densities should be. Selecting $\mathbf{r}_0$ to be an interior point, we obtain for the function $\tilde{\phi}$, representing the disturbance velocity potential of the fictitious flow in the exterior region

$$0 = \iint_S \left[\tilde{\phi}(\mathbf{r}) \frac{\partial G(\mathbf{r}_0,\mathbf{r})}{\partial n} - G(\mathbf{r}_0,\mathbf{r}) \frac{\partial \tilde{\phi}(\mathbf{r})}{\partial n}\right] dS.$$

Subtracting it from Eq.(16), we obtain the interior value of the wall interference potential in terms of the differences of the interior and exterior flow potentials and their normal derivatives along the interface:

$$\phi_w(\mathbf{r}_0) = \iint_S \left\{ \left[\phi(\mathbf{r}) - \tilde{\phi}(\mathbf{r})\right] \frac{\partial G(\mathbf{r}_0,\mathbf{r})}{\partial n} - \left[\frac{\partial \phi(\mathbf{r})}{\partial n} - \frac{\partial \tilde{\phi}(\mathbf{r})}{\partial n}\right] G(\mathbf{r}_0,\mathbf{r}) \right\} dS. \tag{33}$$

Physically, integral (33) can be interpreted as a surface distribution of doublets

$$\frac{\partial G(\mathbf{r}_0,\mathbf{r})}{\partial n} \qquad \text{with density} \qquad \left[\phi(\mathbf{r}) - \tilde{\phi}(\mathbf{r})\right]$$

and a surface distribution of sources

$$G(\mathbf{r}_0,\mathbf{r}) \qquad \text{with density} \qquad -\left[\frac{\partial \phi(\mathbf{r})}{\partial n} - \frac{\partial \tilde{\phi}(\mathbf{r})}{\partial n}\right].$$

The potential $\tilde{\phi}$ is obtained by solving an exterior flow problem (CFD), but ϕ_w is obtained by a surface integration, as in the two-variable method.

The exterior flow can be calculated as a solution of a Neumann problem, satisfying the boundary condition

$$\frac{\partial \tilde{\phi}(\mathbf{r})}{\partial n} = \frac{\partial \phi(\mathbf{r})}{\partial n}, \quad \mathbf{r} \in S, \tag{34}$$

where $\partial\phi(\mathbf{r})/\partial n$ is the normal component of disturbance velocity on the interface. Integral (33) then reduces to the distribution of doublets,

$$\phi_w(\mathbf{r}_0) = \iint_S \left[\phi(\mathbf{r}) - \tilde{\phi}(\mathbf{r})\right] \frac{\partial G(\mathbf{r}_0,\mathbf{r})}{\partial n} dS. \tag{35}$$

Alternatively, the exterior flow can be calculated as a solution of a Dirichlet problem, satisfying the boundary condition

$$\tilde{\phi}(\mathbf{r}) = \phi(\mathbf{r}), \quad \mathbf{r} \in S, \tag{36}$$

integral (33) reduces to the distribution of sources,

$$\phi_w(\mathbf{r}_0) = -\iint_S \left[\frac{\partial \phi(\mathbf{r})}{\partial n} - \frac{\partial \tilde{\phi}(\mathbf{r})}{\partial n}\right] G(\mathbf{r}_0,\mathbf{r}) dS. \tag{37}$$

The latter approach has recently been described by *Rebstock* and *Lee* [29].

Finally, if the walls are adjusted to satisfy the conditions (34) and (36) simultaneously (a perfect match), then from Eq.(33)

$$\phi_w(r_0) \equiv 0,$$

indicating that the flow inside the test section is interference free. The conditions of flow tangency and equal pressures along the interface imply that the desired interface is a stream tube. This streamlining principle for an adaptive wall test section, introduced by *Goodyer* [2], is of course quite general and not just restricted to linear subsonic flow.

The Cauchy integral approach, applicable to two-dimensional flow, proceeds along the similar lines. Considering the complex disturbance velocity $\tilde{w}$ of the fictitious flow, analytic in the exterior region and vanishing at infinity, then for an interior point z_0 it follows

$$0 = \frac{1}{2\pi i}\int_C \frac{\tilde{w}(z)}{z - z_0}\,dz.$$

Subtracting it from Eq.(24), we obtain

$$w_w(z_0) = \frac{1}{2\pi i}\int_C \frac{w(z) - \tilde{w}(z)}{z - z_0}\,dz. \tag{38}$$

This Cauchy type integral can again be evaluated as described in Appendix.

If the normal component of disturbance velocity is continuous across the interface,

$$\tilde{q}_n(z) = q_n(z), \quad z \in C, \tag{39}$$

then from Eqs.(27)-(28)

$$w_w(z_0) = \int_C \left[(q_t(z) - \tilde{q}_t(z)\right] \frac{i}{2\pi(z_0 - z)}\,ds. \tag{40}$$

The wall interference velocity is represented by contour distribution vortices, whose density is equal to the discontinuity of the tangential component of velocity.

Conversely, if the tangential component of disturbance velocity is continuous,

$$\tilde{q}_t(z) = q_t(z), \quad z \in C, \tag{41}$$

then

$$w_w(z_0) = \int_C -\left[(q_n(z) - \tilde{q}_n(z)\right] \frac{1}{2\pi(z_0 - z)}\,ds. \tag{42}$$

The wall interference velocity is represented by contour distribution sources, whose density is equal and opposite to the discontinuity of the normal component of velocity.

The single-step convergence formula of *Judd, Wolf,* and *Goodyer* [30] can be derived from Eq.(38) by taking the limit as as z_0 becomes a point of interface C, by analogy with Eqs.(24) and (29), and eliminating w_w from Eq.(23).

Appendix

The Cauchy type integral, Eq.(24) or (38), is easily evaluated by using a technique from Ref.[31]. Approximating the contour C by line segments, the integral

$$w_w(z_0) = \frac{1}{2\pi i}\int_C \frac{f(z)}{z - z_0}dz \tag{43}$$

reduces to the sum

$$w_w(z_0) = \sum_j \Delta_j w_w(z_0), \tag{44}$$

where

$$\Delta_j w_w(z_0) = \frac{1}{2\pi i}\int_{z_j}^{z_{j+1}} \frac{f(z)}{z - z_0}dz \tag{45}$$

is the contribution of the j-th segment.

Assuming a linear variation of the density function f between the segment end points z_j and z_{j+1}:

$$\begin{aligned} f(z) &= f_j + \frac{f_{j+1} - f_j}{z_{j+1} - z_j}(z - z_j) \\ &= \frac{f_{j+1} - f_j}{z_{j+1} - z_j}(z - z_0) + f_{j+1}\frac{z_0 - z_j}{z_{j+1} - z_j} - f_j\frac{z_0 - z_{j+1}}{z_{j+1} - z_j} \end{aligned} \tag{46}$$

and substituting it in Eq.(45), we find

$$\Delta_j w_w(z_0) = \frac{f_{j+1} - f_j}{2\pi i} + \frac{1}{2\pi i}\left[f_{j+1}\frac{z_0 - z_j}{z_{j+1} - z_j} - f_j\frac{z_0 - z_{j+1}}{z_{j+1} - z_j}\right]\ln\frac{z_{j+1} - z_0}{z_j - z_0}. \tag{47}$$

References

[1] Sears, W.R., "Self Correcting Wind Tunnels," The Aeronautical Journal, Vol.78, March 1974, pp.80-89.

[2] Goodyer, M.J., "The Self Streamlining Wind Tunnel," NASA TMX-72699, Aug.1975.

[3] Kraft, E.M., Ritter, A., and Laster, M.L., "Advances at AEDC in Treating Transonic Wind Tunnel Wall Interference," ICAS Proceedings 1986, pp.748-769.

[4] Smith, J., "Measured Boundary Conditions for 2D Flow," AGARD-CP-335, May 1982, pp.9.1 - 9.15.

[5] Baldwin,B.S., Turner, J.B., and Knechtel, E.D., "Wall Interference in Wind Tunnels With Slotted and Porous Boundaries at Subsonic Speeds," NACA TN 3176, 1954.

[6] Garner, H.C., Rogers, E.W.E., Acum, W.E.A., and Maskell, E.C.,"Subsonic Wind Tunnel Wall Corrections," AGARDograph 109, Oct.1966.

[7] Capelier, C., Chevallier, J.P., and Bouniol, F., "Nouvelle méthode de correction des effets de parois en courant plan," La recherche aérospatiale, Jan.-Feb. 1978, pp.1-11.

[8] Stakgold, I., *Boundary Value Problems of Mathematical Physics*, Vol.II, Macmillan, 1968.

[9] Mokry, M., Digney, J.R., and Poole, R.J.D., "Doublet-Panel Method for Half-Model Wind-Tunnel Corrections," Journal of Aircraft, Vol.24, May 1987, pp.322-327.

[10] Mokry, M. and Ohman, L.H., "Application of the Fast Fourier Transform to Two-Dimensional Wind Tunnel Wall Interference," Journal of Aircraft, Vol.17, June 1980, pp.402-408.

[11] Mokry, M., "Subsonic Wall Interference Corrections for Finite-Length Test Sections Using Boundary Pressure Measurements," AGARD-CP-335, May 1982, pp.10.1 - 10.15.

[12] Rizk, M.H. and Smithmeyer, M.G., "Wind-Tunnel Interference Corrections for Three-Dimensional Flows," Journal of Aircraft, Vol.19, June 1982, pp.465-472.

[13] Gakhov, F.D., *Boundary Value Problems*, Pergamon Press, 1966.

[14] Chevallier, J.P., "Survey of ONERA Activities on Adaptive-Wall Applications and Computation of Residual Corrections," Wind Tunnel Wall Interference Assessment/Correction 1983, NASA CP 2319, 1984, pp.43-58.

[15] GARTEUR Action Group AD(AG-23), "Two-Dimensional Transonic Testing Methods," NLR TR 83086 U, July 1981.

[16] Archambaud, J.P. and Chevallier, J.P., "Utilisation de parois adaptables pour les essais en courant plan," AGARD-CP-335, May 1982, pp.14.1 - 14.14.

[17] Paquet, J.B., "Perturbations induites par les parois d'une soufflerie - methods intégrales," Thèse Ing. Doc., Université de Lille, 1979.

[18] Ashill, P.R. and Weeks, D.J., "A Method for Determining Wall-Interference Corrections in Solid-Wall Tunnels from Measurements of Static Pressure at the Walls," AGARD-CP-335, May 1982, pp.1.1 - 1.12.

[19] Ashill, P.R. and Keating, R.F.A., "Calculation of Tunnel Wall Interference from Wall-Pressure Measurements," Journal of the Royal Aeronaut. Soc., Jan.1988, pp.38-53.

[20] Lo, C.F. and Kraft, E.M., "Convergence of the Adaptive-Wall Wind Tunnel," AIAA Journal, Vol.16, Jan.1978, pp.67-72.

[21] Barche, J., "Zur Ermittlung von Wandinterferenzen," Zeitschrift für Flugwiss. und Weltraumforschung, 4, 1980, pp.389-396.

[22] Labrujère Th.E., "Correction for Wall-Interference by Means of a Measured-Boundary-Condition Method", NLR TR 84114 U, Nov.1984.

[23] Maarsingh, R.A., Labrujère Th.E., and Smith, J., "Accuracy of Various Wall-Correction Methods for 3D Subsonic Wind Tunnel Testing," AGARD-CP-429, Sept.1987, pp.17.1 - 17.13.

[24] Mineck, R.E., "Wall Interference Tests of a CAST 10-2/DOA 2 Airfoil in an Adaptive-Wall Test Section," Supplement to NASA TM 4015, Dec.1987.

[25] Amecke, J., "Direkte Berechnung von Wandinterferenzen und Wandadaptation bei zweidimensionaler Strömung in Windkanälen mit geschlossenen Wänden," DFVLR-FB 85-62, Nov.1985; also NASA TM-88523, Dec.1986.

[26] Niederdrenk, P. and Wedemeyer, E., "Analytic Near-Field Boundary Condition for Transonic Flow Computations," AIAA Journal, Vol.25, June 1987, pp.884 - 886.

[27] Kraft, E.M. and Dahm, W.J.A., "Direct Assessment of Wall Interference in a Two-Dimensional Subsonic Wind Tunnel," AIAA-82-0187, Jan.1982.

[28] Sears, W.R. and Erickson, J.C.Jr., "Adaptive Wind Tunnels," Ann.Rev.Fluid Mech., Vol.20, 1988, pp.17-34.

[29] Rebstock, R., and Lee E.E.Jr., "Capabilities of Wind Tunnels With Two Adaptive Walls to Minimize Boundary Interference in 3-D Model Testing," Transonic Symposium, NASA Langley, April 1988.

[30] Judd, M., Wolf, S.W.D., and Goodyer, M.J., "Analytical Work in Support of the Design and Operation of Two Dimensional Self Streamlining Test Sections," NASA CR 148196, March 1976.

[31] Hromadka II, T.V., *The Complex Variable Boundary Element Method*, Springer-Verlag, 1984.

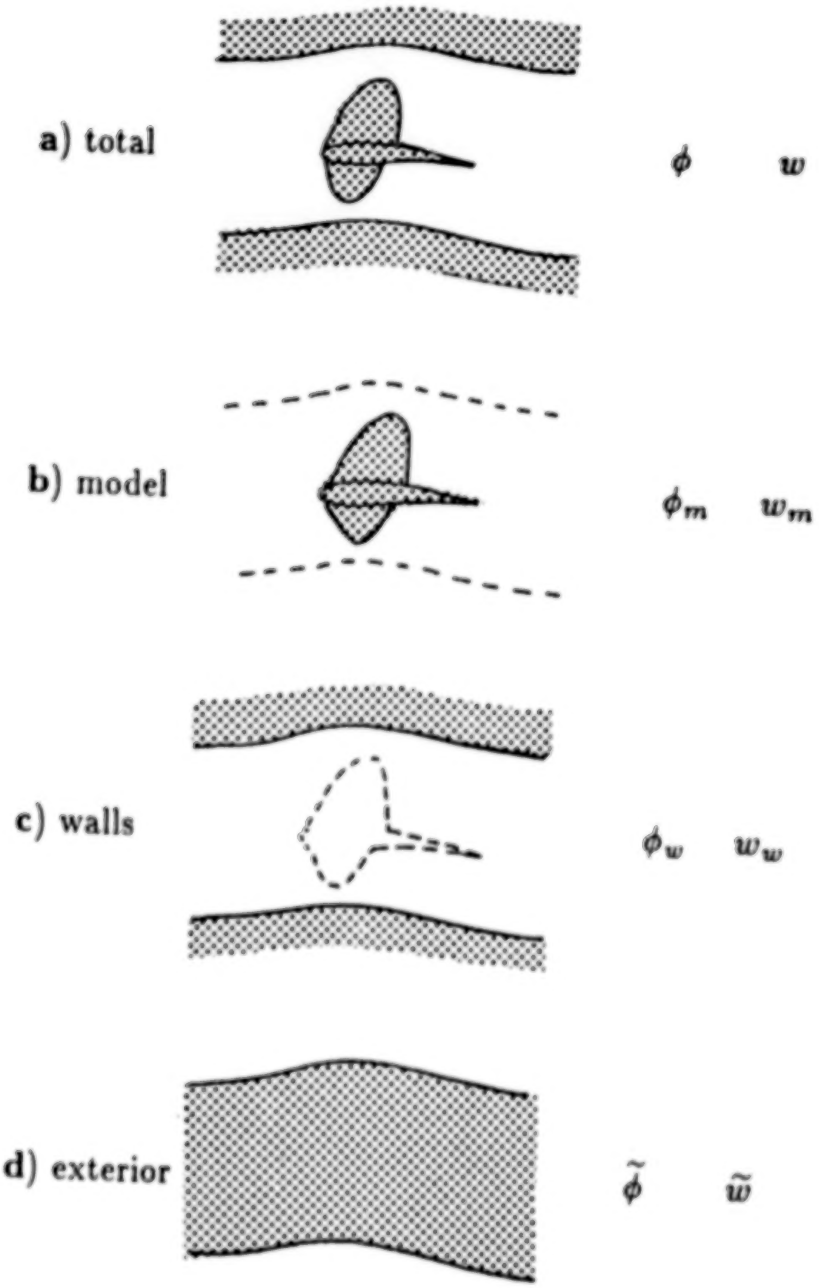

Fig. 1 Linearized flow regions.

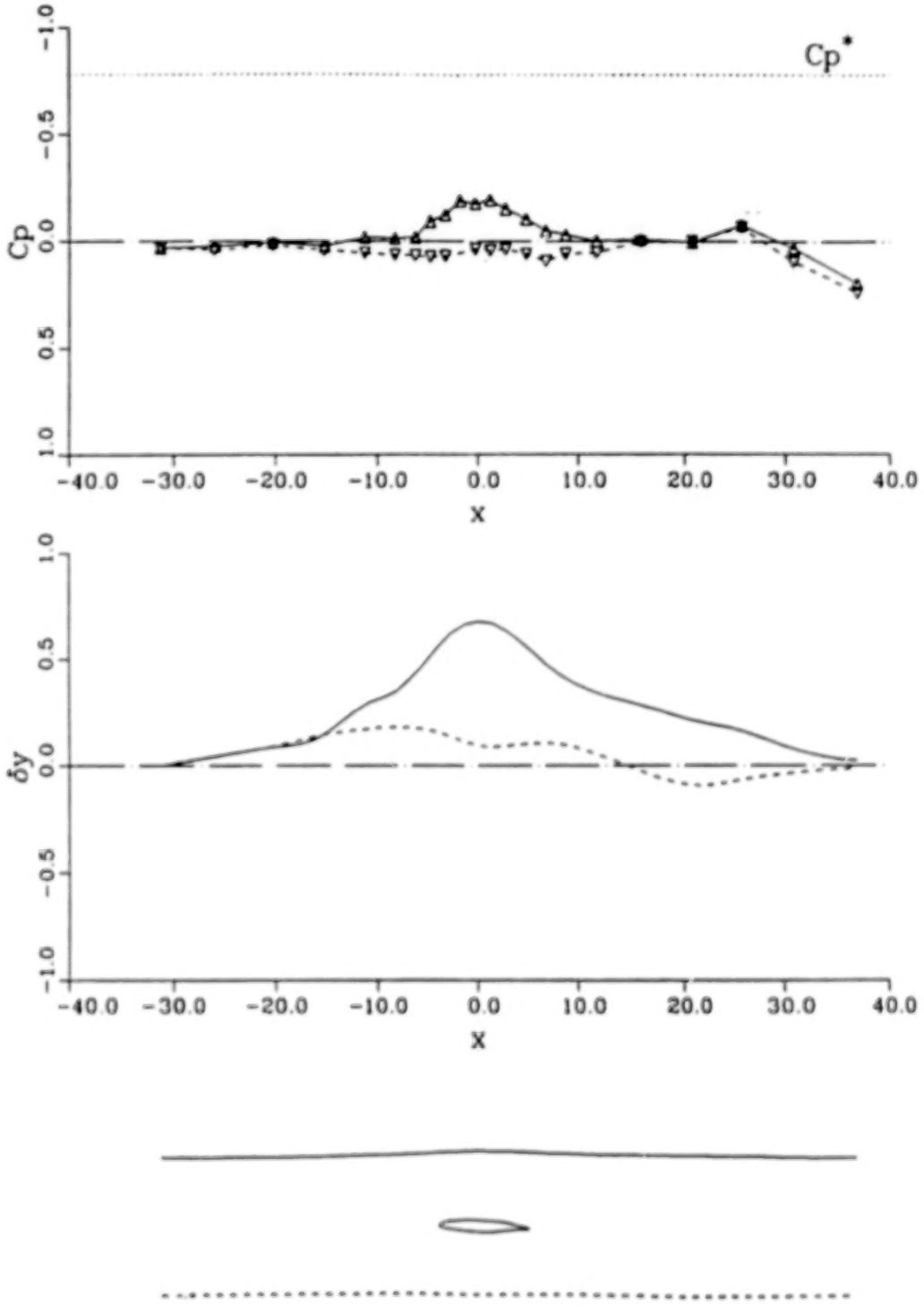

Fig. 2 Wall deflections and wall pressure coefficients; 9-in chord CAST 10 airfoil in the 13-in × 13-in test section of NASA TCT, $M_\infty = 0.700$, $\alpha = 1.20°$, $C_N = 0.50$.

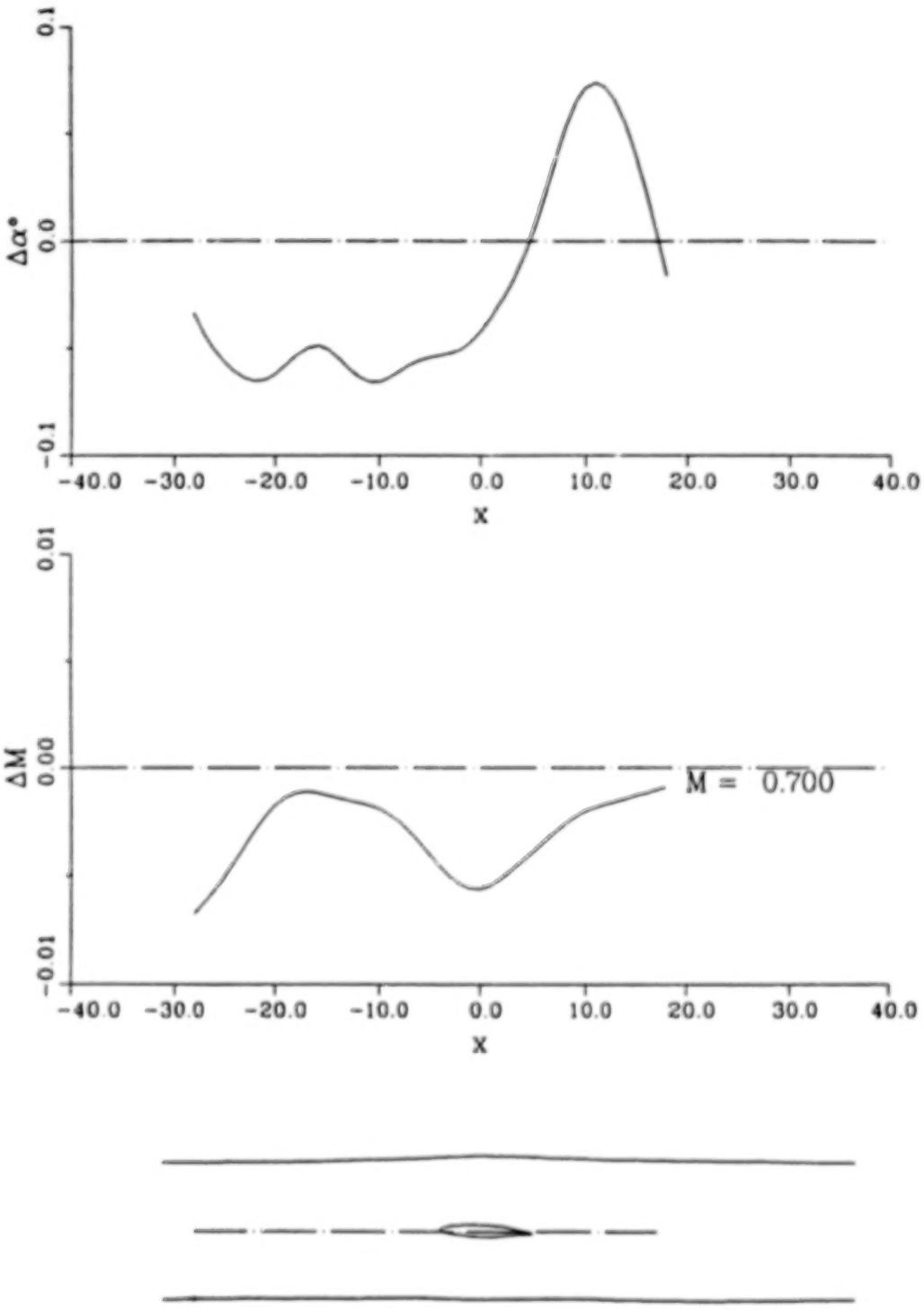

Fig. 3 Residual corrections along test section axis, evaluated by two-variable method from data of Fig.2, $M_\infty = 0.700$.

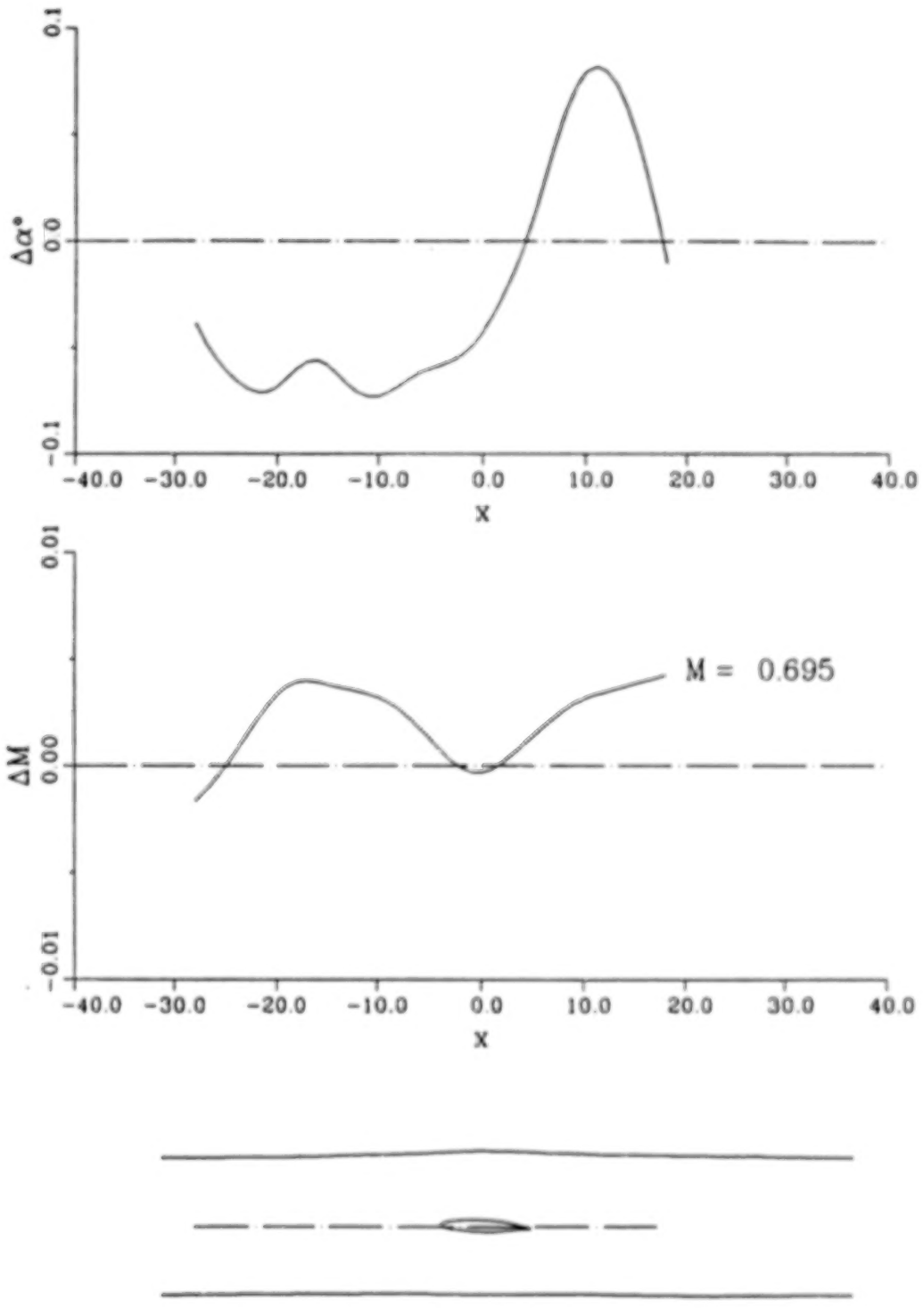

Fig. 4 Residual corrections along test section axis, evaluated by two-variable method from data of Fig.2, setting $M_\infty = 0.695$.

Comparison of NAE Porous Wall and NASA Adaptive Wall Test Results Using the NAE CAST-10 Airfoil Model

Raymond E. Mineck
Advanced Configurations Branch
NASA Langley Research Center
Hampton, Virginia

Wind tunnels can now simulate flows over airfoils at high Reynolds numbers and high subsonic speeds. Methods to correct for (or reduce) test section wall interference at these test conditions must be validated. The National Aeronautical Establishment (NAE) of Canada and NASA have a cooperative agreement to study this area. NAE designed, built, and tested a CAST-10 airfoil model in its conventional Two-Dimensional High Reynolds Number Facility. The results were corrected using classical correction techniques. NASA then tested the same model in its 0.3-meter Transonic Cryogenic Tunnel with the adaptive wall test section. The adaptive wall test section reduced the wall interference to what was expected to be an acceptable level.

This paper will compare the corrected NAE results with the uncorrected NASA results. It will also compared the NAE results with NASA results after residual corrections for top and bottom wall interference. Finally, a comparison of both sets of results corrected for interference from all four walls will be presented.

TASK:

- Study wall interference for 2-D airfoil tests at high Reynold's numbers and high subsonic speeds.

APPROACH:

- Test a supercritical airfoil model in a traditional porous test section and apply classical corrections.
- Test the same airfoil model in an adaptive wall test section.
- Compare the results. Correct the results for any residual interference to try to improve the correlation.

The model has a 9.00-inch chord and a 15.00-inch span for testing in the NAE tunnel. The close manufacturing tolerances led to a very accurate representation of the airfoil contour. The largest deviation from the design ordinates was .0001 $\frac{z}{c}$. A chordwise row of orifices was centered at the mid-span with 45 orifices on the upper surface and 23 on the lower surface. Six orifices were arranged in a spanwise row at the 90-percent chord location on each surface. The diameter of the orifices from the leading edge to the 22-percent chord location was 0.010 inches. The diameter of all other orifices was .014 inches. A strip of carborundum grit #320 (average grit size of 0.0011 inches) was used to trip the boundary layer on each surface. The strip started at the 5-percent chord location and was 0.1-inches wide.

The chord line was defined as the line from the leading edge through the center of the trailing edge. This line is 0.88° nose up from the $z = 0.0$ reference line used to define the airfoil. The angle of attack was measured from this chord line.

Tests were conducted at Mach numbers from 0.3 to 0.8 at chord Reynolds numbers of 10, 15, and 20×10^6. At each test condition, the angle of attack was varied from near zero lift through stall. The NASA test angles of attack were chosen such that the section normal force coefficients were nearly the same for both tests. This paper will present results for 10×10^6 chord Reynolds numbers only.

CAST-10 Airfoil Model

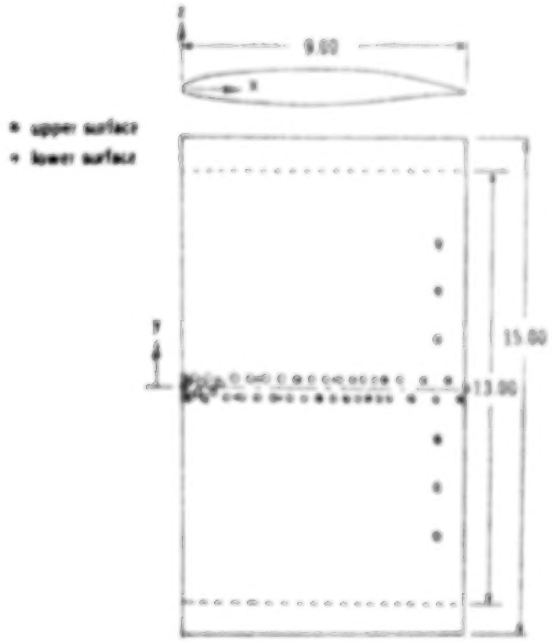

The model was first tested in the NAE 5 ft × 5 ft Blowdown Wind Tunnel. This tunnel achieves the high Reynolds numbers by testing at elevated stagnation pressures (up to 310 psi). The stagnation temperature is about room temperature. The tunnel has two interchangeable test sections: one for 3-D testing (either full or semi-span models) and the other for 2-D testing (airfoil models). The 2-D testing configuration, referred to as the NAE Two-Dimensional High Reynolds Number Facility, was used for these tests. The empty test section Mach number range is from 0.10 to 0.95. This combination of test conditions yields Reynolds numbers up to 50×10^6/ft.

NAE 5 ft x 5 ft Blowdown Wind Tunnel

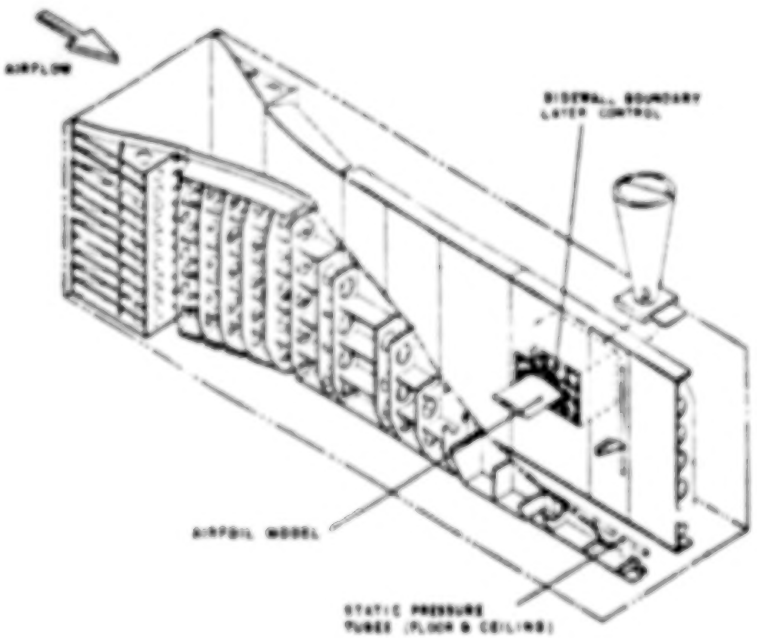

The NAE Two-Dimensional High Reynolds Number Facility test section is 141-inches long, 60-inches high, and 15-inches wide. It has solid, parallel sidewalls and porous top and bottom walls. The top and bottom walls are covered with a 30 mesh screen to reduce the edgetone noise in the test section. A 1-inch-diameter, 128-inch-long static pipe is attached to the top and bottom walls. Each pipe has 60 static pressure orifices. For the 9.00-inch airfoil used in these studies, the test section was 14.2 chords long and 6.7 chords high. The model aspect ratio was 1.7.

The airfoil model was mounted on a porous turntable within an 18-inch by 24-inch porous panel on each sidewall. Moderate suction was applied to the porous region to prevent the sidewall boundary layer from prematurely separating. A four-tube, total pressure rake was mounted 1.8 chords downstream from the trailing edge. The rake was traversed through the model wake to obtain the drag.

The measured data were corrected for top and bottom wall interference using the method of Mokry and Ohman. The large size of the test section relative to the model insured that the assumptions used to develop the correction technique would not be violated. The corrections to the Mach number and angle of attack were moderate.

NAE Two-Dimensional High Reynolds Number Facility

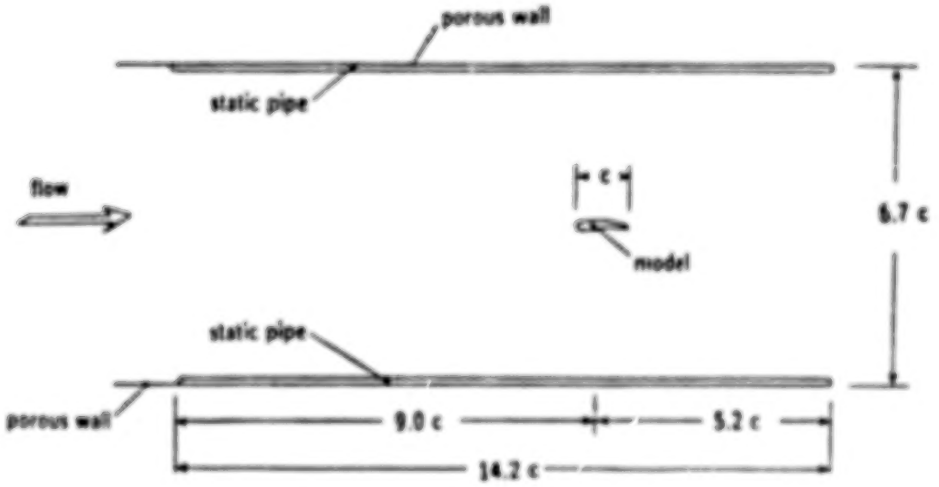

The NASA 0.3-meter Transonic Cryogenic Tunnel achieves high Reynolds numbers through a combination of elevated stagnation pressures and cryogenic stagnation temperatures. It is a fan-driven, cryogenic pressure tunnel. Nitrogen, rather than air, is used as a test gas. The range of stagnation temperature is from 80 K to 327 K and the range of stagnation pressure is from about 17 psi to 88 psi. The empty test section Mach number range is from about 0.20 to 0.95. This combination of test conditions yields Reynolds numbers up to 100×10^6/ft.

NASA 0.3-meter Transonic Cryogenic Tunnel

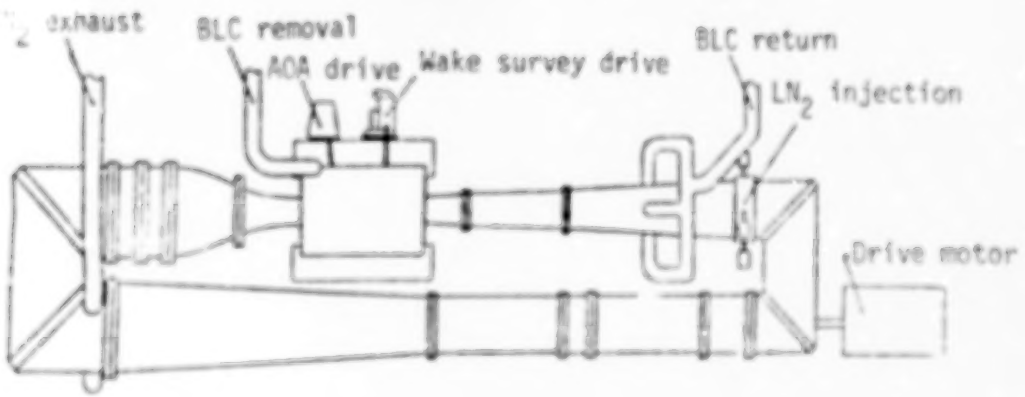

The adaptive wall test section is 13 inches high and 13 inches wide at the entrance of the test section. The solid sidewalls are fixed and parallel. The top and bottom walls are solid and flexible. The forward 55.8-inches of each flexible wall form the test section. The wall shape is controlled by 18 independent jacks. For the 9-inch airfoil used in this test, the test section was 6.2 chords long and 1.4 chords wide. The model aspect ratio was 1.4.

The 15-inch span model was positioned in special turntables so that the chordwise pressure row was aligned with the centerline of the test section. A six-tube, total pressure rake was mounted 1.2 chords downstream of the trailing edge.

The flexible wall position was determined iteratively using the measured wall shape and static pressures. The algorithm is based on the work of Goodyer and Wolf. The small size and short length of the test section relative to the model should lead to significant wall interference if the walls are not properly positioned.

0.3-m TCT Adaptive Wall Test Section

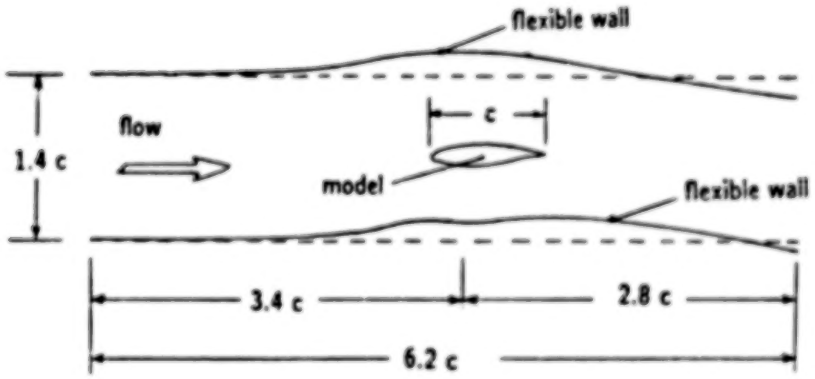

The results from the NASA tests were expected to be practically interference free. Therefore, the uncorrected NASA results are compared to the corrected NAE results. The airfoil chordwise pressure distributions are compared first. In general, the chordwise pressure distributions were in good agreement. The shock locations and trailing edge pressure coefficients agreed well for angles of attack below stall. However, the NASA pressure coefficients were less negative upstream of the beginning of the pressure recovery region. For this case, the peak local Mach number on the lower surface is about 0.009 smaller for the NASA results. Assuming that there is a residual error in the NASA results, the actual Mach number for the NASA tests could be 0.009 smaller than measured.

Comparison of Typical Chordwise Pressure Distributions

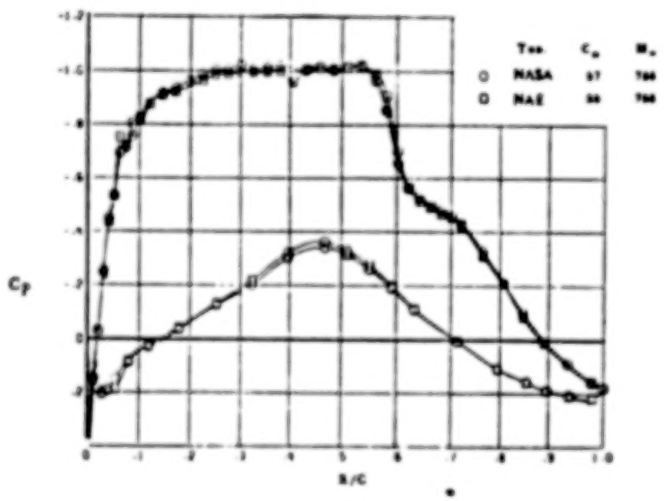

The shock locations were determined by fitting a straight line through the pressures just upstream and just downstream of the pressure rise associated with the shock. A third line was fitted through the pressure rise. The shock location was defined as the midpoint of the two intersections of the fitted lines. Because of the spacing of the orifices, the shock location could be determined with an accuracy of about 2 percent chord. Both sets of data show the same trends. Below the design Mach number, the shock moves aft with increasing normal force until stall. Above the design Mach number, the shock location tends to move slightly forward with increasing normal force. There is a small shift in the curves. When the results are cross-plotted at constant c_n, the maximum shift is equivalent to an error in Mach number of about 0.005. Again assuming there is a residual error in the NASA results, the corrected NASA Mach number could be 0.005 smaller than the measured Mach number.

Comparison of Shock Locations

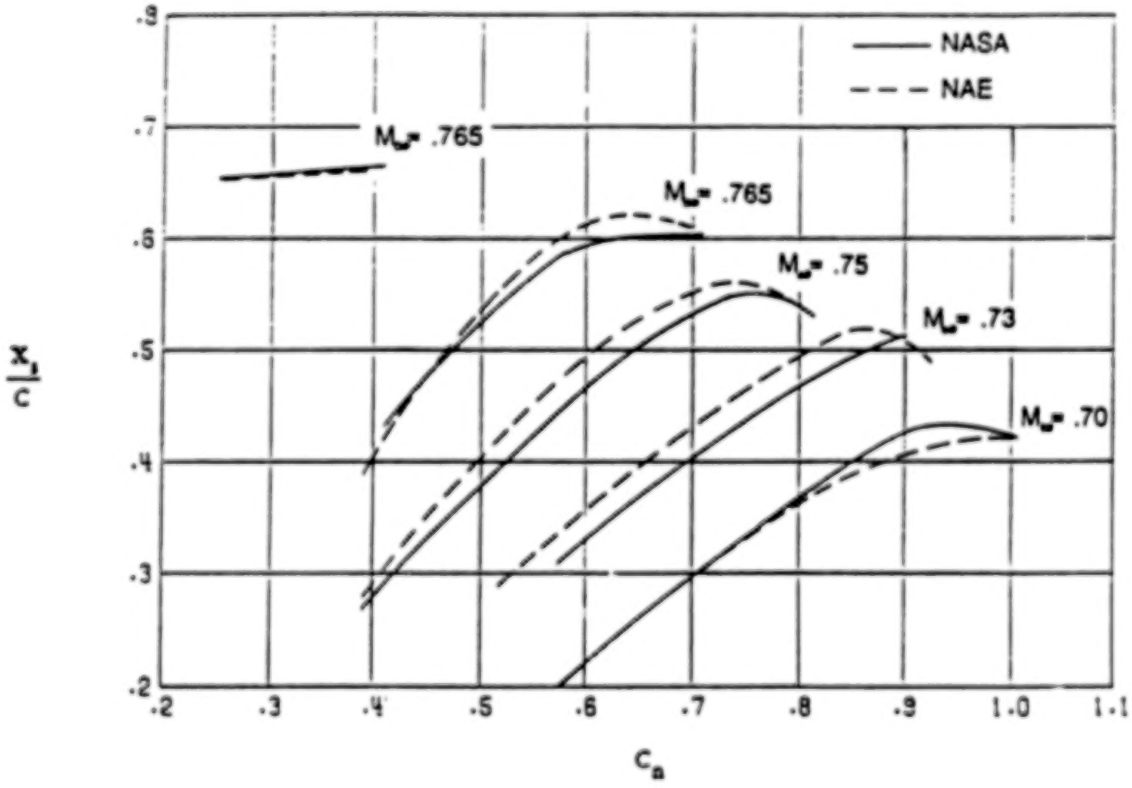

The trailing edge pressure coefficients are sensitive to the condition of the boundary layer. Since the boundary layer was tripped the same way and at the same location in both tests, comparing the trailing edge pressures can be used to check for residual interference. The trailing edge pressures are in reasonable agreement for those angles of attack below stall with $C_P \approx .2$. Near stall, the curves break. The angle of attack for this break does not follow a consistent trend. The reason is not known.

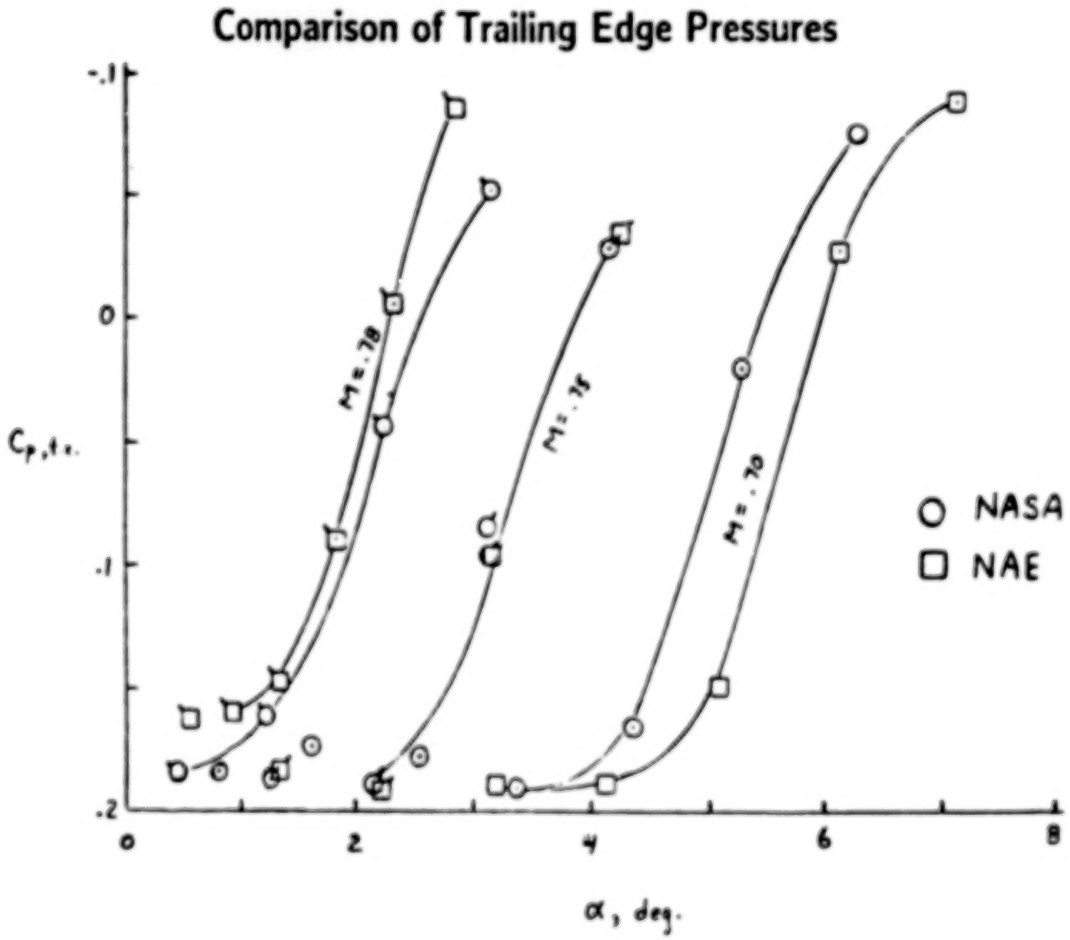

The uncorrected NASA results were expected to have a low level of residual interference from the top and bottom walls. Problems with the adaptive walls prevented data acquisition near zero lift and near stall for some of the test conditions. In general, the angle of attack for the NASA tests was less than the angle of attack for the same normal force for the NAE tests. If the problem was a simple misalignment, the difference would not show up in the normal force — drag polar. This is not the case. The drag for a given normal force is smaller for the NASA tests. The pitching moment data (not shown) was in good agreement. The slopes of the normal force curves and the drag rise characteristics can be examined to help understand the differences.

Comparison of the Integrated Force Coefficients

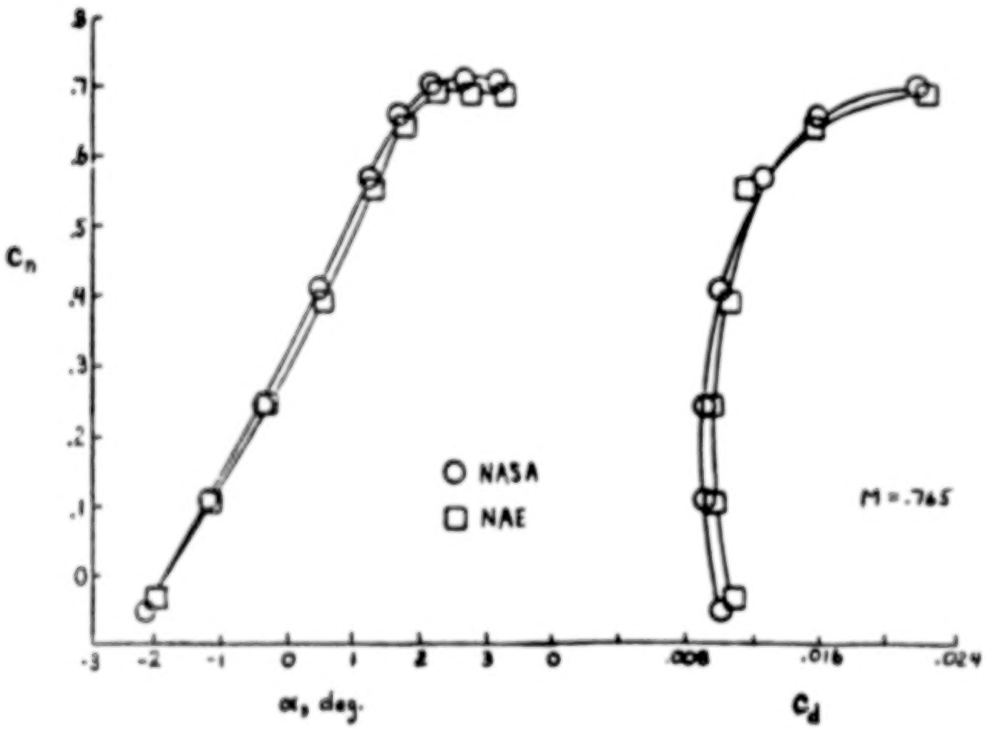

The slope of the normal force curve was measured from the faired data at $c_n \approx .4$. Both sets of data show the same trends. The maximum value of normal force curve slope occurs at $M \approx .78$. In general, the slopes are larger for the NASA results. The differences in the slopes are accentuated by the rapid change in slope with Mach number. Again, assume that there is a residual error in the NASA results. If the difference was attributed to a residual interference in the Mach number, the peaks would not line up. Also, it would indicate the NASA Mach number was higher than measured. This doesn't agree with the previous speculation. The difference could be attributable to an overcorrection of the lift interference which decreases with increasing lift.

Comparison of the Normal Force Curve Slopes

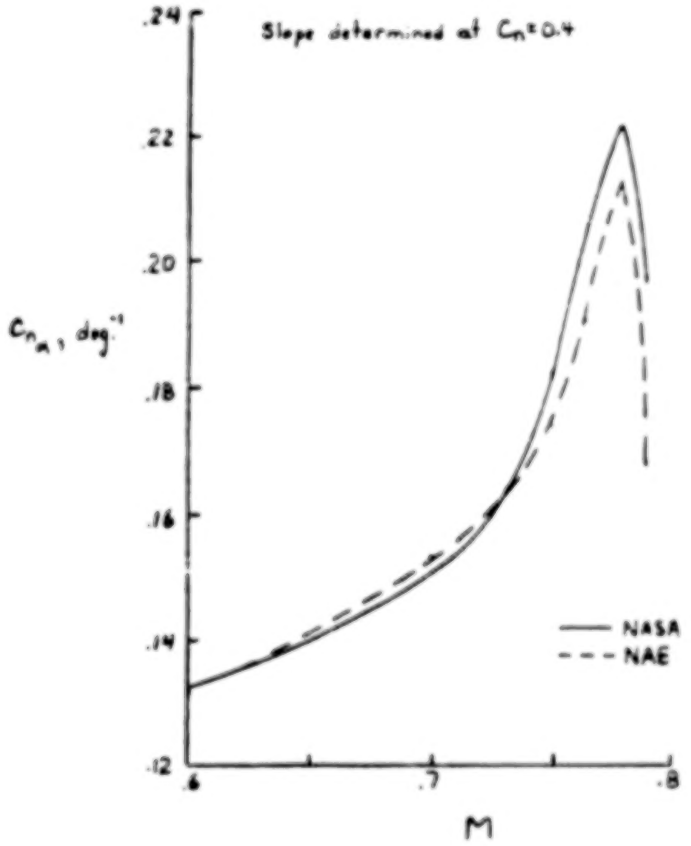

The drag rise was determined from the faired normal force — drag polars with c_d values determined at $c_n \approx 0.4$. The drag level was lower for the NASA tests. The trends around the design Mach number of 0.765 are different. If the NASA corrected Mach number were lower than the measured Mach number, the correlation at the higher Mach number would be improved.

Comparison of the Drag Rise

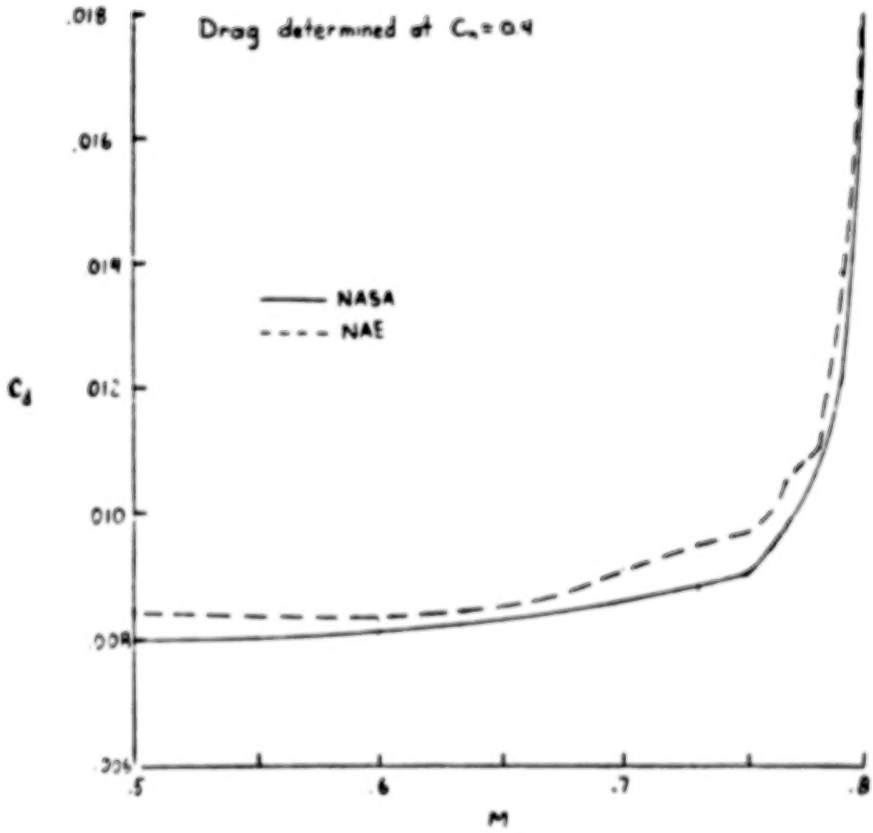

The above comparisons speculated that a residual error remained in the NASA results. When these results were published, there were no production correction techniques which would treat the non-planar boundary condition at the flexible walls. Green of NASA Langley has modified the non-linear correction technique developed by Kemp. This modified code will treat top and bottom walls only or all four walls. The NASA results were corrected using the top and bottom wall (2 wall) option. The code predicted a wall induced downwash which decreased the angle of attack. The correction increased with increasing normal force coefficient. The code also predicted that the actual Mach number was less than the measured Mach number. The correction also increased with increasing normal force coefficient. The effect of the 2-D wall correction on the correlation is mixed as shown on the next page.

Effect of Correcting the NASA Integrated Force Coefficients for Top and Bottom Wall Interference

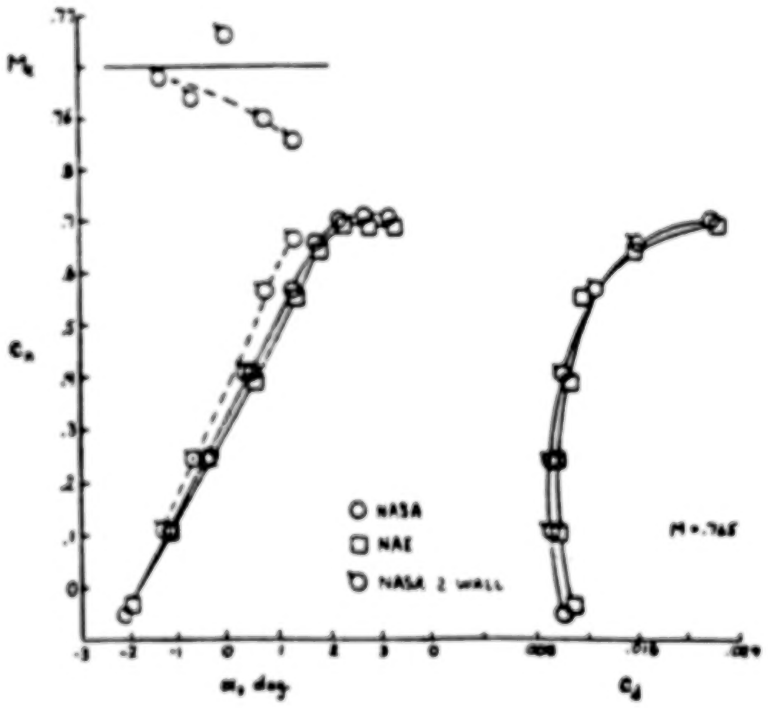

The corrected NASA results were faired and the corrected normal force curve slopes computed. In all cases, the correction drastically degrades the correlation. It is possible that the correction technique is being used incorrectly or that the test section is too short. It is also possible that some of the assumptions used to develop the code are being violated. These results are undergoing further study. They should <u>not</u> be used to form any conclusions of the validity of the NASA results or the correction code at this time.

Effect of Correcting the NASA Normal Force Curve Slopes for Top and Bottom Wall Interference

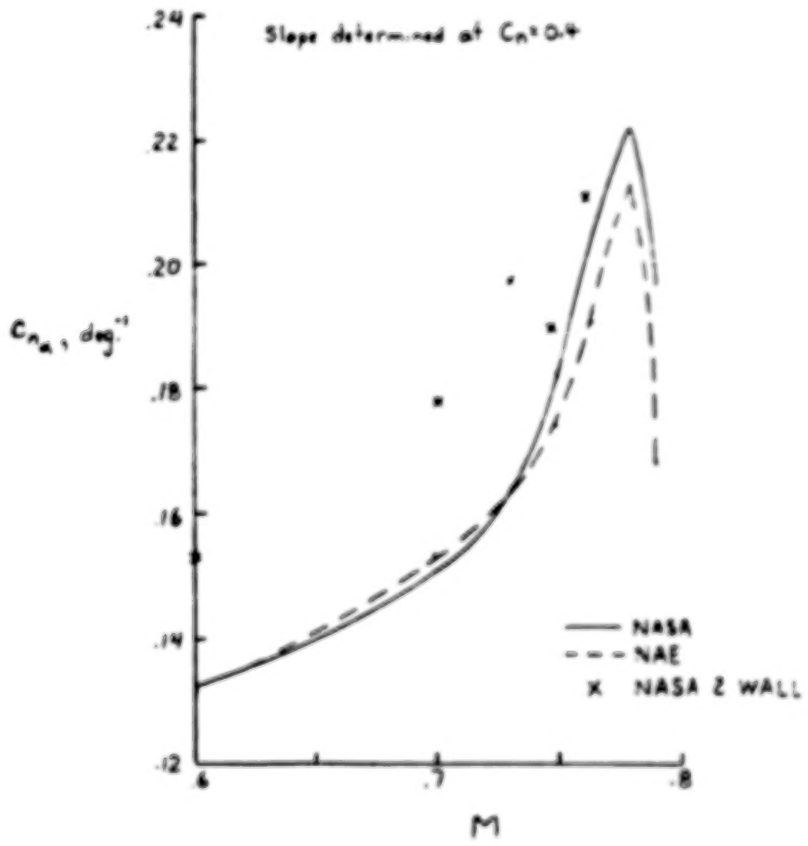

The corrected NASA normal force — drag polar was faired and the drag determined as before. The correction does not have much of an impact on the correlation.

Effect of Correcting the NASA Drag Rise for Top and Bottom Wall Interference

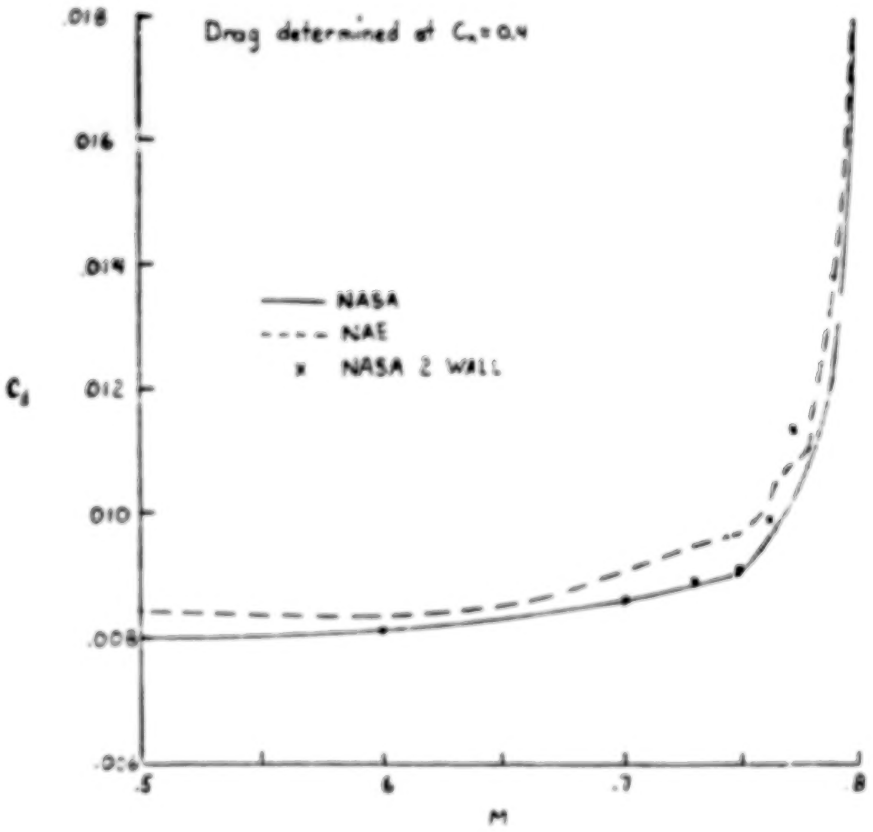

Both tunnels have similar sidewall boundary-layer layer characteristics and the model, as tested, has similar aspect ratios. Neither the NAE wall correction technique for the NASA wall adaption technique directly accounts for the changes in the sidewall boundary layer. The lockage changes will be sensed by the wall static pressures. The effect measured at each wall will be different since the test section heights are so different. If the measured effect is small and can be neglected, the analytical approach by Murthy can be used to correct both sets of data. Since this is only a blockage correction, only the Mach number (and dynamic pressure) will be corrected. The sidewall correction will not affect the angle of attack. Correcting the results for the sidewall interference improves the correlation at the highest Mach numbers where there is a large gradient. It does little to improve the correlation elsewhere.

Effect of Applying the Murthy Sidewall Boundary Layer Correction to the Mach Number

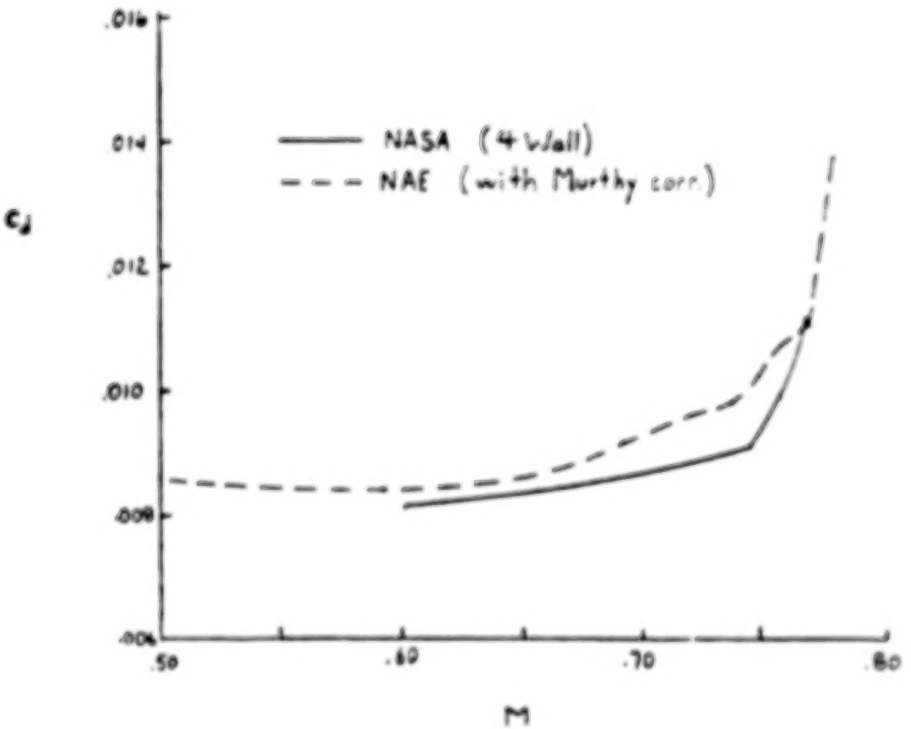

I wish to express my appreciation to the National Aeronautical Establishment of Canada for all its efforts in support of this cooperative agreement. I would like to thank Mr. Lars Ohman and his staff for their assistance and cooperation. Their efforts helped to make this cooperative program a success. I wish to also thank the staff of the 0.3-m TCT for their help in preparing and testing the model and reducing the data. Finally, I would like to express my deepest appreciation to Dr. Y. Y. Chan for his patience, cooperation, insight, and understanding.

CONCLUSIONS

- The adaptive wall test section reduced the wall interference
- Uncorrected adaptive wall and corrected porous wall results:
  - Showed similar pressure profiles and shock locations
  - Showed similar trends of normal force curve slope and drag rise
  - Differences suggest a residual Mach number and angle of attack interference remains
- Correcting adaptive wall results for top and bottom wall residual interference does not improve the correlation
- Correcting results for sidewall interference has a small effect on the correlation

EXPERIENCE WITH SOME REPEAT TESTS ON THE 9" CHORD CAST10-2/DOA 2 AIRFOIL MODEL IN THE LANGLEY 0.3-M TCT ADAPTIVE WALL TEST SECTION

A. V. MURTHY
Vigyan Research Associates, Hampton, Virginia

and

E. J. RAY
Langley Research Center, Hampton, Virginia

INTRODUCTION

A co-operative testing program is in progress between the Langley Research Center (NASA) and the National Aeronautical Establishment (NAE, Canada) to validate two different techniques of airfoil testing at transonic speeds. The procedure employed is to test the same airfoil model in the NAE two-dimensional tunnel and the Langley 0.3-m Transonic Cryogenic Tunnel (0.3-m TCT). The airfoil model used in testing was CAST10-2/DOA2 super-critical airfoil.

The NAE tunnel has a cross section of 15" x 60", and has conventional perforated walls for the ceiling and the floor. With the airfoil chord length of 9" employed in these tests, the tunnel height/airfoil chord ratio is 6.67. Due to large h/c ratio, the wall interference effects will be small. Hence, wall interference corrections can be applied to the test data with greater confidence.

The Langley 0.3m-TCT has a relatively small cross section of 13"x13", giving a (h/c) ratio of 1.44 for the same 9" chord model. The approach employed in the 0.3-m TCT aims towards eliminating the wall effects by using active walls. The top and bottom walls are flexible. By changing the wall shapes during a test in an iterative manner, the wall interference effects are reduced. The method employed to change the wall shapes was developed by the University of Southampton (England). This method, known as adaptive wall technique originally conceived and tested in the National Physical Laboratory (England), is beginning to find potential application in 2D and 3D transonic testing.

The current test program provided an opportunity to validate the adaptive wall technique in the 0.3-m TCT. The relatively long chord airfoil represents a severe test case to test the efficacy of the adaptive wall technique under cryogenic conditions. The program also involved removal of side wall boundary-layer thus increasing the complexity of the wall adaptation technique. This paper deals with some salient results obtained regarding repeatability of test data and possible residual interference effects.

OUTLINE

- **Background**
- **Method: Adaptive wall technique**
  University of Southampton, England
- **Comparison of data from different entries**
- **Side wall boundary-layer removal effects.**
- **Top and bottom wall interference effects**
- **Conclusion**

0.3-m TCT Adaptive Wall Test Section

The 0.3-m TCT adaptive wall test section has rigid side walls and adjustable top and bottom walls. The length of the test section is 67" long. Jacks driven by stepper motors move the top and bottom walls to the required shape during a test. The tunnel reference Mach number is measured near the upstream anchor location of the top wall (x=-31.25"). The test section has provision for removing the boundary-layer on the side walls. The removal location is upstream of the model. The boundary-layer removal region is about 6" wide, and extends from ceiling to floor. The removal medium is a perforated plate. The perforations in the plate were drilled using the electron beam technique. The boundary-layer mass removed from the side walls exhausts to atmosphere through digital flow control valves.

0.3-m TCT ADAPTIVE WALL TEST SECTION

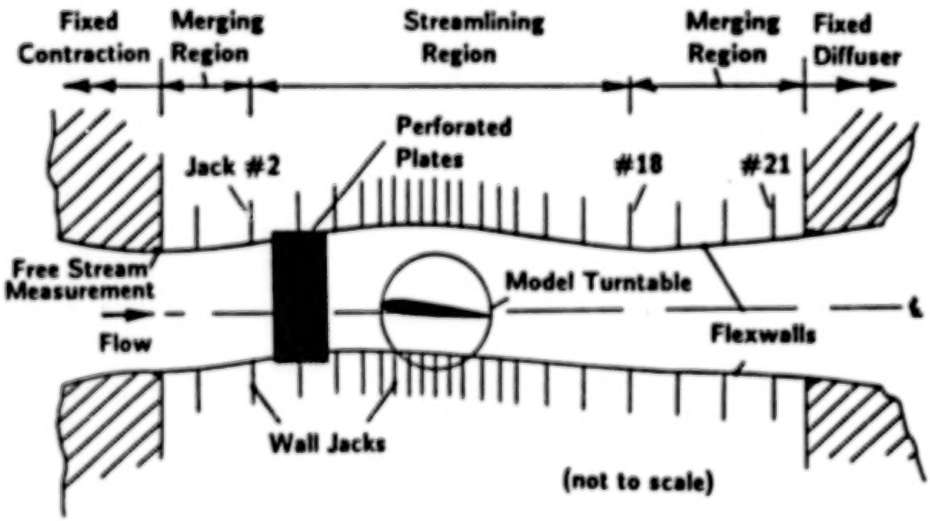

CAST10-2/DOA2 Airfoil test program

The first entry of the CAST10-2/DOA2 airfoil model to the 0.3-m TCT was during November 1986. By then, the tests in the NAE tunnel were over and the corrected data were available for comparison. It was gratifying to note that the 0.3-m TCT test in the relatively smaller test section for the large chord model agreed with the data from the much larger NAE tunnel.

Encouraged by this good agreement, the same model was employed in side wall boundary-layer removal tests conducted about a year later. The purpose of the later test was primarily to examine the wall adaptation process in the presence of side wall boundary-layer removal. The test data, under no boundary-layer removal conditions, were expected to provide a base line comparison with the earlier tests. Surprisingly, the two test data did not agree. The differences were large compared to the test accuracy.

Possible speculations for the differences included facility related hardware and instrumentation problems, or the presence of perforated plates for side wall boundary-layer removal. Further tests by replacing the perforated plates with solid plates confirmed our previous experience that at least the perforated plate was not the cause for the observed differences. It was difficult to identify specific reason(s) for the differences. Therefore, two additional entries (Entry III and IV) were made after a thorough calibration of the instrumentation and careful planning of the test details.

0.3-m TCT ADAPTIVE WALL TEST SECTION

CAST10-2/DOA2 Airfoil Test Program

Entry No.	Tunnel Configuration	Sidewall BL Removal	Test Date	Comments
I	Solid Plate Inserts	–	November 1986	Good agreement with NAE data
II	Perf. Plate Inserts	0 - 1.6%	September 1987	Differences with Entry I data
III	Solid Plate Inserts	–	May 1988	Further Investigation
IV	Perf. Plate Inserts	0 - 1.6%	July 1988	Further Investigation

Test conditions for Entry III and Entry IV

Most of repeat tests were at a Mach number of 0.765 and a chord Reynolds number of 20 million. The model had transition strips (carborundum grit no. 320) on both the surfaces to ensure a turbulent boundary-layer. The objective was primarily to reduce the uncertainty in transition location which can affect the test data.

The side wall boundary-layer removal was in passive mode. The maximum flow removal rate was about 1.6% of the test section mass flow.

MODEL AND TEST CONDITIONS

TEST SECTION

Height, h (Nominal)	:	13.0 inches
Width, b	:	13.0 inches
Top & bottom walls	:	Adjustable
Side walls	:	Fixed
Boundary-layer removal	:	Upstream

MODEL

Airfoil	:	CAST10-2/DOA2
Chord	:	9.0 inches
Chord/height (c/h)	:	0.69
Aspect ratio (b/c)	:	1.44

TEST CONDITIONS

Mach number	:	0.765 & 0.78
Reynolds number	:	20×10^6
Transition	:	Fixed
Boundary-layer removal	:	0 - 1.6%

Side wall boundary-layer thickness

The empty test section side wall boundary-layer thickness is a measure of extent of side wall interference on the test data. A boundary-layer rake mounted on the turntable in the empty test section was used to measure the boundary-layer thickness. The measurements showed that the displacement thickness is about 1.3% of the test section width when there is no removal, and reduces to about 0.6% under maximum removal conditions.

The extent of side wall boundary-layer influence will be of the same order in all the entries. Hence, the differences in the test data obtained during different entries will be largely due to residual top and bottom wall interference.

CHANGE IN SIDE WALL BOUNDARY-LAYER THICKNESS AT MODEL STATION WITH UPSTREAM REMOVAL

(Empty test section measurements)

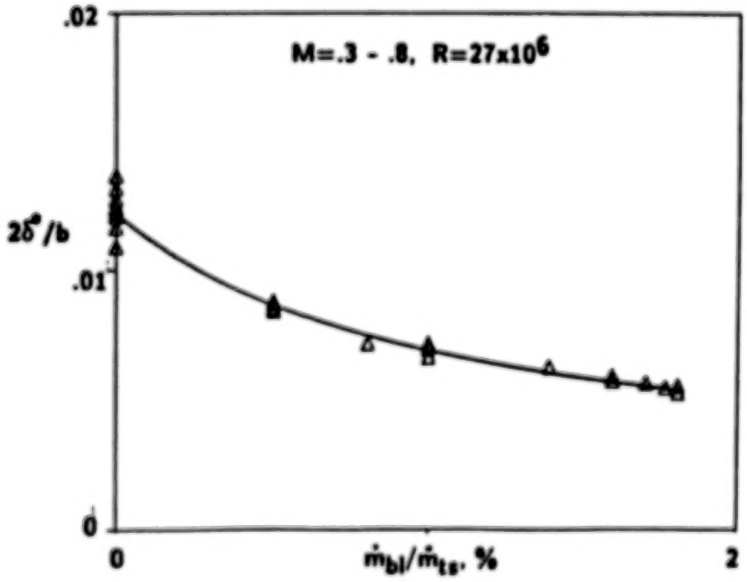

Comparison of data from Entry I and Entry II (M=0.765)

The normal force data at the reference Mach number of 0.765 between the two entries agree closely up to about 1.1 degree angle of attack corresponding to a normal force coefficient of about 0.6. Beyond 0.6, the normal force coefficients are much lower than the values obtained during entry I. However, the agreement up to 0.6 needs closer examination. The corresponding agreement is not reflected in the variation of the drag coefficient. The drag coefficients are consistently higher in the second entry. This suggests the possibility of a higher effective Mach number near the model region, while the reference Mach number in both the tests remained close to 0.765.

COMPARISON OF TEST DATA FROM TWO DIFFERENT ENTRIES

CAST10-2/DOA2 Airfoil (9" Chord)

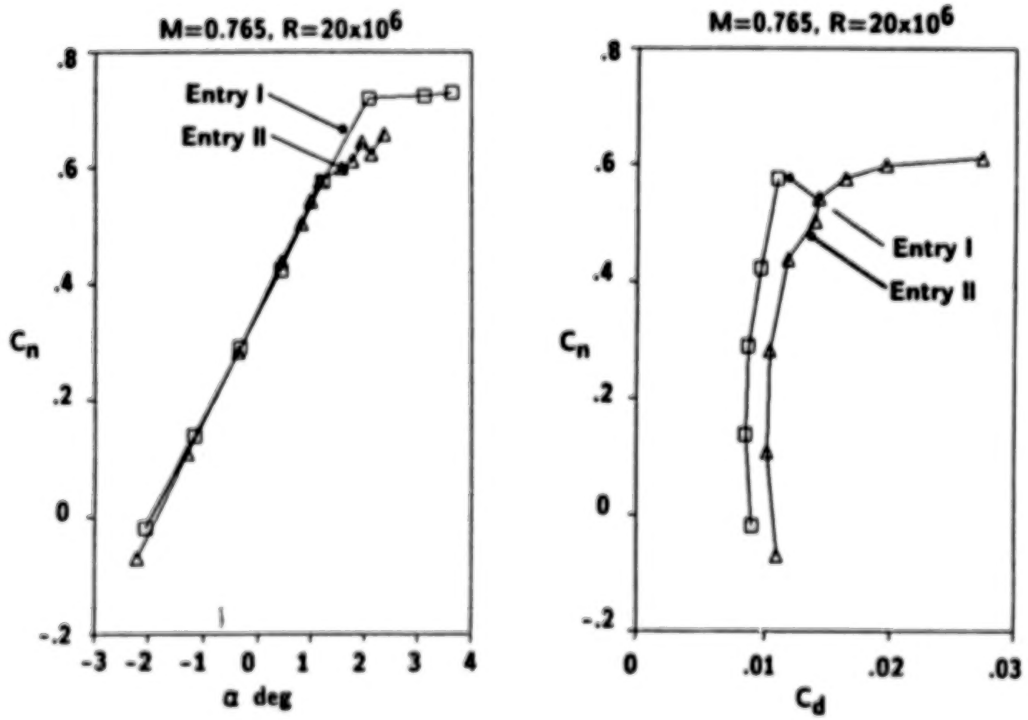

Comparison of data from Entry I and Entry II (M=0.78)

At a slightly higher reference Mach number of 0.78, the same trend is observed for the variation in normal force and drag force coefficients. However, the difference are much larger.

In all these cases, the conditions set for the streamlining of walls were satisfied. This led to the question whether non-unique solutions for wall shapes exist with the adaptive wall testing technique employed. The answer to this question was not simple and straightforward. More analytical and experimental investigation was necessary to determine the cause for the differences between the two sets of data.

COMPARISON OF TEST DATA FROM TWO DIFFERENT ENTRIES

CAST10-2/DOA2 Airfoil (9" Chord)

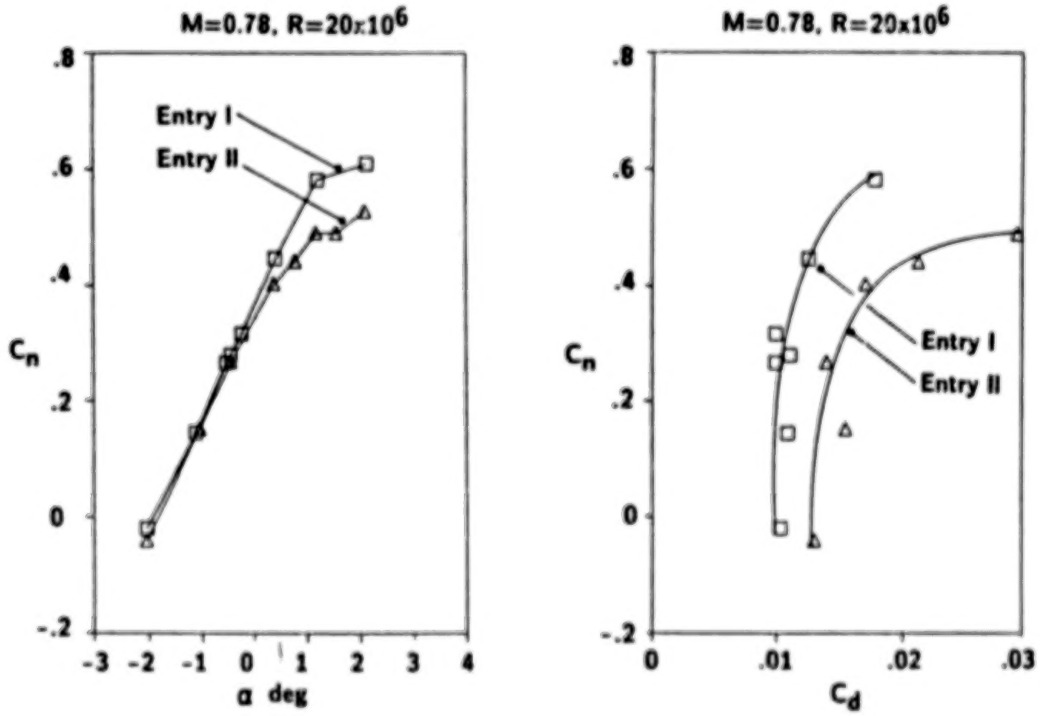

Comparison of test data from Entry I and Entry III

The purpose of the third entry was to reduce uncertainties to the possible extent any facility related hardware and instrumentation problems. The perforated plates used for side wall boundary-layer removal in the second entry was replaced with the solid plate inserts. The pressure instrumentation was recalibrated to ensure the required accuracy standards were met. The availability of an advanced personal computer based pressure, temperature and Mach number controller for the tunnel helped in maintaining steady flow conditions during the test.

With this careful planning of the tests, it was possible to closely repeat the data obtained during the first Entry. In some cases, the iteration process was stopped manually when the wall streamlining accuracy was close to set values, to avoid oscillatory and/or divergence of the solutions. Despite this, the repeatability was quite good. Both the normal force and drag data show good repeatability between Entry I and Entry II. Since the data were at much closer intervals, Entry III data shows clearly the non-linear variation of the normal force with angle of attack.

COMPARISON OF RESULTS FROM ENTRY I AND ENTRY III
CAST10-2/DOA2 Airfoil (9" Chord)

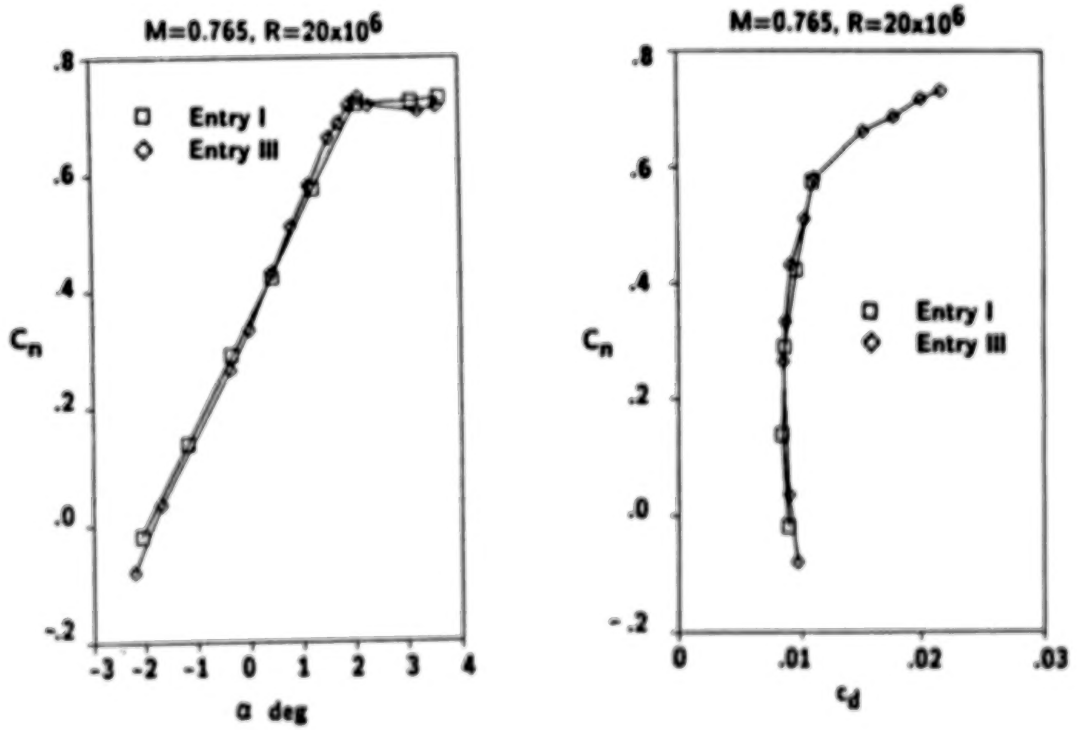

Side wall boundary-layer removal tests

Following the successful demonstration of the repeatability, the perforated plates were reinstalled on the side walls to study the side wall boundary-layer removal effect. Also, we felt it necessary to reconfirm the presence of perforated plates in the Entry II was not the cause for the discrepancy in the test data.

The figures show the normal force and drag coefficient variation for three levels of side wall boundary-layer removal; 0%, 1.0% and 1.6% of the test section mass flow. The iterative streamlining technique worked successfully. The side wall boundary-layer removal did not have a significant effect on the airfoil characteristics. The drag levels appear to be slightly lower for the highest bleed case of 1.6%. However, whether this is really due to side wall boundary-layer effect needs to be ascertained with a detailed assessment of residual interference effect.

SIDEWALL BOUNDARY-LAYER REMOVAL EFFECTS
CAST10-2/DOA2 Airfoil (9" Chord)

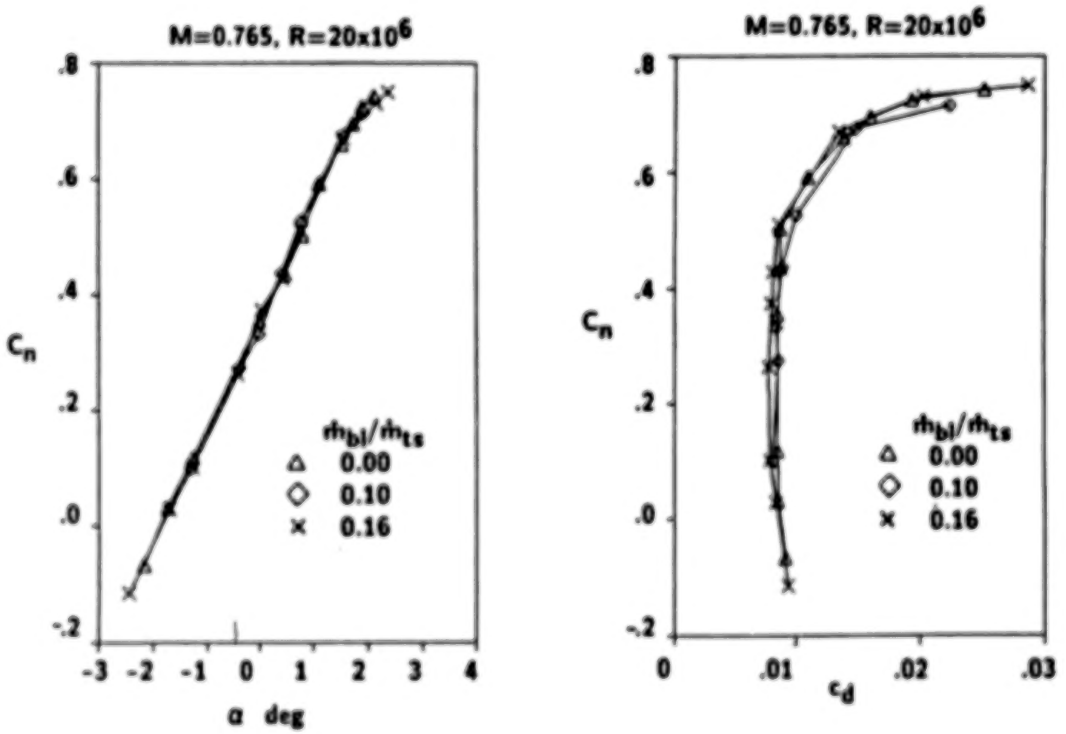

Side wall boundary-layer removal effect on wall streamlining
(Angle of attack: 1.14 degree)

The side wall boundary-layer removal has two effects. First, the boundary-layer thickness at the model station will be smaller. This will reduce the extent of three-dimensional flow field at the airfoil/side wall junction. The force data shows that this effect is not felt significantly at the mid-span where the pressure measurements are made. Second, the free stream Mach number near the model region drops due reduction in mass flow downstream of the boundary-layer removal station. This is an undesirable effect. In conventional wind tunnels, this requires a proper calibration of the test section flow to determine the Mach number correction.

The adaptive wall technique automatically responds to boundary-layer removal effects. Both the top and bottom walls move towards the tunnel centerline to maintain the same upstream reference Mach number conditions in the region of the model. The figure shows the local Mach number on the airfoil and the corresponding wall shapes for conditions with and without side wall boundary-layer removal. While there is no significant effect on the airfoil Mach number distribution, the wall shapes are quite different showing the strong effect of Mach number change due to change in mass flow. Both the top and bottom walls move roughly by the same amount from the shapes corresponding to zero removal conditions. This indicates that the side wall boundary-layer removal is uniform over the height of the test section.

EFFECT OF SIDE WALL BOUNDARY-LAYER REMOVAL ON WALL STREAMLINING
M=0.765, R=20x10^6,α=1.14 deg

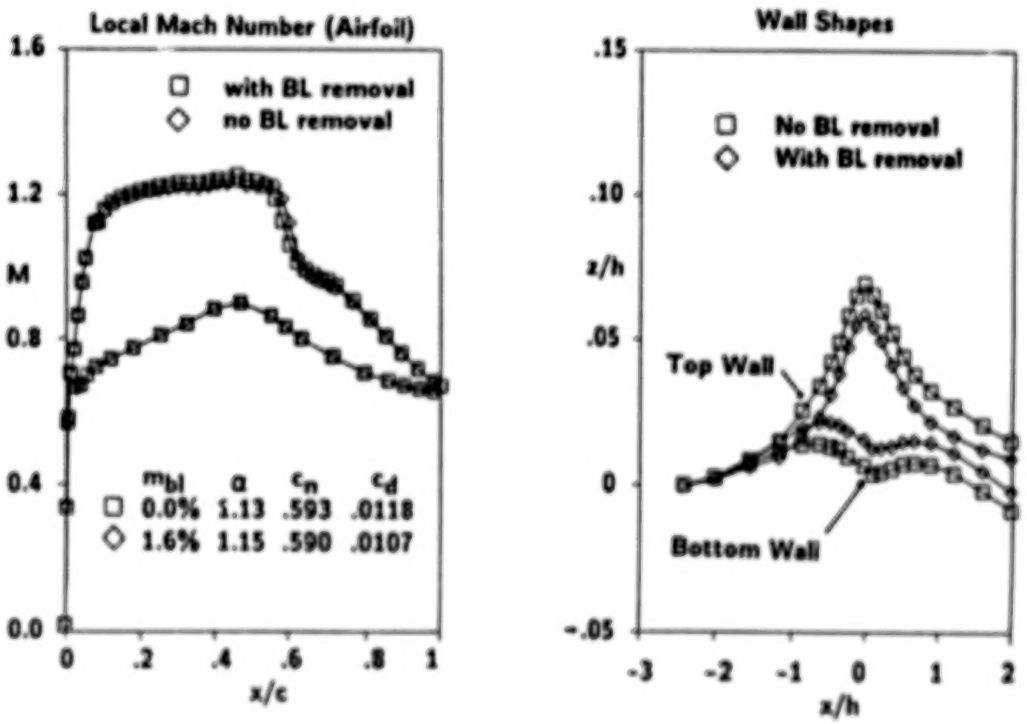

Side wall boundary-layer removal effect on wall streamlining
(Angle of attack: 1.91 degree)

Since the side wall boundary-layer removal does not have a major effect on the airfoil characteristics, the changes in the wall shapes are primarily a function of the amount of mass flow removal only. The airfoil Mach number distribution and the wall shapes at a much higher incidence of 1.91 degrees demonstrate this point. The change in wall shapes from zero removal conditions are about the same as for the 1.1 degree incidence case.

EFFECT OF SIDE WALL BOUNDARY-LAYER REMOVAL
ON WALL STREAMLINING
M=0.765, R=20x10^6,α=1.91 deg

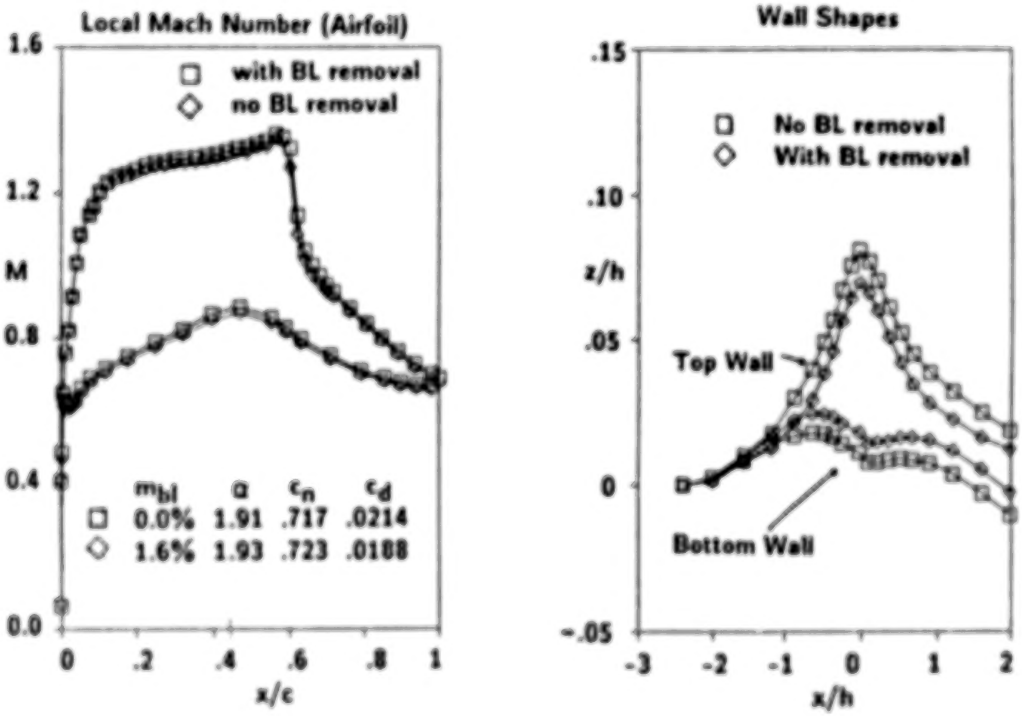

Summary of force data from different tests
(M=0.765, R=20 mil)

The repeatability of the test data over a wide range of varying conditions during different entries is quite good with the adaptive wall technique. The normal force and drag data taken during different entries, with and without side wall boundary-layer removal, agree closely. The data from the NAE tunnel is shown in solid symbols. The agreement between various tests is good. Some differences at higher lifts are quite small and require detailed examination of the test data. It is remarkable to note that the adaptive wall technique employed in the 0.3-m TCT is successful under most complex flow conditions, such as side wall boundary-layer removal, in a fairly smaller test section.

COMPARISON OF FORCE DATA FROM DIFFERENT TESTS
CAST10-2/DOA2 Airfoil (9" Chord)

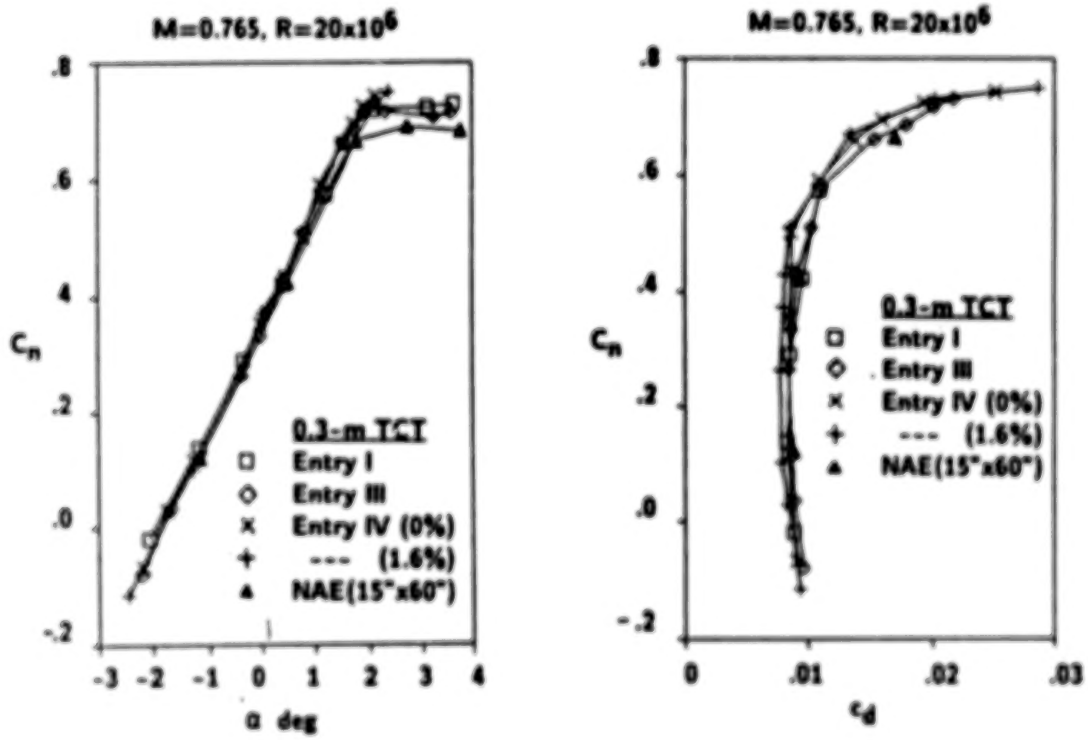

Further study of differences in Entry II

(Comparison of wall shapes and airfoil Mach numbers at 1.90 degree incidence)

The test data taken during different entries proved the repeatability of the adaptive wall technique. However, one question remained unanswered. Whether, the differences noted during the second entry were reproducible. If so, whether the possibly non-unique solutions can be identified during the progress of the test.

To understand the problem, three conditions of angle of attack were considered. The initial wall shapes for these conditions were taken from previous data records.

The first case was at angle of attack of 1.9 degree corresponding to high lift conditions. The wall streamlining process was initiated from previously streamlined shapes. Both had different wall contours and different normal force and drag coefficients. It was surprising to note that for both the wall shapes, the streamlining process converged around the same value. In one of the cases, there is strong indication of trailing edge separation, and also the top wall deflections are less.

COMPARISON OF TWO DIFFERENT SOLUTIONS
M=0.765, R=20x10^6

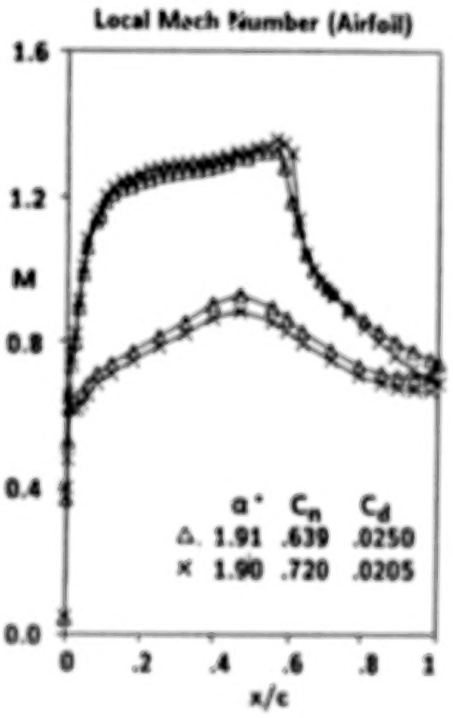

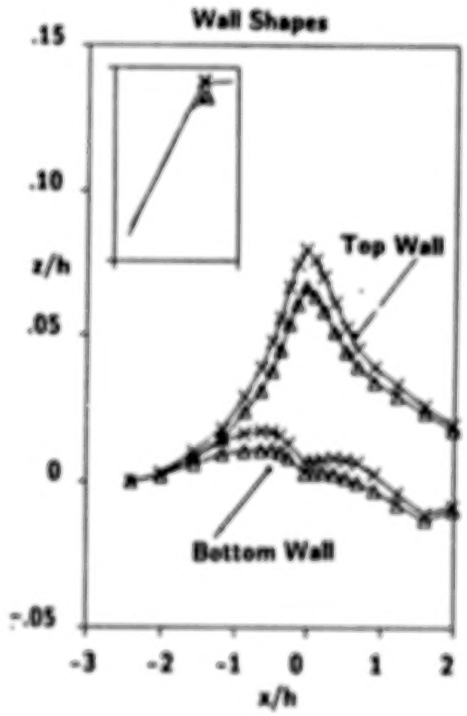

Further study of differences in Entry II

(Comparison of wall shapes and airfoil Mach numbers at 1.10 degree incidence)

The next case considered was at a normal force coefficient of about 0.6, where the Entry II results appeared to break away from the Entry I results. In both the cases the normal forces are about the same value. However, the airfoil pressure distributions are much different. In one of the cases, the shock is much aft and the trailing edge appears to be on the verge of separation. The drag is correspondingly higher. The shock positions are quite different in two cases.

COMPARISON OF TWO DIFFERENT SOLUTIONS
M=0.765, R=20x10^6

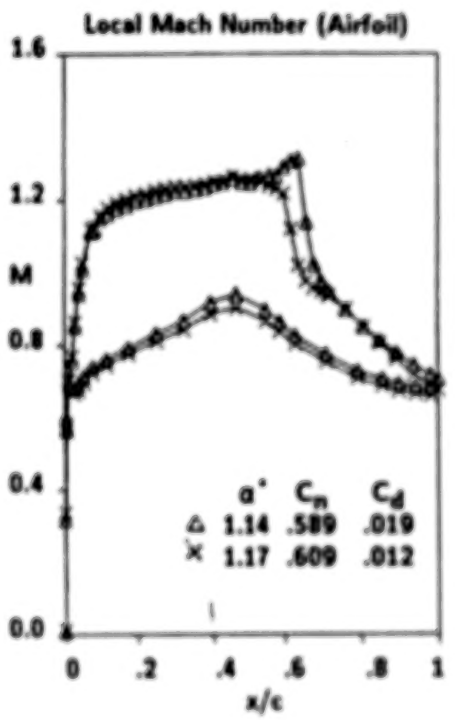

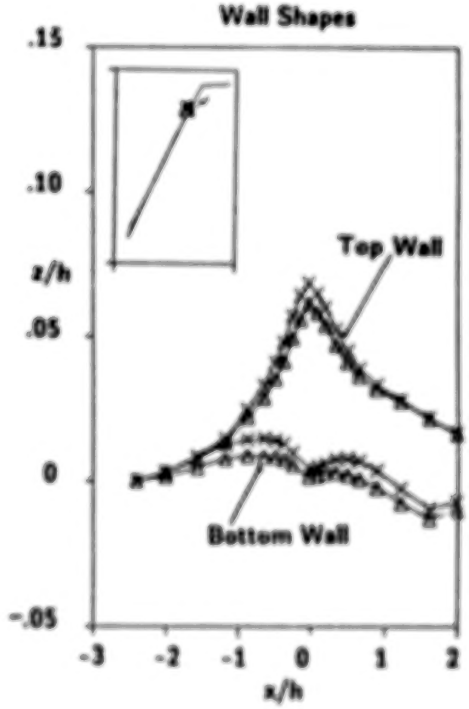

Further study of differences in Entry II
(Comparison of wall shapes and airfoil Mach numbers at -.36 degree incidence)

The next comparison was at a much lower normal force coefficient of about 0.3. There is flow separation at the trailing edge in both the case. Again, the wall shapes and the airfoil pressure distributions are quite different. The local Mach numbers on the airfoil are much higher for the case corresponding to the second Entry initial conditions. The shock appears much stronger with correspondingly higher drag levels.

COMPARISON OF TWO DIFFERENT SOLUTIONS
M=0.765, R=20x10^6

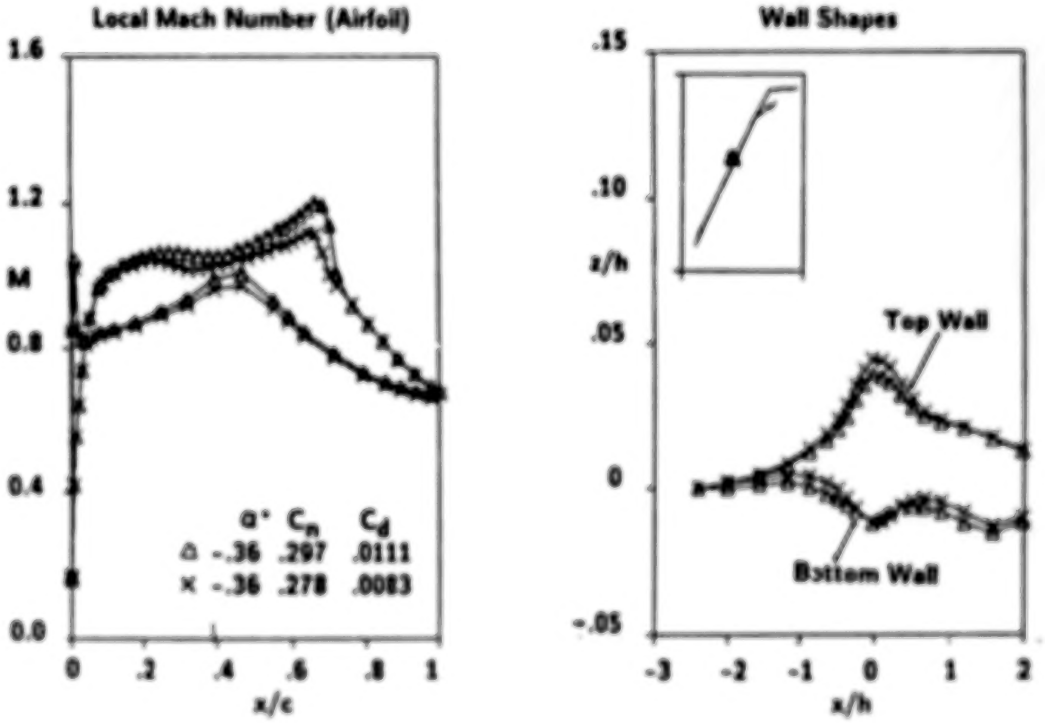

Wall interference assessment

The detailed study of the three cases discussed suggests that the residual interference levels may be different for the two cases, while the wall shapes might have satisfied the required conditions for streamlining. If so, interference assessment will provide an additional tool to reject solutions involving high levels of interference.

The two-variable method based on Cauchy's integral formula, using the flow velocity and inclination at the wall, is particularly suitable for residual interference assessment. The method does not require model description and can take into account the curved top and bottom wall shapes.

WALL INTERFERENCE ASSESSMENT

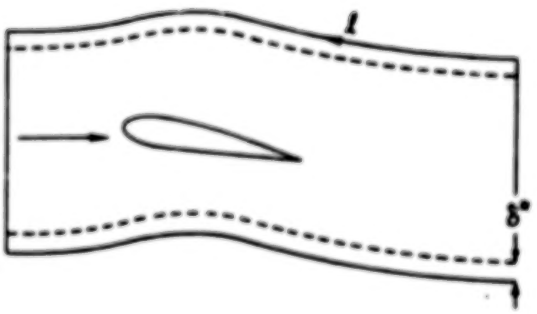

- Two Variable Method
- Cauchy's Integral Formula (Ashill & Weeks)
- Applied to Coutoured Walls
- No Model Description Required
- Approximation

  Interpolation at upstream and downstream ends

  Boundary-layer growth not included

Interference Velocity

$$W_w(z) = \frac{1}{2\pi L}\int_l \frac{W(\zeta)}{(\zeta - z)}\,d\zeta$$

$$W_w(z) = \beta u_w - i v_w$$
$$z = x/\beta + iy$$
$$\zeta = \xi/\beta + i\eta$$

Interference corrections:

Blockage: $u_w(x,y) = (1/\beta)\ \mathrm{Re}\ (W_w(z))$

Incidence: $v_w(x,y) = -\ \mathrm{Im}\ (W_w(z))$

Wall interference assessment - Preliminary results

The results of the preliminary calculation using the Cauchy's formula are shown for the three cases discussed earlier. The calculations show that for conditions corresponding to Entry II results the effective Mach number near the model is much higher. The data corresponding to Entry I giving good agreement with the NAE data, has smaller negative corrections. The higher effective Mach number near the model for the Entry II test conditions also explains the higher drag levels.

The above calculations show that the method can identify cases involving high corrections and can be used as an additional tool for assessing the quality of streamlining. The method is amenable for on-line calculations.

WALL INTERFERENCE ESTIMATION

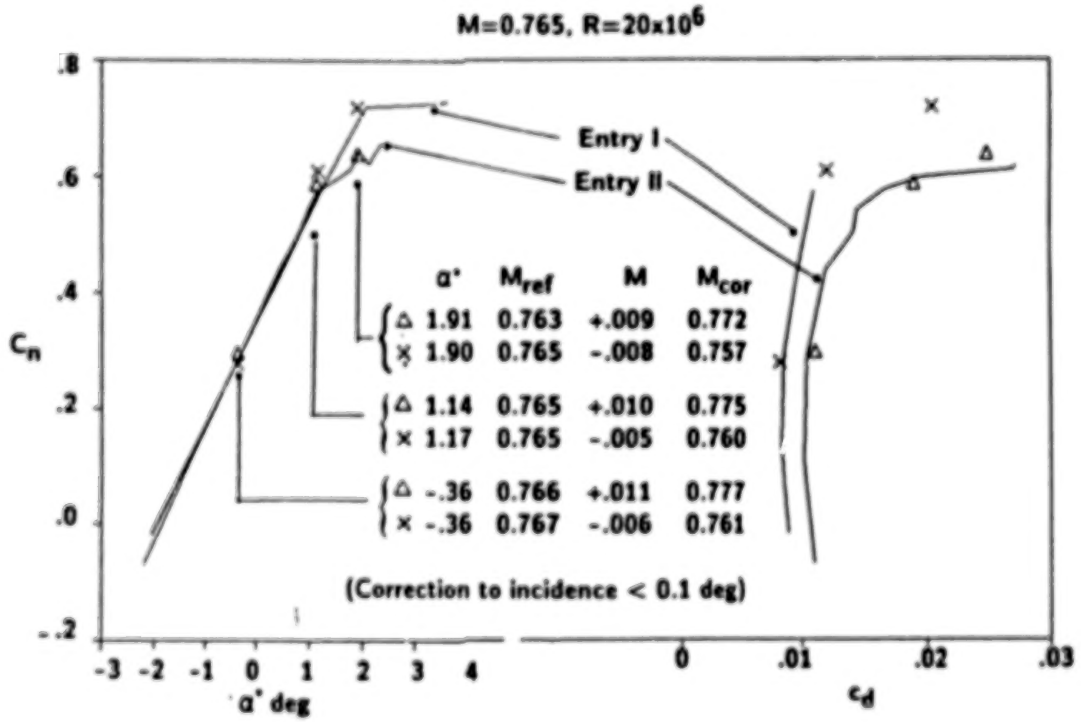

CONCLUSIONS

- Repeatability of the test data demonstrated with different tunnel entries.
- Walls streamlined successfully with and without side wall boundary-layer removal on a long chord model (c/h=0.69).
- Side wall boundary-layer removal did not have significant effect on airfoil characteristics.
- Top and bottom walls contracted with side wall boundary-layer removal to correct for change in Mach number.
- Difference in test data between Entry I and Entry II is not due to any extraneous test condition or limitation.
- Present streamlining procedure may lead to wall shapes having excessive blockage interference.
- Cauchy's formula provides a quick estimate of the residual interference and can be used on-line.
- Refinements to the present streamlining procedure will improve long term repeatability of the test data.

COMPARISON OF TWO- AND THREE-DIMENSIONAL NAVIER-STOKES SOLUTIONS WITH NASA EXPERIMENTAL DATA FOR CAST-10 AIRFOIL

R. Charles Swanson, NASA Langley Research Center
Rolf Radespiel, NASA/DFVLR Research Associate
V. Edward McCormick, North Carolina State University

ABSTRACT

The two-dimensional (2-D) and three-dimensional Navier-Stokes equations are solved for flow over a NAE Cast 10 airfoil model. Recently developed finite-volume codes that apply a multistage time stepping scheme in conjunction with steady state acceleration techniques are used to solve the equations. Two-dimensional results are shown for flow conditions uncorrected and corrected for wind tunnel wall interference effects. Predicted surface pressures from 3-D simulations are compared with those from 2-D calculations. The focus of the 3-D computations is the influence of the sidewall boundary layers. Topological features of the 3-D flow fields are indicated. Lift and drag results are compared with experimental measurements.

INTRODUCTION

Wind-tunnel measurements play a key role in the evaluation of aerodynamic prediction techniques. Therefore, accurate determination of the appropriate flow conditions for free air corresponding to a given experiment is necessary. In order to obtain these conditions, procedures are required to provide corrections to the experimental Mach number and angle of attack. The corrections are needed to remove the wind-tunnel-wall interference effects. The range of validity of such correction methods must be defined to indicate when measured data can be used to validate aerodynamic computational schemes.

In the present work, there are three principal objectives related to the problems of aerodynamic computer code validation and wind-tunnel-wall interference. The first objective is to evaluate the capability of a typical wind-tunnel-wall interference correction technique [1] to compute free-air conditions in the case of transonic flow. The second one is to compare numerical solutions with data from a recent experiment with a two-dimensional Cast 10 wing. The final aim is to determine the influence of the sidewall boundary layers in a wind-tunnel flow. These objectives are achieved by solving the two-dimensional (2-D) and three-dimensional (3-D) Navier-Stokes equations. Some recently developed finite-volume codes that apply a multistage time stepping scheme in conjunction with steady-state acceleration techniques are used to solve the equations.

In this paper, pressure and skin-friction distributions from Navier-Stokes solutions are presented for the following conditions:

1. Small supersonic region on upper surface of airfoil.
2. Large supersonic region on upper surface of airfoil.

To emphasize the validity, as well as the breakdown of the computed wall interference corrections, 2-D results are shown for both the uncorrected and corrected flow conditions. The predicted pressures are compared with the experimental data of [2]. Tables I and II summarize the flow conditions considered in this investigation. Points 77 and 81 of [2] are the representative cases. A 2-D solution for Point 78 is also presented.

As indicated in Table II, the representative cases are also computed with a 3-D simulation of the wind-tunnel flow. A comparison is made between the 2-D and 3-D predicted surface pressures. Corrections to the flow conditions due to the upper and lower tunnel walls are used. The focus in the 3-D calculation is the influence of the sidewall boundary layers. Pressure contours and skin-friction lines are displayed to characterize the flow. Topological features of the 3-D flow fields are indicated. Finally, lift and drag predictions are compared with experimental measurements.

TABLE I - Flow Conditions from Experiment of Mineck [2] and for Two-Dimensional Navier-Stokes Calculations

POINT	M_{uncorr}	α_{uncorr}	M_{corr}	α_{corr}	ΔM	$\Delta\alpha$
76	.7658	-1.1769	.7611	-1.3681	- .0047	- .1912
77	.7656	- .3724	.7581	- .6794	- .0075	- .3070
78	.7664	.4887	.7634	.1735	- .0030	- .3152
79	.7661	1.2568	.7540	.7997	- .0121	- .4571
80	.7662	1.6945	.7518	1.1595	- .0144	- .5350
81	.7666	2.1594	.7468	1.5722	- .0198	- .5872

TABLE II - Flow Conditions from Experiment of Mineck [2] and for Three-Dimensional Navier-Stokes Calculations

POINT	M_{uncorr}	α_{uncorr}	M_{corr}	α_{corr}	ΔM	$\Delta\alpha$
77	.7656	- .3724	.7620	- .6540	- .0036	- .2816
81	.7666	2.1594	.7540	1.5810	- .0126	- .5784

MATHEMATICAL FORMULATION

Both the 2-D and 3-D Navier-Stokes equations are considered. The dominant viscous terms for the airfoil and wind-tunnel flows investigated are retained. The viscous transport processes associated with the streamwise direction are neglected. The cross-derivative viscous terms are neglected.

- Mass-averaged Navier-Stokes equations
- Boundary conditions: no slip and adiabatic surface
- Initial solution: free stream
- Constitutive relations
  1) Ideal gas law
  2) Power law for molecular viscosity
- Turbulence closure
  1) Eddy viscosity hypothesis
  2) Algebraic model for viscosity (i.e., Baldwin and Lomax)

In this figure, the basic elements of the present procedures for the numerical solution of the Navier-Stokes equations are given. A modified five-stage Runge-Kutta scheme is used to advance the solution in time. Artificial dissipation terms are added to the difference equations, and they are third order in the smooth region of the flow field. These terms are included for several reasons: (1) to enhance the coupling of the difference equations, (2) to control nonlinear instabilities, and (3) to eliminate oscillations at shock waves.

Three techniques are employed to accelerate convergence to steady state. With local time stepping, the solution at any point in the domain is advanced at the maximum time step allowed by stability. This results in faster signal propagation and, thus, faster convergence. Implicit residual smoothing can be regarded as simply a mathematical step applied after each Runge-Kutta stage to extend the local stability range. Finally, a multigrid method involves the application of a sequence of meshes to a discrete problem to accelerate convergence of the time-stepping scheme. Successively coarser meshes can be generated by starting with the desired fine mesh and eliminating every other mesh line in each coordinate direction. An equivalent fine grid problem is defined on each coarse grid. Appropriate operators are introduced to transfer information between the meshes. There are two main advantages of the multigrid method. First, less computational effort is required on the coarser meshes. Second, information is propagated faster on the coarser meshes due to larger allowable time steps.

Details of the two-dimensional scheme are given in [3]-[5], and the extension to three dimensions is discussed in [6].

- Time integration with 5 stage Runge-Kutta scheme
- Finite-volume spatial discretization -- central differencing
- Second-order accuracy in time and space
- Controlled artificial dissipation -- blending of second and fourth differences
- Acceleration techniques for steady-state solutions
  1) Local time stepping
  2) Implicit residual smoothing
  3) Multigrid

DEFINITION OF MESHES

With a C-type grid, one set of grid lines wraps around the airfoil, and the other set is normal to the airfoil. The normal mesh spacing at the airfoil is 1×10^{-5} chords. For the 3-D case, streamwise planes containing C-type meshes are stacked in the spanwise direction. The distance from the sidewall to the first spanwise point is 2×10^{-5} chords, and approximately 30 grid planes are located within the sidewall boundary layer.

- Two dimensions
  1) C-type grid
  2) 320 streamwise cells (192 on airfoil) , 64 normal cells
- Three dimensions
  1) C-H mesh topology
  2) 256 streamwise cells (192 on airfoil) , 64 normal cells , and 48 spanwise cells

SURFACE PRESSURES FOR CAST 10 AIRFOIL
Point 77

This figure shows a comparison of 2-D Navier-Stokes predictions for the surface pressures with the experimental data of Mineck [2]. Results are given for both the uncorrected and corrected flow conditions. There is better agreement with the data when corrected flow conditions are used.

$Re_\infty = 10^7$

Uncorrected flow conditions

$M_\infty = .766$, $\alpha = -.372$

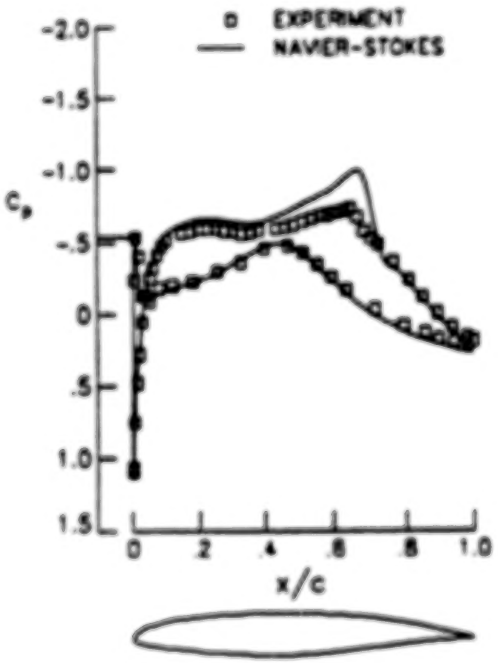

Corrected flow conditions

$M_\infty = .758$, $\alpha = -.679$

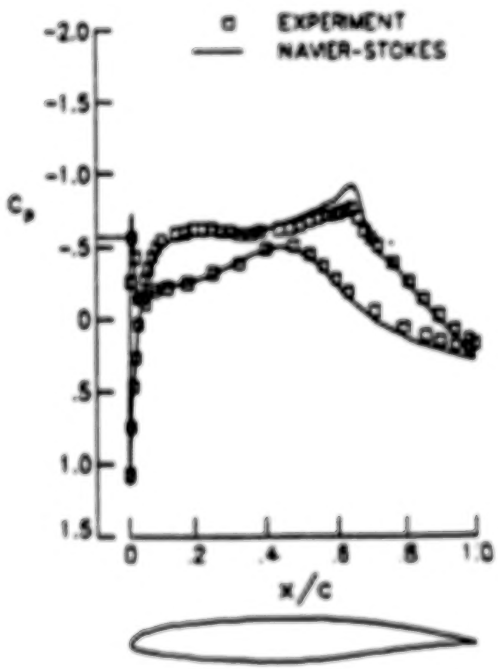

SKIN FRICTION FOR CAST 10 AIRFOIL
Point 77

Calculated skin-friction distributions for the upper surface of the Cast 10 airfoil at both the uncorrected and corrected flow conditions are presented. The decrease in the skin friction at the shock wave is significantly smaller for the case of corrected flow conditions.

UPPER SURFACE , $Re_{\infty} = 10^7$

Uncorrected flow conditions

$M_{\infty} = .766$, $\alpha = -.372$

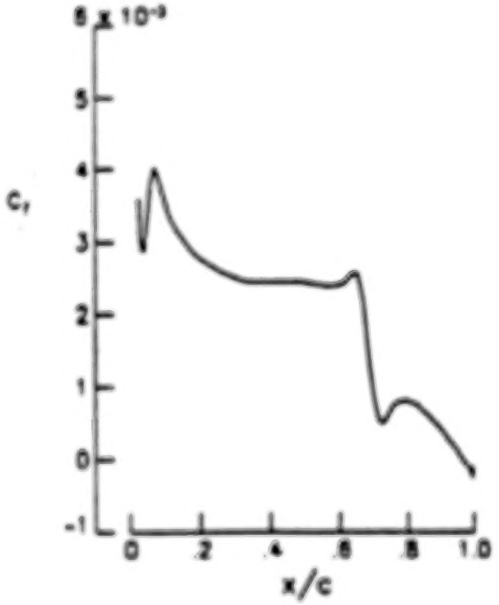

Corrected flow conditions

$M_{\infty} = .758$, $\alpha = -.679$

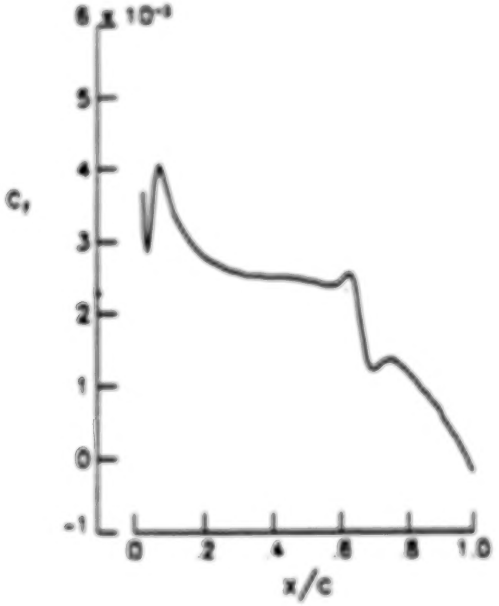

SURFACE PRESSURE FOR CAST 10 AIRFOIL
Point 81

In this figure, computed pressures are compared with experimental data at the uncorrected and corrected flow conditions. There is better agreement with the data when the uncorrected flow conditions are used. The discrepancy between the predicted and measured shock position is probably due to the turbulence model. The corrections for wind-tunnel-wall interference effects are too large. The large supersonic region on the wing results in a behavior of the sidewall boundary layer that is not properly modeled in the wall interference correction code.

$Re_\infty = 10^7$

Uncorrected flow conditions

$M_\infty = .767$, $\alpha = 2.159$

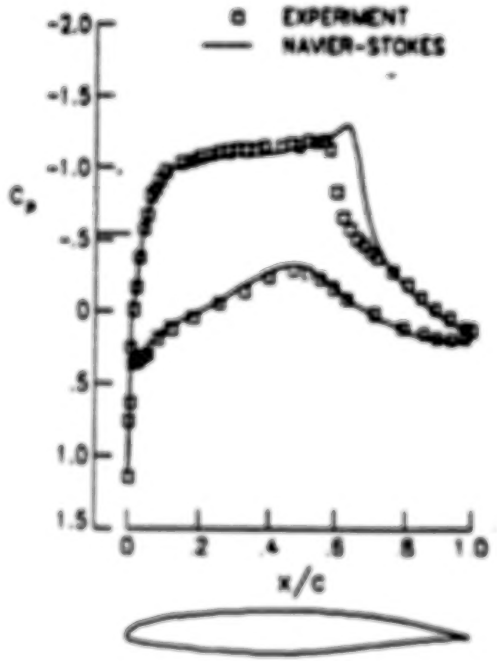

Corrected flow conditions

$M_\infty = .747$, $\alpha = 1.572$

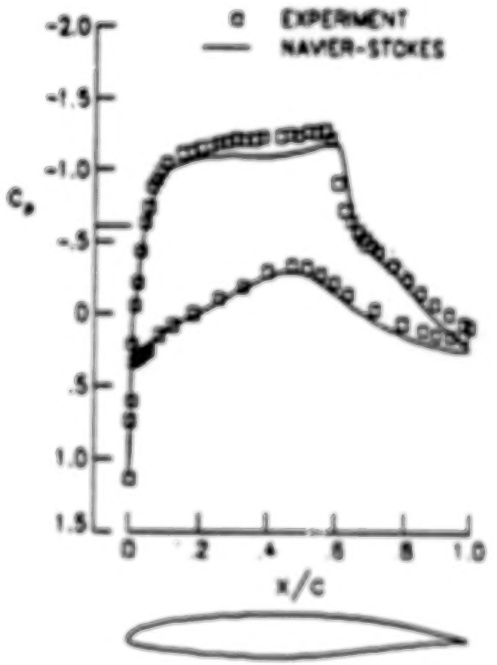

SKIN FRICTION FOR CAST 10 AIRFOIL
Point 81

This figure presents predicted skin-friction variations for the upper surface of the Cast 10 airfoil. The solution based upon corrected flow conditions exhibits a small separation region at the shock and one at the airfoil trailing edge. With the uncorrected conditions, the separation induced by the shock merges with that at the trailing edge.

UPPER SURFACE , $Re_\infty = 10^7$

Uncorrected flow conditions

$M_\infty = .767$, $\alpha = 2.159$

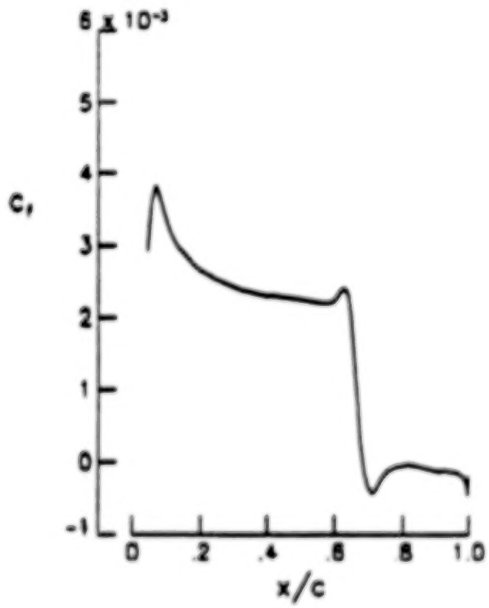

Corrected flow conditions

$M_\infty = .747$, $\alpha = 1.572$

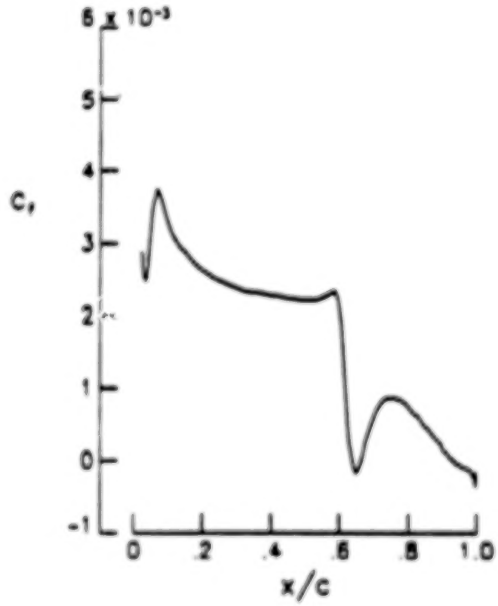

SURFACE PRESSURES FOR CAST 10 AIRFOIL
Point 78

The surface pressure distributions in this figure represent a noticeable departure from those shown previously. They exhibit a weak compression of the upper surface flow followed by acceleration and a shock wave. The computed solution using the corrected Mach number and angle of attack agrees better with the experimental data than the solution using the uncorrected values. However, the weak compression upstream of the shock is still not captured.

$Re_\infty = 10^7$

Uncorrected flow conditions

$M_\infty = .766$, $\alpha = .489$

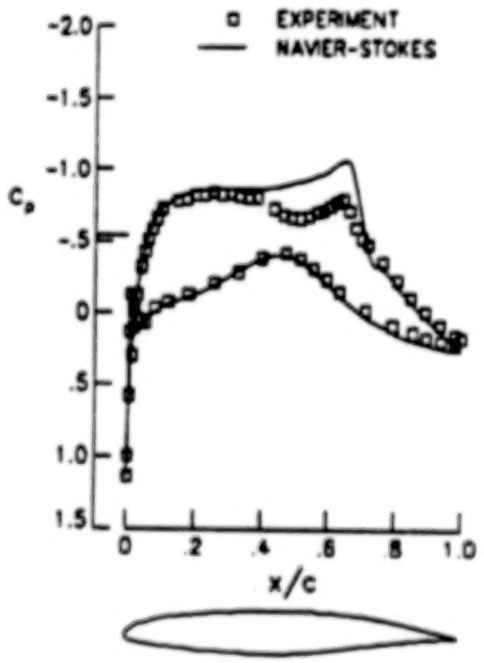

Corrected flow conditions

$M_\infty = .763$, $\alpha = .174$

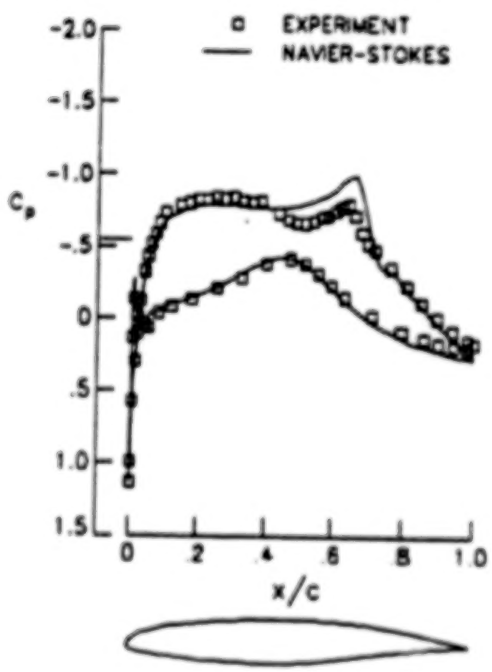

3-D SIMULATION OF CAST 10 AIRFOIL IN WIND TUNNEL

For the 3-D simulation no-slip boundary conditions have been applied on part of the sidewall so that the computed thickness of the sidewall boundary layer matches the values measured in the empty wind tunnel. At the outer boundaries of the computational domain characteristic variable boundary conditions assuming one-dimensional flow normal to the boundary have been employed, and the free-stream conditions are obtained by superimposing the flow field of a single vortex to the onset flow. Due to the displacement effect of the sidewall boundary layer, the Mach number in the test section is not the same as the free-stream Mach number. Therefore, the dependence of the test section Mach number with respect to the free stream was first calibrated by a simulation of the empty wind tunnel. When specifying the flow conditions for the simulations of the airfoil in the tunnel, the wind-tunnel corrections of Mach number and angle of attack for the upper and lower walls as predicted by the method of [1] have been included. Following the ideas of Hung, et al. [7], the turbulence model of Baldwin and Lomax was extended to treat corner flows.

In all simulations, a steady-state solution of the flow has been obtained within 200 multigrid cycles on the fine mesh.

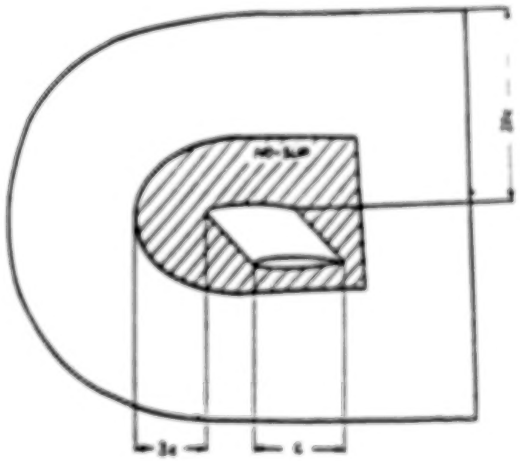

SURFACE PRESSURES FOR CAST 10 AIRFOIL
Point 77

To demonstrate the viscous sidewall effects, results of the 3-D simulation are now compared to those of the 2-D code at the same flow conditions. For $M_\infty = 0.762$, $\alpha = 0.654$, and $Re_\infty = 10^7$, the influence of the viscous sidewall on the pressure distribution along the centerline of the wind tunnel is small.

INFLUENCE OF VISCOUS SIDEWALL

$$M_\infty = .762\ ,\ \alpha = -.654\ ,\ Re_\infty = 10^7$$

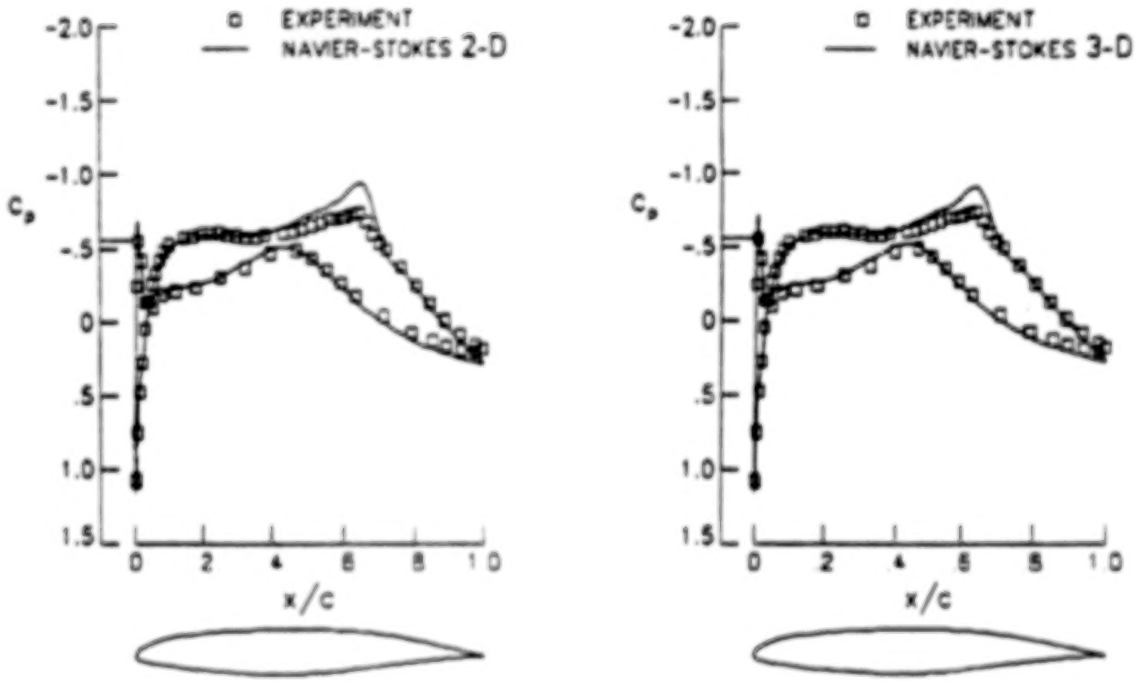

SURFACE PRESSURES FOR CAST 10 AIRFOIL
Point 81

For $M_\infty = 0.754$, $\alpha = 1.581$, and $Re_\infty = 10^7$, the influence of the viscous sidewall on the pressure distribution along the centerline of the wind tunnel is larger. Due to the variation of the displacement thickness of the sidewall boundary layer along the airfoil, the flow is more accelerated at the upper side of the airfoil, and the shock is moved upstream.

INFLUENCE OF VISCOUS SIDEWALL

$$M_\infty = .754 \ , \ \alpha = 1.581 \ , \ Re_\infty = 10^7$$

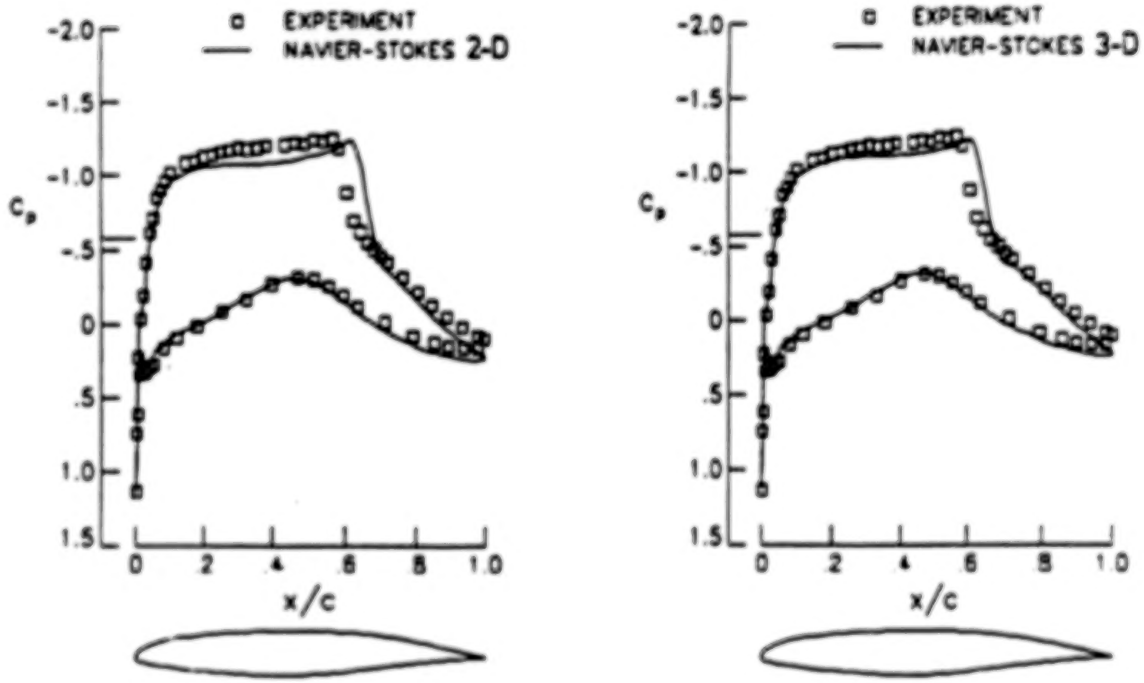

FLOW OVER UPPER SURFACE OF CAST 10 AIRFOIL
Point 77

The pressure contours and the skin-friction lines on the upper surface of the airfoil for $M_\infty = 0.72$, $\alpha = -0.654$, and $Re_\infty = 10^7$ show that the shock is weakened as the sidewall is approached. There is incipient separation at the trailing edge. A small separation around a nodal point occurs in the corner between the trailing edge and the sidewall.

$M_\infty = .762$, $\alpha = -.654$, $Re_\infty = 10^7$

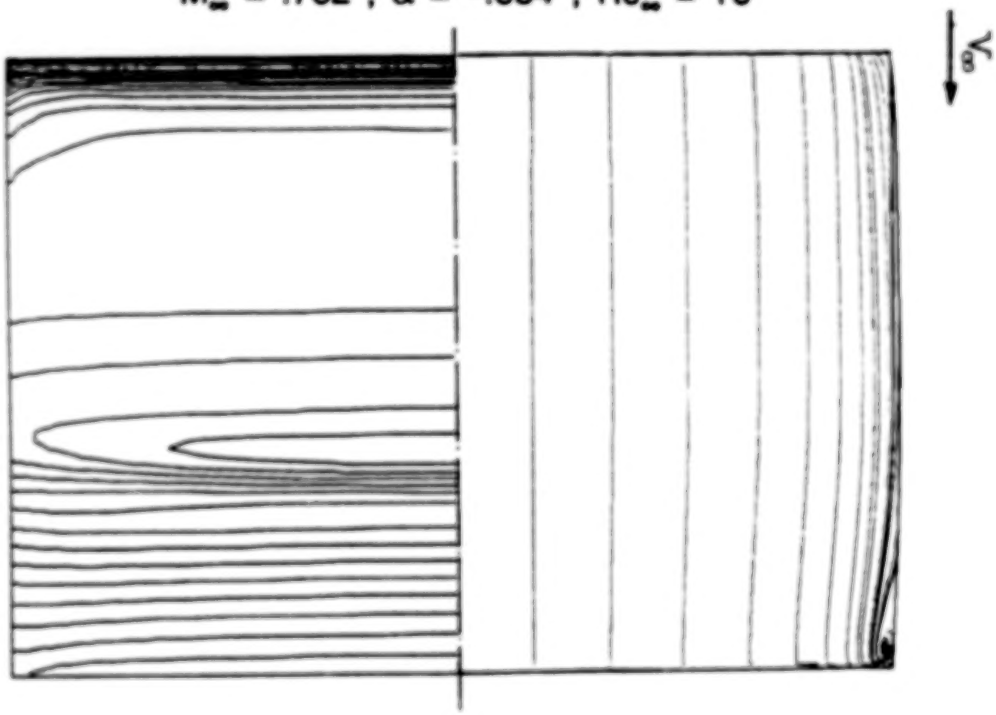

Pressure contours

Skin-friction lines

FLOW OVER UPPER SURFACE OF CAST 10 WING
Point 81

For $M_\infty = 0.754$, $\alpha = 1.581$, and $Re_\infty = 10^7$, shock induced and trailing-edge separations occur. These separations are weakened towards the sidewall because the pressure gradients are smaller near the sidewall. The nodal-type separation in the corner between the trailing edge and the sidewall has grown considerably relative to the previous case.

$M_\infty = .754$, $\alpha = 1.581$, $Re_\infty = 10^7$

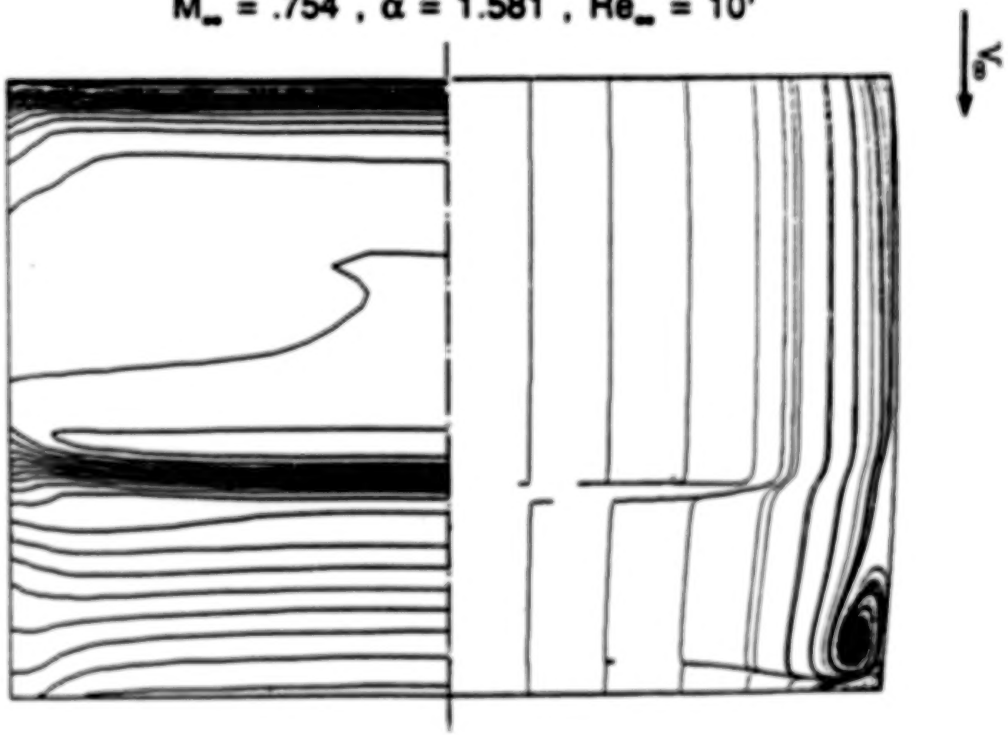

Pressure contours

Skin-friction lines

SKIN-FRICTION LINES FOR WING AND SIDEWALL
Point 77

The skin-friction lines along the wing and sidewall for $M_\infty = 0.762$, $\alpha = -0.654$, and $Re_\infty = 10^7$, show the existence of a sidewall separation upstream of the leading edge of the wing. The wavy behavior of the sidewall streamlines around the trailing edge indicates three-dimensional flow in the corner between the sidewall and the wing.

CAST 10 AIRFOIL , $M_\infty = .762$, $\alpha = -.654$, $Re_\infty = 10^7$

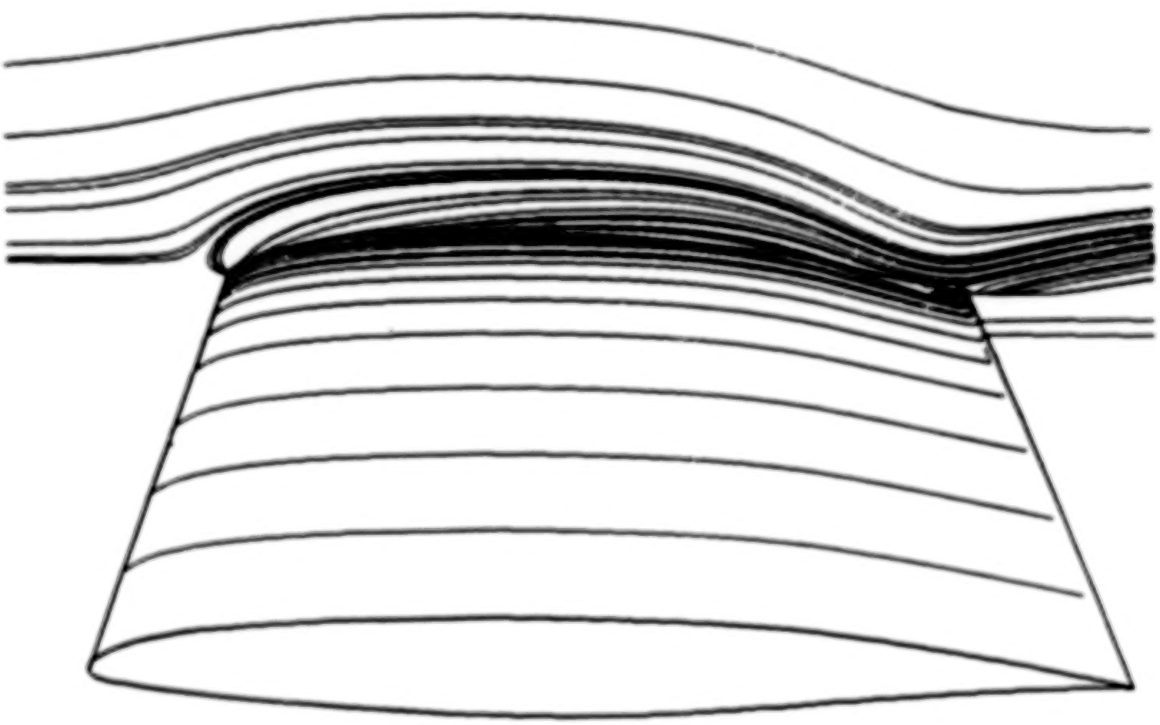

DETAILS OF WING-SIDEWALL JUNCTURE REGION
Point 77

CAST 10 AIRFOIL , $M_\infty = .762$, $\alpha = -.654$, $Re_\infty = 10^7$

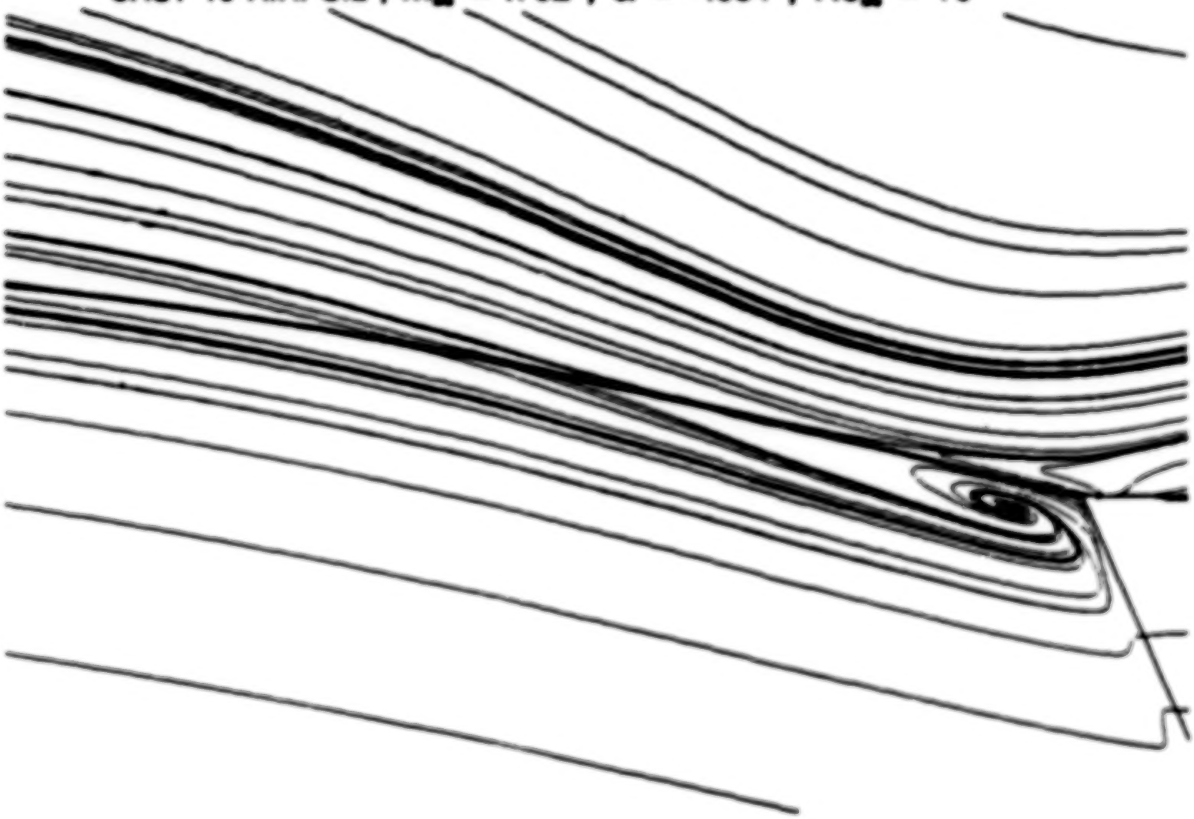

SKIN-FRICTION LINES FOR WING AND SIDEWALL
Point 81

For M_∞ = 0.754, α = 1.581, and Re_∞ 10^7, the sidewall boundary layer separates at the shock and near the trailing edge of the wing, forming a complex flow structure with saddle points and nodal points, which are designated in the figure on the next page by S and N, respectively.

CAST 10 AIRFOIL , M_∞ = .754 , α = 1.581 , Re_∞ = 10^7

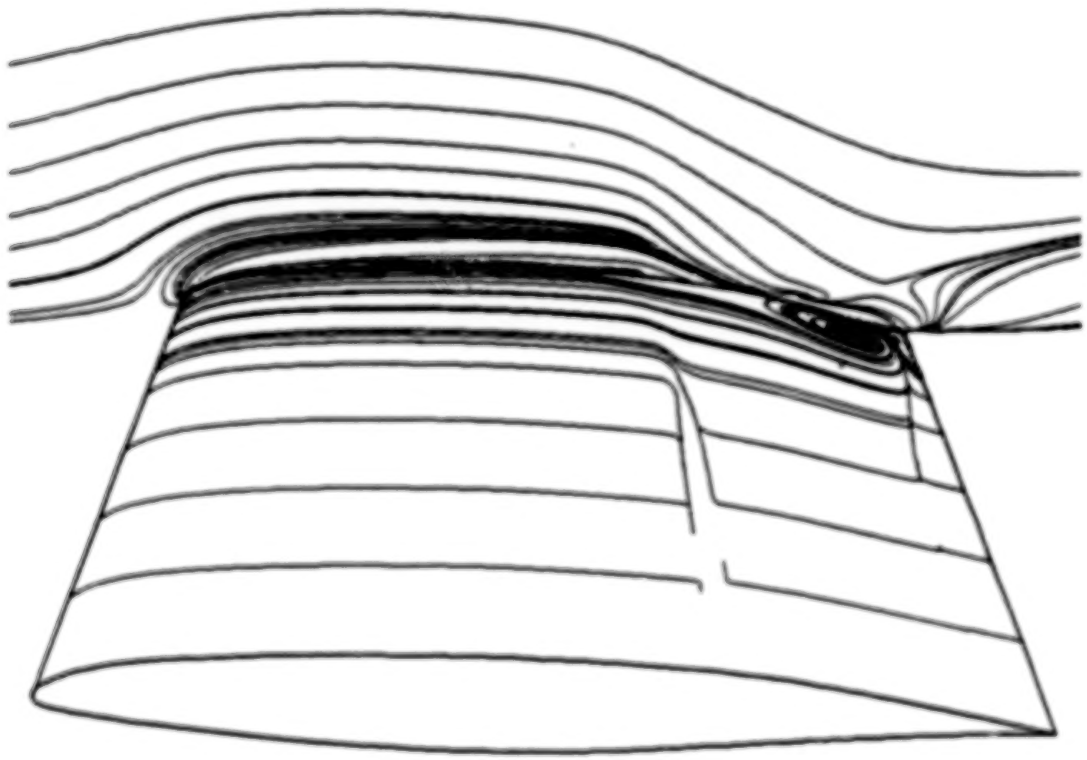

DETAILS OF WING-SIDEWALL JUNCTURE
Point 81

CAST 10 AIRFOIL , $M_\infty = .754$, $\alpha = 1.581$, $Re_\infty = 10^7$

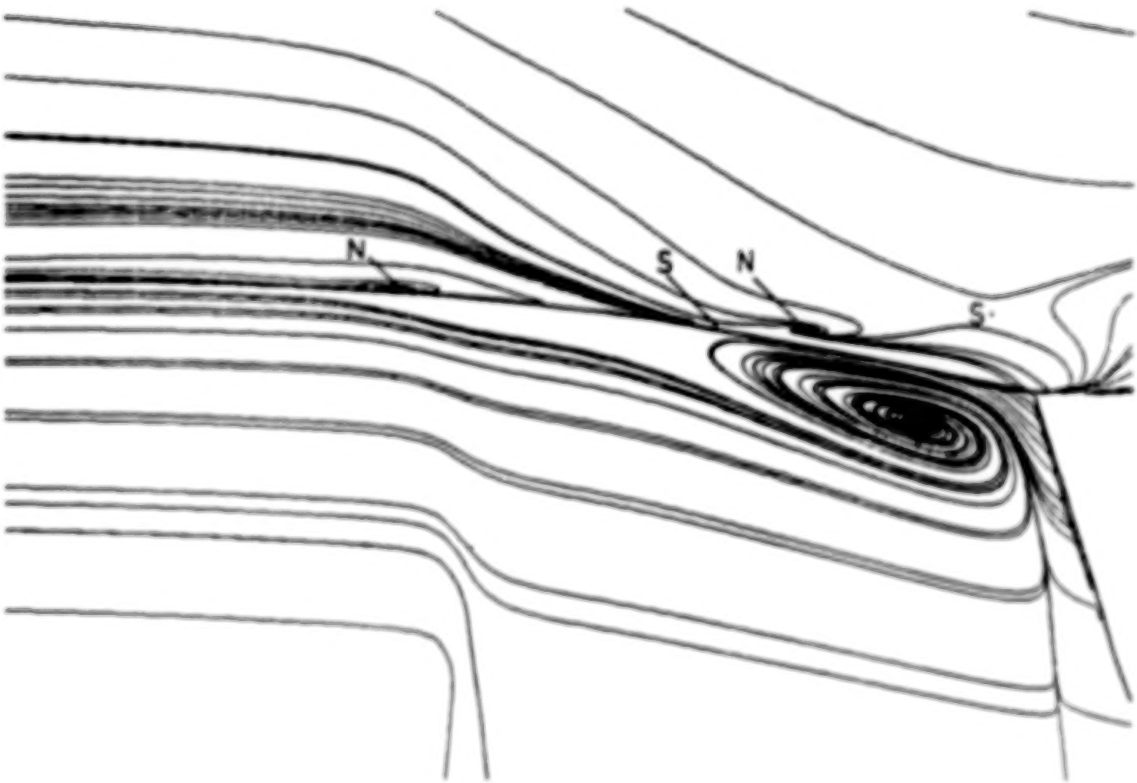

LIFT CURVE FOR CAST 10 AIRFOIL

This figure compares the computed lift curves with the experimental ones for the uncorrected and corrected flow conditions. The predicted lift coefficients are higher than the corrected ones (denoted by square symbol) at the lower angles of attack. As indicated previously, the calculated wall interference corrections are too large at the higher angles of attack, which explains the change in experimental lift curve slope for the corrected conditions. The predicted centerline sectional lift coefficients from the 3-D calculations are indicated with the solid symbol.

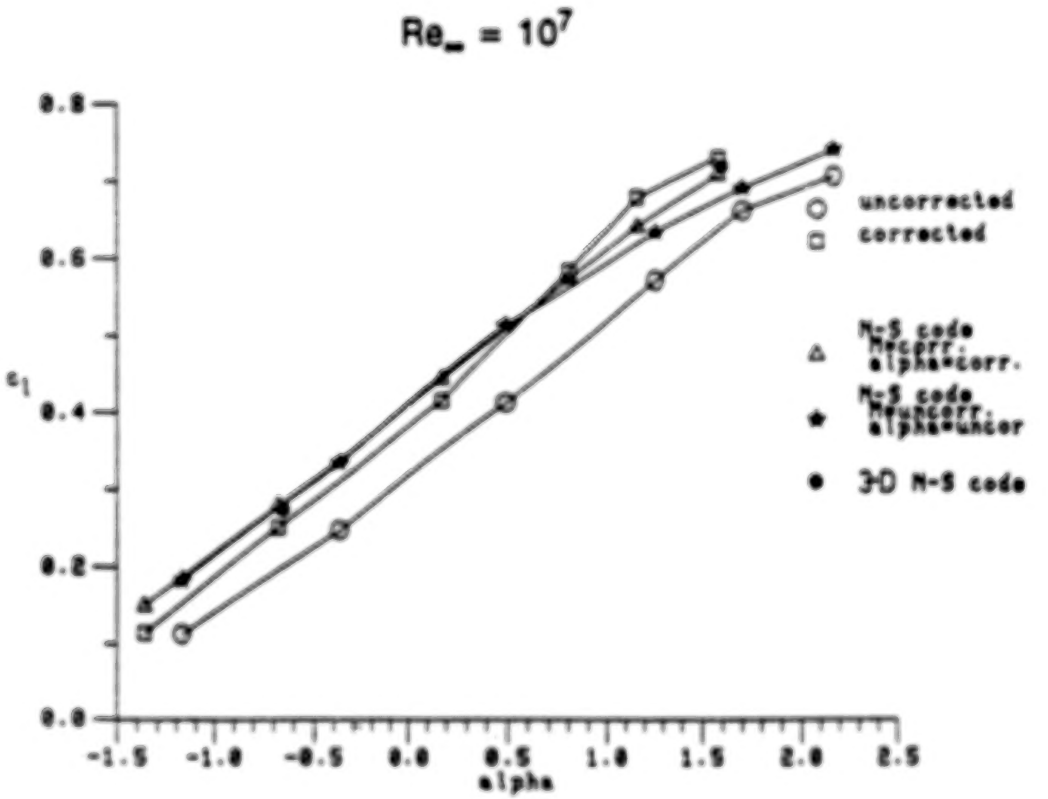

DRAG POLAR FOR CAST 10 AIRFOIL

The computed and experimental drag polars are compared in this figure. There is a strange behavior at the higher angles of attack exhibited by the numerical values based on corrected flow conditions. This occurs because the wind-tunnel-wall interference corrections are too large. The large corrections are a consequence of the breakdown in the theory used to compute the influence of the sidewall boundary layers.

$Re_\infty = 10^7$

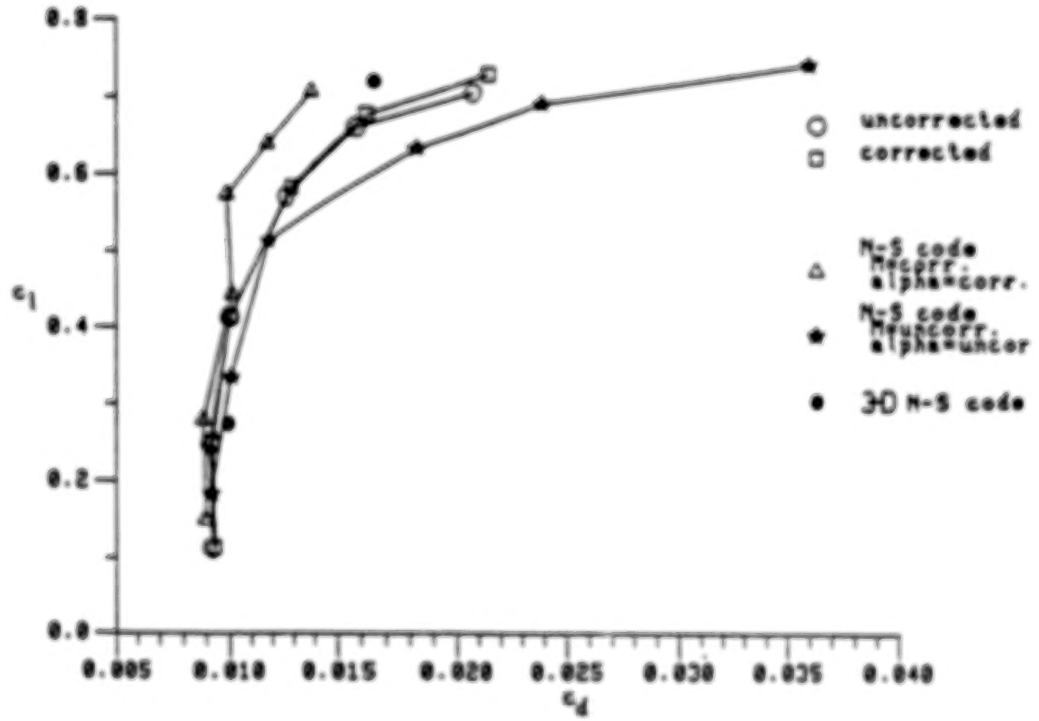

SPANWISE DISTRIBUTION OF DRAG

The spanwise distribution of drag has been computed by integrating pressure drag and friction drag along the airfoil sections. The experimental values have been also included for $M_\infty = 0.762$, $\alpha = -0.654$, and $Re_\infty = 10^7$, whereas for $M_\infty = 0.754$, $\alpha = 1.581°$, and $Re_\infty = 10^7$ there was no experimental drag available [2]. The comparisons show constant drag over 60% of the span and a drag maximum at about 10% of the half span away from the wall. A part of the local increase of the drag may be attributed to the fact that the flow was assumed to be completely turbulent near the sidewall, and boundary-layer transition at 5% of the chord was gradually introduced between 0.25 and 0.35 of the half span. Of course, there is also induced drag to be considered, because the lift is varying over the wing.

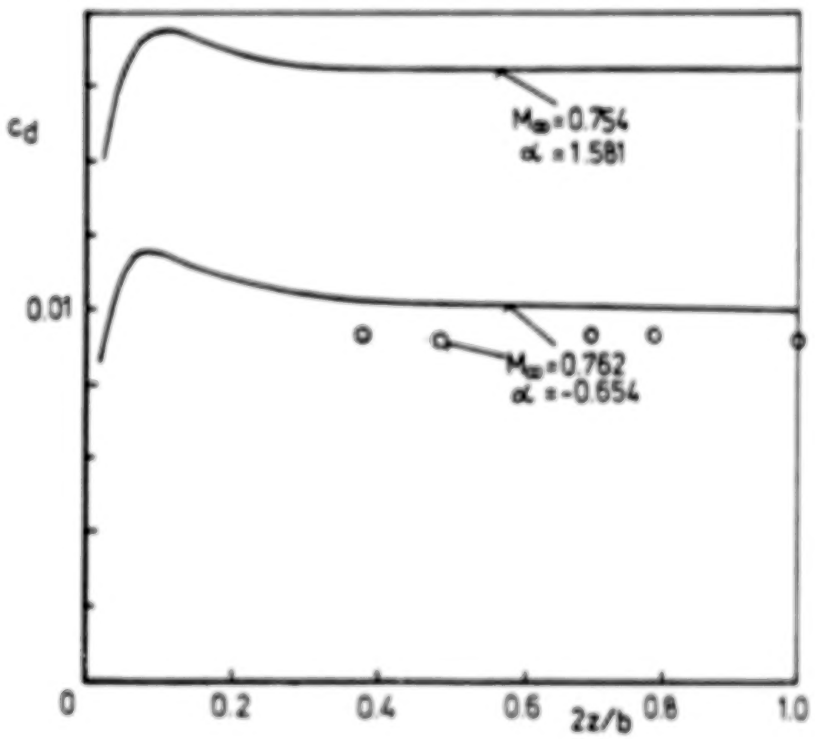

CONCLUDING REMARKS

- Corrections for Mach number and angle of attack due to wind tunnel wall interference effects are required.
- Standard wind tunnel wall interference corrections due to sidewall boundary layers are inadequate in the case of a large supersonic flow region on the upper surface of the wing.
- Three-dimensional simulations of the flow in the wind tunnel have shown that the influence of the sidewall is small for a small supersonic flow region on the wing. For a large supersonic region, the effect of the viscous side wall is to accelerate the flow upstream of the shock and to move the shock upstream.
- For the case of a large supersonic flow region on the upper surface of the wing, the 3-D prediction using only wind tunnel corrections for the upper and lower walls and simulating the sidewall boundary layers is in better agreement with the measured data than the 2-D solution using wind tunnel corrections for all walls.
- For some cases it may be impossible to find wind tunnel corrections such that good agreement is obtained between predictions of 2-D codes and measurements. To address this issue, a 3-D simulation including the upper and lower wind tunnel walls is necessary.
- The Baldwin-Lomax algebraic turbulence model is not adequate to obtain the correct shock wave position for the higher angles of attack considered for Cast-10 airfoil.

REFERENCES

[1] Green, L. L.; and Newman, P. A.: "Transonic Wall Interference Assessment and Corrections for Airfoil Data from the 0.3-m TCT Adaptive Wall Test Section," AIAA Paper 87-1431, 1987.

[2] Mineck, R. E.: "Wall Interference Tests of a CAST 10-2/DoA 2 Airfoil in an Adaptive-Wall Test Section," NASA TM 4015 with Supplement, Dec. 1987.

[3] Arnone, A.; and Swanson, R. C.: "A Navier-Stokes Solver for Cascade Flows," ICASE Report No. 88-32, July 1988.

[4] Radespiel, R.; and Swanson, R. C.: "An Investigation of Cell Centered and Cell Vertex Multigrid Schemes for the Navier-Stokes Equations," AIAA Paper 89-0548, Jan. 1989.

[5] Swanson, R. C.; and Turkel, E.: "Artificial Dissipation and Central Difference Schemes for the Euler and Navier-Stokes Equations," AIAA Paper 87-1107, AIAA 8th Computational Fluid Dynamics Conference, Honolulu, Hawaii, June 9-11, 1987.

[6] Radespiel, R.: "A Cell-Vertex Multigrid Method for the Navier-Stokes Equations," NASA TM, in publication.

[7] Hung, C.-M.; and Buning, P. G.: "Simulation of Blunt-Fin-Induced Shock-Wave and Turbulent Boundary-Layer Interaction," J. F. M. Vol. 154, pp. 163-185 (1985).

*U.S. GOVERNMENT PRINTING OFFICE 1989-727-016/80005

NASA

Report Documentation Page

1. Report No.	2. Government Accession No.	3. Recipient's Catalog No.
NASA CP-3052		

4. Title and Subtitle	5. Report Date
CAST-10-2/DOA 2 Airfoil Studies Workshop Resultr	November 1989
	6. Performing Organization Code

7. Author(s)	8. Performing Organization Report No.
Edward J. Ray and Acquilla S. Hill, Compilers	L-16633
	10. Work Unit No. 505-61-01-09

9. Performing Organization Name and Address	11. Contract or Grant No.
NASA Langley Research Center Hampton, VA 23665-5225	
	13. Type of Report and Period Covered: Conference Publication

12. Sponsoring Agency Name and Address	14. Sponsoring Agency Code
National Aeronautics and Space Administration Washington, DC 20546-0001	

15. Supplementary Notes

16. Abstract

During the period of September 23 through 27, 1988, the Transonic Aerodynamics Division at the Langley Research Center hosted an International Workshop on CAST-10-2/DOA 2 Airfoil Studies. These airfoil studies were the outgrowth of several cooperative study agreements among the NASA, the NAE of Canada, the DLR of West Germany, and the ONERA of France. Each of the visiting organizations was represented by at least two participants. NASA and visiting researchers reviewed both theoretical and experimental CAST-10 airfoil results that had been obtained from an extensive series of tests and studies. These results provided an opportunity to make direct comparisons of adaptive wall test section (AWTS) results from the NASA 0.3-Meter Transonic Cryogenic Tunnel and ONERA T-2 AWTS facilities with conventional ventilated wall wind-tunnel results from the Canadian High-Reynolds Number Two-Dimensional Test Facility.

The overall results of the workshop were very positive. Correlations of corrected "conventional" results, AWTS data, and predictions were generally good. The present report contains the individual papers presented during the workshop. A summary of the major activities and accomplishments of the workshop is included.

17. Key Words (Suggested by Author(s))	18. Distribution Statement
High Reynolds number testing Adaptive wall test section Cryogenic pressure tunnel facilities Supercritical airfoil technology	Unclassified - Unlimited Subject Category 09

19. Security Classif. (of this report)	20. Security Classif. (of this page)	21. No. of pages	22. Price
Unclassified	Unclassified	264	A12

NASA FORM 1626 OCT 86 For sale by the National Technical Information Service, Springfield, Virginia 22161-2171 NASA-Langley, 1989

National Aeronautics and
Space Administration
Code NTT-4

Washington, D.C.
20546-0001

Official Business
Penalty for Private Use, $300

SPECIAL FOURTH-CLASS RATE
POSTAGE & FEES PAID
NASA
Permit No. G-27

NASA

POSTMASTER: If Undeliverable (Section 158
Postal Manual) Do Not Return